INVESTIGATION INTO THE EFFECT OF LOW TEMPERATURE IN THE FEMORAL HIP STEM ON THE EXTRACTION FORCE REQUIRED DURING REVISION TOTAL HIP ARTHROPLASTY

A Thesis submitted to The University of Manchester for the degree of

Doctor of Philosophy

in the Faculty of Science & Engineering

2016

ADEODATO ISRAEL BOTELLO ARREDONDO

SCHOOL OF MECHANICAL, AEROSPACE AND CIVIL ENGINEERING

Table of Contents

Final Word Count 44,027

List of Figures

List of Tables

Abbreviations

THA	Total Hip Arthroplasty
RTHA	Revision Total Hip Arthroplasty
HA	Hydroxyapatite
PMMA	Poly(Methyl Methacrylate)
LN_2	Liquid nitrogen
CAD	Computer Aided Design
CAE	Computer Aided Engineering
FEA	Finite Element Analysis
FE	Finite Element
NJR	National Joint Registry
MIS	Minimally Invasive Surgery
NHS	National Health Service
ASA	American Society of Anaesthesiologist
RSR	Retrograde Stem Removal
ISO	International Organization for Standardization
ASTM	American Society for Testing and Materials
TUS	Therapeutic Ultrasound
g.e.s.	global element size

Nomenclature

q_x, q_y, q_z,	Heat transfer rate in the x, y, and z directions respectively
q''_x, q''_y, q''_z	Heat flux in the x, y, and z directions respectively
k	Conductive heat transfer coefficient
T	Temperature
x, y, z	Position coordinates
h	Convective heat transfer coefficient
T_s	Temperature at the surface
T_∞	Temperature of the fluid
U	Internal energy
ρ	Density
S	Surface area of a solid body
r	External energy per unit volume
∇	Gradient operator
V	Volume
c	Heat capacity
t	Time
Δ	Difference operator
E	Young's modulus
G_1, G_2	Shear moduli in z and θ direction respectively
Knn, Ktt, Kss	Elastic stiffness in r, z, and θ directions respectively
Ra	Surface roughness coefficient
τ	Shear stress

K	Stiffness
A_s	Area of custom femoral stem in contact with bone-cement
P	Force
γ	Shear strain
δ	Displacement
W	Strain Energy
Q	Volumetric flow

Abstract

The University of Manchester, Adeodato Israel Botello Arredondo, Doctor of Philosophy, Investigation into the effect of low temperature in the femoral hip stem on the extraction force required during revision total hip arthroplasty, June 2016.

Improvements in Total Hip Arthroplasty (THA) technology, methods of fixation, and cementing techniques of the prosthetic components have resulted in major problems when Revision Total Hip Arthroplasty (RTHA) is required, making the removal of well-fixed femoral stems a challenging and difficult surgical procedure. The promotion of osseointegration in cementless THA means removal of a cementless stem in RTHA is a particularly demanding task. Despite the numerous tools and methods that can be employed to remove the femoral component, the surrounding soft and osseous tissue can be severely damaged by the established revision techniques because no surgical procedure is able to remove a well-fixed femoral stem without causing any damage. This thesis investigates cooling the femoral prosthesis in order to lower the force required to extract the implant during RTHA of cementless femoral stems. Based on this concept, a new methodology was developed, consisting of cooling the neck of the femoral stem to a low temperature and immediately extracting the stem from the femur. As a proof of concept, to demonstrate the potential feasibility of the new method, experimental tests involving the removal of a cemented stem were considered; this was because, amongst other reasons, (i) the difficulty of simulating osseointegration in laboratory experimentation in a controlled and repeatable way, (ii) the favourable similarities of the mechanical and thermal properties of bone cement and bone, (iii) the fact that it has been determined that to pull-out cemented stems requires 60% to 70% of the pulling force to remove cementless stems, thus experimentation on cemented stems can provide a relatively good indication of the behaviour with cementless stems, (iv) the repeatability of the experimental procedure associated with the use of cemented stems. Three sets of in-vitro case studies were carried out with custom-made titanium stems cemented into a trapezoidal steel mould, a composite cylinder and a composite femur using polymethyl-methacrylate with a minimum cement mantle thickness of 3mm. First, a trapezoidal steel mould was employed for four case studies with the femoral neck stem cooled to temperatures of -76ºC, -58ºC, -49ºC, and -40ºC. Composite bones were used for the second set of case studies, in which stems were cemented into a) composite cylinders and b) composite femurs. Three case studies were performed for the cylindrical specimens: -76ºC, -49ºC, and -40ºC. Two case studies were considered for the composite femoral specimens: -76ºC, and -40ºC. In each of the tests, after reaching the temperature of interest, the specimen was immediately clamped in a materials testing machine, and the stem pulled out at a constant rate of 0.5 mm/min. Control tests were undertaken at room temperature for comparison purposes. Results from the first set of case studies showed that the force required to remove the titanium stem was reduced to 56.5% of the control force at a temperature of -76ºC, while for temperatures of -58ºC, -49ºC, and -40ºC the release force was reduced by 39%, 28%, and 31% respectively. Subsequent case studies with the cylindrical and femur composites also showed a reduction in the release force compared to their respective control force. The composite cylinder specimens exhibited reductions of 50%, 57% and 53% of the release force for temperatures of -76ºC, -49ºC, and -40ºC while, in the composite femur specimen the release force was reduced by 65% for a temperature of -40ºC. The results confirmed that the force required to remove a well-cemented femoral stem was reduced after cooling to temperatures below -40ºC allowing easier extraction of the stem. A finite element model was developed to analyse the thermal conditions in the femoral stem and surrounding material. The model can be used to ensure the required thermal balance can be obtained whilst avoiding conditions which may lead to tissue damage. The model was validated using the results of the experiments in which the temperature at strategic points on the stem was monitored during cooling. Furthermore, a concept design of a medical device based on the new methodology was developed.

Declaration

No portion of the work referred to in the Thesis has been submitted in support of an application for another degree or qualification of this or any other university or other institute of learning.

Copyright

Acknowledgements

I want to gratefully acknowledge the PhD scholarship financial support provided by the National Council on Science and Technology of Mexico (CONACYT).

I would like to express my deepest gratitude to my supervisor Prof Teresa Alonso-Rasgado for her support, patience, and guidance throughout my entire PhD programme. To Prof Timothy Board for trusting in me and supporting this project. Without their help this work could not be done.

I want to thank Dr Alan Walmsley for sharing his knowledge and academic experience, for his patience and time invested in constructively criticize this work. His guidance and recommendations helped to improve this work.

To the Bioengineering Research Group and colleagues: Dr David, Dr Jaya, Dr Emmanuel, Mr Isidro et al. for their support and help.

To my family and friends for the moral support and love I have always received from them, which is invaluable.

Finally, to my loving Romina for her support, patience, and encouragement throughout these years.

Chapter 1
Introduction

1.1 Overview

The hip is a joint of the human body that connects the torso and the lower limb. The hip is a ball-socket type joint, and it consists of the acetabulum, which is part of the pelvis, and the head of the femur. The joint is covered by ligaments and muscles that help support the weight of the body and give a full range of leg motion. Nonetheless, disease, or trauma, can affect the hip joint functionality.

As one of the most successful types of orthopaedic surgery, artificial reconstruction of the hip joint, known as Total Hip Arthroplasty (THA), has been of great benefit to patients by providing pain relief, restoring movement of the lower limb, and improving the quality of the patient's life [1, 2]. This surgery has also advanced orthopaedics through the implementation of different surgical approaches [3-5] and prostheses designs [6, 7].

The artificial hip joint is composed of two parts: the acetabular socket that partially replaces the acetabulum, and the femoral component (stem) that replaces the dissected part of the femur (head and neck), as shown in Figure 1.1. The material in which the components are manufactured varies; the acetabular cup can be made of metal or polymer, whereas the femoral stem is usually made of metal with the head made of metal or ceramic [8-11]. Both components are designed in such a way that they can adhere to the bone with the help of a rough or porous surface, and polymethyl methacrylate (PMMA) bone cement for smooth surfaces. Therefore, the artificial hip joint can be cementless or cemented [2, 12].

Despite the positive advances in surgical techniques and implant design to increase the effectiveness of the THA, these prosthetic mechanical joints tend to fail over time because of dislocation, the presence of loosened components caused by wear between components, infections, femoral stem fracture and/or femur fracture [13-17]. In order to restore the artificial hip joint after a failure, the surgeon has to perform a

Revision THA using a similar surgical approach to a primary THA. The complexity of the revision surgery depends on the design of the components and how the primary prosthesis was fixed in the medullary canal of the femoral bone, cemented or uncemented [18-20].

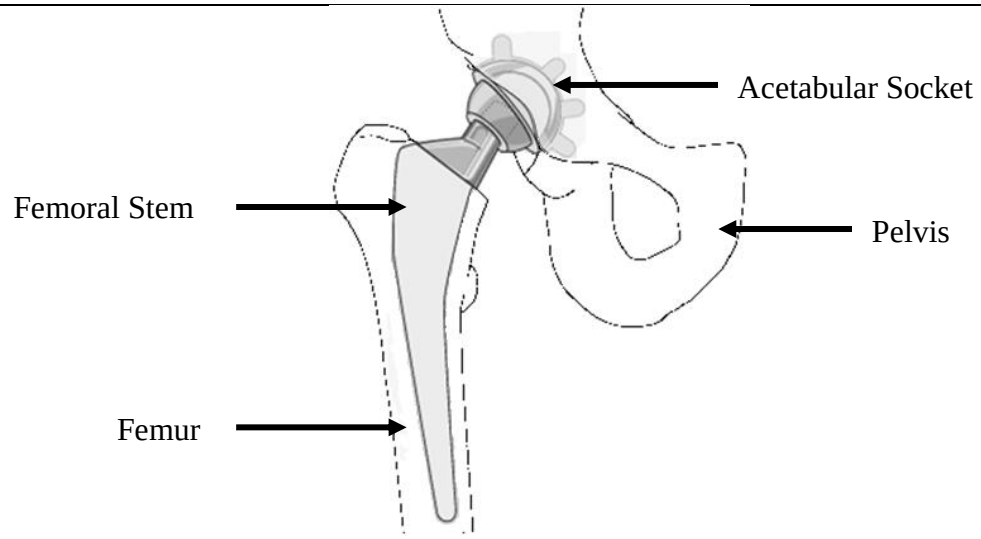

Figure 1.1 Artificial Hip Joint.

Particular attention must be given to the removal of the femoral stem, which presents significant challenges for the surgeon during Revision THA, since the procedures to remove femoral stems are difficult and could damage the general structure of bone and tissue while in surgery [21-25].

1.2 Research Background

The increased incidence of hip arthroplasty has resulted in a continuing revision burden. In the UK, a total of 86,488 surgical hip procedures were performed in 2012, from which the rate of revision surgery was 12%. The revision rate was relatively constant in 2011 and 2012, but in 2013 there was a decrease of 3% in the 'revision' burden, and year 2014 reported a reduction of 16.2% compared to year 2013 [26-28].

Revision total hip arthroplasty is well known for its complications and risks, such as intra-operative and postoperative damage to soft tissue surrounding the hip joint and fracture of the femur while in surgery, particularly because over 60% of the 10,040 revision surgeries carried out in the UK as reported in the year 2013, involve the removal of the femoral stem [26]. As a result of advances in the design of alternative surface finishes such as porous surfaces and hydroxyapatite coatings, the bonding strength of the femoral stem with the bone or cement has been increased [29-31], making it increasingly difficult to remove the prosthesis from the femur.

Studies indicate that the maximum shear stress required to remove a cemented femoral stem with polished surfaces ranges from 0.2 MPa to 0.38 MPa, and 5.16 MPa to 12 MPa for grit-blasted and pre-coated surfaces [32-34]. In practice, these values can rise to 20 MPa and may also depend on factors such as the bone-cement used and the cementing technique, in addition to surface finish and geometry of the stems [29, 32].

For cementless stems, in vivo experiments have also reported that the force required to remove a coated titanium implant, cylindrical (20 mm long and 5 mm diameter) or plate (5x10x2 mm), with bone ingrowth varies from 1.7 kN to 10.7 kN (with corresponding shear strength of 5 MPa – 30 MPa) depending on the harvest time, which ranged from 2 weeks to 52 weeks [35-40].

In vitro experimental studies of cemented implants were undertaken, and the maximum force measured with the aid of materials testing machines was obtained. Tests were performed by using geometries such as blocks (6.4x12.8x25.6 mm) and cylinders (6.4 mm diameter and various lengths 12.8 mm, 50 mm, and 60 mm), with various surface roughness (1 μm < Ra < 3 μm), show that the force required to remove the implants varies from 1.23 kN to 6.5 kN (1.16 MPa – 18 MPa shear stress), depending on the surface finish of the implants [32-34, 41, 42].

To remove the femoral prosthesis, the surgeon can use various methods such as the retrograde removal technique, extended trochanteric and cortical window osteotomies amongst others. Despite the efforts and experience of the surgeon, complications are frequently reported, potentially leading to bone damage and fracture and, therefore, increasing the risk for the patient [18, 20, 43].

Because of the complications mentioned above, and the fact that the removal of both cemented and uncemented stems is extremely challenging, a less destructive method to remove a femoral implant, whether cementless or cemented, is needed. In order to facilitate ease of removal of the femoral stem, the development of a new technique should be focused on the disruption of the implant-bone or implant-cement bonding interface, and should lead, as a consequence, to a less complicated reconstruction of the bone and soft tissues, reducing the trauma to the bone and minimizing the damage to the surrounding soft tissues.

In order to effectively remove the femoral stem by disrupting the implant-bone, or implant-cement, bonding interface and at the same time safeguard the structural integrity of bone tissue, the effect of low temperature on the thermo-mechanical properties of the femoral implant can be used as a feasible strategy to remove the femoral stem. However, care should be taken when low temperatures are used since the risk of damaging healthy living tissue is always present [44-46].

Very few researchers have conducted experimentation concerning the removal metallic rods from bone tissue after being exposed to low temperature. From the studies reviewed, Steinmann rods and small titanium pins (10 mm by Ø0.8 mm) have been implanted in canine femurs and rat tibiae respectively. The specimens have been used to perform biomechanical pull-out tests after storing and keeping the implanted specimens at low temperature, -20°C and -70°C, for a period of 2 to 4 weeks [47, 48]. After harvesting and testing mechanically the specimens, the results showed no significant difference in maximum pull-out force required and interfacial shear strength between specimens pulled at room temperature and those that were pulled after being frozen. However, after analysing the work done by Diefenbeck [47] and Huss [48], this thesis recommends that the mechanical pull-out should be performed immediately after the cooling temperature of interest is achieved and not after several days to avoid thermal equilibrium from the materials involved (prosthesis-bone or prosthesis-bone cement). The objective is to induce a thermal shock to the interface between the materials, and the cooling process should be tried at temperatures much lower than -20°C in order to investigate if lower temperatures do affect the value of the force required to remove the prosthesis from the bone.

1.3 Objectives and Methodology of the Research

The aim of this research is to investigate the effect of low temperature in the femoral stem in order to reduce the force needed to remove a primary femoral prosthesis during revision total hip arthroplasty. A new methodology is proposed which involves the application of low temperature over the neck of the femoral stem before proceeding to remove it from the femur. Low temperature is expected have an effect on the thermo-physical properties of the titanium stem by shrinking the material and weaken the interface between the prosthesis and the bone (or bone-cement), thus the femoral prosthesis can be removed from the femur during a RTHA by requiring a lower force.

The two specific objectives in the present study to prove the new methodology where low temperature can reduce the force required to remove an implanted femoral stem were:

I. Experimental feasibility study and verification of the new methodology.

II. Develop a concept design of a medical device working under the new methodology.

To accomplish the aim of the research, in-vitro experimental work was undertaken by means of implanting a titanium stem using bone cement after analysing the similarities in mechanical and thermal properties with bone, see Table 1.1. Moreover, previous Section 1.2 provided information with regard to the force required to remove a well-cemented stem whose values range from 1.23 to 6.5 kN, which represent 60% to 70% of the value of the pulling force required to remove a cementless stem. The experimental work was undertaken to verify the feasibility of the technique by simulating the removal of the femoral prosthesis at a revision total hip arthroplasty. The cooling methodology was applied to custom titanium stems (manufactured according to the requirements such as contact area, general dimensions, and reusability), which were cemented into both a custom made mould and two different geometries of synthetic bone (composite cylinders and composite femurs), thus making two scenario studies. Verification was achieved by measuring the maximum force required to remove a simplified femoral stem by performing a mechanical pull-out test after applying different cooling temperatures as case studies for each scenario study.

In addition, standardization of cement preparation, injection, curing and setting time, as well as mantle thickness can be controlled. This should allow consistent characteristics of the interface between the femoral stem and the bone-cement to assure experimental repeatability, in contrast with the possible lack of control in the process of implanting the femoral stem in living bone, which could lead to unsuccessful bone ingrowth in the implanted stem resulting in areas with uneven bonding strength (interface strength).

Table 1.1 Mechanical and thermal properties of femoral cortical and acrylic bone cement at 22°C [49-53].

Mechanical Properties	**Cortical Bone**	**Cancellous Bone**	**Acrylic Bone Cement**
Elasticity Module (GPa)	17	0.2	2.4
Poisson's ratio	0.29	0.30	0.33
Thermal Properties	**Cortical Bone**	**Cancellous Bone**	**Acrylic Bone Cement**
Expansion coefficient $\left(\frac{1}{^\circ C}\right)$	27.5e-6	0.1 e-6	72.2e-6
Density $\left(\frac{kg}{m^3}\right)$	1800	1300	1190
Specific heat capacity $\left(\frac{J}{kg^\circ C}\right)$	1500	2290	1450
Conductive heat transfer coefficient $\left(\frac{W}{m^\circ C}\right)$	0.25	0.29	0.18

1.4 Structure of the Thesis

A literature review regarding the hip anatomy and the pathologies leading to a primary hip arthroplasty is presented in Chapter 2. Total hip arthroplasty is introduced, as well as the various surgical approaches and methods used in surgery. The chapter presents the bearing systems and methods of fixation of the components in an artificial hip, as well as the characteristics of the materials they are made of. Moreover, indications for revision total hip arthroplasty are introduced as well as the characteristics

of the surgery and its complications. Cryosurgery is introduced, and the mechanisms of thermal injury are discussed.

Chapter 3 describes the new methodology and introduces the basic concepts on which it is founded. It also provides details of the mechanical and thermal properties of the materials involved in the hip prosthesis and the materials used in the experimental study. The Chapter presents experiments of the first scenario study, a titanium femoral stem was implanted in a steel mould specially designed to allow a minimum bone-cement mantle thickness of 3mm. The specimen was cooled to four cooling temperatures of interest: -76°C, -58°C, -49°C, -40°C. After achieving the temperature of interest, the mechanical pull-out test was performed. The maximum release forces were measured to confirm the feasibility of the new methodology.

Chapter 4 follows the experimental work by describing the second scenario study, performed by using material composites from Sawbones®, and consisted in two case studies. Firstly, the titanium stems were cemented in cylindrical composites. The temperatures studied were: -76°C, -49°C, and -40°C. Secondly, the femoral stems were cemented in a composite femur and tested at two temperatures of interest: -76°C and -40°C. The results from the tests performed with composite materials were compared to those obtained in previous experimental work done in Chapter 3.

Chapter 5 presents the design process of a concept medical device based in the reported results of this thesis. A concept design that functions under the principles of the proposed methodology was developed to initiate the design and manufacture of the final medical device. User needs, requirements, and specifications of the concept design as well as the directives that must be followed to gain approval for the medical device to be launched on the market were taken into account of the design process.

Chapter 6 provides details of the development of the numerical model in Abaqus CAE® to perform the Finite Element Thermal Analysis. Five (3D) numerical models from the geometry representing the titanium stem cemented in a steel mould were developed as part of computational work. The following case studies were simulated: 1) simulation of the cooling procedure over the specimen for 20 minutes, 2) simulation of the cooling procedure to four different cooling temperatures of interest: -76°C, -58°C, -49°C, -40°C. The numerical model provided relevant information for future work

regarding the distribution of temperatures in the femoral stem, and the appropriate thermal conditions of safety for the surrounding materials after being exposed to low temperatures.

Finally, Chapter 7 summarises the conclusions of the experimental work, the concept design, and the computational model. The chapter closes by acknowledging recommendations and future challenges.

1.5 Original Contribution of the Author

1.5.1 Papers to be Published

- Botello A.I., Alonso T., Walmsley A., Board T., "New Methodology for Orthopaedic Surgery - Impact of Thermal Stress", Journal of Orthopaedic Research. Submission pending.

Explains and demonstrates the effects of the new methodology on the release force of a titanium stem cemented in a mould of steel.

- Botello A.I., Alonso T., Walmsley A., Board T., "New Methodology for Orthopaedic Surgery - Impact of Thermal Stress Over Synthetic Bone I", Journal of Orthopaedic Research. Submission pending.

Explains and demonstrates the effects of the new methodology on the release force of a titanium stem cemented in a composite cylinder, which mimics the mechanical and thermal properties of bone tissue.

1.5.2 Intellectual Property

A concept design of an orthopaedic medical device utilizing low temperatures in a surgical treatment for revision hip arthroplasty is presented, and is being processed by University of Manchester Intellectual Property.

Chapter 2
The Hip and Total Hip Arthroplasty

2.1 Introduction

In the 1960's at Wrightington Hospital in the United Kingdom, Sir John Charnley introduced the concept of low friction arthroplasty, pioneering the modern era of arthroplasty. Total hip arthroplasty is probably one of the most successful advances in orthopaedic surgery and has continued improving in the present century[54]. The National Joint Registry shows a total of 620,400 primary hip replacements between the years 2003 and 2013. In 2013 a total of 80,194 primary hip replacements were performed, an increase of 3745 compared to 2012 [27].

This chapter gives an overview of the hip joint anatomy and its function in the daily activities of the human being, and introduces Total Hip Arthroplasty and outlines two different methods to insert the prosthetics and restore the hip joint. In one of these methods, acrylic cement is used, while the other method promotes osseointegration for improved adherence to the bony tissue.

In addition, the different methods and complications of performing this surgery are explained in this chapter with the purpose of visualising the main issues that need to be addressed concerning the stem-cement interface, to further develop a new removal methodology.

2.2 Hip Anatomy

The hip is one of the largest weight-bearing joints, and it is where the torso and the lower limb are connected by a ball-socket joint, as seen in Figure 2.1. The hip joint is surrounded by a capsule and is stabilized by tendons, ligaments and muscles. The structure of the hip joint comprises of a hip socket (the acetabulum), which is part of the pelvis, and the quasi-spherical head of the femur. In a healthy hip, a layer of articular

cartilage covers the femoral head and the acetabulum. This cartilage cushions and protects the bones from direct friction[55, 56].

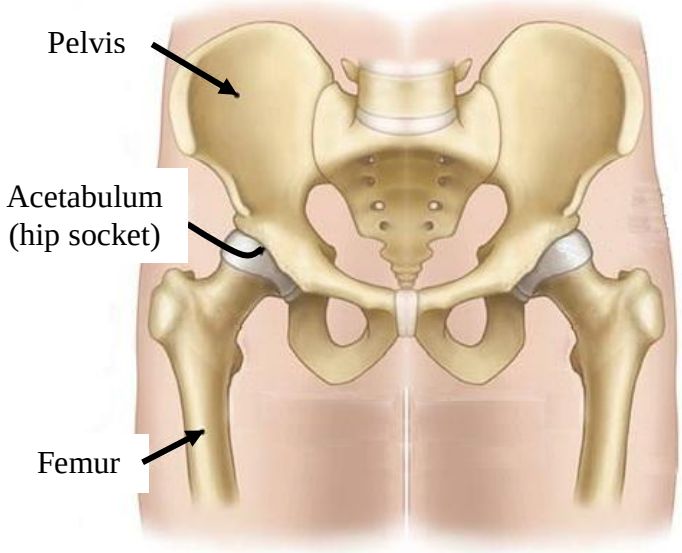

Figure 2.1 The hip anatomy, anterior view. Modified.[57]

Synovial fluid fills the gap between the acetabulum and the femoral head and allows a full range of unrestricted motion. Figure 2.2 shows a more detailed structure of the hip joint and its components [55, 56].

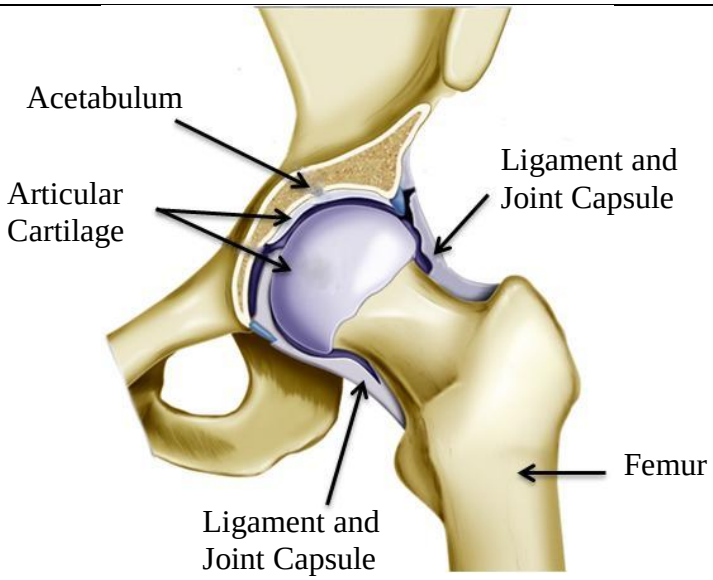

Figure 2.2 Structure of a natural hip joint. Modified [58].

Nevertheless, trauma or pathological diseases can affect the hip joint's bearing system, which allows motion and load transfer from the torso to the lower limb. A gradual degeneration of the articular cartilage and synovial fluid occur because of wear and tear over time. This degeneration causes an exposure of the bone accompanied by pain as the femoral head and the acetabulum begin to have direct contact [1, 59].

2.3 Total Hip Arthroplasty

The basic prosthesis structure and surgical technique proposed by Sir John Charnley for THA remains almost unchanged. He proposed the replacement of the damaged articulating hip joint with artificial components composed of two parts: the femoral component or stem with a head that replaces the dissected part of the femoral head, and a socket acting as the acetabular cup. The materials and the designs of the femoral stems and acetabular cups have evolved in time towards more resistant and safe components. Major initial problems caused concerns because of the infection rate, aseptic loosening, osteolysis, and bone resorption because of debris particles created by the wear of the components [54, 60].

THA is one of the most effective procedures in orthopaedics and trauma surgery, with the intention of restoring the quality of life of young and elderly patients. These patients commonly suffer from a hip disorder such as rheumatoid arthritis, traumatic arthritis, osteoarthritis and avascular necrosis, as well as deformities and fractures located in either or both the acetabulum or the proximal zone of the femur. Most patients who suffer from hip disorder exhibit a limited range of motion in their everyday activities, such as walking, rising from a sitting position, taking off and putting on garments of the lower limb. Clinical indications include severe pain in the zones of the groin, thighs, and buttocks. The functional capacity of the lower limb is significantly restored by THA surgery, and it brings fast relief to the continuous hip pain that the patient suffers [54, 61-63].

The National Joint Registry for England, Wales and Northern Ireland (NJR) has reported hip replacement procedures (708,311 cases since 2003 [28]). A total of 86,488 hip procedures were recorded in the NJR in 2012 which represented a 7.5% increase

from the year 2011. Of this number, 764,48 were primary hip arthroplasty surgeries [26]; compared to the year 2012, primary hip replacement procedures increased 4.9% in 2013 and 5.1% in 2014 [27, 28].

Indications for primary hip THA are diverse: osteoarthritis, avascular necrosis, fractured neck of the femur, dysplasia of the hip and congenital dislocations are some examples. Diagnosis for THA varies with the age of the patient, and the most affected groups are 50-59 years and older. From the indications mentioned, osteoarthritis is the most prevalent indication for surgery, followed by avascular necrosis and congenital dislocation. In 2012, 70,188 cases of osteoarthritis were reported, representing 92% of primary hip replacement procedures. In 2013, the occurrence of osteoarthritis increased by 4% compared to 2012 [1, 26, 27], osteoarthritis remains as the predominant diagnosis since 2003 in 93% of the cases [28].

2.3.1 Surgical Approaches and General Technique

Surgical approaches for THA must grant sufficient access through the muscular tissues that surround the hip joint to prepare appropriately the acetabulum and the proximal femur for implantation.

By choosing an appropriate surgical approach, the surgeon aims to keep any trauma that could be caused in surrounding muscles, tendons and ligaments to a minimum. Figure 2.3 shows the right side of the hip in the transverse plane, and the various surgical approaches to the hip [64, 65].

A general description of the most common surgical approaches for total hip replacement follows:

2.3.1.1 Anterior Approach (Smith-Petersen)

The classical anterior approach uses the internervous plane between the sartorius muscle and the tensor fascia lata superficially and between the rectus femoris and gluteus

medius. The advantages of this approach are: the hip is closer to the skin anteriorly than posteriorly; the approach follows laterally the anatomic interval between the zones of innervations of the superior and inferior gluteal nerves laterally and the femoral nerve medially; and it exposes the hip without detachment of the muscles and tissues from either the femur and pelvis [64].

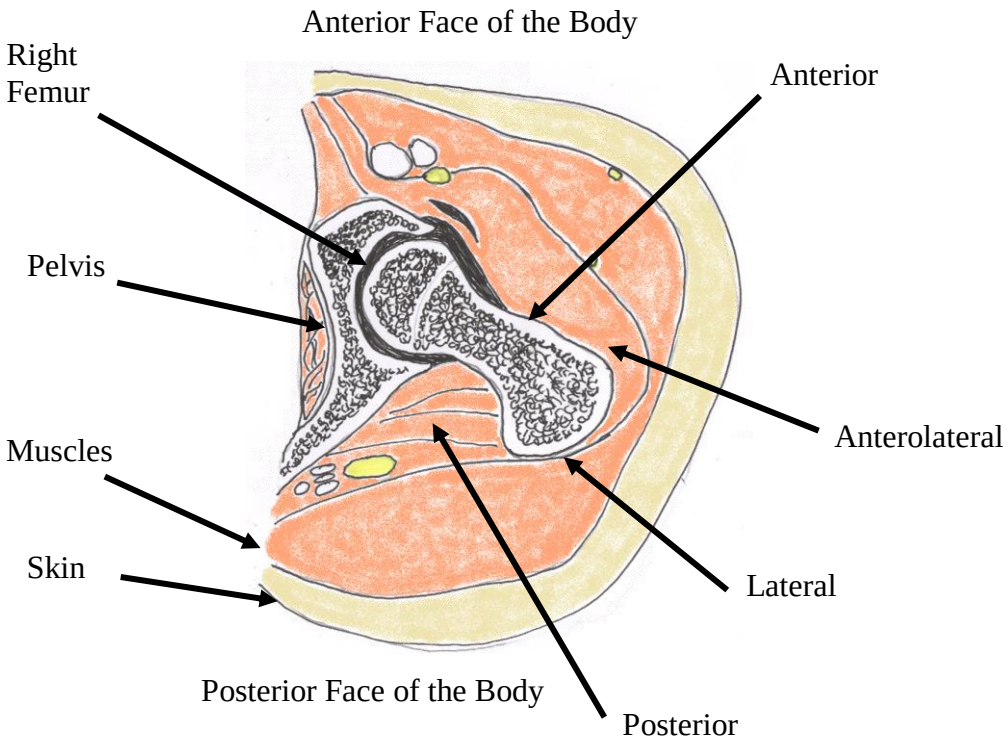

Figure 2.3 Different surgical approaches to the hip (transverse plane view of the right hip): 1) Anterior, 2) Anterolateral, 3) Lateral, 4) Posterior.

2.3.1.2 Anterolateral Approach (Watson-Jones)

The anterolateral approach exploits the intermuscular plane between the tensor fascia lata and the gluteus medius. In this approach, the abductor mechanism is detached, and the surgery can be performed in the lateral or supine position. The supine position helps the surgeon to evaluate more accurately the leg length discrepancy [64, 65].

2.3.1.3 Direct Lateral or Transgluteal Approach (Hardinge)

In this approach, the periosteum covering the greater trochanter is bisected safeguarding the tendinous insertion of the vastus lateralis distally and gluteus medius and minimus proximally. The transgluteal approach enhances access to the femur for reaming and the hip joint in general; trochanteric osteotomy is also avoided with this approach [4, 65].

2.3.1.4 Lateral Transtrochanteric Approach

Sir John Charnley popularized the lateral transtrochanteric approach for THA to allow good visibility of the abductor muscles, posterior and anterior hip, and a full view of the acetabulum[62]. The necessity for trochanteric osteotomy has been widely discussed, but it remains popular for revision surgery and reconstruction of hips with dysplasia [4].

2.3.1.5 Posterior and Posterolateral Approach

The posterior and posterolateral approach is also called the Moore Southern approach and is commonly used and preferred by surgeons for THA to expose the hip. It is considered technically simple by giving easy and quick access to the hip joint with wide visibility of the femur and acetabulum. This approach requires less dissection and the abductor mechanism is not interfered with. One drawback of this approach is that 9 out of 100 patients might experience joint dislocation postoperatively [64-66].

2.3.1.6 Minimally Invasive Approaches

Minimally invasive surgery (MIS) involves modifications to classical approaches and is a relatively modern practice. Some surgeons tend to support claims of better outcomes and faster healing of patients than after conventional surgery, nevertheless, unbiased controlled studies are needed to support such statements. MIS in essence, is a technique that aims to preserve soft tissues and musculature of the hip by making smaller incisions (smaller than 15cm) than those made in conventional approaches [2, 67].

From the NRJ data for 2011, the patient position used in 93% of the cases was lateral and there was an increase in the use of the posterior approach to 61% compared to 59% in 2011 [26]. 2013 was similar; the patients were positioned laterally and the approach to make the incision was posterior in 65% of procedures [27].

2.3.1.7 General Surgical Technique [2, 66, 67]

Once the patient has been positioned and anaesthetized on the operating table, the skin of the surgical site is cleaned and draped. The surgeon makes an incision over the hip joint according to the previously selected approach. The surgeon gains access to the bones of the hip joint by carefully separating the ligaments and muscles that cover the joint [2, 66, 67].

After reaching the hip joint, the femoral head is dislocated from the acetabulum. Once the acetabular socket is exposed, cartilage and bone debris are cleared using a drill with a hemispherical reamer. The hemispherical reamer has appropriate dimensions according to the acetabular shell to be fitted for the patient's new hip.

The femoral head can then be cut with a reciprocating saw, starting at approximately 1.5-2 cm above the lesser trochanter up to the level of the piriformis fossa, approximately at 35^{o} to the femoral shaft axis. Depending on the surgeon's preference, the osteotomy can be performed in one or two planes [2, 66, 67].

The surgeon prepares the femoral canal by first compacting the proximal cancellous bone at the osteotomy. Once this is done, a chisel is used to enter the femoral canal laterally; broaches of different sizes are used to increase the dimension of the femoral canal. The smallest broach is recommended in the first instance, then changing to a bigger broach until axial and rotational stability is achieved. The final broach is selected according to the femoral stem to be fitted in the patient from the pre-operative planning. By leaving the last broach in the femoral canal, the calcar is milled to achieve a flat resection surface.

A trial femoral head and neck are tested with the last broach still in situ. At this point, any adjustment needs to be assessed. For the case of a cementless hip arthroplasty, the trial femoral head, neck trial and broach are removed from the canal, and the permanent cementless femoral stem is inserted with the aid of an impactor for the final few centimetres [2, 66, 67].

The neck and taper of the stem are carefully cleaned to remove any particle of debris, and the femoral head is placed onto the taper by gently taping it with the head impactor [2, 66, 67]. Before reducing the hip, the surgeon must check that the bearing surfaces are clean [2, 66, 67].

2.3.2 The Hip Implant Systems

The components of an artificial hip joint vary in size, design and the material they are made of. The use of metal alloys, ceramics and polymers provide the surgeon with a wide variety of choices to construct the best hip system for the patient. Figure 2.4 shows the components of a total hip replacement: the acetabular cup, a liner, the femoral stem, which can be modular or a single piece, and the femoral head [68-70].

The acetabular components can be made of metal, ultra-high molecular-weight polyethylene or ceramic backed by metal. The femoral components are made of metal alloys based on titanium or cobalt-chromium. The balls that substitute the femoral head may also be made of metal alloys, or ceramics (aluminium oxide or zirconium oxide); this part is smoothly polished to avoid wear of the bearing system as much as possible.

The design of femoral stems must deliver specific strength and stiffness to give mechanical stability, and surface properties that ensure biocompatibility and enhance attachment to bone. As the preferred material to design stems, titanium alloys have excellent mechanical, physical and biological performance in medical applications; they have the advantage of being non-carcinogenic (no adverse effects on tissue) and allow the bone to bond directly and easily [12, 71, 72]. On the other hand, titanium and titanium alloys are not used as bearing systems, either in medicine or engineering, since it would be impractical to apply very special surface treatments to allow good sliding contact between components and at the same time avoiding severe wear with continuous use [71, 73, 74].

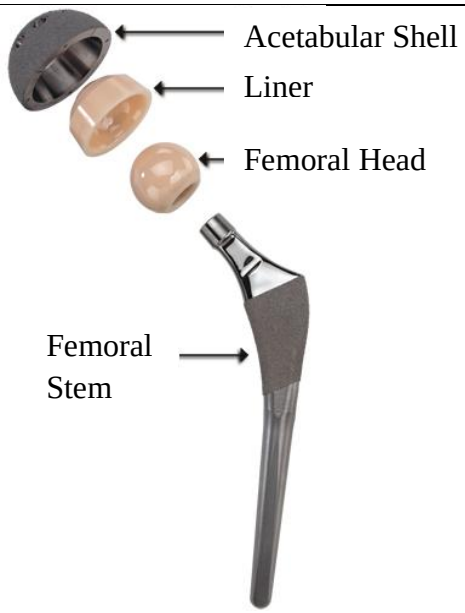

Figure 2.4 Artificial hip components [75].

2.3.3 Materials in Hip Arthroplasty

The materials used for total hip arthroplasty or any biomedical application must have specific characteristics, which can be grouped into five general categories [76, 77]:

a) **Biocompatibility:** to avoid any rejection response from the body as an undesirable organism. Reactions such as hypersensitivity, metal ion release,

carcinogenesis are some of the issues that cause failure of the prosthesis [77, 78].

b) **Highly resistant to corrosion, degradation and wear:** to maintain the mechanical and chemical properties of the materials. Change in any of the material properties may result in damage of the components of the prosthesis and/or the bone and soft tissue. Since these materials replace the natural parts of the body, they should replicate their functions such as flexibility, mobility and withstanding weight-bearing loads [77, 78].

c) Sterilizability: sterilization is very important for medical materials and devices. Therefore, materials used must be able to undergo the sterilization processes [77, 78].

d) Balance of mechanical properties: such as low rigidity, shape memory or superelastic properties, fracture toughness, and elastic modulus as close as possible to that of cortical bone. The properties must ensure a good and lasting performance of the implant [77, 78].

e) Functionality: which depends on the characteristics of the material of being able to be shaped according to the function it will perform [77, 78].

2.3.4 Bearing Systems of the Artificial Hip

The artificial hip joint has contact/bearing characteristics between the components once the surgeon has decided which bearing system is best for the patient [79]. The list below describes the different possible material interactions that a surgeon may select:

a) **Metal-on-Metal:** both components, ball and socket are made of stainless steel or cobalt-chrome alloy, see Figure 2.5.

b) **Ceramic-on-Ceramic:** the acetabular socket has a ceramic liner and the ball/head of the stem is made of ceramic, see Figure 2.6.

c) **Metal-on-Polyethylene:** the acetabular cup is made of metal, the acetabular liner is polyethylene, and the head of the stem is made of metal, see Figure 2.7.

d) **Ceramic-on-Polyethylene:** the acetabular cup is made of metal, the acetabular liner is polyethylene and the head of the stem is made of ceramic, see Figure 2.8.

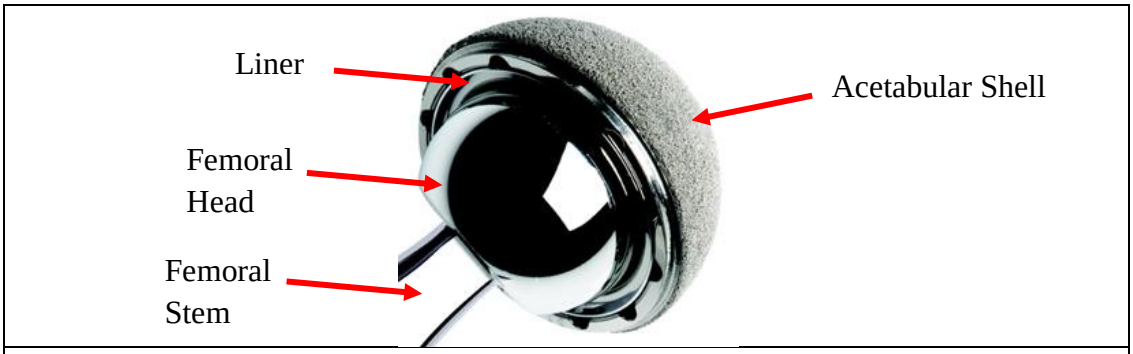

Figure 2.5 Metal-on-metal bearing system [8].

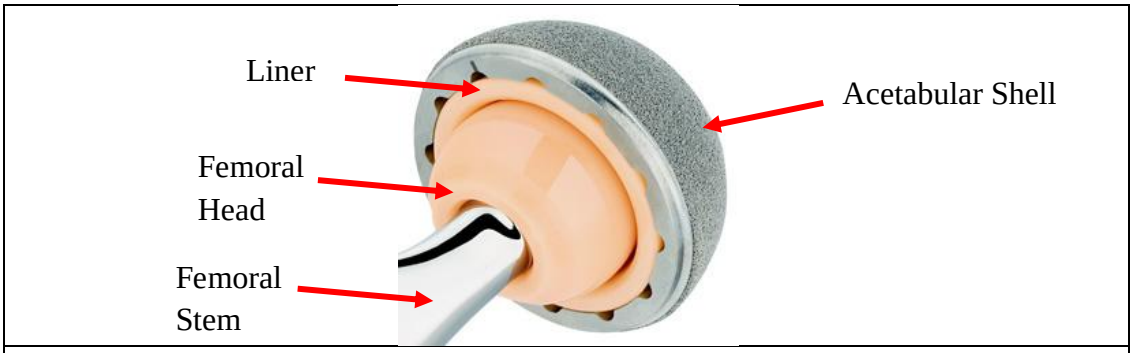

Figure 2.6 Ceramic-on-ceramic bearing system [8].

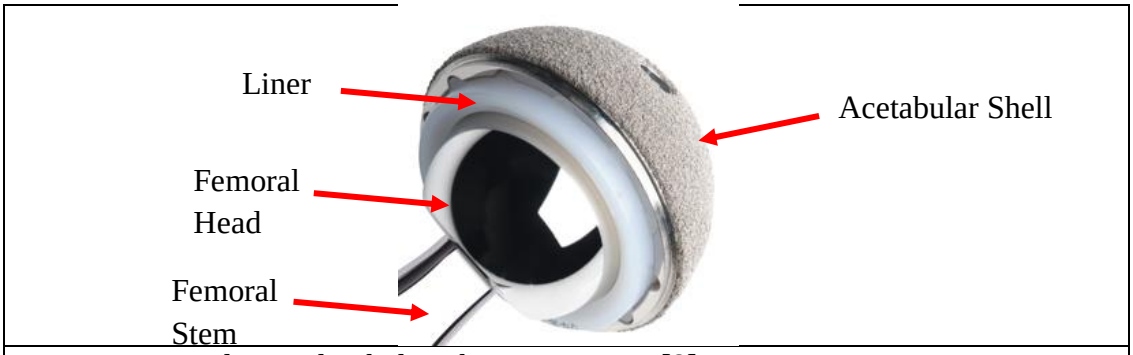

Figure 2.7 Metal-on-polyethylene bearing system [8]

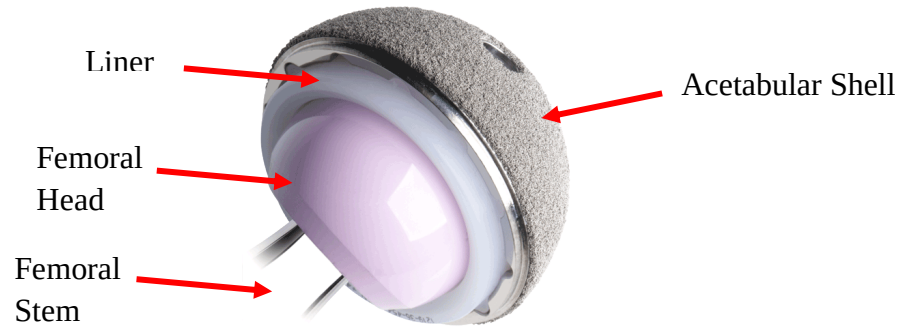

Figure 2.8 Ceramic-on-polyethylene bearing system [8].

Though there has been an effort to reduce the wear rate, the controversy over which bearing system is best for a successful artificial hip joint is a question that remains open and has led to an increasing number of investigations on the topic [80]. All combinations of materials have resulted in reactions leading to implant failure. These reactions are mainly caused by contact friction between the acetabular cup and the stem head. Impingement of hard-on-hard bearing systems has been studied concerning its relation to dislocation and damage of the prosthesis [80]. Squeaking may occur in hard-on-hard bearings, metal-on-metal bearings can cause wear debris which leads to infection, inflammatory pseudotumors and necrosis in the local soft-tissue; severe destructive osteolysis is produced as a reaction to debris and corrosion, opposite to ceramic wear particles as they are relatively inert [10, 81-85].

The trends of hip bearing systems have changed since 2003. According to the NJR, between 2003 and 2014 there were significant variations in the choice of bearing systems and the method of fixation of the prosthetic components [26-28]. Figure 2.9 shows these trend differences with the specific type of fixation.

It can be seen from Figure 2.9 that the selection of metal-on-metal bearing systems rose significantly rise between 2003 and 2009, whereas after 2009 the metal-on-metal option was virtually eliminated, due to the high index of complications such as metal debris, and carcinogenesis [10]. Of the 83,125 primary hip procedures reported in 2014, 47,752 bearing systems were metal-on-polyethylene, 17,791 ceramic-on-polyethylene, 13,744 ceramic-on-ceramic, and only 79 cases were metal-on-metal bearing systems [28]. On the other hand, the use ceramic-on-poly and metal-on-poly

have increased over the years being ceramic-on-poly the preferred bearing system to date.

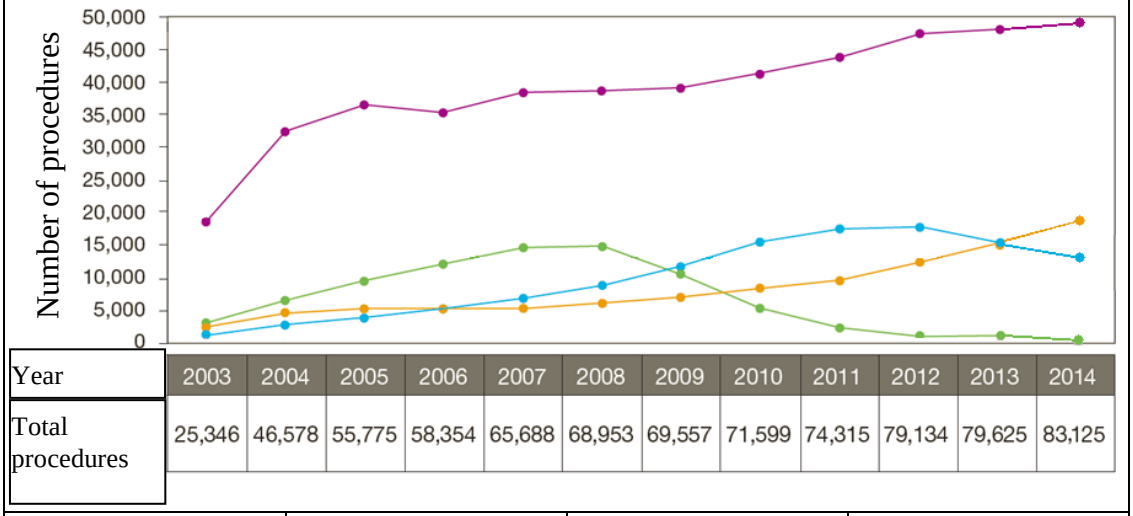

Figure 2.9 Hip bearing systems, trends from 2003 to 2013. Modified [27].

2.3.5 Methods of Fixation of the Femoral Implant

There are two main methods for fixing the femoral stem into the femoral medullary cavity, namely using acrylic bone cement for fixation or in the case of an uncemented femoral stem, the latter is designed with a porous coating to stimulate bone ingrowth as fixation [86, 87].

In order to fix the stem into the medullary cavity, the surfaces of the components vary in design. The surface of the femoral stem goes through different manufacturing processes to attain the desired surface finish. The surface finish can be smoothly polished, have a degree of roughness or coated with hydroxyapatite (HA) or metal particles in order to have a porous surface.

For a brief description of the characteristics of these methods see Table 2.1, and for an extended overview of this topic refer to the next subsection.

Table 2.1 Characteristics of surface finishes [29-31, 38, 88-98].

Finish	Characteristics
Smooth polish	Roughness ratio less than 0.75 µm, e.g. matt finish.
Roughness	Roughness values ranging from 0.5 µm to 9 µm.
Hydroxyapatite coating	Surface roughness varies from 1.3 µm to 9 µm. HA thickness from 20 µm to 50 µm.
Metal porous coating	Produced by impacting micro spheres of calcium aluminate ceramic, titanium, titanium alloys, Co-Cr-Mo, or steel. Pore sizes vary from 75 µm to 650 µm, 450 µm being the optimal pore size, though 1 mm pores are also effective for bone ingrowth. Porous surface thickness varies from 100 µm to 400 µm

Depending on the surface finish, bonding strengths vary. For bone ingrowth in porous tantalum the mean bonding strength is of 18.5 MPa, and for beaded cobalt–chrome implants 9.3 MPa [90, 92]. Bonding strength obtained from hydroxyapatite coatings ranges from 30 MPa for Co-Cr–Mo implants [38, 96] to 65 MPa for coated Ti alloy implants [31, 96]. Regarding porosity, it has been found that the optimum pore size should be between 100 µm and 400 µm [29, 93, 95].

2.3.6 Trends of Fixation for Primary THA

The choice of a cemented or uncemented THA is based on the experience of the surgeon and varies between health centres and countries [99, 100], e.g. 91% in the UK to 10% in Austria for cemented THA [99].

Figure 2.10 shows the trends for the preferred method of fixation for primary hip arthroplasties in the UK reported from 2003 to 2013.

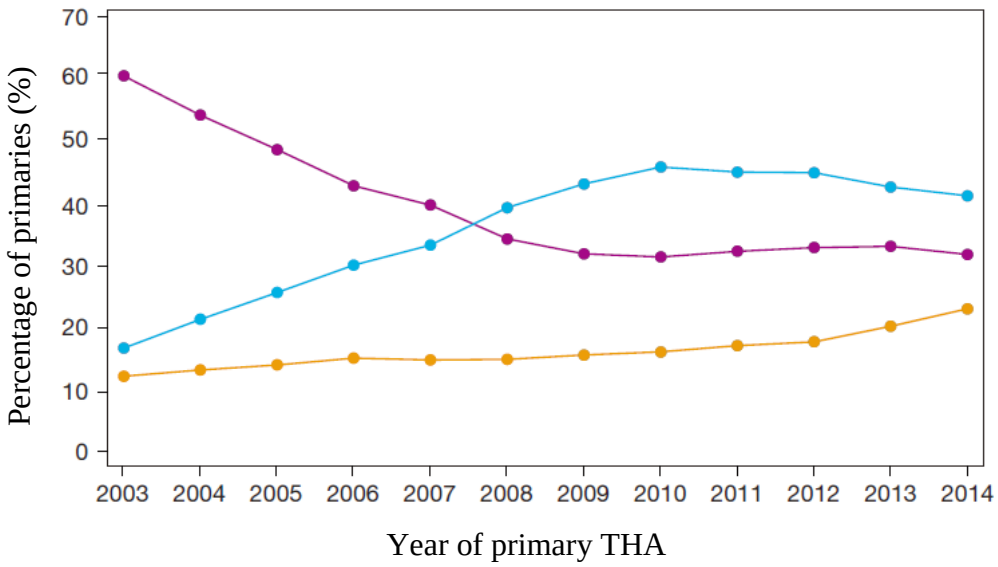

Figure 2.10 Total hip arthroplasty, trends from 2003 to 2013 of methods of fixation. Modified [27].

Regarding fixation of the hip replacement shown in Figure 2.10, in 2003 cemented procedures represented 60.5% of the total activity and their use decreased year on year to 32% in 2009 and remained at an average of 31.8% until the year 2013 [26-28]. On the other hand, uncemented procedures have shown a noticeable increase in use since 2003 from 17% of the total activity to 41.2% in 2014 [26-28]. Hybrid hip arthroplasty, where the femoral stem is implanted using bone-cement and the acetabular cup is cementless, increased from 12% to 23.1% over the same period [26-28]. These changes in fixation methods may be related to the individual success of each component, femoral stem or acetabular cup, in either cemented or uncemented fixation method. Uncemented acetabular cups and cemented stems have been associated with lower rates of loosening, giving place to a rise to the hybrid fixation method [3, 101].

2.3.7 Characteristics of a Cemented THA

The principle of the cemented THA is based on the use of acrylic bone cement to mechanically stabilise the stem into the femoral canal and to effectively transfer

physiological loading from the prosthesis to the bone. Bone cement techniques were originally designed to be used in dentistry, and in late 1940s, Edward Haboush used dental acrylic cement as first attempt of fixation of prostheses for hip arthroplasty [102]. Acrylic cements have been used for more than 40 years in THA surgery since their introduction, and Sir John Charnley continued its development in the 1960's.

The technique consists of filling the space around the implant in the medullary canal of the femur with acrylic cement; polymethyl methacrylate (PMMA) is commonly used for this purpose. The cement compounds (acrylic powder and monomer) are pre-cooled to 4°C before being mixed according to the product standards for use in medicine. The cement is then cured (polymerized) with the monomer for 15 minutes approximately in order to allow adequate adherence to the surface while holding the stem firmly in place.

Cemented THA is highly recommended for adults over 60 years or for patients with a deteriorated quality and density of bone because it is probable that these patients will be unable to go through a lengthy healing period. In this case, the rehabilitation lasts no more than two weeks [103, 104].

2.3.7.1 Bone Cements

There are many bone cements developed with the purpose of substituting the functions of the natural bone. These available bone cements have some slight variations in composition and they possess different mechanical properties [105].

Bone cements must endure multiple and considerable stresses in vivo to provide stable fixation and stability of the prosthesis in the long term. From commercial bone cements the most commonly used are:

a) **Polymethyl methacrylate cement:** is a two-part self polymerizing bone cement (polymethyl-methacrylate powder and methyl-methacrylate monomer) and is the premier and most used cement for orthopaedics since it was invented [103, 105, 106].

b) **Zinc phosphate and zinc polycarboxylate cement:** created mainly to be used in dentistry. It is a brittle cement and has a relatively high compressive strength. It restores superficial defects in teeth. It works as an adhesive in orthodontics [103, 105].

c) **Bioglass:** Composed of 46.1% of SiO_2, 24.4% NaO_2, 26.9% CaO and 2.6% P_2O_5, this bioactive and biocompatible cement is used to repair bone defects and prostheses due to its bone-bonding and osteoconductivity properties [103, 105].

d) **Apatite/wollastonite glass-ceramic:** is the main material used for fabricating orthopaedic parts such as vertebral replacements, iliac crest, filling cavities left in the bone after excision of bone tumours [105].

Among new developments are the inclusion of antibiotic powders to fight infections and reinforce bioactivity, in addition to barium sulphate or zirconium dioxide as radiopacifiers as part of the manufacturing process of the new generation of cements [106-108]. Some of the design criteria for bone cements used in orthopaedics are shown in Table 2.2.

The general preparation and mixing process of bone cements is divided into three main phases [104]:

1. **Mixing phase*:*** The cement powder is mixed with the monomer and stirred homogeneously. This phase lasts for about 1 minute. The mixture is allowed to rest for 15 seconds and in this waiting phase, the cement achieves a suitable viscosity through physical swelling and doughing but remains a sticky dough.

2. **Working phase:** The cement and the implant can be introduced into the medullary canal after the waiting phase. The cement must not be sticky and its viscosity should be suitable for application.

3. **Setting phase:** Primary chain growth is finished and the cement has hardened. Maximum temperature is reached.

Table 2.2 Design Criteria of Modern Bone Cement [103-107, 109-113].

Criterion	Purpose
Mechanical properties as similar as possible to the bone's properties	Eliminate the stress shielding phenomena
Quick setting (5-15 min)	To assist in clinical use and healing of the patient
In situ setting at body temperature	To avoid necrosis caused by thermal injuries
Bonding to bone and medical grade alloys	Elimination of fibrous capsule and loosening of the implant
Bioactive bone in-growth	To enhance chemical attachment and stress attachment
Radio opaque	Subsequent examinations of the implant

2.3.8 Characteristics of a Cementless THA

The objective of the cementless method is to achieve stable fixation of the femoral stem in the medullary canal by promoting osseointegration (bone ingrowth). This is achieved by coating the femoral stem with a material to improve the long-term success of THA. Potentially, the patient's hip can repair itself with time. Currently, there are three strategies to promote osteogenesis and bone ingrowth: the design of implants with irregular or textured surfaces, deposition of metallic or ceramic coatings (hydroxyapatite) manufactured by plasma-spray over solid metal substrates, and the manufacture of implants with porous-coated surfaces prepared by sintering metallic powders or fibres over bone interfacing surfaces of metal substrates [31, 91, 114-118].

Loosening of cemented implants led to new research studies with the purpose of solving this particular problem. The stability of implants was then accomplished by stimulating bone ingrowth into the porous surface of the stem or into the roughness of the stem surface [119, 120]. In general, all porous coatings (made of cobalt-chrome,

stainless steel, or titanium) showed evidence of bone ingrowth and firm stability of the femoral stem in the medullary canal. The bone in-growth depends on many factors such as the right pore size, thickness of the surface layer, the gap between bone and implant in order to gain stability, and the geometry of the femoral stem [30, 89, 90, 121-125]. Figure 2.11a and Figure 2.11b show the results of osseointegration after a period of time; osteogenesis can be seen between the metallic porosity of the femoral stem.

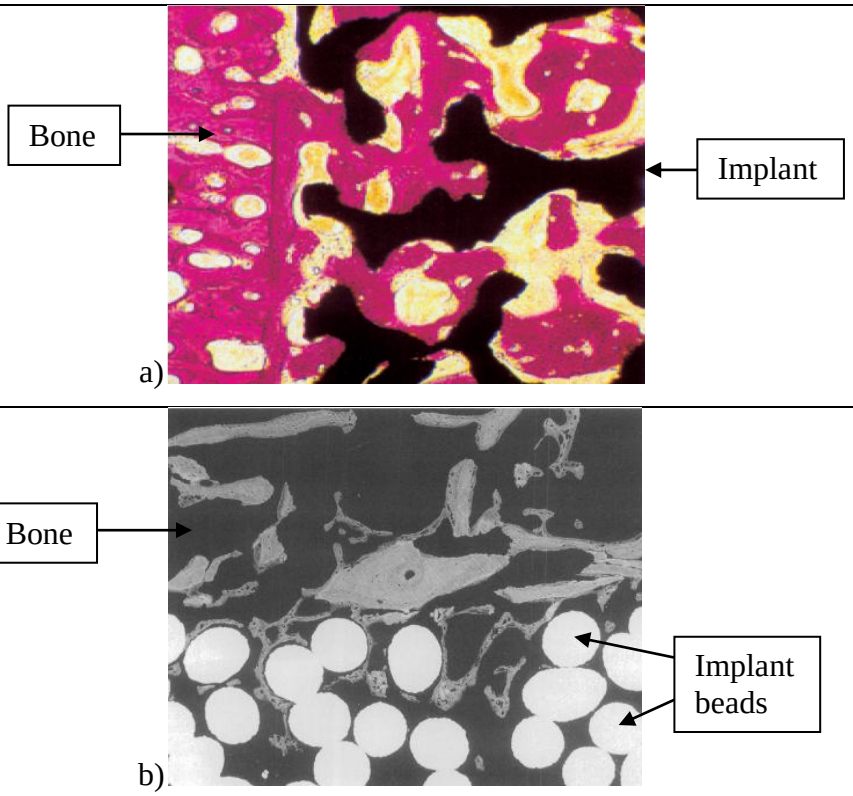

Figure 2.11 a) Photomicrograph of an interface region with bone ingrowth of a four-week implant (black) [90], b) Nature of the ingrown bone in the implant after one month (x 45)[126].

Calcium hydroxyapatite ($Ca_5(PO_4)_3OH$) is the primary inorganic component of bones and teeth. To enhance bone mineralization hydroxyapatite (HA) has been used as a bone-like surface material [96, 127]. HA-coated implants showed a much better bone ingrowth, and faster fixation than non-coated uncemented implants [96, 128, 129].

The optimum pore size to promote osteogenesis and osseointegration between the prosthesis and the bone tissue has been widely investigated to attain an effective

osseous fixation [101, 130, 131]. Bobyn et al. estimated it to be in the range of 50 – 400μm whereas Malchay et al. concluded that good results can be expected from pore sizes of 1 – 2 mm [89, 132].

Regarding the geometry of the femoral stems, the cross-sectional shape and curvature, and surface finish have an important role in the stability of the prosthesis into the medullary canal. The geometrical shape depend on the desired location of fixation of the stem in the medullary canal, which can be at the metaphysic, metaphysic-diaphysis, or at the diaphysis[133]. Porous coating allows bone ingrowth whereas rough surfaces allow bone ongrowth, on the other hand, polished femoral stems are the best option for cemented fixation to reduce or avoid cement particles that may cause osteloysis and gross loosening [101, 133].

Nowadays, stems are designed with and without proximal coatings. The type of coating and the percentage of coated surface of the femoral stem varies from 30% to 90% of the surface. The fully porous coated metal stems show distal fixation with proximal stress shielding. In other designs, the tip of the stem is slim so the diaphysis is not filled, which helps prevent stress shielding [6, 88, 91, 134-139].

Classification of stems depend on the fixation method, cemented stems are categorized into closed beam, French paradox, and taper slip. On the other hand, cementless stems have been widely classified but the principal fixation divisions are the proximal fixation, and the extensive fixation [133].

Figure 2.12 shows femoral stem designs with different surface finishes, from left to right: grooved stem, fully polished stem, fully coated stem, proximally coated stems with distal grooves.

The following section addresses in more detail the topic of revision total hip arthroplasty which is considerably more demanding, complicated for the surgeon, and risky for the patient [14].

a) b) c) d) e) f)

Figure 2.12 Types of femoral stems and surface designs, from left to right: a) grooved stem, b) fully polished stem, c) fully coated stem, d-f) proximally coated stems with distal grooves [140].

2.4 Revision Total Hip Arthroplasty

A Revision THA surgery must be performed after a failed THA. Such failure might occur a number of reasons: dislocation, infection, leg length discrepancy, fracture of the femur, nerve injuries, vascular injuries, stem fracture, loosening, or wear debris and squeaking. All of these causes are associated with several factors such as excessive activity, increased body weight, use of wrong stem size; these factors are accompanied by pain in the hip and limited function and mobility of the patient [82, 141-144].

From the 86,488 hip procedures recorded in the NJR in 2012, 10,040 were revision procedures, of which 88% were single-stage revisions. The 'revision' burden stood at 12% of THA activity in 2012 compared to 11% in 2011 [26]. In 2013, there were 9,751 revision procedures, representing a decrease of nearly 3% of the burden reported in 2012 [27]. In 2014, 8,165 revision procedures were reported, representing a reduction of 16.2% compared to 2013 [28]. Major problems may be found intra-operatively such as femoral fractures and unintentional perforations; in up to 21% of the cases, patient blood loss increases significantly and is time demanding [145]. Worldwide, revision burden has been found to be approximately 12.9% according to

Pabinger et al.[146], and it is estimated to increase as the primary THA incidence increases by 2.3% annually.

Aseptic loosening has been the most commonly recorded indication for revision surgery (40% of cases), followed by infection and adverse soft tissue reactions (25% of 1,330 cases). According to the NJR, patients undergoing revision surgery are less fit than patients undergoing primary replacement, with one third of patients being graded with severe systemic disease, ASA grade 3, for staged revision surgery on the physical status classification system of the American Society of Anaesthesiologists. NHS hospitals incurred most of the burden of revision operations – 83% compared to 15% from independent hospitals. This differs from the activity of primary surgery, where NHS hospitals carried out 69% of primary surgery compared to 27% in the independent sector. When the revision is carried out in a single operation both the cup and stem are removed in 45% of cases, the acetabular component only in 30% and the femoral stem in only 14% of the cases [26].

The average period of time after which a Revision THA is performed is 10 years, and according to NICE guidelines, failure rates should be less than 5% in that period of time for primary THA prostheses in order to meet the regulations [147]. There are cases in which the surgery must be performed in less than 5 years; these variations are related to the patient's daily activities. The diagnosis can refer to developmental dysplasia, osteoarthritis, stem loosening, old septic hip, post-trauma, rheumatoid arthritis (juvenile rheumatoid arthritis), avascular necrosis, and wear debris being the most common [82, 148-150]. Surgery follow ups are continuously performed to monitor the development of the patient's health; these follow-ups occur at 6 weeks, 12 weeks, 6 months, and 1 year after the revision surgery and then every year up to 15 years if the procedure was successful [88, 139, 150].

2.4.1 Surgical Approaches and General Technique

The surgical approaches are the same as for primary THA but in this case, the exposure must be maximized, and the damage to the soft-tissue and bone must be minimized, and theoretically, the revision must remain as simple as possible. Even

though the surgeon always makes an effort to minimize soft-tissue damage and bone trauma, these approaches do not give sufficiently good access to the femur and the femoral canal; for these cases, the extended trochanteric approach is needed or the direct lateral approach[20, 151].

A large number of surgical instruments exist to carry out Revision THA: drills, splitters, curved and flat osteotomes, rongeurs, reversed hooks, trephines, burrs, cement taps, impactors, saws, and in some cases the use of ultrasonic devices is needed. The surgeon must ensure that there is an adequate number of each tool that will be used during the surgery. Figure 2.13 shows the basic medical instruments needed to perform revision surgery, from top to bottom: trephines of different lengths, slap hammer, and flexible osteotomes.

Disadvantages of Revision THA include intra-operative complications, non-planned femoral fractures and perforations. These tend to happen in most of the cases and lead to a reconstruction of the femur, which is highly time-consuming in the operating theatre. Moreover, leading to blood loss, medical cost, and a long and painful recovery for the patient [141, 152].

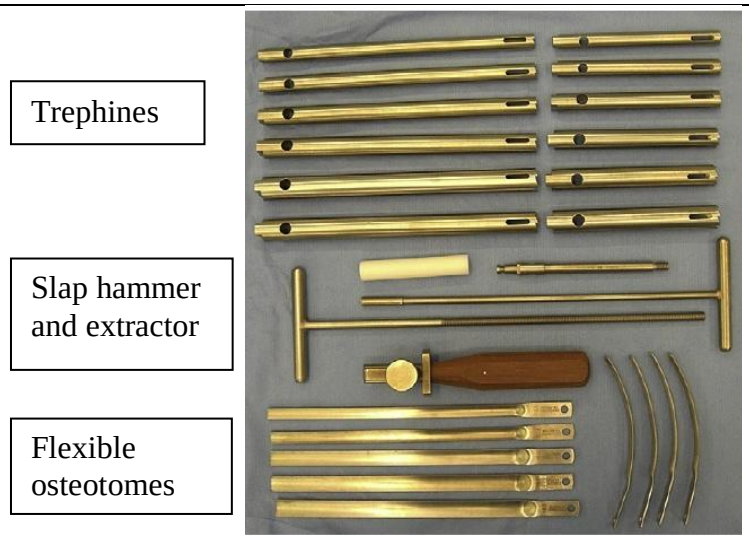

Figure 2.13 Basic tools and instruments to perform RTHA [151].

The different techniques available to perform a Revision THA are described briefly in the following subsections in accordance with the type of fixation that the

femoral component had in the primary THA, cemented or uncemented. The surgeon should be very experienced in this technique due to the difficulties and risks that Revision Total Hip Arthroplasty presents.

2.4.2 Surgical Techniques for Revision of Cemented and Cementless THA

Amongst the surgical techniques used to remove cemented and cementless femoral stems, the most common are:

2.4.2.1 Retrograde stem removal technique (RSR)

Figure 2.14 shows two methods to remove the prosthesis: a) the surgeon can use an extractor to grip the femoral stem and hammer in its retrograde form, b) alternatively, if the femoral stem has a collar, the surgeon can use a carbide bit or tamp to impact upwards against the collar.

This technique is favourable when there is a fractured femoral stem in the medullary canal, but one or both parts of the fractured stem are firmly bonded to the bone or the cement mantle [20, 144]. The retrograde removal technique is mostly used for polished stems and not for roughened or pre-coated stems due to the high risk of bone fracture [144].

2.4.2.2 Cortical window

When the surgeon faces an RTHA with a coated stem or with a rough surface, the removal of the component can become complicated since the cement mantle does not easily yield. In these cases, there is the option of performing a small osteotomy on the femur by creating a distal window from which the femoral stem can be transacted

with a burr, one part of the stem can be easily removed, and the distal part can be removed with the use of a trephine.

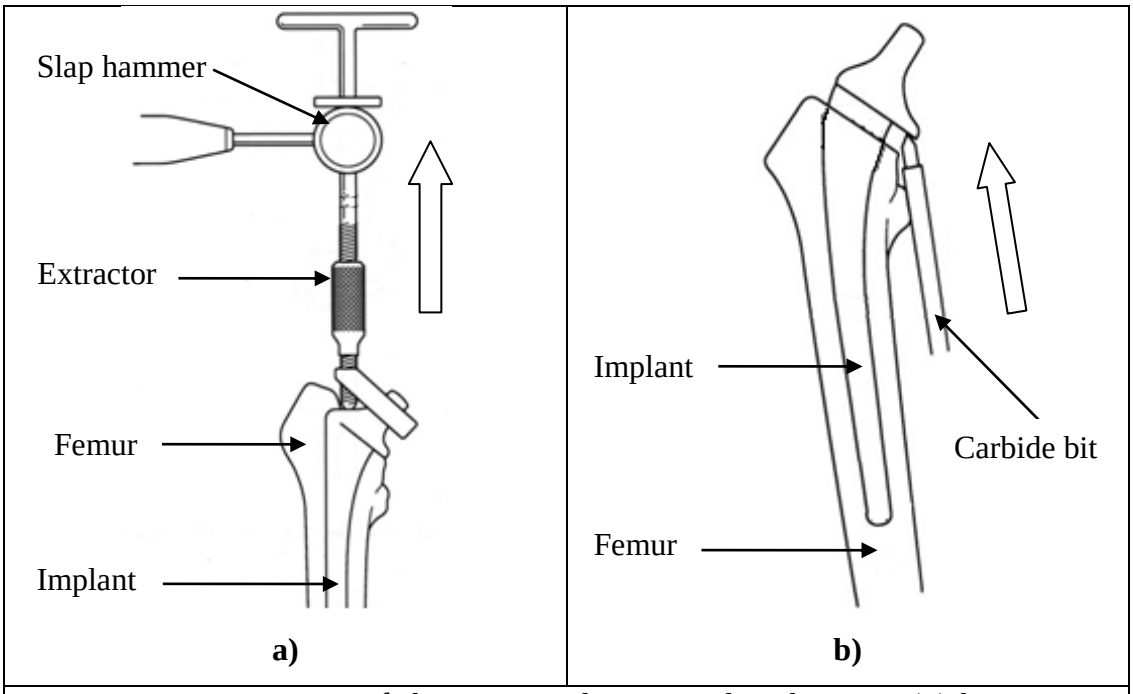

Figure 2.14 Variations of the retrograde removal technique: (a) by using a slap hammer and extractor, (b) by using a carbide bit. Modified [20].

This technique is also performed when removing broken stems. Figure 2.15 shows the four basic theoretical steps in the transection technique, 1) small cortical window and stem cut at the medial zone, 2) removal of the proximal portion of the stem, 3) with the aid of trephines, the remaining distal tip of the stem is removed, 4) an intact femur is left [20, 33, 97, 98, 151, 153].

2.4.2.3 Large cortical window and anterior cortical window

Figure 2.16 shows the large cortical window technique that is needed to approach the stem and cut it into as many parts as necessary to remove it. This technique is widely used by surgeons as an easy way to remove the prosthesis; practically it is a controlled fracture of the femoral bone, which can then be

reconstructed. The anterior cortical window can have a wider opening by drilling holes and controlled fracture lines with osteotomes, the result facilitates direct work on the interfaces and prosthesis [18, 19, 150, 154].

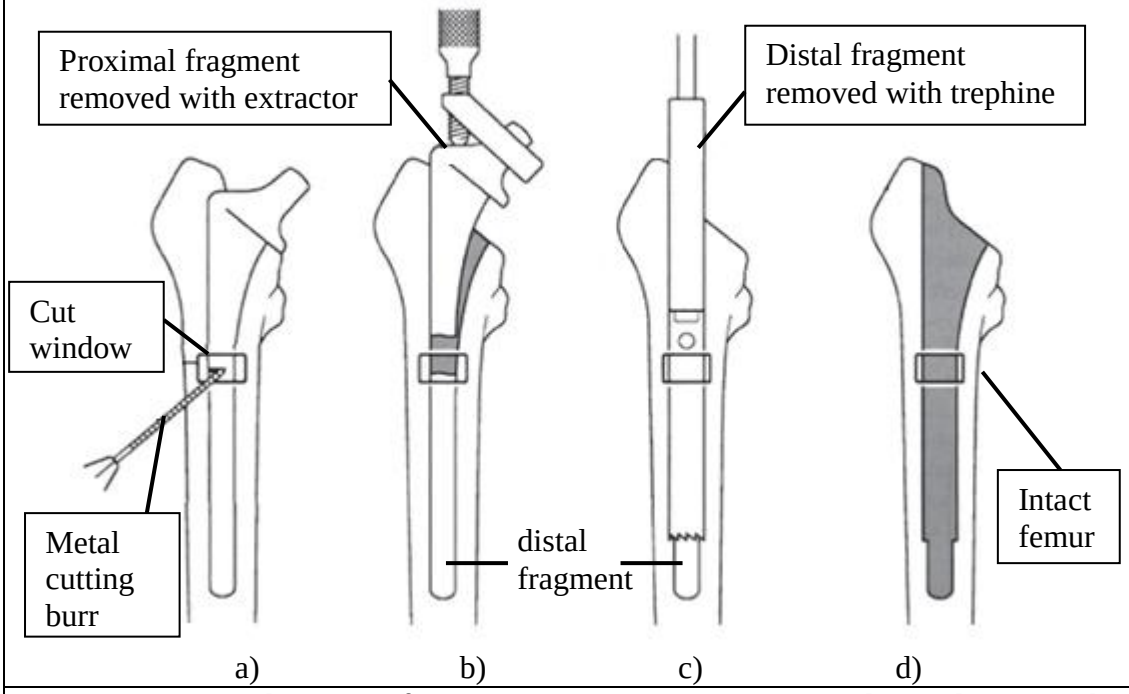

Figure 2.15 Technique of stem transection: (a) cortical window on the bone and stem cut, (b) proximal portion removed, (c) distal tip removed with a trephine, (d) stem removed [20].

2.4.2.1 Extended trochanteric osteotomy

Burrs and osteotomes are not always the best option to remove the cement mantle or to remove the bony ingrowth from the proximal zone or the femoral component since an undesired and uncontrolled fracture may occur. The extended trochanteric technique offers a controlled fracture that can be reconstructed with cables. The resulting wide exposure of the implant allows the surgeon to work directly on the interface to be disrupted by using flexible osteotomes and/or gigli saws. This technique is known to be much more efficient for removing either well-fixed cemented or cementless stems [21, 154-156].

Figure 2.17 shows the basic steps to perform this technique: a) the osteotomy is created by cutting distally from the greater trochanter following the linea aspera, b) a transverse cut made at one third (depending on the case) of the diaphyseal circumference, c) the bone fragment is opened by using osteotomes and d) once opened, the surgeon then proceeds to remove the femoral implant.

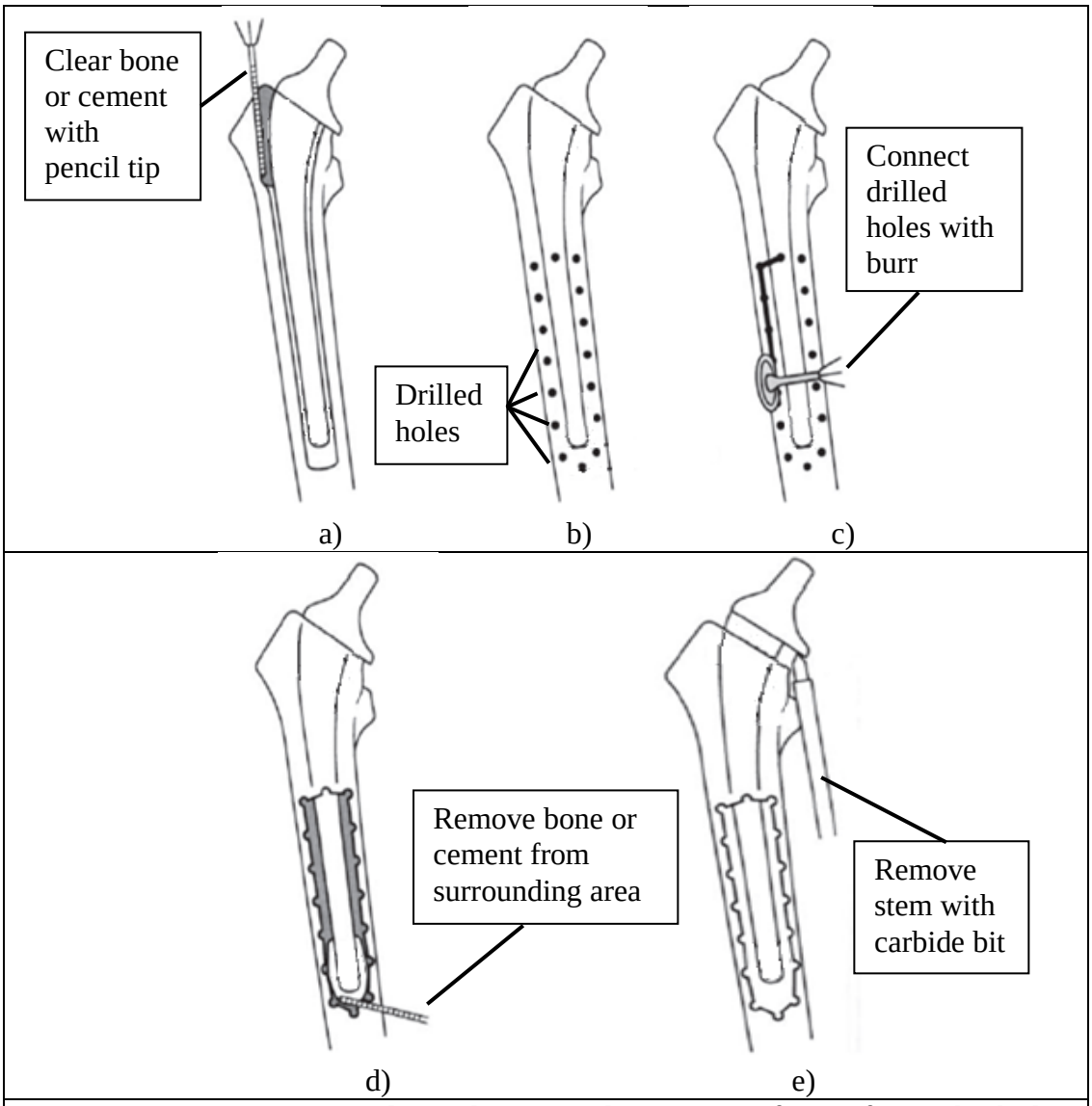

Figure 2.16 Large cortical window, (a) disruption of interface, (b) holes outlining the window's dimensions, (c) holes connected by burr or osteotome, (d) the cement surrounding the femoral implant can then be removed, (e) the stem being removed [20].

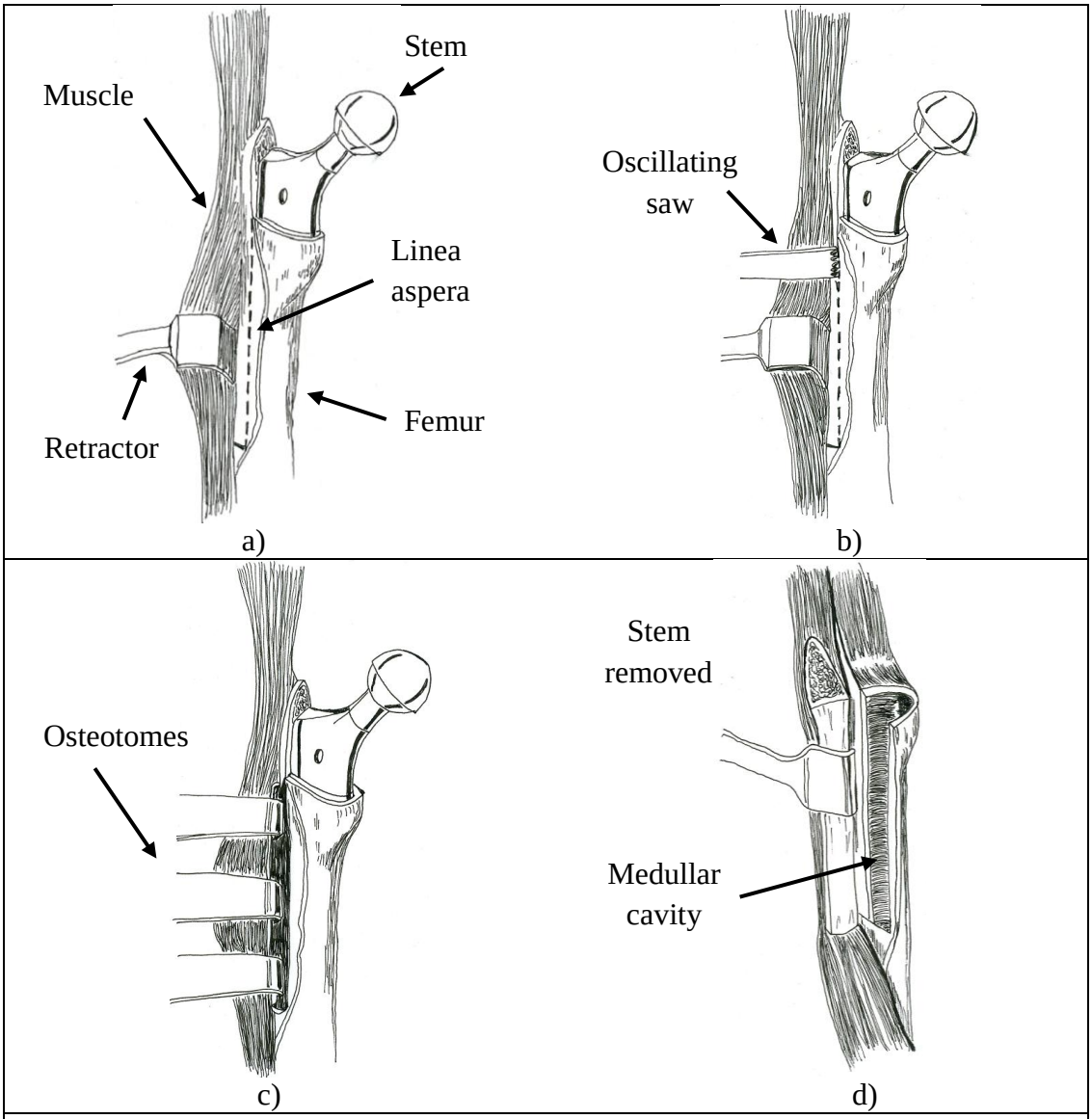

Figure 2.17 Extended trochanteric osteotomy, (a) locate the linea aspera, b) cut along the linea aspera with an oscillating saw, (c) open with the aid of osteotomes, (d) remove the prosthesis once fully opened. Modified [157].

2.4.3 Removal of a Cemented Femoral Stem

Revision of a cemented hip arthroplasty requires the surgeon to be highly skilled; removal of the cemented femoral stem must be carefully planned prior to the operation by the surgeon as unforeseen complications may arise during the surgery. The surgeon must select the appropriate surgical technique, equipment and tools to be used [144].

There is a basic and general theoretical procedure to remove a cemented stem. First, after the artificial joint has been reached, the bonded zones must be identified as well as any damaged areas of the prosthesis component and potential osseous damage, before proceeding to disrupt the cement interface. This can be achieved by removing the cement surrounding the femoral stem using osteotomes. In this step, the surgeon must be very careful not to fracture the greater trochanter, which could lead to a challenging procedure of bone reconstruction. After disrupting the cement bonding and removing some of the cement layer in the proximal zone, the stem can be removed by tapping it in retrograde form. The surgeon can use one of the various extractors to grip and hammer the prosthesis. The surgeon must be careful not to apply an overloaded impact since that could fracture the femoral bone in its medial or greater trochanter zone, leading to reconstruction of the osseous tissue supported by wires [18, 145, 158-160].

After removing the femoral stem, the residual cement layer can be removed with the help of a cement tap or a high-speed drill in some zones. Ultrasound devices may be used to remove the remaining cement mantle inside the femoral canal while minimizing trauma to the bone. The risk of using ultrasonic devices is thermal necrosis of the host bone [20, 151]. Finally, the surgeon will extract the distal plug located in the diaphysis of the femur, avoiding perforation of the femoral canal.

2.4.4 Removal of a Cementless Femoral Stem

The removal of cementless stems can be a very difficult task for the surgeon. The grade of fixation of the prosthesis to the bone is a function of the type of surface that the stem has. The percentage of coating applied or the final surface finish, and the areas they cover are major variables to determine the grade of fixation. The result is a well-fixed implant, which demands more effort to disrupt the bone-implant interface. These factors must be considered by the surgeon when planning the RTHA. The techniques used for the removal of an uncemented femoral stem are the same as the techniques used when cement is used as a method of fixation. Osteotomes and burrs can be used to disrupt the interface and minimize stress on the osseous tissue [137, 143, 161-164].

In the best cases, the stem can be easily removed when it is bonded to the bone solely by the proximal region (trochanteric region), and at specific spots of the porous or coated surface which minimises the quantity of bone to be removed from the interface. Unfortunately, nowadays stems are designed to stimulate bone-ingrowth with more than 50% of the surface finish specifically meant to increase the bonding spots [12]. This requires more instruments: more osteotomes, burrs and trephines must be ready if required as well as oscillating saw blades and gigli saws to disrupt the interface [165].

Cementless RTHA represents a major challenge to the surgeon since it always carries the risk of high trauma to the osseous tissue, blood loss and long recovery time for the patient after surgery. This opens a great field of research into finding ways to improve the methods of surgery and techniques in cementless RTHA [158, 166].

2.4.5 Surgical Complications in RTHA

Various techniques have been introduced to orthopaedics with the objective of lowering the incidence of intra-operative and postoperative damage of soft tissue surrounding the hip joint and the fracture of the femoral bone during revision of total hip arthroplasty. Complications have been reported with all techniques; even if the technique is meant to be as conservative as possible to safeguard bone tissue. Complications depend on several factors such as the design and type of the femoral implant, the integrity of the cement mantle or the bone ingrowth [18, 20, 43].

In vivo and in vitro studies support the clinical experience where performing an osteotomy by making a femoral longitudinal window over the area of difficulty, decreases the resistance of the bone to compression and rotational forces putting the integrity of the artificial hip and health of the patient at risk [43, 144].

It is evident that femoral implant removal has become a more difficult task because of the continuous advances in the design of prostheses and methods of fixation in the medullary canal of the femur. A much more effective, less time consuming, and

less destructive method to remove a femoral implant, whether cemented or cementless, is needed.

2.5 The Use of Low Temperatures in Medicine

In the second half of the nineteenth century, physicists were very interested in achieving and studying low temperatures. In the same period, James Arnott of Brighton started to apply freezing temperatures to be used as cancer treatment and cold anaesthesia. In 1899, Campbell White began to use liquefied air to treat various skin diseases, after which many other methods started to be reported where liquid air or solid CO_2 were used to treat diseases such as varicose leg ulcers, warts, epitheliomas, and carbuncles [167-169].

In 1930, Lortat-Jacob and Solente established cryotherapy as a therapeutical technique in dermatology and gynaecology. In 1938, Temple Fay applied local freezing to patients with Hodgkin's disease, glioblastomas, and advanced carcinomas. The use of cryosurgery continued to grow from the 1930s to the 1960s with the liquefaction of nitrogen, hydrogen, and helium. Liquid nitrogen started to be applied for skin diseases [168, 169].

Cryopreservation and survival of cells and tissues such as spermatozoa, ovaries, embryos, bones, and blood was ensured with the discovery of materials called cryoprotectants such as glycerol and dimethylsulfoxide, both discovered in the late 1940s and late 1950s [168, 169].

Modern cryosurgery started to develop in 1961 when Cooper and Lee officially introduced the freezing surgical technique called cryosurgery. They created a probe made of concentric tubes with liquid nitrogen flowing inside. This probe allowed controlled freezing of depth and area where the probe was placed on the location of the tumour to be removed, or the specific location in the brain to treat Alzheimer disease [167-169].

Cryosurgery started to grow more in the second half of the twentieth century and its application expanded to cataract removal, detached retinas repairs, liver and prostate cancer treatment, plastic surgery, orthopaedics, and dermatology [167, 169].

As an approach to studying the treatment of benign aggressive diseases in the maxillomandibular complex, Costa et al. [44] evaluated the effects of cryosurgery with liquid nitrogen on the femoral diaphysis of rats. Liquid nitrogen was locally and sequentially applied for 1 or 2 minutes in the diaphysis, with 5 minutes of thawing immediately after cooling. The cryoprobe used had a flat tip of 1 mm in diameter. Thermal necrosis was evaluated by studying four parameters: depth and extent of bone necrosis, number of empty osteocyte lacunae and vessel channels. Their results indicated that a 2 minute exposure caused more necrosis than a 1 minute exposure. Unfortunately, their findings were not extrapolated to clinical practice for a better understanding of the mechanisms of thermal injury.

Regarding to the effects of low temperature over the interface strength, Diefenbeck et al. [47] studied the effects of freezing-thawing cycles on intramedullary bone-implant interfaces in rat bones. The variations of the mechanical properties of the bone-implant interface were evaluated in a mechanical pull-out test. After eight weeks of implantation, the animals were sacrificed and the bone-implant specimens were harvested. Two scenarios were studied by pulling-out the implanted titanium rods: 1) after storing the specimens for 14 days at -20°C and thawed, 2) immediately after harvesting the specimen. Their results revealed that there was no significant change in the mechanical properties of the interface, shear strength and maximum force required to extract the implant, between the frozen-thawed and the fresh samples. The researchers did not measure the amount of bone ingrowth on the implanted titanium stem rods.

In a similar study, Huss et al. [48] tested and evaluated the pull-out forces of pins implanted in canine femurs after being stored at -20°C and -70°C for 14 or 28 days. They concluded that the pull-out forces were not affected by freezing temperature or time. Similarly, the researchers did not quantify the quantity of bone integrated in the implants.

Low temperatures are applied to freeze and store biological materials, including thin tissues, blood, reproductive cells, and bone. Preservation of living tissue is difficult; as the cells suffer severe damage during the cooling and thawing processes. However, thermal damage can be used to kill carcinogenic tissue [46, 170-178].

In vivo procedures regarding temperature effect on the construct of hip replacement have also been studied in order to determine the relevance of thermal residual stresses, which could be by means of a heating or cooling process and the effect of the mechanical properties of each of the components of the system individually or as a whole [52, 179, 180]. Even though there are studies that have focused on the thermal effect on the cement-bone or cement-stem interface, they concentrate mainly on the effects of cement curing and the effects of pre-heating or pre-cooling the stem while performing the cementing procedure. Sub-zero temperatures have been widely used in medical surgery to kill unhealthy tissue for cancer treatment; cryosurgery is a tool to be used delicately, since the risk of damaging healthy living tissue is always present [177, 181-183].

2.5.1 Cryogenic Injury

Since the beginnings of cryosurgery, researchers have acknowledged the need to have specific information regarding the thermal parameters of tissue destruction. In the early days, these thermal parameters were not precise, and treatment failures resulted, though it is known that cells differ in vulnerability related to freezing damage [181, 184]. Nevertheless, the critical temperature range falls between -5°C and -50°C, depending of the cell/tissue [181].

The mechanism of damage is itself a complex and vast topic. The rate of cooling constantly varies throughout the frozen lesion. The temperature gradients vary from cryogenic at the cryogenic device to body temperature (36°C), making it very difficult to predict the outcome of the cryosurgery and the relation between freezing exposure and tissue damage [184].

Postoperative complications may occur after cryotherapy where aseptic necrosis starts to appear after thawing in cryosurgery [172]. Researchers have concluded that tumour necrosis is caused by intracellular ice crystal formation and that the rate of freezing plays an important role in the formation of crystals in the cellular compartment [182]. This intracellular ice crystal formation requires temperatures below -40°C, and according to several researchers, this temperature is an important factor in tissue destruction [181]. On the other hand, temperature ranges between -20°C and -25°C are important factor for recrystallization, where ice crystals fuse and form larger crystal structures, which are much more abrasive and lethal to cells [181, 185]. From the mentioned information, the present thesis will recognize the temperature of -40°C as a critical turning point for tissue safety or injury.

For cancer treatment, temperatures as low as -196°C are applied for 3 minutes, slow freezing also causes damage to the structure of tissue because of ice crystal formation of frozen water molecules [186].

In cryosurgery, low cooling rates are defined in the range of 10°C/min or slower. On the other hand, in order to destroy living tissue, high cooling rates can be found to be in the ranges of 22°C/min and up to 50°C/min [45, 181]. Regarding cooling rate, studies have demonstrated that a single and quick freezing process causes less thermal damage than repeated freezing, but high cooling rates are much more lethal to cells [182]. A quick rate also produces intracellular crystals that break the membranes and organelles of the cells [182, 187], but slow thawing has also been demonstrated to be an important key to minimising damage to the cells compared to quick warming of the tissue, which is much more lethal at the cellular level [181, 182, 187].

2.6 Thermally Induced Failure of the Interface in Composite Joints

Previous Section 2.5 presented the use of low temperatures in medicine and the importance of keeping living tissue out of thermal damage by acknowledging its thermal limits. The mechanisms of cryogenic injury have shown that temperature at

-25°C in lethal to cells, and -40°C represents a critical temperature for irreversible thermal damage to tissue.

As basis for a new methodology to facilitate the removal of the femoral stem, it is important to cause an early interface failure between the implant and bone. In order to do so, the structure of the interface must be subjected to mechanical stress and temperature variations to decrease the bonding strength between materials.

Previous investigations related to bimetallic strips and joints revealed that composite materials such as bimetallic strips are considered as efficient structures [188, 189]. These hybrid materials have structural and multi-functional characteristics such as thermal, electrical, magnetic and optical properties and can be used as electrical components and as a result of an excellent bonding interface they can acquire high electrical conductivity with acceptable deformability [188-192]. Bimetallic strips can be manufactured at very high temperatures in the range of 250°C and 1150°C. Other manufacturing techniques use low temperatures in the process, and a high interface strength can be obtained [188-192].

Studies have shown that a bimetal interface manufactured using high temperatures might have a failure mechanism dependent on some of the following factors [188-193]:

a) The stress applied to the interface;

b) The residual stress;

c) The dynamics of the thermal expansion and contraction of the materials and the effect in the interface; and

d) Fatigue caused by continual temperature changes, in the case of bimetallic thermostats.

On the other hand, high strength bonded joints are primarily used in aerospace and nautical vessels where they have an important role in load transfer through the structure [194-196]. These joints are often mechanically fastened and may also use adhesives. Mechanical fastening involves the use of rivets or bolts through the structure

of the joints [195, 197]. Studies on the strength of these joints have shown that failure of the interface is also related to [195, 197]:

a) The stress applied to the interface;

b) The residual stress caused by temperature; and

c) Fastening method: adhesive, mechanical, or hybrid.

The next chapter introduces the new methodology and the fundamentals on which it is based. The experimental setup is described along with the various materials used in the preparation of the specimens to be mechanically tested, after applying the cooling procedure in order to investigate the load required to remove a cemented titanium stem.

Chapter 3
The New Methodology to Remove a Femoral Stem

3.1 Introduction

In previous chapter, it has been mentioned that femoral stem loosening has been a long-term complication of Total Hip Arthroplasty, researchers have focused on solving this problem by improving the cementing and the manufacturing techniques of the femoral stems. Consequently, the fixation of implants to bone or bonding to the bone cement has now become an issue in clinical orthopaedics when conducting Revision Total Hip Arthroplasty surgery. Section 2.4 showed that the problems are closely related to the methods and techniques employed in surgical practice when conducting an RTHA, which may destroy the structure of the femur, extending the surgery time to reconstruct the affected zone, increasing the health risk to the patient, and requiring a longer rehabilitation time. It is, therefore, crucial to preserve the integrity of the bony tissue, and for that reason, better and more effective ways to perform the surgical extraction of the implants are necessary.

This Chapter presents the new methodology proposed to remove a femoral stem during RTHA. The method applies very low temperature to the neck of the femoral stem in order to cause an effect on the thermo-physical properties of titanium alloy, Ti-6Al-4V, specifically thermal properties. Shrinking induced by thermal shock with low temperature should weaken the interface bonding strength between the femoral prosthesis and the bone cement, reducing the force required to remove a femoral stem during RTHA.

For this thesis, the use of orthopaedic bone cement was chosen to implant the stems in order to perform in-vitro experiments and demonstrate the feasibility of the proposed methodology to remove an implanted femoral prosthesis. An analysis and comparison of the material properties between the bone tissue and bone cement were carried out to justify this decision. An analogous thermo-mechanical behaviour was expected due to the close similarities found in the thermal properties of both materials,

as seen in Table 1.1 from Chapter 1, and by following standardized preparation of bone cement for specimens repeatability of the experiments was assured in contrast to the difficulties of simulating osseointegration in-vivo. Moreover, upon reviewing in-vitro and in-vivo experiments, the data showed that the force required to remove a well-cemented femoral stem ranges from 1.23 to 6.5 kN [35-40], which represents the equivalent of 60% to 70% of the force required to remove a cementless stem [32-34, 41, 42]. This means that removing a cemented stem is as challenging as a cementless stem.

The chapter continues by discussing the basic concepts of heat transfer followed by the thermo-physical characteristics of the materials involved in the artificial hip, specifically for a cemented femoral implant. The chapter closes with the first set of experimental work demonstrating the feasibility of the new methodology. The methodology offers the opportunity to safeguard the structure of the femur while easing extraction of the femoral stem by exposing it to low temperatures. Based on the information from Section 2.5 [47, 48, 185, 198], the cooling temperatures were: -76°C as an extreme cooling case, -40 °C as the critical limit of thermal safety, and two intermediate temperatures at intervals of 9°C and 18°C from the critical temperature, thus making a total of 4 temperatures of interest.

In order to prove the concept of the new methodology to remove a femoral stem, the effect of low temperature on the release force of a cemented femoral implant was investigated. This research considered in-vitro experiments in which custom-made titanium stems were implanted with bone cement in two different materials, thus, making two scenario studies:

I. In the first scenario study, a trapezoidal steel mould was used with the aim to prove the concept of the proposed methodology, and understand the effect of low temperature on the release force.

II. Second scenario study, composite bones were used in order to prove the concept in a closer approach to a real case. Two different shapes of composites were used:

    a. Cylindrical composites.

    b. Composite femurs.

After 24 hours of implantation, the specimens from both scenario studies were subjected to two consecutive experimental stages and then compared:

1. First Stage: Cooling Stage

   The neck of the titanium stem was exposed to different cooling temperatures by using liquid nitrogen; the case studies considered for each scenario were as follows:

   a) For the steel mould specimens, four case studies with cooling temperatures at: -76^{o}C, -58^{o}C, -49^{o}C, and -40^{o}C.

   b) For the cylindrical specimens, three case studies were performed: -76^{o}C, -49^{o}C, and -40^{o}C.

   c) For the femur specimens two case studies were considered: -76^{o}C and -40^{o}C as temperatures of interest.

Once the desired temperature was achieved in the cooling stage, each specimen was immediately subjected to the second stage.

2. Second Stage: Mechanical loading test (pull-out)

   The specimens were clamped on an Instron materials testing machine, where the femoral stem was pulled from the neck at a constant crosshead speed of 0.5 mm/min. The mechanical pull-out was deliberately stopped until breakage occurred at the interface between the titanium stem and the bone cement, thus releasing it from the cement mantle.

Figure 3.1 summarises the scenarios and stages that were used in this research studies as a diagram.

3.2 Experimental Methodology Used

In order to demonstrate the feasibility of the new methodology to remove a cemented femoral stem during RTHA, a total of 20 experimental in-vitro tests were

performed. The experiments consisted in removing a custom made femoral stem (Ti-6Al-4V) implanted with bone cement in two different materials: steel mould and composite bones. As a first scenario study, a steel mould was used in order to prove the feasibility of the new methodology. For the second scenario study, Sawbones composite bones were used in two forms: a) as composite cylinders, and b) as composite femurs. In all tests, two consecutive stages were applied: a cooling stage and a mechanical loading test (pull-out).

3.2.1 Stage One: Cooling of Prosthesis

In the first stage: the titanium stem was subjected to very low temperatures, -76°C, -58°C, -49°C, or -40°C, depending on the case as described in Figure 3.1, by immersing its neck into a container with liquid nitrogen. The level of liquid nitrogen in the container was continuously monitored as well as the temperature at different points of interest in the surface of the titanium stem with the aid of 12 T-Type thermocouples connected to a 3530 Orion data logging system and a computer. Once the desired cooling temperature was achieved at the proximal zone of the cemented femoral stem, the stem was immediately removed from the bath of liquid nitrogen and proceeded to be clamped in an Instron materials testing machine to perform the second process.

3.2.2 Stage Two: Mechanical Loading Test (Pull-out)

The second stage, mechanical loading test, takes place consecutively after the cooling procedure. It consisted on clamping the cemented stem in an Instron materials testing machine and pulling the titanium stem from the neck at a constant crosshead speed of 0.5 mm/min until it was released from its container, steel mould or composite bone depending on the case. Force-displacement data was captured while performing the mechanical test.

This new technique should lead to easier extraction of the femoral prosthesis, along with less complicated reconstruction of the bone and soft tissues, reducing the trauma to the patient.

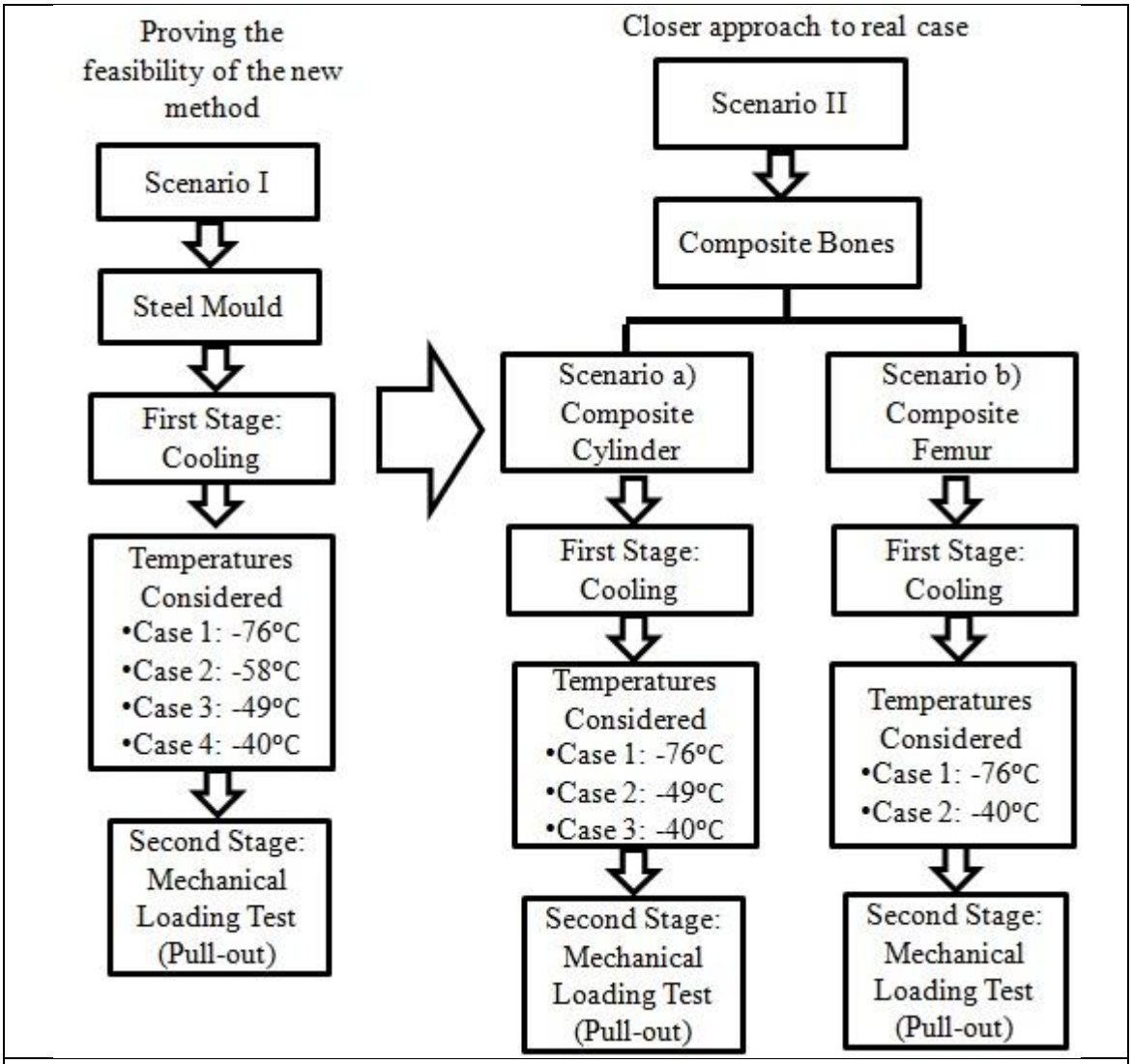

Figure 3.1 General diagram of scenarios and case studies of a cemented titanium stem. First Scenario: implantation in steel mould, Second Scenario: implantation in composite bones: composite cylinder and composite femur.

3.3 The Methodology for Removing the Femoral Stem and Theoretical Background

The complications and the required forces to remove cemented and non-cemented femoral stems were mentioned in Chapter 1 and Chapter 2, as well as the difficulties and limitations that could arise while in surgery. Because of this, an extraction method for the femoral stem with characteristics such as effectiveness and less destructive is needed.

The proposed methodology, uses low temperatures as a way to obtain a temperature gradient with the objective of inflicting thermal stress and contraction of the materials to affect the bonding interface, implant-bone or implant-cement, before applying a pulling mechanical load. Therefore, the application of low temperature should lead to an increase of thermal residual stress, allowing easier disruption of the bonding interface, depending on the method of fixation used in the primary THA.

The following sections on this chapter provide concepts of heat transfer followed by the thermo-physical characteristics of the materials involved in the artificial hip, specifically from a cemented femoral implant, as a way to understand the thermal principles involved in the research.

3.3.1 Fundamentals of Heat Transfer

By following the general purpose of a heat transfer analysis according to Incropera et al. [199], the thermal analysis of this thesis focuses in two objectives: (1) to determine the temperature distribution in the titanium stem and the temperature change rate during the specific case studies, and (2) to determine the working temperature of the system

It is important to understand the elemental concepts of thermodynamics on which the proposed technique is based. Therefore, this section describes how energy is transferred from a system to its surroundings when a temperature difference exists between them. The thermodynamic analysis provides a prediction of the total heat

transferred during a process in which a system goes from one state of equilibrium to another [199].

There are three ways to transfer thermal energy: conduction, convection, and radiation. All heat transfer processes involve at least one of these forms of energy transfer. In this study, two phenomena are considered: conduction between the solid materials, and convection: between the solid materials and the surrounding air. These two phenomena are presented in the following sections. Effects caused by radiation were neglected since experimental tests were performed indoors in an environment at an average room temperature of 23°C.

3.3.1.1 Conduction Heat Transfer

Conduction is a mode of heat transfer in which energy is transported from regions of high temperature within a system to regions of low temperature by the interaction and exchange of energy between elemental particles. The elemental particles (such as atoms or molecules) that are in high temperature regions are at higher energy levels, and as a result, particles oscillate rapidly, collide and move the neighbouring particles (by exchange of kinetic energy) that are at lower energy levels. The net transfer of energy by molecular motion is called energy diffusion [199-201].

The energy transferred per unit time of a conduction heat transfer process can be calculated by the rate equation known as Fourier's Law. For a one-dimension plane wall shown in Figure 3.2, the rate equation is expressed as:

$$q''_x = -k\frac{dT}{dx} \qquad \text{(Equation 3.1)}$$

Where q''_x (W/m^2) is the heat flux, representing the heat transfer rate per unit area perpendicular to the *x*-direction, and it is proportional to the gradient of temperature, *dT/dx*, in that direction. The thermal conductivity coefficient, *k* (W/m°C), is a characteristic transport property of the material [199, 201, 202]. Heat flux is transferred from the zone at higher temperature T_1 (°C), to the zone at lower

temperature T_2 (°C) as shown in Figure 3.2, there is no energy transfer in the y and z directions thus qy=0 and qz=0.

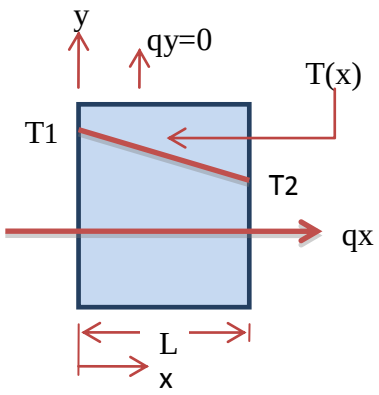

Figure 3.2 One-dimensional conduction heat transfer in a plate with $T_1>T_2$; $q_y=0$ and $q_z = 0$.

3.3.1.2 Convection Heat Transfer

Heat transfer by convection is a complex phenomenon, as it requires a fluid in motion and a fixed surface, in the presence of a temperature gradient. Figure 3.3 shows a hypothetical case where a fluid at ambient temperature flows over a surface with a higher temperature Ts; the transport of thermal energy occurs by the motion of the fluid. The motion of the fluid over the surface improves the energy transfer, and so the rate of heat transfer through a fluid is much higher than the rate by conduction.

Regarding the movement of the fluid, the phenomenon of convection can be classified as free convection, where the flow is induced by buoyant forces as a result of density variations caused by temperature differences in the fluid, or forced convection, in which flow is caused by external means, such as wind, a fan, or a pump [199, 201, 203].

The rate equation for convection heat transfer is expressed as Newton's cooling law:

$$q'' = h(T_s - T_\infty) \qquad \text{(Equation 3.2)}$$

Where *q"* is the convective heat flux (W/m^2), proportional to the temperature differences between the surface and the fluid, T_s (°C)and T_∞ (°C), respectively. The constant of proportionality *h* is given in (*W/m2°*C) and denominated as the convective heat transfer coefficient. This coefficient is not a thermophysical property given that it varies with materials, and depends on the conditions of the boundary layer, which also depends on the geometry of the surface, the nature of the movement of the fluid and a variety of thermodynamic and transport properties of the fluid [199, 201, 203]. Some of the typical values of *h* are shown in Table 3.1.

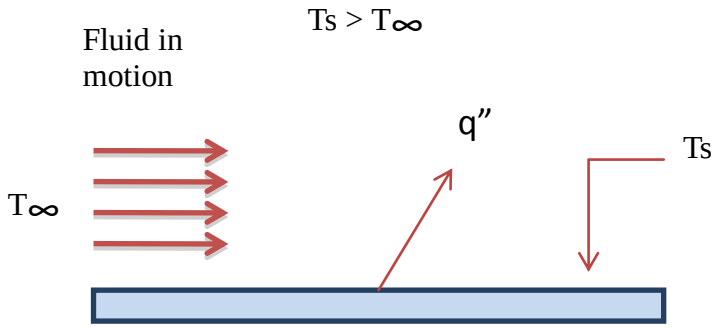

Figure 3.3 Convective heat flux q", from a surface at a temperature Ts, to a fluid in motion with temperature T_∞.

Table 3.1 Typical values for the convection heat transfer coefficient [199, 201].

Process	h (W/m²°C)
Natural Convection	
Gases	2-25
Liquids	50-1000
Forced Convection	
Gases	25-250
Liquids	50-20,000
Convection with phase change	
Boiling or condensation	2500-100,000

3.3.2 Thermo-Physical Properties of Materials

Knowledge of the thermophysical properties of materials is essential to understanding the physical and physiological behaviour of the material under thermal and mechanical loads.

3.3.2.1 Bone Tissue - Femur

The skeletal system supports the body, gives protection to vital organs, and allows muscle to transmit forces. Bone is a non-homogeneous, anisotropic, viscoelastic material, and has a basic extracellular matrix and cellular components. The extracellular matrix is formed by an organic and a mineral phase and gives the mechanical strength characteristics of the bone tissue. The organic phase is made of collagen fibres and the mineral phase is made of deposits of phosphate salt and calcium in the form of hydroxyapatite crystals. The cellular components of bone tissue include various cells including osteoblasts, osteoclasts, and osteocytes [56].

Like all the bones in the body, the femur does not possess a homogeneous structure, as seen in Figure 3.4a. It is made of two types of bone: cortical bone tissue and trabecular bone tissue.

The cortical (compact) bone is a dense tissue commonly located on the outer layer of bones. It is composed of osteons formed of concentric lamellae. The trabecular (cancellous) bone has a porous structure and is formed of trabeculae, which are generally oriented in the direction of the mechanical load; the image on the right of Figure 3.4b shows the lines that follow the corresponding principal stresses applied to the femur. Since bone is an anisotropic material, its strength and stiffness depend on the direction of the loads acting on the bone. Mechanically speaking, this means that the femur is longitudinally strong, thus tolerating compressive loads, and weak in the transversal direction [51, 204].

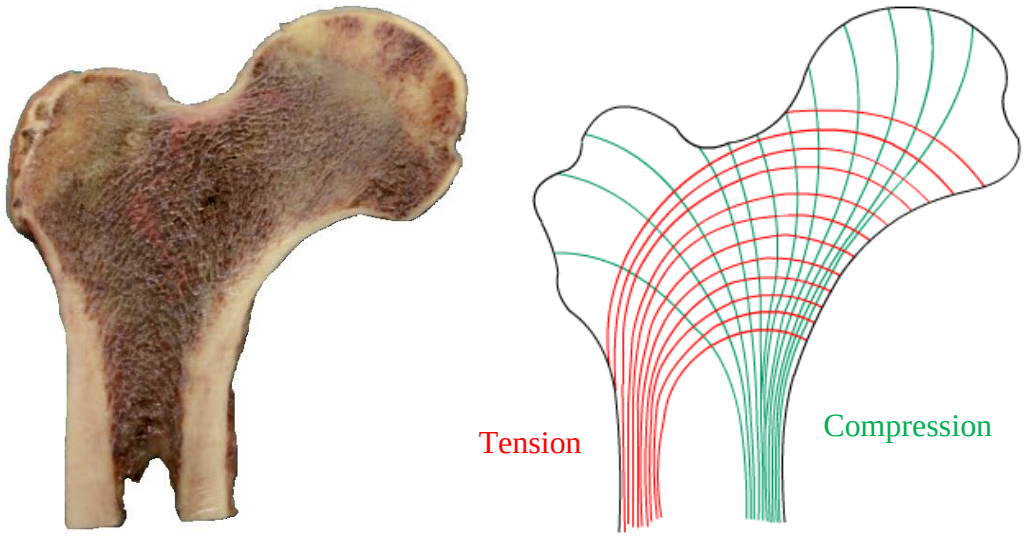

a) b)

Figure 3.4 a) proximal cross section of femur, b) direction of principal stresses. Modified [205]

The typical thermal and mechanical properties of cortical and cancellous bone at room temperature can be seen in Table 3.2. Nevertheless, these mechanical properties vary with the age of the person [49, 50, 206-208].

Table 3.2 Mechanical and thermal properties of femoral cortical and cancellous bone at 22°C [49, 50, 206-208].

Mechanical Properties	**Cortical Bone**	**Cancellous Bone**
Elasticity Module (GPa)	17	0.2
Poisson's ratio	0.29	0.30
Thermal Properties	**Cortical Bone**	**Cancellous Bone**
Expansion coefficient $\left(\frac{1}{^{\circ}C}\right)$	27.5e-6	0.1 e-6
Density $\left(\frac{kg}{m^3}\right)$	1800	1300
Specific heat capacity $\left(\frac{J}{kg^{\circ}C}\right)$	1500	2290
Conductive heat transfer coefficient $\left(\frac{W}{m^{\circ}C}\right)$	0.25	0.29

3.3.2.2 The Titanium Femoral Stem

Different metals and metal alloys have been widely used as prosthetics for total hip replacement as well as for many other joint replacement surgeries. Among those materials stainless steel, Co-Cr-Mo, Ti alloys and many more specialized alloys such as Au-Pd [71] are used.

An alloy of titanium with 6% aluminium and 4% vanadium, Ti-6Al-4V, has been used for medical prostheses since the 1950s, mainly because of its excellent mechanical and biological properties, and other characteristics such as [71, 73, 209-211]:

1. Young's Modulus, lower compared to steel (stainless steel E = 180 GPa).
2. Higher strength to weight ratio. This characteristic is very helpful since the natural limits of human anatomy constrain the design (volume, geometry) of the implants.
3. Improved erosion and corrosion resistance to body fluids that cause the release of undesired metallic ions.
4. A very thin conductive oxide surface film.
5. Excellent creep resistance.
6. Biocompatibility properties, to reduce problems of bone resorption due to the difference between the bone and the prosthesis.
7. Bio-adhesion, which allows integration of bone to the implant.

These characteristics combined in titanium alloys make them highly tolerant to damage. The Ti-6Al-4V alloy is an alpha-beta alloy that has significantly higher yield and ultimate tensile strength than the alpha alloy [212].

Regarding thermal properties, titanium and titanium alloys have been studied at sub-zero temperatures. These alloys have very high ratios of strength to weight at cryogenic temperatures and are the preferred alloys for many applications at temperatures from -196 to -269°C [213]. Cohen et al. [214] demonstrated that titanium

alloy samples showed no difference in breaking and bending forces after cooling to -96°C compared to untreated samples. In other studies, Ti-6Al-4V demonstrated exceptional mechanical behaviour at such temperatures [215].

The variation of the mechanical and thermal properties of Ti-6Al-4V in the range of temperatures that will be used in the present study, 22°C to -76°C, are shown in Table 3.3. For the Young's Modulus and the Poisson's ratio at cryogenic temperatures [210, 212], it can be seen that they have a small variation from 2% to 3.5% in that range of temperatures, and the change is linearly related to temperature change.

Variation of thermal properties as functions of temperature: thermal conductivity and thermal expansion are plotted in Figure 3.5, Figure 3.6 respectively [210, 212, 216-218]. From Figure 3.5, it can be seen that the thermal conductivity varies linearly in the range of temperature shown, from -200°C to 25°C. On the other hand, it can be seen from Figure 3.6, that the thermal expansion follows a quadratic function.

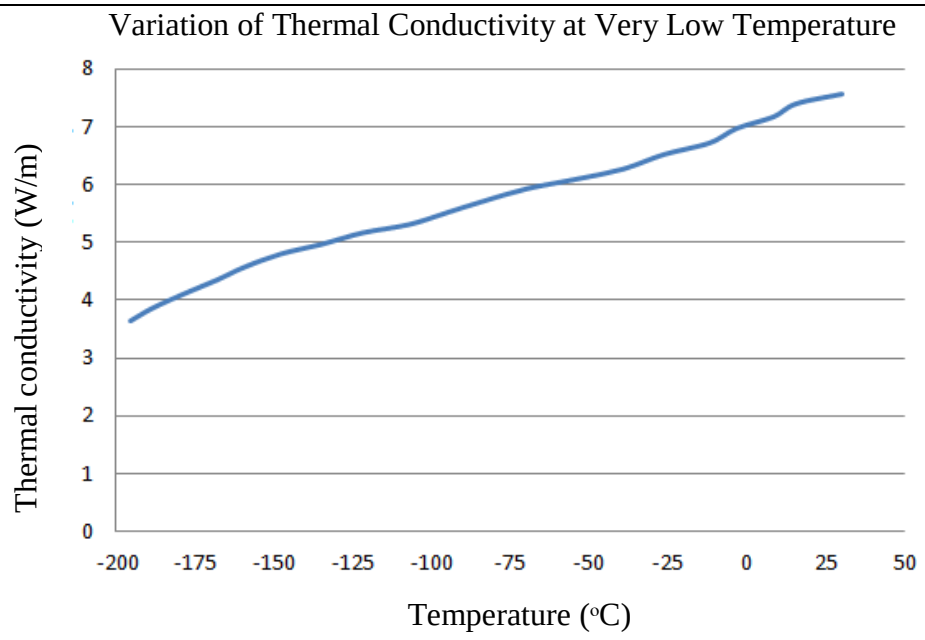

Figure 3.5 Thermal conductivity at cryogenic temperatures for Ti-6Al-4V alloy.

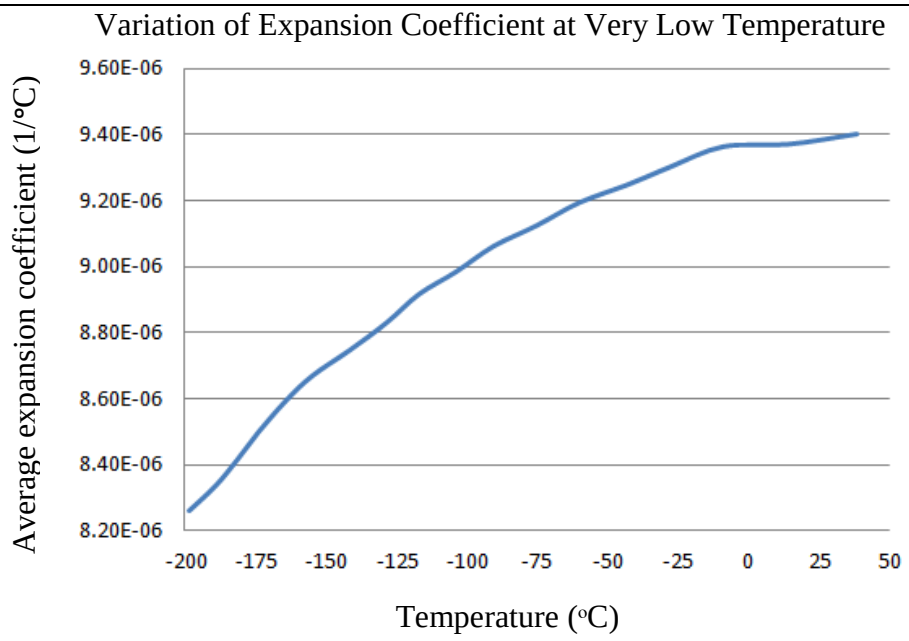

Figure 3.6 Expansion coefficient variations at cryogenic temperatures for Ti-6Al-4V alloy.

Table 3.3 also shows the variation of thermal properties as functions of temperature, 22°C to -76°C. The specific heat, thermal conductivity and thermal expansion can be seen to have a variation of 11%, 20%, and 2.6% respectively [74, 210, 212, 216-219]. This means that at lower temperatures, this titanium alloy stores less thermal energy and is less conductive.

Regarding the thermal expansion coefficient, by using as a first approximation the well known equation for linear expansion for an isotropic material,

$$\Delta L = L\alpha_L \Delta T \qquad \text{(Equation 3.3)}$$

where L (mm) is a length measurement, ΔL (mm) is the change in length caused by the change in temperature, ΔT (°C), α_L (1/°C) is the linear thermal expansion coefficient of the material, it is possible to calculate the contraction of a cube of 1000 mm^3 made of titanium alloy and an ambient temperature of 22°C, the cube would contract about 8.55 μm in all directions at -76°C.

Table 3.3 Mechanical and thermal properties of Ti-6Al-4V at different temperatures [74, 210, 212, 216-219].

Mechanical Properties	Temperature				
	22°C	-40°C	-49°C	-58°C	-76°C
Elasticity Module (GPa)	112	114	115	115.6	116
Poisson's ratio	0.323	0.319	0.318	0.318	0.317
Thermal Properties					
Expansion coefficient $\left(\frac{1}{^{\circ}C}\right)$	9.4e-6	8.89e-6	8.85e-6	8.82e-6	8.73e-6
Density $\left(\frac{kg}{m^3}\right)$	4850	4297	4252	4215	4160
Specific heat capacity $\left(\frac{J}{kg^{\circ}C}\right)$	544.25	504.74	498.26	491.2	475.23
Conductive heat transfer coefficient $\left(\frac{W}{m^{\circ}C}\right)$	7.44	6.29	6.14	6.00	5.73

3.3.2.3 Cement Poly Methyl Methacrylate - (PMMA)

The bone cement used in this research was SmartSet® HV by DePuy®. The polymeric material is based on Methyl Methacrylate (MMA) as the monomer, and a polymer powder, Poly (Methyl Methacrylate) (PMMA). The use of bone cement in hip arthroplasty is to fill the space between bone and the femoral stem by anchoring it in the femoral canal. It is important to know that bone cement bears the weigh and transfers the loads between the prosthesis and the femur, for that reason, the mechanical behaviour of bone cement resembles that of bone by having similar mechanical properties. Moreover, acrylic bone cement thermal properties are also designed to mimic bone tissue.

Initially, PMMA was used in dentistry because of its transparency, durability, strength and biocompatibility. It was through the work of Charnley in the late 1960's that PMMA bone cement emerged as a leading synthetic biomaterial in modern

orthopaedics. Since its invention, PMMA cement has been used in many replacement operations; the main functions of the cement are to stabilize the prosthesis and transmit static and dynamic loads from the prosthesis to the bone and/or increase the carrying capacity of the entire prosthetic system [105, 110]. Bone cement behaves as a brittle material, being weak under tensile loads. However, it is strong under compressive loads which is the main direction of the loads in a hip implant [220].

As mentioned in Chapter 2, there are several bone cements on the market and since they vary in composition, they also possess different mechanical and thermal properties. Mixing technologies also affect the performance of the cement mantle once extruded in the femoral canal. Therefore, the recommended mixing and cementing techniques must be followed closely [221]. In the present study, the bone cement was mixed under vacuum conditions and extruded with the aid of a handgun in the femoral canal, (the cementing procedure will be explained in detail in Section 3.3.2 from this Chapter.

The physical, thermal and mechanical properties of some acrylic bone cements have been investigated and documented [52, 53, 103, 222, 223]. The investigations have one or multiple objectives such as characterizing new compositions, improving mechanical properties, controlling curing time and curing temperature, and reinforcing the chemical structure to improve the biocompatibility [103, 220, 224]. The studies were mainly performed under dry conditions at room temperature of 23±1°C, in a controlled environment after 24 hours of ageing, and followed testing standards from ISO 5833: 2002 and ASTM F451-99a [103, 113, 225]. However, researchers suggest that a more robust methodology and experimental setup is needed to accurately obtain the mechanical, thermal and physical properties of the cements, and that should involve mimicking the physiological conditions to which the cement will be exposed, such as temperature and moisture [103, 223, 225-227].

From the data collected, the average values of the mechanical and thermal properties of acrylic bone cement measured at room temperature of 22°C, are shown in Table 3.4.

3.3.2.4 Composite Bones

As mentioned in Section 3.1, composite bones are used in the second scenario study in order to implement a closer approach to a real case. In the present work, fourth-generation Sawbones® composite models were considered. These composite bones provide an accurate reproduction of the biomechanical characteristics of human bone when placed under diverse loads such as bending, torsion, tension and compression. Such accuracy is achieved by the combination of glass fibre and epoxy resin as a single phase material formed by injection moulding in the manufacturing process [228, 229].

Table 3.4 Mechanical and thermal properties of acrylic bone cement at 22°C [52, 53, 180, 220, 223, 224].

Mechanical Properties	
Elasticity Module (GPa)	2.4
Poisson's ratio	0.33
Thermal Properties	
Expansion coefficient $\left(\frac{1}{^{\circ}C}\right)$	72.2e-6
Density $\left(\frac{kg}{m^3}\right)$	1190
Specific heat capacity $\left(\frac{J}{kg^{\circ}C}\right)$	1450
Conductive heat transfer coefficient $\left(\frac{W}{m^{\circ}C}\right)$	0.18

The use of composite bones has increased continuously in research related to orthopaedic, biomechanics, and surgical education, all of which traditionally involved cadavers. Cadaveric bones have their drawbacks, for example: availability, preservation, discrepancies between specimens, and much more importantly, cadaveric bone have no potential for biological ingrowth for cementless implants and no venous back pressure for the case of cemented implants [228, 229].

Working with synthetic bones offers advantages over human cadaveric bones, such as low cost, easy storage, no toxicity, easier handling and mounting of the

composite materials to the test machines and experimental setup in general, and finally, they do not deteriorate with time[230]. The biomechanical testing materials also provide a reliable and constant medium for experimental work as an analogy to healthy bone or customised properties replicating pathologies such as decreased cancellous bone density [228, 229, 231, 232].

Heiner et al. [233, 234] and Gardner et al. [235] measured and evaluated the structural properties of fourth-generation composite femurs and tibias from Sawbones®. The femurs and tibias were tested under loads of torsion, bending, tension and compression. The results were compared to the values from the third-generation composite bones and natural bones. The results showed that the fourth-generation composites had improved tensile and compressive properties, fracture and fatigue resistance, better thermal stability and an increased moisture resistance. The values were much closer to the mechanical properties of natural bone, making the fourth-generation of composite bones much more reliable.

Dunlap et al. [236] studied the structural properties of third- and fourth-generation composite bones. Results and analyses showed that the fourth-generation composite bone resemble more closely to biological bone with respect to the flexural rigidity, failure strength, and torsional stiffness. Other researchers have also studied composite bones, and they demonstrated good agreement in the material properties when compared to healthy human bone in both wet and dry controlled environments [237-240].

The thermal properties of composite bones were reported as part of an in-vitro study analysing diverse particular thermal phenomena between composite bones and human bone samples, such as comparing the heat distribution from thermographic images after applying therapeutic ultrasound (TUS) for 5 minutes. Temperature rise was also studied while using drills and trephines in orthopaedic surgery, and the consequences of thermal necrosis of bone after using such tools. The effects of thermally treating hip prostheses were also studied prior to implantation and the thermal effects of bone cement curing over the bone while implanting a femoral prosthesis [241-243].

Table 3.5 shows the mechanical and thermal properties, at room temperature of 22°C, of short fibre reinforced epoxy composites (cortical bone analogue), and solid rigid polyurethane (cancellous analogue).

Table 3.5 Mechanical and thermal properties of composite cortical and trabecular bone at 22°C [234, 241-244].

Mechanical Properties	**Composite Cortical Bone**	**Composite Cancellous Bone**
Elasticity Module (GPa)	16	2.84
Poisson's ratio	0.30	0.06
Thermal Properties	**Composite Cortical Bone**	**Composite Cancellous Bone**
Expansion coefficient $\left(\frac{1}{^{\circ}C}\right)$	63e-6	63e-6
Density $\left(\frac{kg}{m^3}\right)$	1640	320
Specific heat capacity $\left(\frac{J}{kg^{\circ}C}\right)$	1640	1570
Conductive heat transfer coefficient $\left(\frac{W}{m^{\circ}C}\right)$	0.45	0.05

3.4 Impact of Temperature on the Release Force of a Cemented Titanium Stem in a Steel Mould

As a way to demonstrate the effectiveness of the new methodology, this section of Chapter 3 presents the first scenario of study by performing in-vitro experimentation of a titanium stem cemented in a steel mould and by following the experimental methodology introduced in Section 3.2.

In order to perform standardized experimental work, procedures such as the cement preparation, injection, curing, setting time, and mantle thickness needed to be controlled and standardized. The requirements for acrylic bone cements [103, 104] and DePuy®'s instruction leaflet for self-curing cements were taken into account for the

preparation of DePuy® SmarthSet® High Viscosity bone cement. The standardized procedures were followed to achieve the mixing time of the chemical components, maximum working time over the mixed dough, setting time, and maximum curing temperature.

To reproduce the removal of the femoral stem in RTHA, a pull-out experimental test was performed, and the impact of cooling on the force required to release a cemented femoral implant was investigated and reported in this chapter.

3.4.1 Materials Used for Steel Mould Specimens

To investigate the required force to release a cemented femoral titanium stem in the first scenario study, customised stems with equivalent geometry to DePuy®'s Corail® size 11 were cemented in a specifically designed steel mould and pull-out tests were performed at 4 cooling temperatures of interest: -76℃, -58℃, -49℃, and -40℃. Control tests at ambient temperature, approximately 23℃, were also carried out enabling results to be compared.

The stems were cemented in a steel mound and instrumented with 12 T-Type quick response thermocouples, which were used to record temperatures at strategic points on the surface of the titanium stems; details are shown in Section 3.3.2. Liquid Nitrogen (LN_2) was used to cool the neck of the stems to the required test temperature. The steel mould-stem assembly was then clamped in an Instron materials testing machine and mechanically tested by pulling out the femoral stem.

3.4.1.1 The Titanium Femoral Stem

For this study, custom titanium stems, Ti6Al4V, were used. The double tapered custom made stems had a trapezoidal cross section and a total length of 165 mm. In addition to the relative roughness produced by the milling machining of the customized femoral stem, the surface of the stems was sand-blasted to produce an opaque finish

(Ra<1µm) in order to standardize the surface for the stem-cement interface in the present study. The resulting stem-cement interface area of the customized titanium stem was 6500 mm^2, with a stem-neck area of 1620 mm^2.

Figure 3.7a shows the custom-made titanium stem used for the experiments. More detail regarding the dimensions of the titanium stem can be seen in Appendix A2. Figure 3.7b show three titanium stems, one with a glossy finish as result from the milling manufacture, and two samples after being sandblasted.

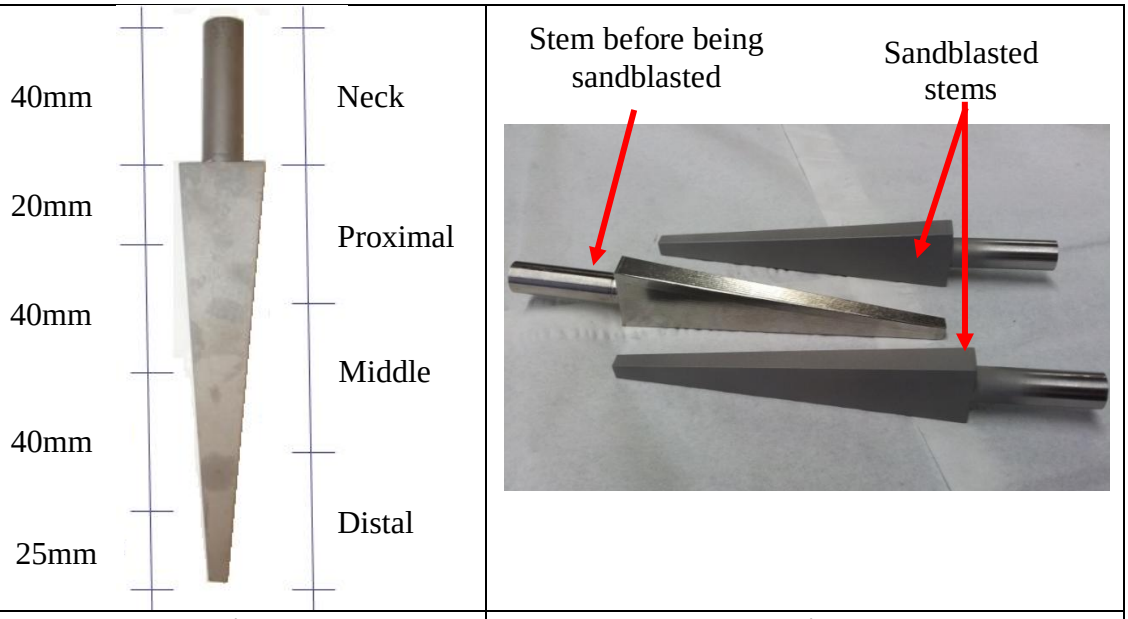

Figure 3.7 a) Custom made Titanium stem showing dimensions, and zones of interest, b) Titanium stems before and after being sandblasted.

The obtained roughness of the custom made titanium stem is equivalent to the cemented prostheses in the market such as: Charnley (by DePuy Johnson & Johnson) average roughness of Ra=0.75µm [2], Exeter (by Stryker Howmedica) matt finished with roughness of 0.658µm<Ra<1.159µm [245], Muller (by Zimmer) straight stem with roughness of 0.5µm <Ra<1.5µm [2, 246]. These values are 10 to 50 times higher than the surface roughness of the polished femoral stems such as the Exeter (by Stryker Howmedica) with polished finish of 0.01µm<Ra<0.059µm [2, 245], and the C-stem (by DePuy Johnson & Johnson) with a polished finish of Ra<0.02µm [2]. On the other hand, by comparing the customized femoral stem to the cementless Corail (by by

DePuy Johnson & Johnson), the hydroxyapatite coating delivers a roughness of 3µm<Ra<10.2µm [31].

3.4.1.2 Steel Mould

In order to implant the titanium stem, a trapezoidal and tapered steel mould was designed to simulate the femur encasing the stem, and with the objective of allowing a constant and minimum bone-cement mantle thickness of 3 mm, as recommended in literature [97, 247, 248]. Figure 3.8a shows the steel moulds in which the femoral stem was implanted. As shown in Figure 3.8b, a removable cap was manufactured to be placed on the top of the mould, thus keeping the cement in the cavity while the stem was being pulled out with the Instron machine.

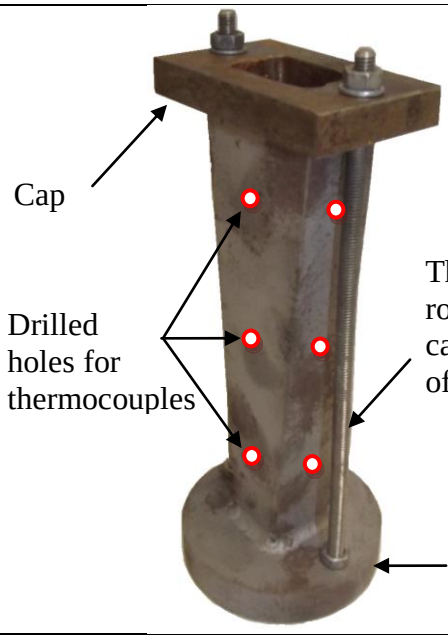

a) b)

Figure 3.8 a) Steel moulds used for the tests, b) Steel Mould with cap and 2 mm drilled holes for thermocouples.

With the purpose of inserting the thermocouples, three 2 mm diameter holes were drilled on each face of the mould making a total of 12 holes (one thermocouple for each hole). These holes were located so as to coincide directly with the middle of the

three zones of interest on the stem (proximal, middle, and distal); the holes were positioned at 20 mm, 60 mm, and 100 mm from the edge of the mould. The location of the drilled holes in the steel mould and contact locations on the titanium stem (once implanted in the steel mould) can be observed in Figures 3.9a and 3.9b respectively.

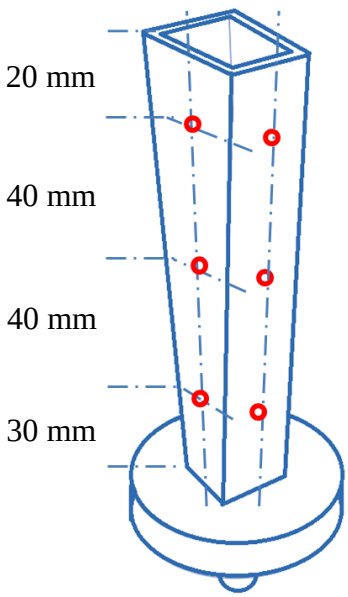

a)

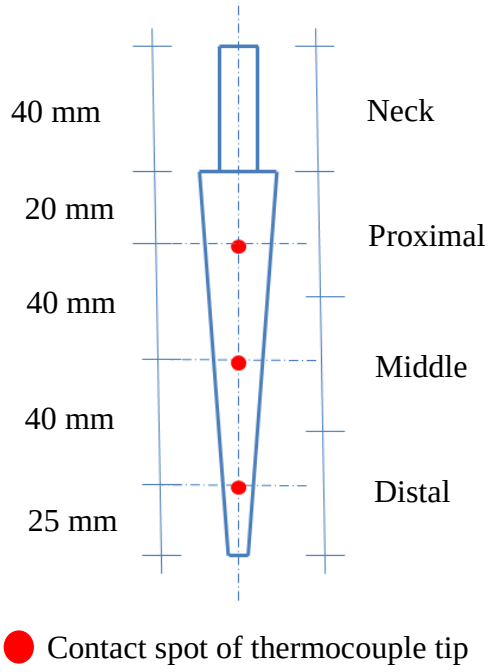

b)

Figure 3.9 a) Drilled holes at two faces of the steel mould, b) contact spots of thermocouples at one surface of the titanium stem.

3.4.1.3 Bone Cement – Polymethyl-Methacrylate (PMMA)

SmartSet® HV bone cement is a self-curing, radio-opaque, polymethyl methacrylate based cement used to fix a metal or polymeric prosthesis to living bone in arthroplasty procedures. The bone cement does not have intrinsic adhesive properties, but depends instead on close mechanical interlock between the irregular bone surface and the prosthesis. SmartSet® HV bone cement is a two-component system, consisting of separate, sterile liquid (Methyl Methacrylate) and powder (Methyl Acrylate copolymer) components, which are mixed at the point of use to produce the cement.

3.4.1.4 T-Type Thermocouples

T-Type (copper - constantan) thermocouples were considered to measure the desired low temperatures due to their working temperature range, from -200°C to 350°C, their fast response and low sensitivity of 43 µV/°C. The thermocouples are a pair of twisted leads with 0.2 mm of diameter, one made of copper and one made of constantan, and welded together at one end. The twister pair leads are protected with solid PFA (perfluoroalkoxy polymer resin) insulation. Figure 3.10a shows the thermocouples connected to a data logger's cartridge prior to be inserted and embedded in the steel mould.

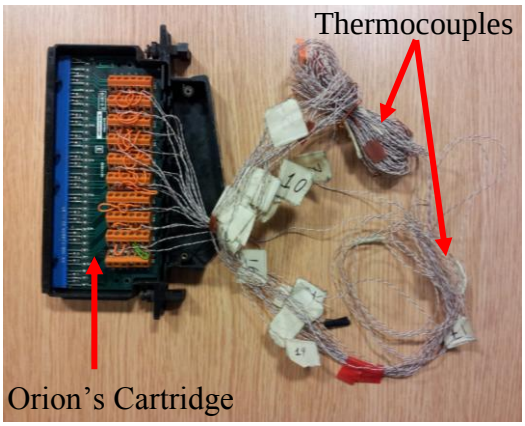

a)

b)

Figure 3.10 a) Thermocouples connected to Orion's cartridge, b) Orion 3530 data logger.

Figure 3.10a shows a total of 18 thermocouples connected to the data logger's cartridge which was posteriorly connected to the Orion 3530 data logger. From those 18 thermocouples, 12 were used to measure the temperature at strategic points on the surface of the titanium stem, 2 as monitors of liquid nitrogen level in the container, and 2 as monitors of room temperature. Real time data acquisition was achieved in the combination of a data logger ORION 3530 (Solartron/Schlumberger, Franborough, UK) shown in Figure3.10b, and a computer. The data logger was set to read and record the temperature at two-second intervals.

3.4.1.5 Liquid Nitrogen (LN_2)

Liquid nitrogen chosen as cooling agent because it is chemically inactive, non-explosive, and non-toxic [249]. At an atmospheric pressure of 1 bar, liquid nitrogen boils at -196.6°C, and has a density of 808.9 kg/m^3 [46, 249]. The use of liquid nitrogen in an open container at atmospheric conditions in a big space (room), allowed the achievement of low temperatures with minimum risk. Low temperature protecting gloves and a Dewar flask were used to handle the liquid nitrogen in the experimental working area. Figure 3.11 shows the equipment used to handle the liquid nitrogen during experimentation.

Figure 3.11 Safety equipment: Dewar flask and insulated gloves.

3.4.2 Experimental Methodology for Steel Mould Specimens

3.4.2.1 Cementing Procedure and Instrumentation of the Steel Mould Specimens

Before cementing the stem in the steel mould, both were sandblasted and wiped with alcohol cleansing pads to remove sand residues from the surfaces of the stem and the steel mould.

Figure 3.12 shows the material and equipment used for the preparation of the cement: a box of SmartSet CEMVAC 40g containing the polymer powder and liquid monomer, mixing syringe, hand gun, and DYMAX14 vacuum pump (240 mbar).

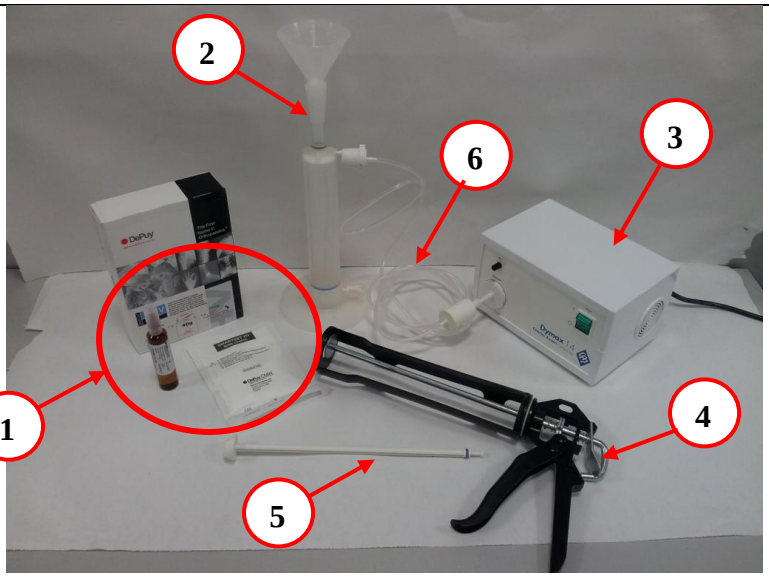

Figure 3.12 Equipment used for the cementing procedure: 1) bone cement components: PMMA powder sachet and liquid monomer ampoule, 2) cement syringe, 3) vacuum pump, 4) syringe hand gun, 5) hermetic central rod, 6) vacuum hose connector.

The bone cement was prepared according to the manufacturer's guidelines. Figures 3.13 to 3.16 shows a pictographic description of the general steps followed in the process of cement preparation:

1) Assemble the syringe in the stand and secure with the plastic pin provided. The bag containing the powder component is opened and the entire contents are emptied into the clean and dry mixing vessel (cartridge/syringe). The syringe is hermetically connected by a filter/vacuum hose to a vacuum pump, which is NOT activated, as seen in Figure 3.13a.

2) The sealing plug is removed. The ampoule containing the liquid monomer is opened and completely emptied into the mixing vessel/syringe, as seen in Figure 3.13b.

3) The ampoule is removed from the nozzle once it has been emptied. The syringe is then sealed by inserting the provided hermetic central rod. The mixer is positioned at the bottom of the syringe, as seen in Figure 3.13c.

4) The vacuum pump is turned ON immediately, and a waiting time of 10 seconds is given to allow maximum vacuum before mixing, as shown in Figure 3.14a.

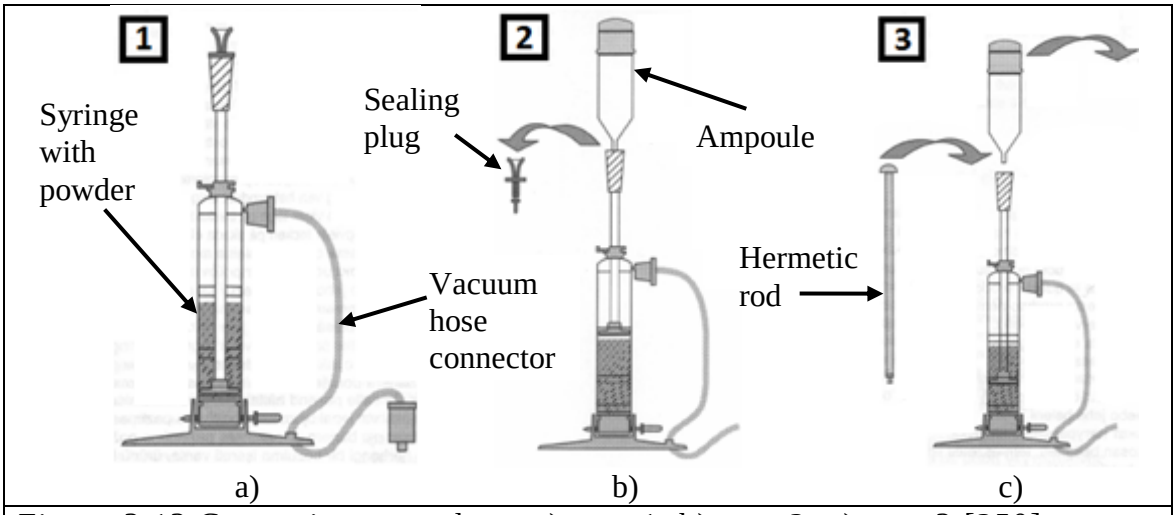

Figure 3.13 Cementing procedure, a) step 1, b) step 2, c) step 3 [250].

5) After this waiting time, the components are mixed by pulling and pushing the piston of the syringe and giving half a revolution to the piston at the end of each cycle. This has to be done 8 to 11 times at a constant rhythm, taking approximately 10 seconds, as shown in Figure 3.14b.

6) After mixing, the piston is left at the top of the syringe and the vacuum is maintained for 15 seconds, as seen in Figure 3.15a.

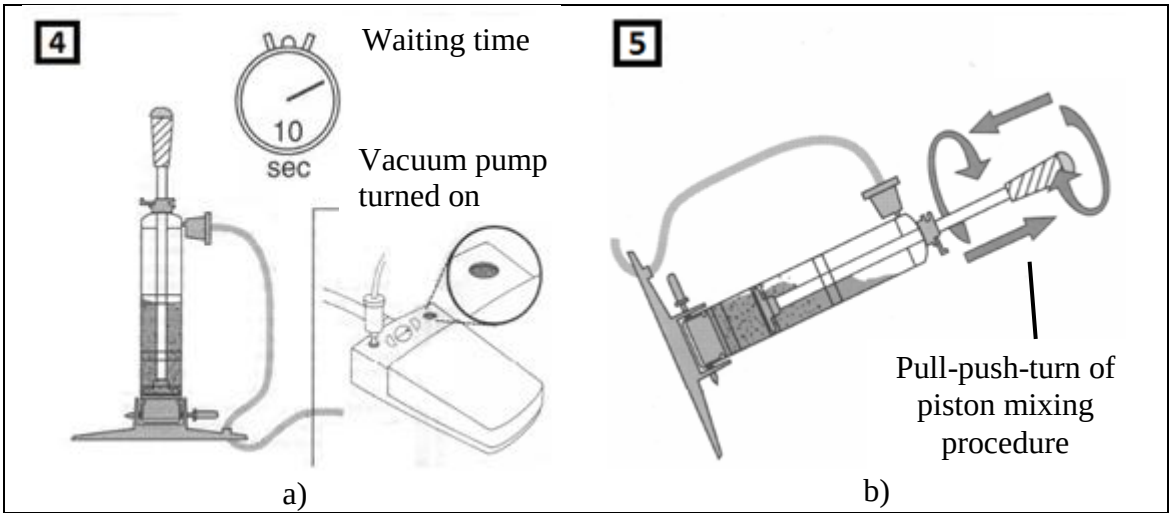

Figure 3.14 Cementing procedure, a) step 4, b) step 5 [250].

7) The pump is then turned off and the filter/vacuum hose is removed from the syringe. The locking pin is removed from the base of the syringe, as shown in Figure 3.15b.

8) The central rod is removed. The nozzle is locked by a locking plate and the edge is removed, as seen in Figure 3.15c.

9) The syringe is removed from the mixing stand and then inserted into the hand gun, as shown in Figure 3.16a.

10) The cement is injected into the steel mould, as shown in Figure 3.16b.

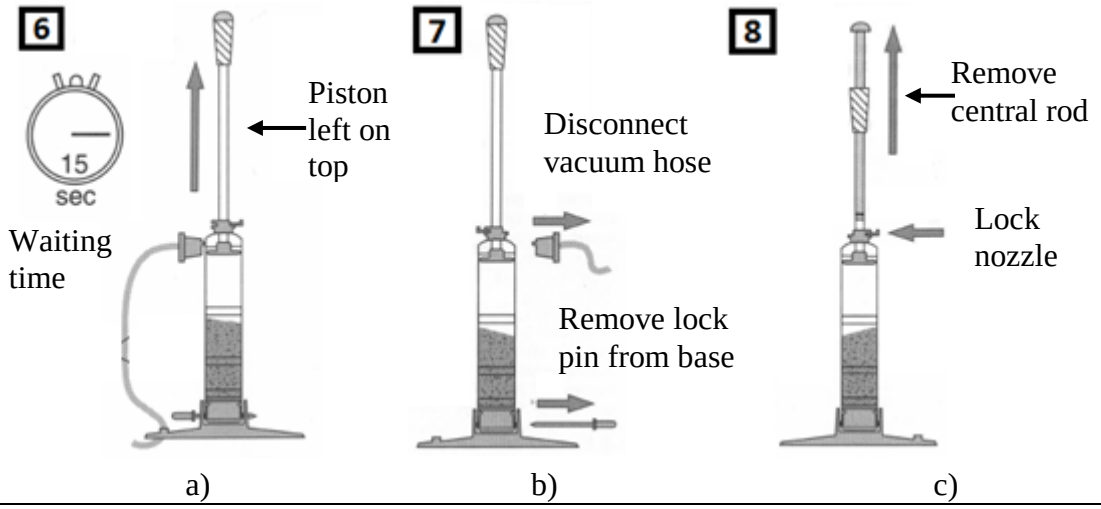

Figure 3.15 Cementing procedure, a) step 6, b) step 7, c) step 8 [250].

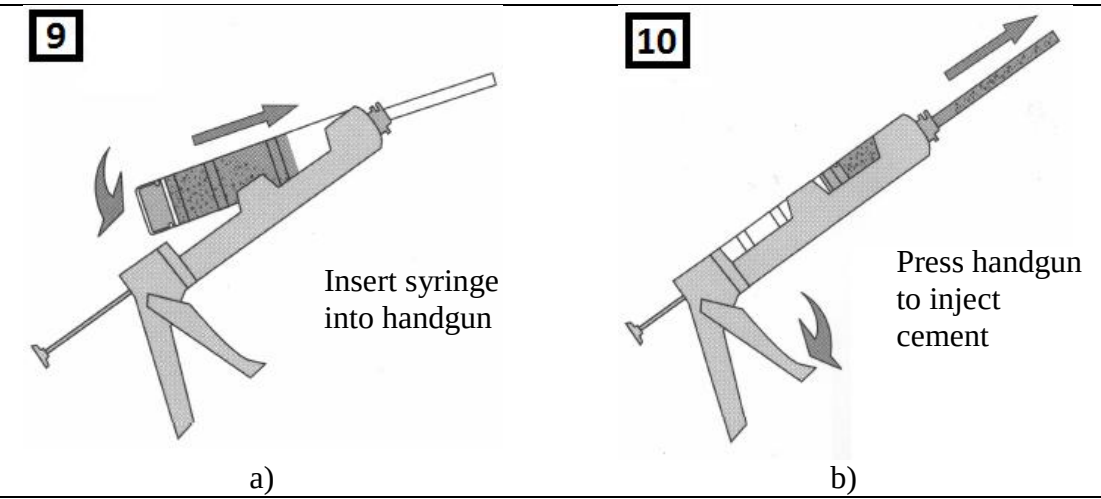

Figure 3.16 Cementing procedure, a) step 9, b) step 10 [250].

An approximate working time of about 6 minutes is available before the bone cement starts to harden. The preparation of cement and cementing process takes approximately 10 minutes, though the bone cement continues to cure for several hours. The recommended times associated with the preparation of the bone cement are given in Table 3.6.

Table 3.6 Times associated with the preparation of SmartSet® HV bone cement:

Action/Activity	Time
Vacuum mixing time	30 secs
Waiting and Minimum Extrusion time	20 secs
Working time	400 secs
Hardening time	125 secs
TOTAL TIME	605 secs

Prior to injecting the bone cement into the mould, the stem and mould were vertically aligned and clamped in the Instron 4507 Universal Material Testing machine, leaving enough space to inject the cement into the mould, as shown in Figure 3.17. The Instron machine limit-switch was setup at the level where the upper surface of the body of the stem was horizontally aligned with the upper edge of the steel mould. This also served as safety precaution to avoid damage to the specimens and the materials testing machine.

After injecting the cement into the mould, the stem was inserted into the mould at a rate of 2 mm/s (constant crosshead speed). The insertion of the stem was stopped by the automatic limit-switch of the Instron machine. Immediately, after this procedure, 12 steel rods, with diameter of 1.5mm, were inserted through the holes in the steel mould to provide space for thermocouples, one per hole for a total of 12 thermocouples.

When the cement was set, the steel rods were removed leaving behind 12 holes passing through the bone cement reaching the surface of the titanium stem. Figure 3.18a show two cemented specimens and Figure 3.18b shows a close up picture of a cemented titanium stem. A total of 12 T-Type thermocouples were inserted through the holes in the steel mould and the cement, one per hole, and embedded onto the surfaces of each stem in order to monitor the surface temperature of the stem.

The locations of the thermocouples were chosen to represent the proximal, middle, and distal zones of the stem; these were spaced 4 cm from each other, leaving a distance of 2 cm and 2.5 cm from the proximal and distal edges respectively, as shown in Figure 3.19. Low-temperature varnish was used to secure the thermocouples to the stem after cementing. A setting time of 24 hours was allowed for all the specimens.

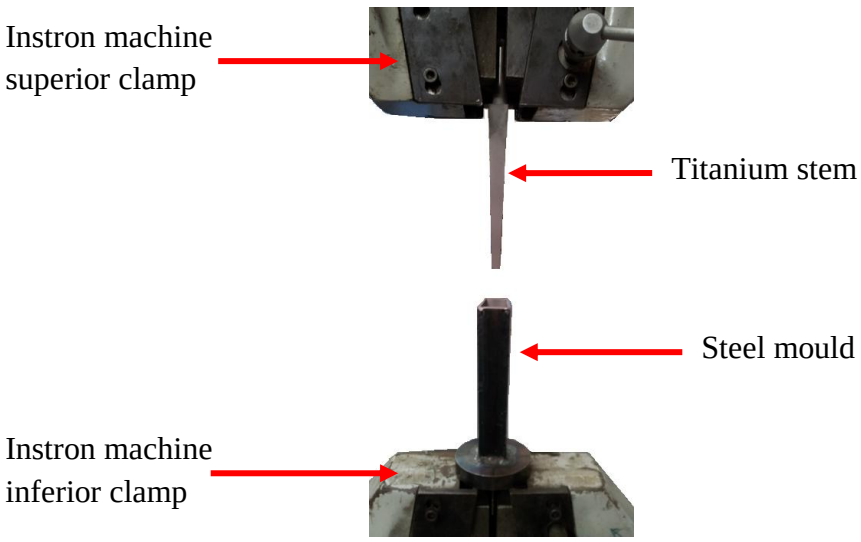

Figure 3.17 Specimen clamped ready for cementing.

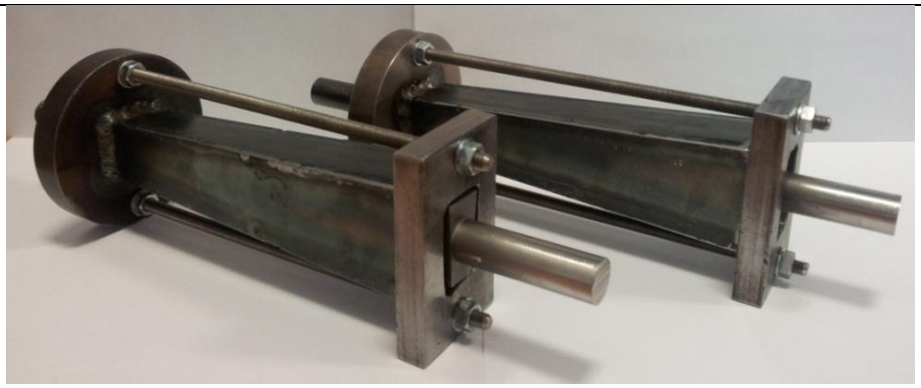

a)

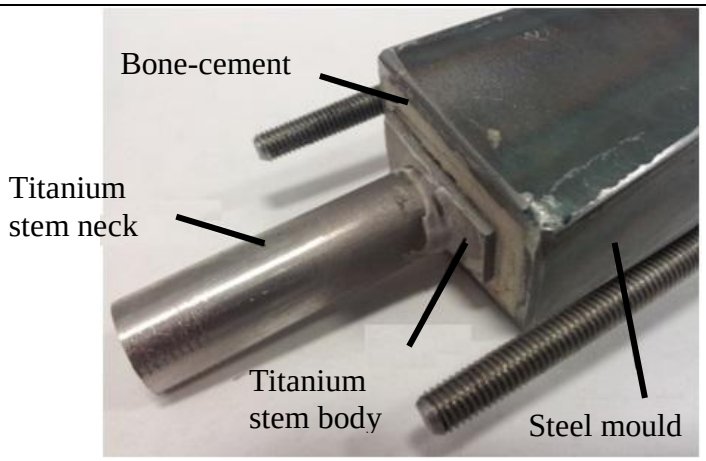

b)

Figure 3.18 a) Samples cemented in steel mould, b) sample close-up.

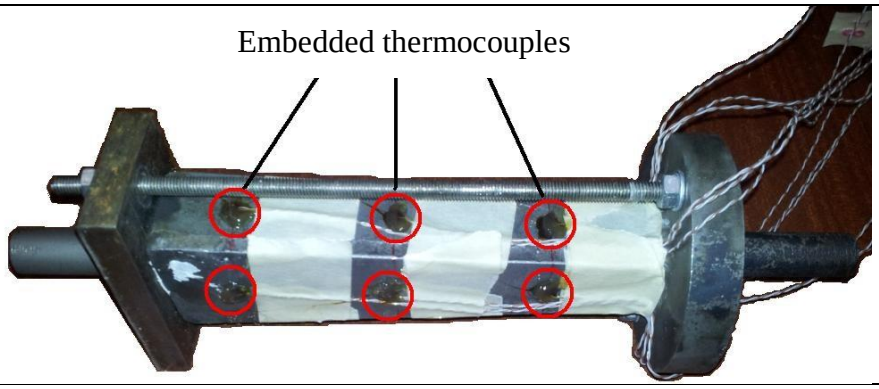

Figure 3.19 Specimen showing 6 of the 12 embedded thermocouples.

3.4.2.2 Cooling Stage Preparation

The experimental setup is shown in Figure 3.20. First, the stem-mould specimen was clamped (1) with the neck of the stem facing down (2) at a fixed height but not yet

immersed in the liquid nitrogen, LN_2. The thermocouples were connected to a 3530 Orion data logging system (3), and the data logger was set to read and record the temperature at two-second intervals. The container (4) was filled with approximately 2 litres of LN_2 to reach the desired level. To keep the level of LN_2 constant, two thermocouples (5) were attached inside the container at the specific height to monitor the level of LN_2. The container was covered with the lid with a funnel attached and the data logger started to capture data. The neck of the stem was immersed in the liquid Nitrogen (LN_2) through an opening in the polystyrene container lid.

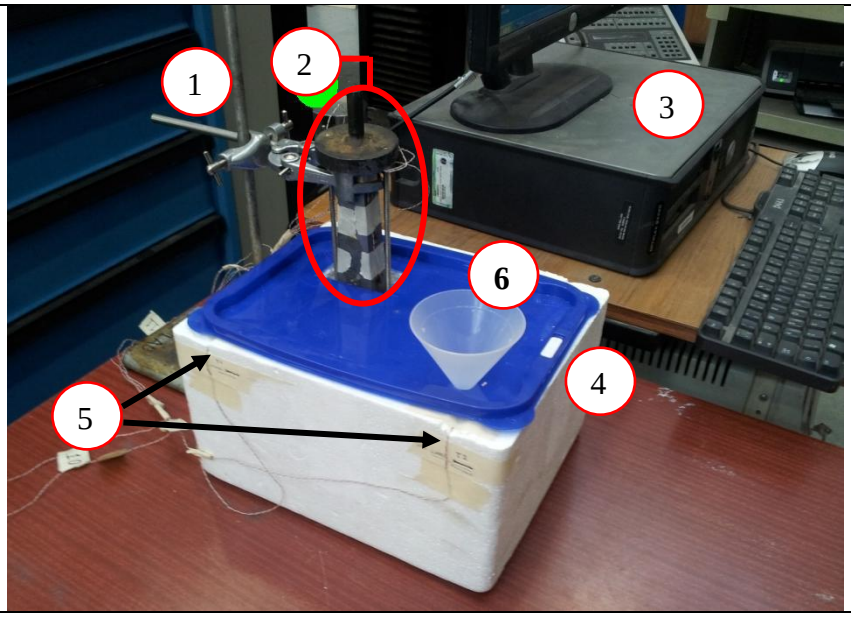

Figure 3.20 Setup for cooling procedure. 1) Clamp, 2) Specimen with cemented femoral stem, 3) Orion 3530 data logger and pc, 4) Polystyrene container with LN_2, 5) Thermocouples as level sensors of LN_2, (6) Funnel.

When the LN_2 level monitor showed the slightest change in temperature, LN_2 was carefully poured through another small opening with an attached funnel (6), thus the LN_2 level was kept constant. When the temperature of interest was reached, the specimen was removed from the LN_2 bath and clamped into the Instron machine.

The specimens were cooled to different temperatures of interest, and the time taken to reach the temperature was recorded during each cooling process. Table 3.7 shows the temperatures of interest at the proximal zone of the titanium stem for each cooling test of the first case scenario.

Table 3.7 Temperatures of interest for Scenario Study with Steel Mould

	Temperature (^{o}C)
Case 1	-76
Case 2	-58
Case 3	-49
Case 4	-40

3.4.2.3 Mechanical Loading Stage (Pull-out)

The time interval between removing the specimen from the LN_2 bath and clamping in the Instron machine was 60 seconds. Once the specimen was clamped as shown in Figure 3.21, the mechanical pull-out was activated.

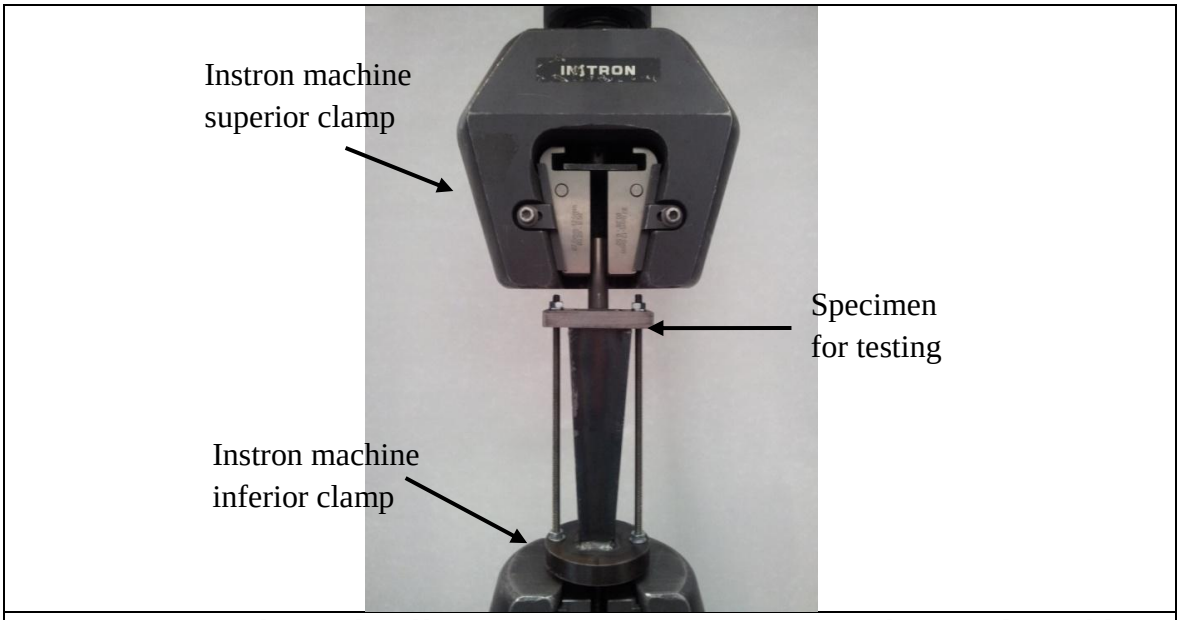

Figure 3.21 Mechanical pull-out test setup: stems cemented in steel mould.

The titanium stem was pulled from the mould at a constant crosshead speed of 0.5 mm/min until it was completely detached from the bone cement. Force-time data and the temperatures on the surface of the stem were continuously recorded from the Instron machine and Orion data logger while performing the pull-out test.

3.4.2.4 Steel Mould: Control Pull-Out Test

A total of 2 control tests were performed 24 hours after cementing the titanium stems. The average room temperature was 23°C for all tests. Figure 3.22 shows the average force plotted versus time from recorded forces during the control (room temperature) pull-out tests from the specimens. The average maximum force required to remove the titanium stem from the bone cement was 14.55 kN at a time of 350 seconds. The plot has linear behaviour from time 0 to 100 seconds, then the slope is much more steeper but keeps its linear behaviour to the end of the pull-out test. At the maximum force, the stem suddenly detaches from the cement mantle after δ_c = 2.9137 mm of displacement.

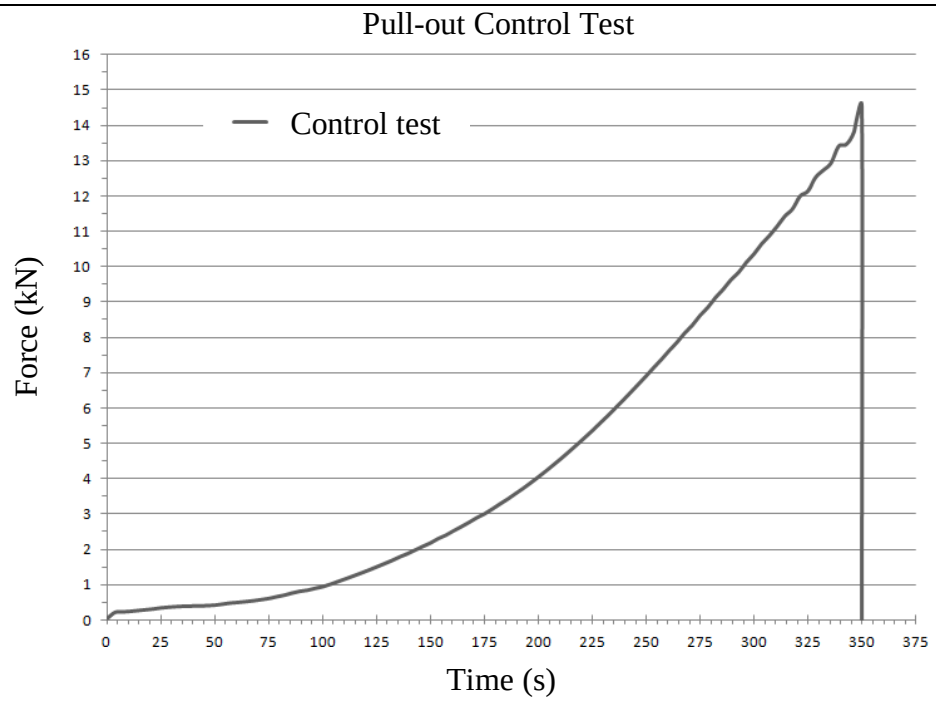

Figure 3.22 Characteristic behaviour of specimens pulled at room temperature.

The force-time plot from Figure 3.22 describes a brittle failure, similar to the observations of Di Franco et al. [197], and Khandaker et al. [251] on failure of composite materials. By visual inspection, no residues or particles of bone cement were

found on the surfaces of the titanium stem, and the cement mantle remained entirely in the steel mould.

From the force-time graph of the Control test, and knowing the Instron's crosshead speed of 0.5 mm/min, the strain energy was obtained using Equation 3.4, in order to ascertain how much mechanical energy was needed to break the stem-cement interface and therefore release the femoral stem from the cement mantle. Strain energy was calculated as the area under the force-displacement curve using the integral equation:

$$W = \int_0^x P(\delta) d\delta \qquad \text{(Equation 3.4)}$$

where W (J) is the strain energy, $P(\delta)$ is the force (kN) as function of displacement (mm), and $d\delta$ is the differential of displacement, evaluated in the interval from 0 to x, where x is the final displacement. The strain energy obtained was W_c = 13.24 J.

Moreover, in order to know the maximum strength of the interface between the stem and bone cement, when structurally failing in shear, the shear stress was calculated using the following equation:

$$\tau = \frac{P}{A_s} \qquad \text{(Equation 3.5)}$$

where τ (MPa) is the shear stress, P (N) is the maximum force obtained at the end of the test, and A_s (mm^2) is the area of the stem in contact with bone-cement. By substituting the maximum force obtained for the control test, P = 14.55 kN, and the area of the stem which is 6500 mm^{2}in Equation 3.4, the shear stress for the control test had a value of τ_c = 2.24 MPa.

3.5 Experimental Results of Cooled Steel Mould Specimens

A total of 8 tests were carried out, 2 for each temperature of interest. The readings of temperature from the 12 thermocouples and the force-time results from the pull-out test from each case study were normalized in a time interval. For time normalization, the start and end point of each test of every case study was known, thus an interval from 0 to 100% was set, where 0 represents the start and 100% represents the end of the stage, cooling or pull-out test depending on the case. The results were then averaged and plotted to be properly compared.

By visual inspection, the cement mantle remained completely in the steel mould, and no residue of bone-cement was found on the surfaces of the titanium stem. Figure 3.23a shows the titanium stem after being pulled-out from the cement mantle, Figures 3.23b and 3.23c show the cement mantle in the steel mould, and the titanium stem showing no residues on its surface respectively.

a)

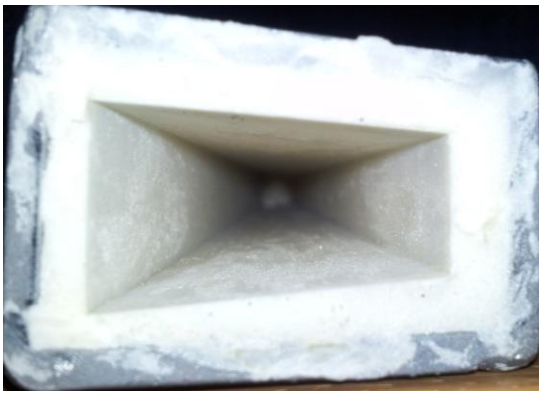

b)

c)

Figure 3.23 a) Titanium stem after pull-out test, b) cement mantle in steel mould, c) removed titanium stem.

Figures 3.24 to 3.27 show the results obtained for a) temperature and b) force, both plotted versus time, from the tests performed with the steel mould for the four cooling case studies at temperatures of interest: -76°C, -58°C, -49°C, and -40°C. The results of temperature are plotted from -80°C to 30°C on its Y axis, and the results of force are plotted from 0 kN to 10 kN in its Y axis. Both plots share the same time range in the X axis, depending on the case study showed in each figure, which corresponds from the end of the cooling stage to the end of the mechanical pull-out which is the failure of the bonding interface. The plots have markers numbered from 1 to 3, to distinguish the relevant intervals of time during the experimental tests, which are delimited by the solid vertical lines. The results of temperature and force are described respectively in the following two subsections.

3.5.1 Temperature Results

In the first instance, Figures 3.24a to 3.27a show the results of temperature vs time after the proximal thermocouple achieved the specific temperature of interest for each case study: -76°C, -58°C, -49°C, and -40°C respectively. Each plot represents the mean of four temperature readings from the four thermocouples positioned in a particular region of interest on the stem (proximal, middle, and distal), making a total of 12 thermocouples. As mentioned before, Y axis presents temperature values from -80°C to 30°C, and X axis corresponds to time units in seconds from the end of the cooling stage to the end of the pull-out test. The numbered markers, 1 to 3, distinguish relevant time interval zones in the experimental tests (delimited by solid vertical lines) in terms of temperature as follows:

Zone#1: Temperature of the specimen recorded while being clamped in the Instron machine.

Zone#2: Temperature readings of the specimen during the mechanical pull-out stage, linear behaviour of the force.

Zone#3: Temperature readings of the specimen during the mechanical pull-out stage, non-linear behaviour of the force.

The temperature plots from Figures 3.24a to 3.27a display the same trend in all case studies. Zone#1 starts from the time at which the proximal thermocouples detected the achievement of the temperature of interest: 300, 308, 178, and 194 seconds for the temperatures at -76°C, -58°C, -49°C, and -40°C respectively, and ended 60 seconds after, which was the start of the mechanical pull-out. At this zone, Zone#1, all case studies registered an increase in temperature in the proximal area after removing the specimens from the bath of LN_2, the approximate rates were of 13, 7.1, 7.8, and 0.2°C/min for each case study respectively. On the other hand, middle and distal thermocouples recorded a decrease of temperature in the same time interval of Zone#1. For case study 1 to case study 4, the rates in the middle zone were approximately of -4.7, -5.5, -6.8, and -7.4°C/min respectively; the registered rates in the distal zone were approximately of -6, -4.1, -4.8, and -3.9°C/min for each case study respectively.

In the time interval of Zone#2 from Figures 3.24a to 3.27a, the proximal zone of the titanium stem continued to warm up at an approximate rate of 8, 6.9, 6.3, and 4.5°C/min for case study 1 to case study 4 respectively. Compared to the Zone#1, it was observed that the temperature registered from the thermocouples at middle zone of the stem started to stabilize, and the rate of change in temperature decreased to values of approximately 1.1, -0.2, -0.3, and -1.1°C/min for each case study respectively. On the other hand, the temperature readings at the distal area of the stem showed that temperature at that area continued to decrease at a rate of -1.4, -1.7, -1.9, and -2.2°C/min for case study 1 to case study 4 respectively.

In relation to Zone#3, Figures 3.24a to 3.27a showed that proximal and middle temperature readings of the stem were warming up for all case studies. The approximate rates were of 6.7, 5.3, 4.9, and 6.1°C/min in the proximal zone and of 2.5, 2, 1.5, and 2.1°C/min for the middle zone for case study 1 to case study 4 respectively. The distal zone continued to cool down until the end of the mechanical pull-out stage at an approximate rate of -0.2, -0.1, -0.4, and -0.9°C/min for each case study respectively.

In general, after removing the specimen from the LN_2 bath and until the end of the pull-out tests, it was observed from Figures 3.24a to 3.27a that the temperature of the stem in the proximal zone gradually increased at an average rate of approximately 9.2, 6.4, 6.3, and 3.6 °C/min respectively for each case study. Whereas the middle zone

of the femoral stem registered a decrease in temperature at an average rate of approximately 0.4, 1.2, 1.9, and 2.2 °C/min for each case study respectively. Temperature at the distal zones continued to decrease at a rate of approximately 1.9, 2, 2.4, and 2.3°C/min for each case study respectively.

3.5.2 Force Results

Figures 3.24b to 3.27b show the results of the force obtained from the mechanical pull-out tests performed with the steel mould for the four cooling case studies at temperatures of interest: -76°C, -58°C, -49°C, and -40°C. The Y axis presents the units of force from 0 kN to 10 kN, and the X axis represents the units of time in seconds whose limits are the same as for the temperature plots, starting from the achievement of the temperature of interest at the proximal area to the end of the mechanical pull-out with the release of the femoral stem from the cement mantle. The circled numbers (1 to 3) from the plots in Figures 3.24b to 3.27b, mark relevant time interval zones from the mechanical pull-out test (delimited by solid vertical lines), and they are described as follows:

Zone#1: End of cooling - clamping interval - mechanical pull-out starts.

Zone#2: Linear region and sudden reduction in force.

Zone#3: Non-linear region with second increase in force until failure of the interface and complete release of the stem.

Upon inspection of the Figures 3.24b to 3.27b, it can be seen that all four case studies displayed similar characteristics in the obtained force-time curves. Zone#1 represents the time taken to clamp the specimen to be tested in the Instron machine, and ends at the moment in which the mechanical pull-out started. The behaviour of the force plot consists of two distinct stages. In the first stage (Zone #2) the force increases almost linearly until it reaches a maximum value after which it rapidly drops, signifying a brittle-type failure in the interface between the titanium stem and the bone cement; a cracking sound was heard at this point in the tests but the stem was not released at that moment. The second stage (Zone #3) is characterized by a non-linear force-time curve

at which the force increases to a maximum point and then decreases until the stem-cement interface completely fails and the stem is released from the cement mantle (Zone #3). This mechanical behaviour is similar to that found by Di Franco et al. [197] while studying thermally treated hybrid joints, where the adhesive joint was found to fail in the elastic zone, and the mechanical joint failed plastically.

It was noticed that from the start of the mechanical pull-out test to the moment of the maximum force was reached, the temperature in the proximal region was warmer approximately with an increment of 24^{o}C and 19^{o}C for the case studies at -76^{o}C and -58^{o}C respectively. On the other hand, case studies at -49^{o}C and -40^{o}C were approximately 15^{o}C and 14^{o}C warmer at the moment the maximum force was reached, respectively.

The maximum force measured in the linear zone (6.32kN, 8.85kN, 10.45kN, 10.04kN) increases in value as the temperature of interest at the proximal thermocouple increases, that is -76^{o}C, -58^{o}C, -49^{o}C, and -40^{o}C respectively. For Case 1, the maximum force to remove the femoral stem, 6.32kN, was lower than the control force by 56.5%. Similarly, other case studies (-58^{o}C, -49^{o}C, and -40^{o}C) also showed a reduction in force to remove the prosthesis from the cement mantle compared with the control test by 39%, 28%, and 31% respectively. Moreover, the release force was found to be approximately 40% higher when the temperature of interest was -40^{o}C compared to the force required at -76^{o}C, the lowest temperature used in the study. In addition, a change in slope was observed at a particular point in time of the experiment in all case studies, at time 400, 390, 275, and 270 seconds for Case 1 to Case 4 respectively. It was observed that the proximal temperature had warmed up approximately 5^{o}C in Case1 and Case 3 whereas Case 2 and Case 4 registered an increment of approximately 2^{o}C at the moment of slope change.

The maximum force reached in the non-linear region was, in general, less than that in the linear region, 45% less for Case 2, 38.8% for Case 3 and 4.32% for Case 4. Particularly in Case 1, the maximum force reached during the non-linear behaviour was 0.5% higher than the maximum force during the linear stage. Comparing the resulting maximum force at the linear zone (Zone #2) between the case studies, there is a

maximum difference of 39% between the forces. The difference in the maximum force at the non-linear zone (Zone #3) between the case studies was 24.4%.

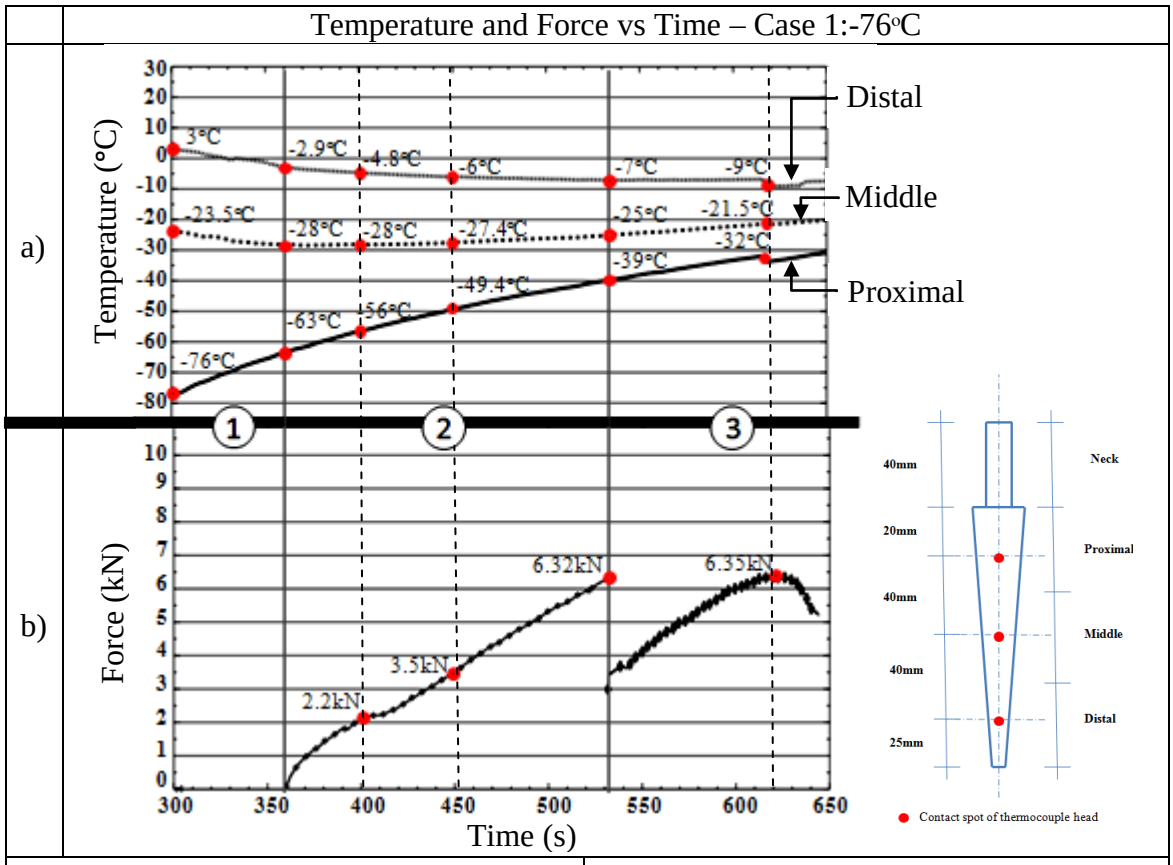

Figure 3.24 Experimental results for case study 1 at a temperature of -76°C plotted after removing the specimen from the LN_2 bath. a) Temperature readings in the three zones of interest of the stem: proximal, middle, and distal. b) Pull-out test: force vs time; different stages in the experimental tests are marked as follows: 1) End of cooling, clamping interval, mechanical pull-out starts, 2) Linear region and sudden drop in force, 3) Non-linear region with second rise in force and complete release of the stem.

The displacement also varied between experiments. The control test at room temperature had a displacement of δ_c=2.92 mm at the moment of failure, the cooled cases had a total displacement of δ_1=1.43 mm, δ_2=1.24 mm, δ_3=1.22 mm, and

δ_4=1.45 mm respectively. The extension at the elastic region in each cooling case represented a displacement of 49%, 42.5%, 42%, and 50% compared to the control test.

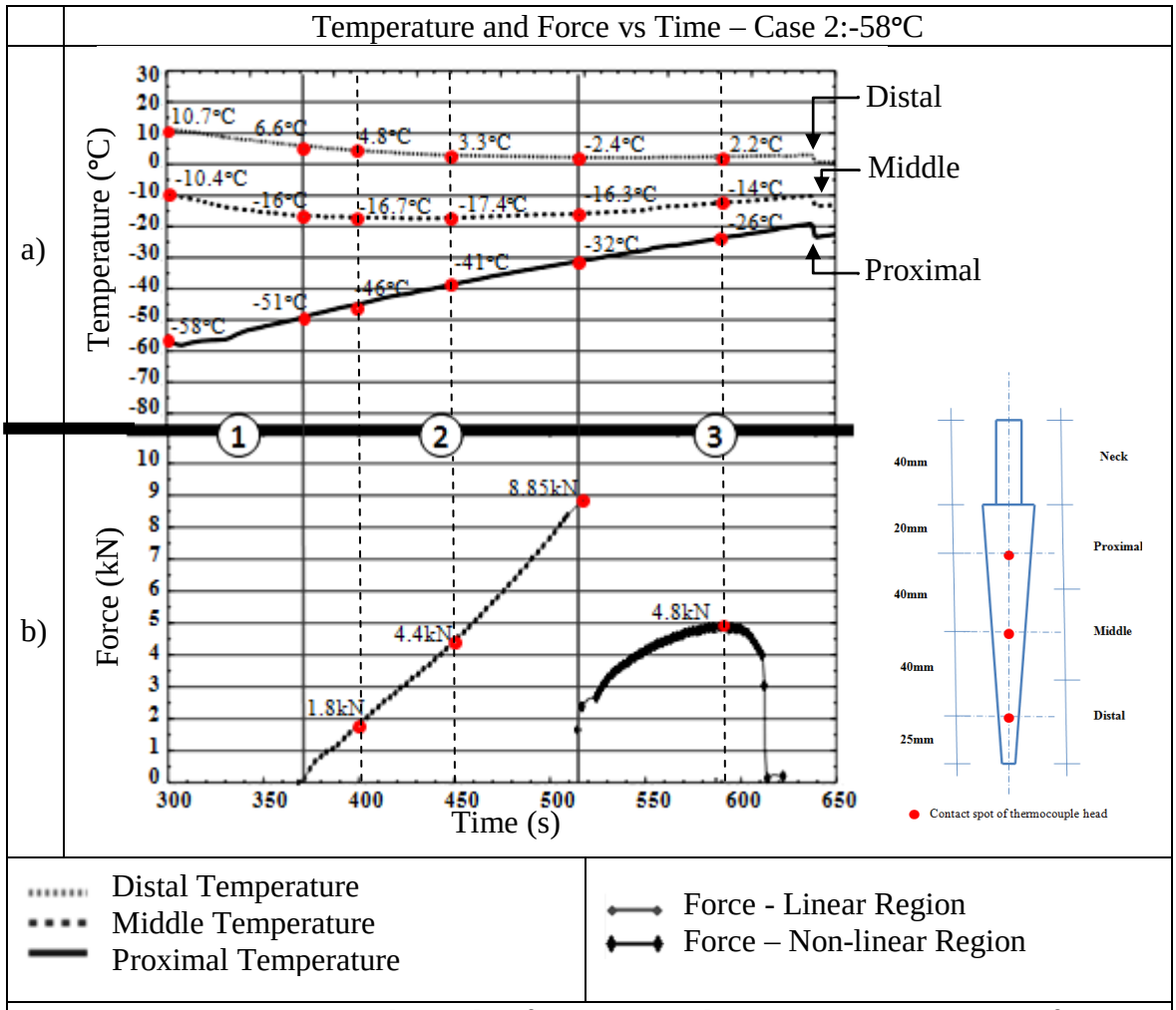

Figure 3.25 Experimental results for case study 2 at a temperature of -58°C plotted after removing the specimen from the LN_2 bath. a) Temperature readings in the three zones of interest of the stem: proximal, middle, and distal. b) Pull-out test: force vs time; different stages in the experimental tests are marked as follows: 1) End of cooling, clamping interval, mechanical pull-out starts, 2) Linear region and sudden drop in force, 3) Non-linear region with second rise in force and complete release of the stem.

Regarding the maximum shear stress, Case 1 showed a value of τ_1= 0.97 Mpa, a reduction of 56.7% compared to the control test. The rest of the cooling cases resulted in reductions of 39%, 28%, and 31% of the maximum shear respectively compared to the control test.

The amount of mechanical energy required to break the bonding interface between the prosthesis and the bone cement was calculated with the total strain energy. The case studies at the temperatures of interest of -40°C and -49°C required approximately 90% of the energy needed to pull out the titanium stem at ambient temperature, which had a value of W_c = 13.24 J. Case 1 and Case 2 required less energy to release the stem from the cement mantle, 75% and 65% respectively, compared to the control test.

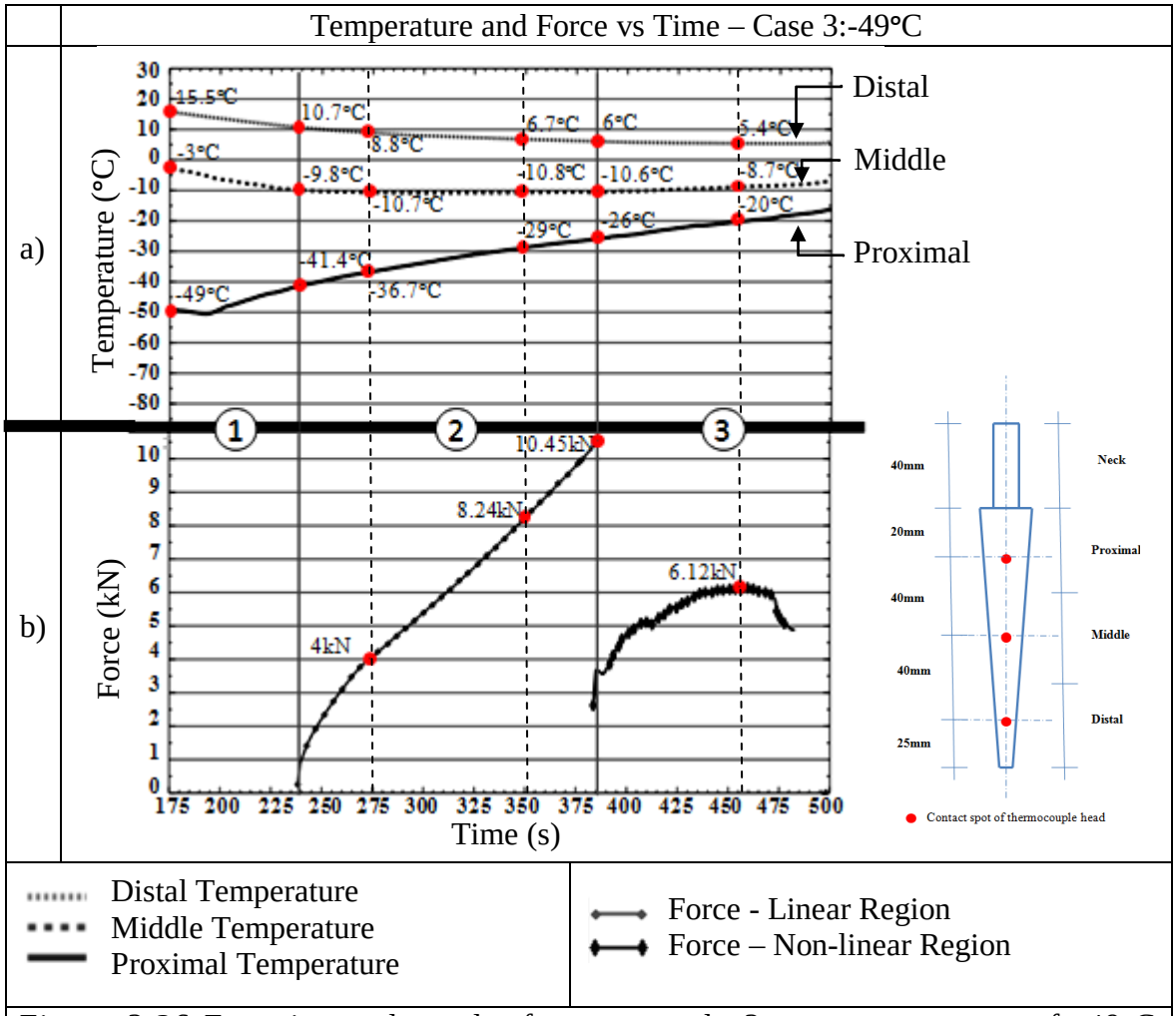

Figure 3.26 Experimental results for case study 3 at a temperature of -49°C plotted after removing the specimen from the LN_2 bath. a) Temperature readings in the three zones of interest of the stem: proximal, middle, and distal. b) Pull-out test: force vs time; different stages in the experimental tests are marked as follows: 1) End of cooling, clamping interval, mechanical pull-out starts, 2) Linear region and sudden drop in force, 3) Non-linear region with second rise in force and complete release of the stem.

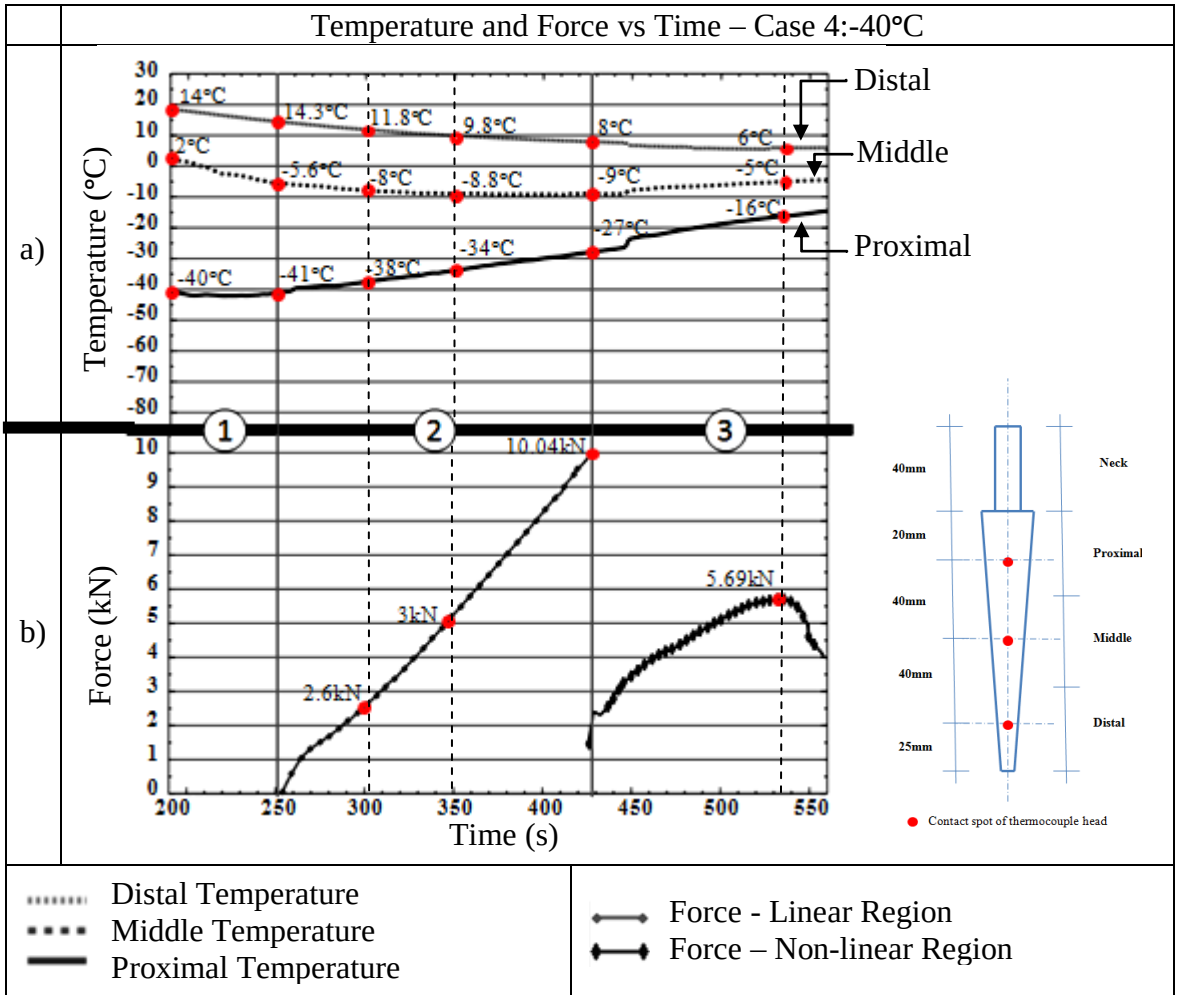

Figure 3.27 Experimental results for case study 4 at a temperature of -40°C plotted after removing the specimen from the LN_2 bath. a) Temperature readings in the three zones of interest of the stem: proximal, middle, and distal. b) Pull-out test: force vs time; different stages in the experimental tests are marked as follows: 1) End of cooling, clamping interval, mechanical pull-out starts, 2) Linear region and sudden drop in force, 3) Non-linear region with second rise in force and complete release of the stem.

The following chapter presents the second case scenario by applying the same experimental procedure in two different geometries, cylindrical and femur-like, made of composite materials that replicate the mechanical and thermal properties of real human femur.

Chapter 4
Impact of Temperature on the Release Force of a Titanium Stem Cemented in Composite Bone

4.1 Introduction

The previous chapter introduced the proposed methodology as a new alternative to remove a femoral stem during RTHA by means of applying low temperature at the neck of the stem before mechanically pulling it out from the steel mould where it was cemented. The results demonstrated that the new methodology is effective by showing a considerable reduction of the force needed to remove a cemented femoral stem by 56.5%, compared with the control test.

As a second scenario, this chapter studies the effects of the proposed methodology in a closer approach to a real case where a titanium stem is cemented in materials with bone-like thermal and mechanical properties, as is the case of Sawbones® composite bones. Two cases are studied with two different geometries, first by implanting the stem in composite cylinders, and second, by implanting the stem in composite femurs. The studied temperatures of interest were: -76°C, -49°C, and -40°C for the composite cylinders, and -76°C and -40°C for the composite femurs.

4.2 Impact of Temperature on the Release Force of a Titanium Stem Cemented in Cylindrical Composite

As first instance, experiments were performed to investigate the force required to release a titanium femoral stem fixed in bone-cement and composite cylinders manufactured from Sawbones®. The necks of the stems cooled until the proximal zone of the titanium stem achieved the cooling temperature of interest (-76°C, -49°C, and -40°C for each case study respectively) by immersing them in liquid nitrogen (LN_2)

after which pull-out tests were performed on them; control tests at ambient temperature were carried out and results were compared.

4.2.1 Materials Used for Composite Cylinder Specimens

4.2.1.1 The Titanium Femoral Stem

As described in Chapter 3, customized Ti-6Al-4V stems were used for the experimental work presented in this chapter. To obtain proper anchoring and a strong implant-cement interface, the same sandblasting procedure was employed as described in previous chapter to generate a matt finish and to clean the surface of the stem; Figure 3.5a from section 3.3.1.2 shows the manufactured titanium stem.

4.2.1.2 Composite Cylinders

In order to implant the femoral stems with bone-cement, fourth generation Sawbones® composite cylinders of 40 mm outer diameter and 150 mm in length were used to reproduce both cortical and cancellous bone; the cortical bone is a 3 mm shell (cylindrical wall) made of short fibre filled epoxy. The cylinder is filled with high-density polyurethane foam of 320 kg/m^3 to mimic healthy cancellous bone. Two samples of the composite cylinders are shown in Figure 4.1.

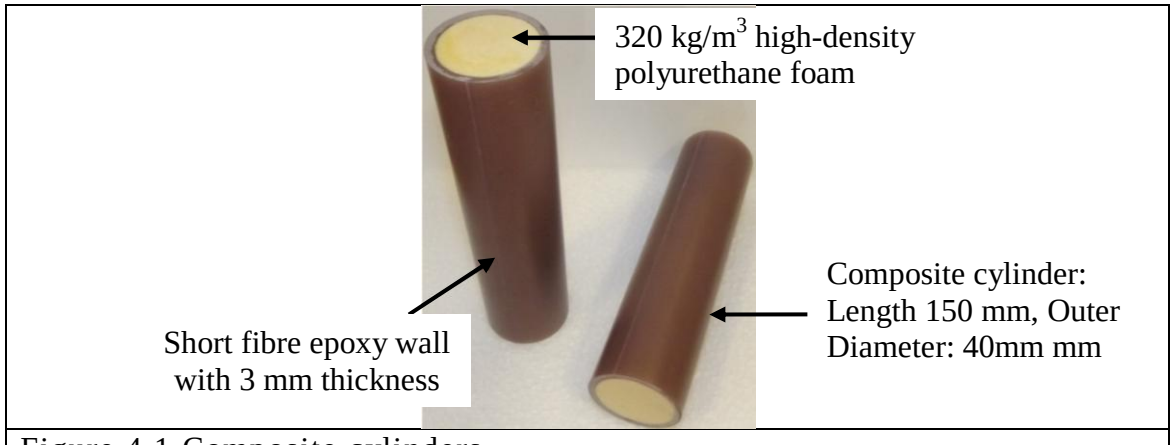

Figure 4.1 Composite cylinders.

The preparation of the composite cylinders for testing started with the making of a centred hole of 15 mm in diameter and 135 mm in depth. In order to make the hole, the composite cylinder was fastened in a lathe's chuck as shown in Figure 4.2a. The tailstock of the lathe was used for drilling, with the aid of a drill chuck attachment and a drill bit of Ø15 mm by 250 mm. The hole was drilled to the desired depth of 135 mm, allowing a remaining mantle of cancellous bone of 15 mm thick at the bottom. Figure 4.2a shows two cylinders after drilling the centre hole. The following step in the preparation was to reshape the hole to fit the femoral stem by drawing a centred trapezoidal guide to limit the boundaries of the expansion of the canal as shown in Figure 4.2b.

Once the trapezoidal guide was drawn over the surface where the hole was drilled, the expansion of the "medullary canal" in the cancellous bone was carried out with the aid of two custom-made steel broaches as shown in Figure 4.3a. To guarantee a consistent trapezoidal shape of the canal the first broach (Broach no. 1), had the same shape and dimensions of the titanium stem, see Figure 4.3b. The length of broach no.1 was 100 mm, shorter than the titanium stem by 25 mm to avoid damage of the cylinder at the bottom while broaching the canal. In order to start reshaping the canal, the cylinder was vertically fastened in a clamp with the hole facing up. The first broach was vertically aligned with the centre line of the hole, and proceeded to broach into the circular canal to create the double tapered shape.

Once the canal was reshaped, a 6 mm thicker broach (Broach no.2 shown in Figure 4.3c) was used, with objective of widening the canal by 3 mm in all directions, except the depth of the canal. This expansion allowed a cement mantle with a minimum thickness of 3 mm for good anchoring of the titanium stem in the composite cylinder as discussed in Chapter 3 [97, 247, 248]. The expansion was undertaken by vertically aligning the Broach no.2 with the centre line of the cylinder, and proceeded to broach into the trapezoidal canal.

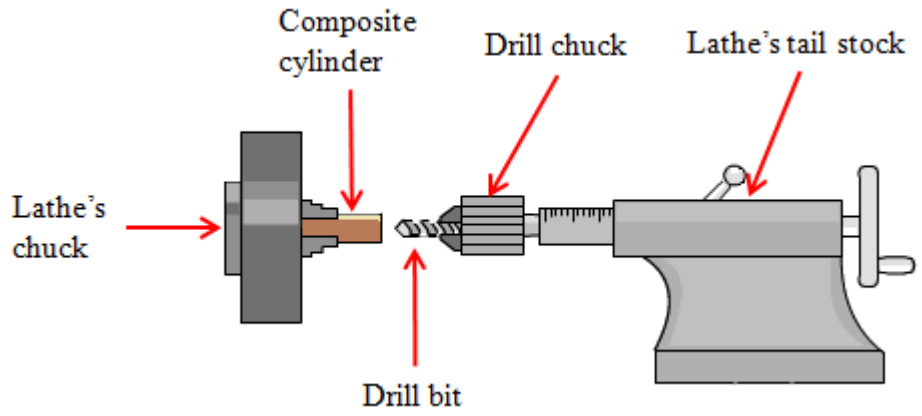

a)

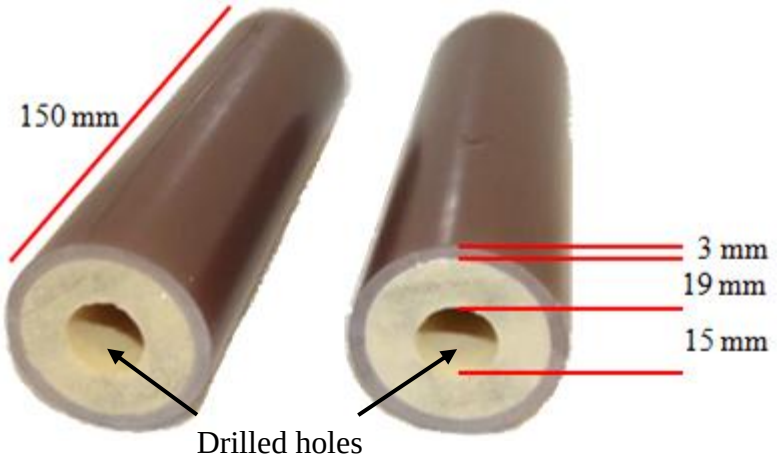

b)

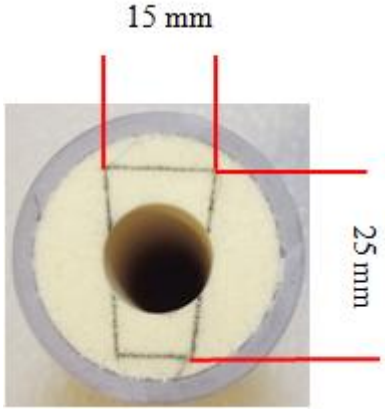

c)

Figure 4.2 Composite cylinders: a) drilling of centred hole, b) drilled holes Ø15 mm, b) marks of trapezoidal shape to expand the "medullary canal".

a)

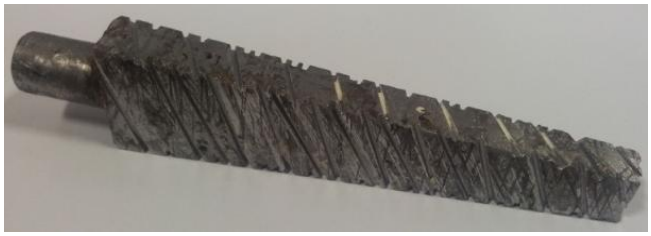

b)

c)

Figure 4.3 Custom made steel broaches to expand the "medullary canal", b) Broach no.1same dimensions as titanium stem but shorter in length by 20 mm, b) Broach no.2 thicker by 6 mm.

To facilitate the insertion of 12 T-Type quick response thermocouples through the cylinder to record temperatures at strategic positions on the surface of the titanium stems, a total of 12 holes of 2 mm diameter were drilled in the cylinders (one per thermocouple). The distances between the holes were at 20 mm, 60 mm, and 100 mm from the upper surface as shown in Figure 4.4. The positions correspond to the middle of the three zones of interest on the stem (proximal, middle, distal zones).

Figure 4.4a shows the cylinder clamped in the power drill with the drill bit pointing perpendicularly to one of the inner surfaces of the trapezoidal medullary canal. A controlled feed speed was used in order to avoid hairline fractures in the cylindrical cortical shell. Figure 4.4b shows the distances between 3 of the 12 holes drilled in the cylinder.

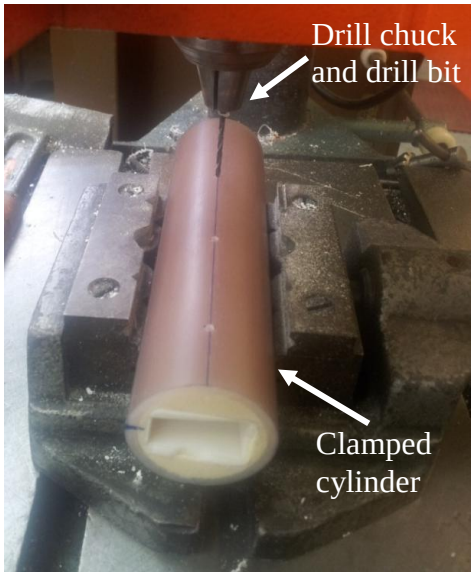

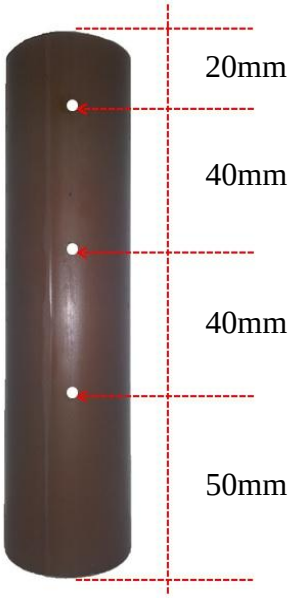

a) b)

Figure 4.4 Composite cylinder with 2 mm drilled holes for thermocouples. a) composite cylinder clamped in drill, b) distances between 3 drilled holes.

4.2.1.3 Bone Cement – Polymethyl-Methacrylate (PMMA), T-Type Thermocouples, and Liquid Nitrogen (NL_2)

For these experiments, the same type bone cement was used (SmartSet HV), as well as the type of thermocouples (T-Type) and liquid nitrogen as cooling agent, as previously described in Sections 3.3.1.3 to 3.3.1.5 from Chapter 3.

4.2.2 Experimental Methodology for Composite Cylinder Specimens

4.2.2.1 Cementing Procedure and Instrumentation of Composite Cylinders

Once the cement was prepared, the stems were cemented in the composite cylinders with the aid of a clamp designed to hold the specimen firmly. Figure 4.5 shows the bottom and top plates of the clamp.

The bottom plate was fixed to the Instron's moving crosshead with three M10 screws. Both plates featured a circular pocket to help centring and holding the cylinder.

Four M10 threaded rods were used to locate and adjust the top plate, which was tightened with four nuts. The drawings showing specific dimensions of the plates can be found in Appendices A3 and A4. The top plate kept the cement in place while the stem was being pushed in through the rectangular opening. Figure 4.6 shows the clamped cylinder and titanium stem ready for the bone cement to be injected.

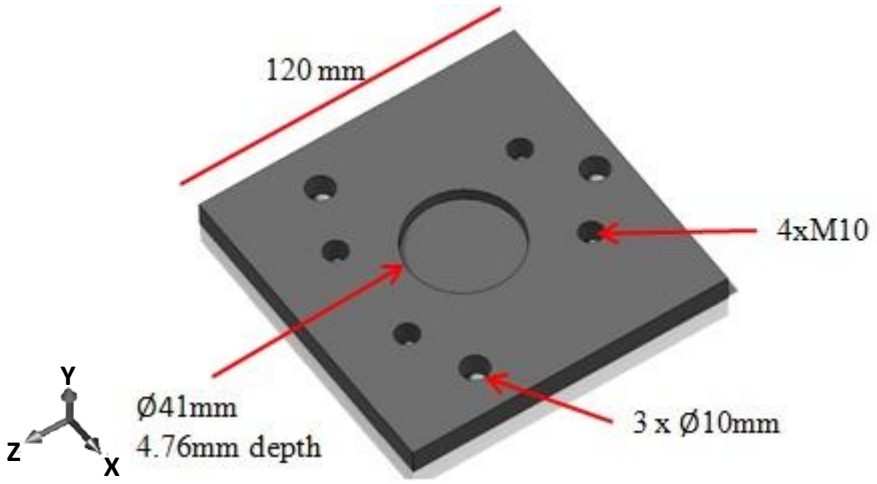

a)

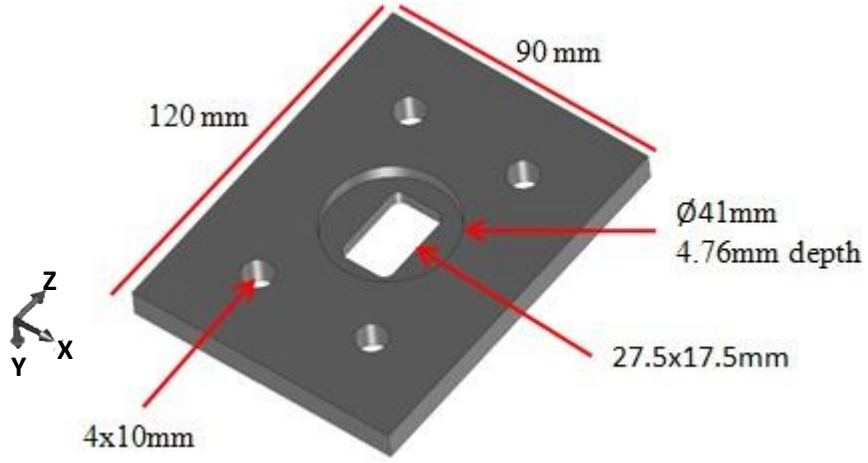

b)

Figure 4.5 Parts of the clamp used in the experiments: a) bottom plate, b) top plate (pictured upside-down). Geometry in SOLIDWORKS® 2010.

One pack of bone-cement (SmartSet® CEMVAC® [250]) of 40g was sufficient for the cementing of each specimen, and the bone cement was prepared according to the

instruction leaflet from DePuy® as shown in Table 3.6 from the previous chapter, in Section 3.3.2.1.

Before proceeding with the cementing, the stem and cylinder were vertically aligned while clamped in the Instron machine as shown in Figure 4.6, leaving enough space for the cement to be injected into the medullary canal. Immediately after injecting the cement into the cylinder, the stem was inserted at a constant crosshead speed of 2 mm/s and automatically stopped by a limit-switch when the body of the stem was completely inserted into the "medullary canal".

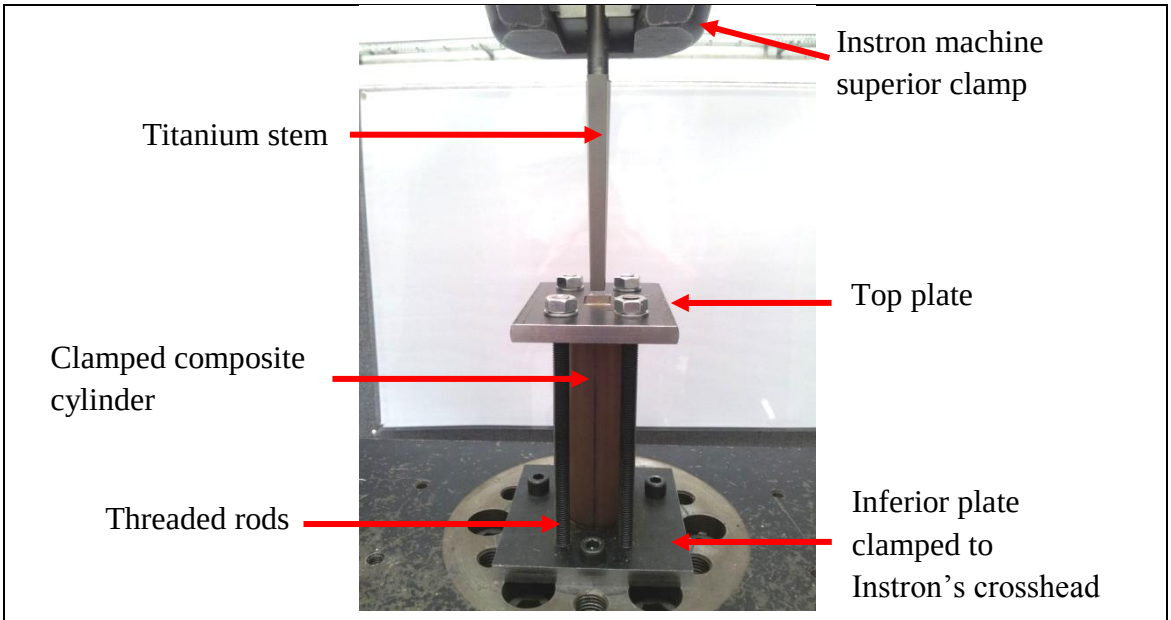

Figure 4.6 Clamped cylinder and titanium stem ready for cementing procedure.

Figure 4.7a shows the specimen with 1.5 mm steel rods inserted through the drilled holes in the composite cylinder while the specimen was held in the Instron machine waiting for the cement to set. After 15 minutes of setting, the specimen was removed from the clamping system, and the steel rods were removed leaving behind holes passing through the specimen walls. Figure 4.7b shows a cemented titanium stem for a control pull-out test, with no thermocouples attached.

As part of the instrumentation, a total of 12 T-Type thermocouples (1 per hole) were inserted through the small holes in the specimens, and secured with low

temperature varnish so that their tips could make contact with the surface of the stem and monitor the temperature on it. Figure 4.8 shows the specimen with the embedded thermocouples. All specimens were allowed to set for 24 hours before being tested experimentally.

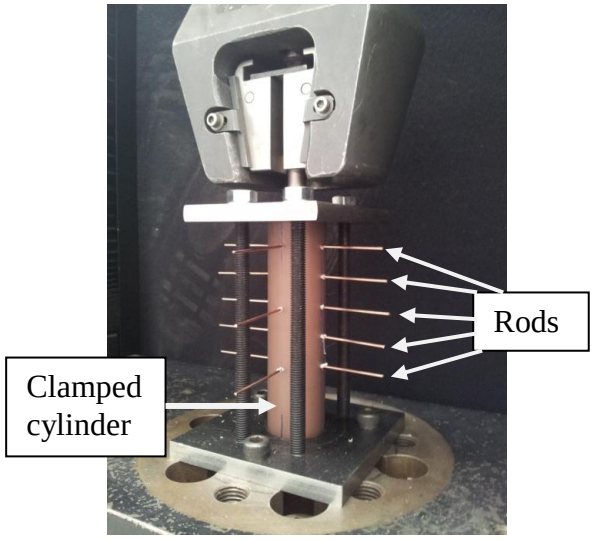

a)

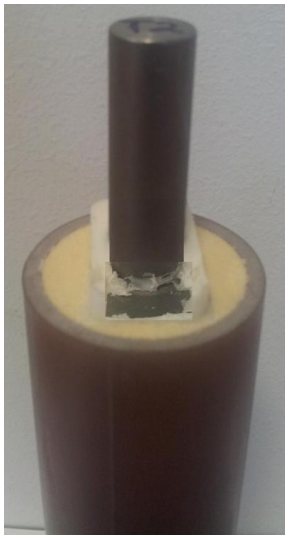

b)

Figure 4.7 a) Clamped cylinder with inserted 1.5 mm rods for instrumentation and b) titanium stem cemented in composite cylinder (sample).

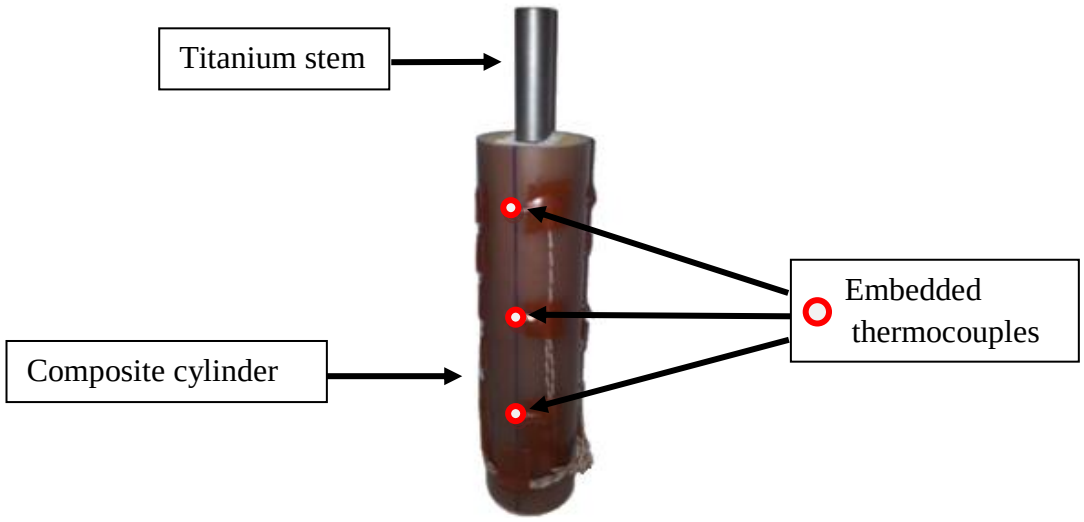

Figure 4.8 Titanium stem cemented in composite cylinder showing 3 of the 12 embedded thermocouples (sample).

4.2.2.2 Cooling Stage Preparation: Composite Cylinders

Figure 4.9 shows the stem-cylinder specimen clamped (1) with the neck of the stem facing down (2) at a fixed height above a polystyrene container (4) filled with Liquid Nitrogen (LN_2). The neck of the stem was then lowered through an opening in the lid of the container until it was immersed in the LN_2. To prevent While performing the cooling, the thermocouples were connected to an Orion 3530 logging system (3), and the data was recorded at two-second intervals. Two thermocouples (5) were attached through the lid at a specific height to monitor the level of LN_2 and keep it constant. When this level monitor showed the smallest change in temperature, LN_2 was poured into the container through an attached funnel (6) to ensure a constant level of LN_2 in the container, see Figure 4.9.

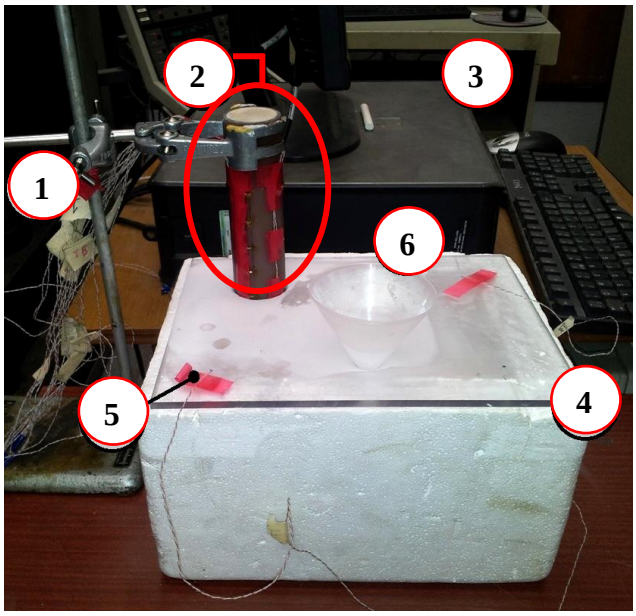

Figure 4.9 Setup for cooling procedure.1) Clamp, 2) Cemented stem, 3) Orion 3530 data logger, 4) Polystyrene container for LN_2, 5) Thermocouples as level sensors of LN_2, 6) Funnel.

The specimen was removed from the LN_2 bath immediately the proximal thermocouples reached the required temperature of interest for the test and clamped in the Instron machine after which the pull-out test procedure was followed.

The Table 4.1 shows the temperatures of interest at the proximal zone of the femoral titanium stem for the case studies performed in the present scenario study performed with composite cylinders.

Table 4.1 Temperatures of Interest for Scenario Study with Composite Cylinders

	Temperature (°C)
Case1	-76
Case 2	-49
Case 3	-40

4.2.2.3 Mechanical Loading Stage (Pull-out): Composite Cylinders

Once the cooling procedure was finished, the specimens immediately removed from the LN2 bath, and proceeded to be clamped in the Instron materials testing machine, were the femoral stem was pulled from the cylinder at a constant crosshead speed rate of 0.5 mm/min until it became completely detached from the bone cement. Force-time and stem surface temperature data were continuously recorded from the Instron machine and Orion data logger during each pull-out test (see Figure 4.10).

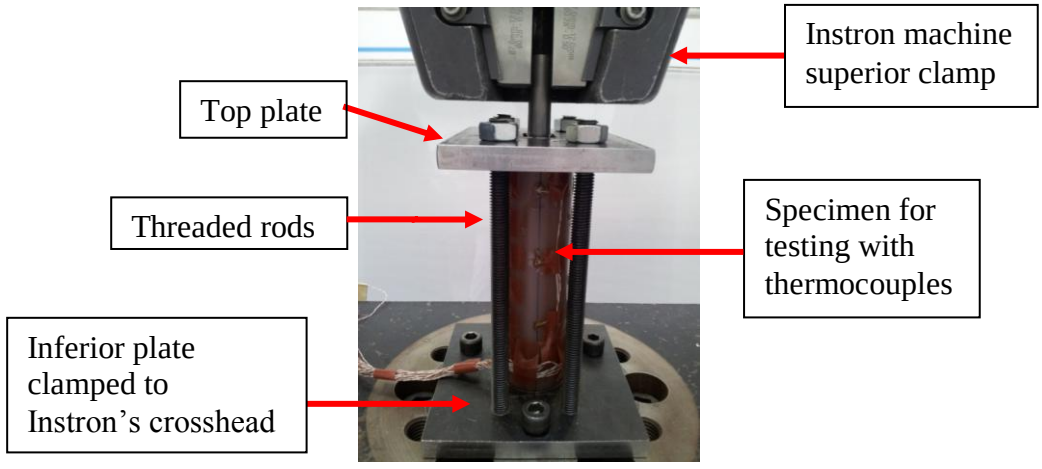

Figure 4.10 Mechanical pull-out test setup of a titanium stem cemented in composite cylinder.

4.2.2.4 Composite Cylinders: Control Pull-Out Test

Figures 4.11a and 4.11b show a removed titanium stem specimen and the cement mantle in the composite cylinder respectively. By visual inspection, the cement mantle remained completely in the cylinder, and no residue of bone-cement was found on the surfaces of the titanium stem. The porous characteristics of the simulated cancellous bone in the composite cylinder allowed the bone-cement to have a strong bond with the cylinder itself.

The control tests showed a maximum force of 13.98 kN at the moment the interface failed, and the stem was released from the cement mantle, with average time of 204.6 seconds and displacement of δ_{c1} = 1.71 mm. Figure 4.12 shows an averaged force-time curve from the control pull-out tests. The interface failed at the maximum force with the stem suddenly coming out of the cement mantle. The linear increase of the force and the abrupt drop in the force indicates a brittle failure of the bonded interface between the titanium stem and the bone-cement. This behaviour is similar to that reported in the literature regarding adhered composite joints [195, 197, 252].

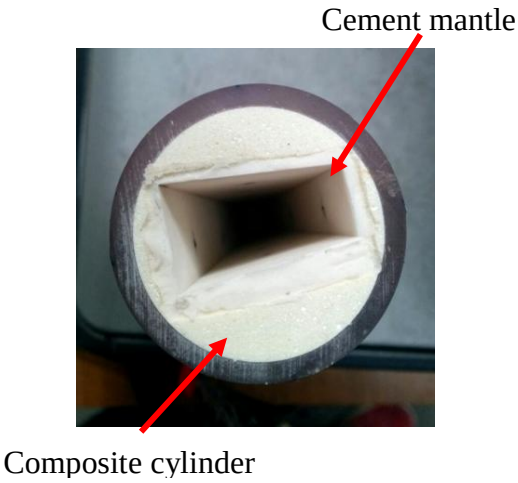

a) b)

Figure 4.11 a) Removed titanium stem, b) cement mantle in composite cylinder.

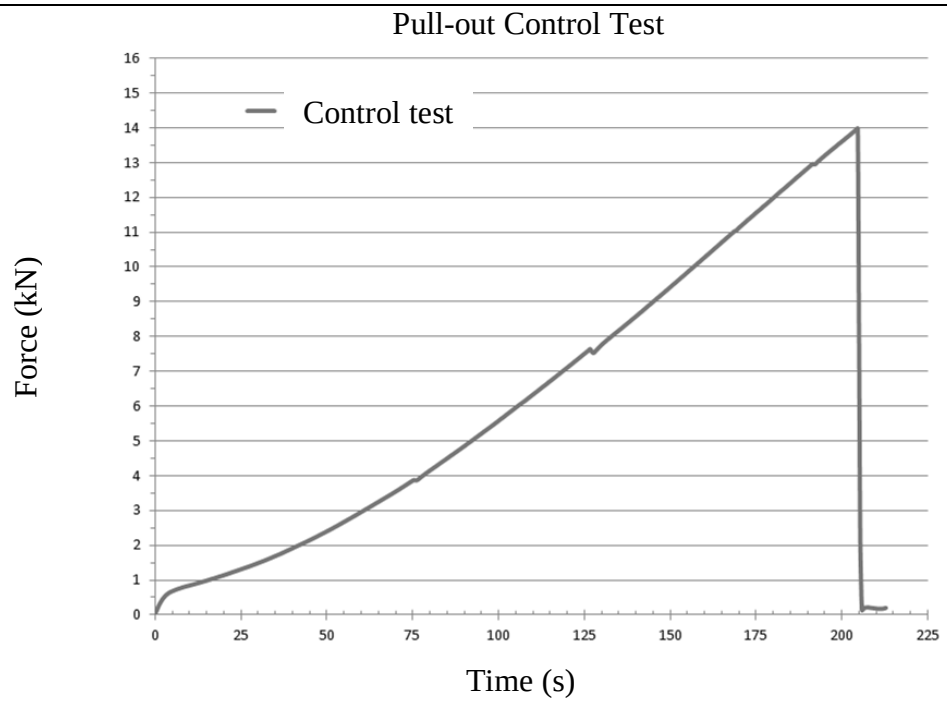

Figure 4.12 Characteristic behaviour of specimens pulled at room temperature, showing a brittle behaviour.

The maximum shear stress at failure had a value of τ_{cc} = 2.15 MPa, and a strain energy of W_{cc} = 10.66 J. Compared to the tests presented in Chapter 3 where the titanium stem was cemented in a steel mould, the energy required to pull out the stem was lower by 19.5%, that is a reduction of 2.5 J. On the other hand, shear stress was lower by 4% with respect to the steel mould test. This reduction in energy can be observed by comparing the force vs time plots, Figure 3.22 and Figure 4.12, where the titanium stem of control test for the composite cylinder was released at 205 seconds, whereas the stem of control test of the steel mould was released at 350 seconds.

4.3 Experimental Results of Cooled Composite Cylinder Specimens

A total of 8 tests were performed, 2 control tests and 2 for each case study. The readings of temperature (12 thermocouples at specific points of interest as described in Section 4.2.2) and the results from the pull-out test were averaged over a normalized time period as described in Chapter 3. Figure 4.13 shows the general experimental methodology that was explained and followed in Section 4.2.2.

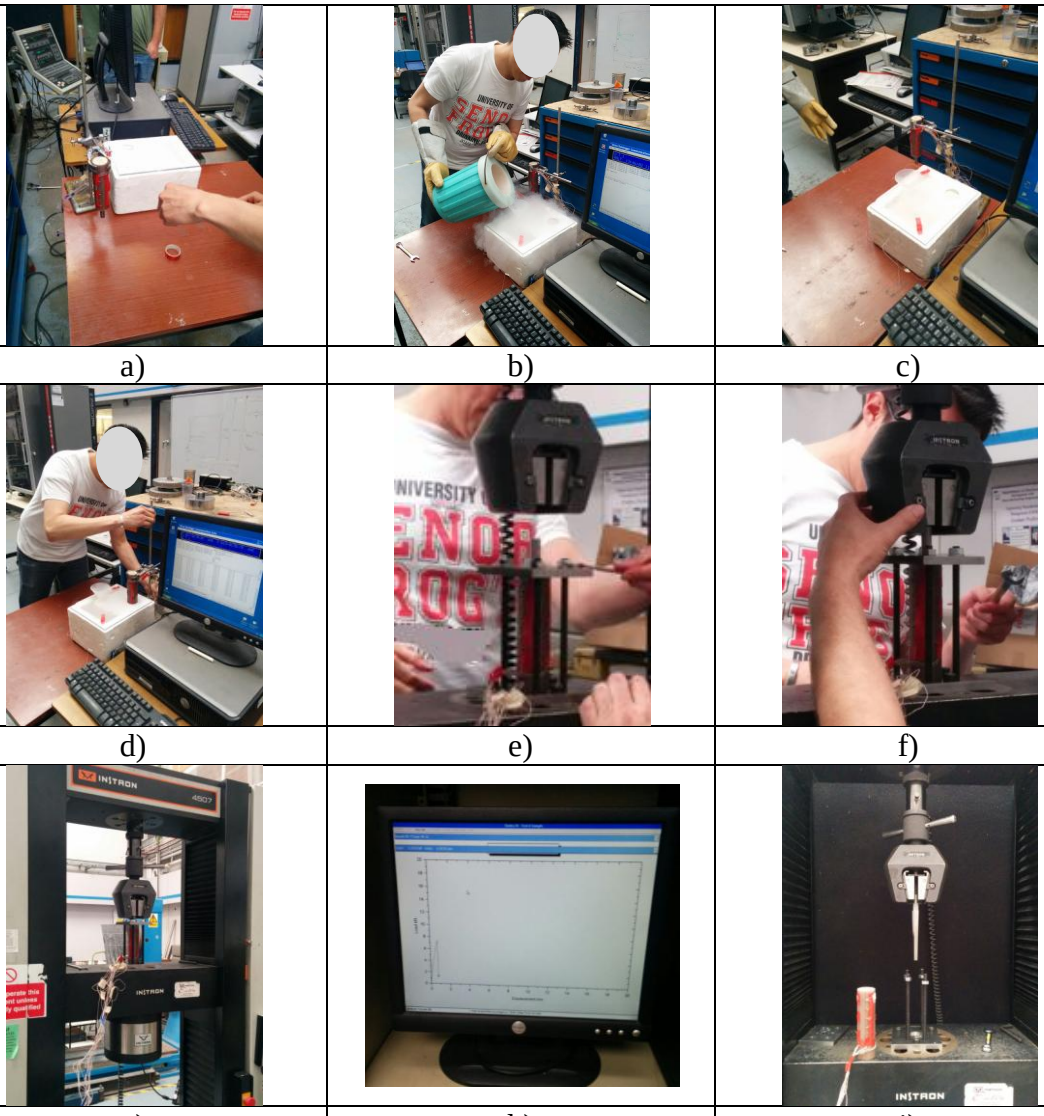

Figure 4.13 The various steps and stages while performing experimental tests with composite cylinders. a) setup preparation, b) filling the container with LN_2, c) setup ready, d) start of cooling stage, e) fastening the specimen to Instron's crosshead, f) clamping the neck of the stem to the superior clamp of Instron machine, g) mechanical pull-out test, h) and load-displacement data acquisition, i) specimen after titanium stem was removed.

The averaged results of temperature and force from the experimental tests performed with cylindrical composites at three different temperatures of interest in the proximal region of the titanium stem are shown in Figures 4.14 to 4.16. Three case studies were considered for composite cylinders: case study 1 at -76°C, case study 2 at -49°C, and case study 3 at -40°C. Description of the results for the temperature and force are presented in the following two subsections respectively.

4.3.1 Temperature Results

Figures 4.14a to 4.16a show the averaged results of the temperature readings plotted versus time from the three case studies considered with composite cylinders: Case 1 to Case 3 which correspond to the temperatures of interest: -76°C, -49°C, and -40°C in the proximal zone of the titanium stem. Each temperature plot represents the averaged readings of the four thermocouples at each zone of interest of the stem (proximal, middle, and distal), making a total of 12 thermocouples. These results of temperature are plotted from -80°C to 30°C on its Y axis. X axis represents the time interval (in seconds) of the plot starts from the end of the cooling stage to the end of the mechanical pull-out. The circular markers in the plots from Figures 4.14a to 4.16a, numbered from 1 to 3, indicate important time intervals in the experimental test. The time intervals are delimited by solid vertical lines, and they are described as follows:

Zone#1: Temperature of the specimen recorded while being clamped in the Instron machine.

Zone#2: Temperature readings of the specimen during the mechanical pull-out stage, linear behaviour of the force. Failure of the interface and release of the stem.

Zone#3: Temperature readings of the specimen at the end of the mechanical pull-out stage.

The temperature plots from Figures 4.14a to 4.16a show that each case study achieved its corresponding cooling temperature of interest in the proximal zone (-76°C, -49°C, and -40°C) at different times: 518, 284, and 280 seconds respectively; the mechanical pull-out started 120 seconds after removing the specimens from the bath of LN_2. During that time interval, represented as Zone#1, an increase on temperature was registered by the proximal thermocouples in all case studies. The approximate warming rates in this proximal area of the titanium stem were of 5.6, 5.2, and 1.8°C/min for each case study respectively. At the same Zone#1, thermocouples continued to register a decrease in temperature in each case study (Case 1 to Case 3 respectively) with

approximate cooling rates of -3, -3, -2.5°C/min in the middle zone, and -0.7, -0.3, -0.2°C/min in the distal zone from the titanium stem.

In the time interval of Zone#2 from Figures 4.14a to 4.16a, the rate of warming increased considerably at the proximal zone of the titanium stem to 8.9, 7, and 7.2°C/min for each case study (Case 1 to Case 3 respectively). The warming of the proximal zone of the femoral stem was, in part, consequence of the interaction of the neck to the surroundings and the direct contact with the upper jaw of the Instron machine to which it was clamped to. For each case study, the temperature registered at middle and distal zones of the stem continued to decrease at rates of approximately -2.0, -1.6, and -1.2°C/min; and -0.8, -0.5, and -0.3°C/min respectively.

Zone#3 from Figures 4.14a to 4.16a, showed that the proximal temperature readings of the stem continued to warm up for all case studies with approximate rates of 7.4, 5.7, and 3.7°C/min, Case 1 to Case 3 respectively. The middle and distal zones showed thermal stabilization and posteriorly an increase in temperature at approximate rates of -0.3 and -0.2°C/min respectively for Case 2, and 0.4 and 1°C/min respectively for Case 3. On the other hand, the middle and distal temperatures of Case 1 continued to decrease until the end of the mechanical pull-out at an approximate rate of -1.2 and -0.8°C/min respectively.

From the moment the temperatures of interest were achieved and the neck of the stem was removed from the bath of liquid nitrogen, the temperature at the proximal zone of the titanium stem increased as a consequence of the interaction of the specimen with the surrounding environment (average temperature 25°C). The proximal zone was observed to be warming up at a rate of 7.4, 5.7, and 3.7 °C/min for each case study (-76°C, -49°C, and -40°C respectively). The temperature in the middle zone continued to decrease at an approximate average rate of -1.5 °C/min for all case studies. On the other hand, temperature at the distal zones remained almost constant, with an average decrease rate of -0.4 °C/min.

4.3.2 Force results

Figures 4.14b to 4.16b show the averaged results of the force plotted versus time from the three case studies considered with composite cylinders: case study 1 at -76°C, case study 2 at -49°C, and case study 3 at -40°C. The results are plotted from 0 kN to 7 kN on its Y axis, and the time on X axis. Similarly to the temperature plots, the time interval covers the end of the cooling stage to the end of the mechanical pull-out. The circular markers in the plots from Figures 4.14b to 4.16b, numbered from 1 to 3, indicate the relevant time intervals in the experimental tests which are delimited by solid vertical lines, and they are described as follows:

Zone#1: End of cooling, clamping of cylindrical specimen in the Instron machine, mechanical pull-out stage starts.

Zone#2: Linear behaviour of the force, failure of the interface and release of the stem.

Zone#3: End of the mechanical pull-out stage.

The force-time curves in Figures 4.14b to 4.16b show similar behaviour in the 3 case studies for the cooling tests with composite cylinders. A brittle failure of the interface occurred when the force reached maximum value causing the stem to be released from the cement mantle and composite bone. For these tests performed with composite cylinders, the results for the mechanical pull-out did not exhibit a non-linear behaviour as occurred with the tests performed with the steel mould.

Upon analysing Figures 4.14b to 4.16b, Zone#1 represents the time that was needed to clamp the composite cylinder in the Instron machine to perform the mechanical pull-out test. Once the specimen was clamped, the mechanical pull-out test started at an overall experimental time of 638, 404, and 400 seconds for Case 1, Case 2, and Case 3 respectively. The force to remove the femoral stem was recorded, and the resulting plot showed a linear behaviour until a maximum value of the force was reached and the interface between the titanium stem and the cement failed thus releasing the prosthesis from the cement mantle, Zone#2. The force plots displays two changes in slope for all case studies in the Zone#2. The first change in slope occurred relatively

quickly at the beginning of the mechanical stage that is 12, 16, and 12 seconds after starting to pull-out the stem for each case study respectively. At that specific time, the proximal temperature had increased by approximately 1.7°C (average) in all case studies. The change in slope remained constant with a linear behaviour for approximately 50, 60, and 28 seconds for Case 1, Case 2, and Case 3 respectively, representing an increment of temperature in the proximal area of the femoral stem of 8°C for Case 1 and Case 2, and a change in temperature of 3°C for Case 3. The slope remained constant until the moment stem was released from the cement, that was at an overall experimental time of 774, 546, and 494 seconds. It was observed that from the start of the mechanical pull-out test to the moment of the maximum force to release the femoral stem from the cement mantle was reached (6.93kN, 6.05kN, and 6.52kN for each case study respectively) the temperature in the proximal region was warmer approximately 20^{o}C, 17^{o}C, and 11^{o}C for Case 1, Case 2, and Case 3 respectively (temperatures of interest reached: -76^{o}C, -49^{o}C, and -40^{o}C for each case study correspondingly). Although the femoral stem was already loosened and out from the cement mantle by approximately 3 mm, at the beginning of the Zone#3 from the force plots in Figures 4.14b to 4.16b, the Instron machine continued to register a decrement of the force. The experiment was terminated after 90 seconds.

The thermal treatment reduced the force required to remove the stem compared with the force at room temperature, which was 13.98 kN. The release forces were reduced by approximately 53%, 57%, and 50% for the temperatures of interest studied at -40^{o}C, -49^{o}C, and -76^{o}C respectively.

With respect to the displacement at failure registered by the Instron machine, the control test had a displacement of δ_{cc}=1.71 mm, the cooled cases at -76°C, -49°C and -40°C had a total displacement of δ_{c1}=1.14 mm, δ_{c2}=1.19 mm, and δ_{c3}=0.76 mm respectively. These changes in extension for each cooling case represented a displacement of 66.6%, 69.6%, and 44.4% of the control test. Compared with the results of the elastic region from Chapter 3, the failure occurred at a lower extension in all cases with a difference of 41.5%, 20.4%, and 48% for the tests at 22°C, -76°C, and -40°C respectively. The case study at -49°C exhibited a difference in extension of only 3.2%.

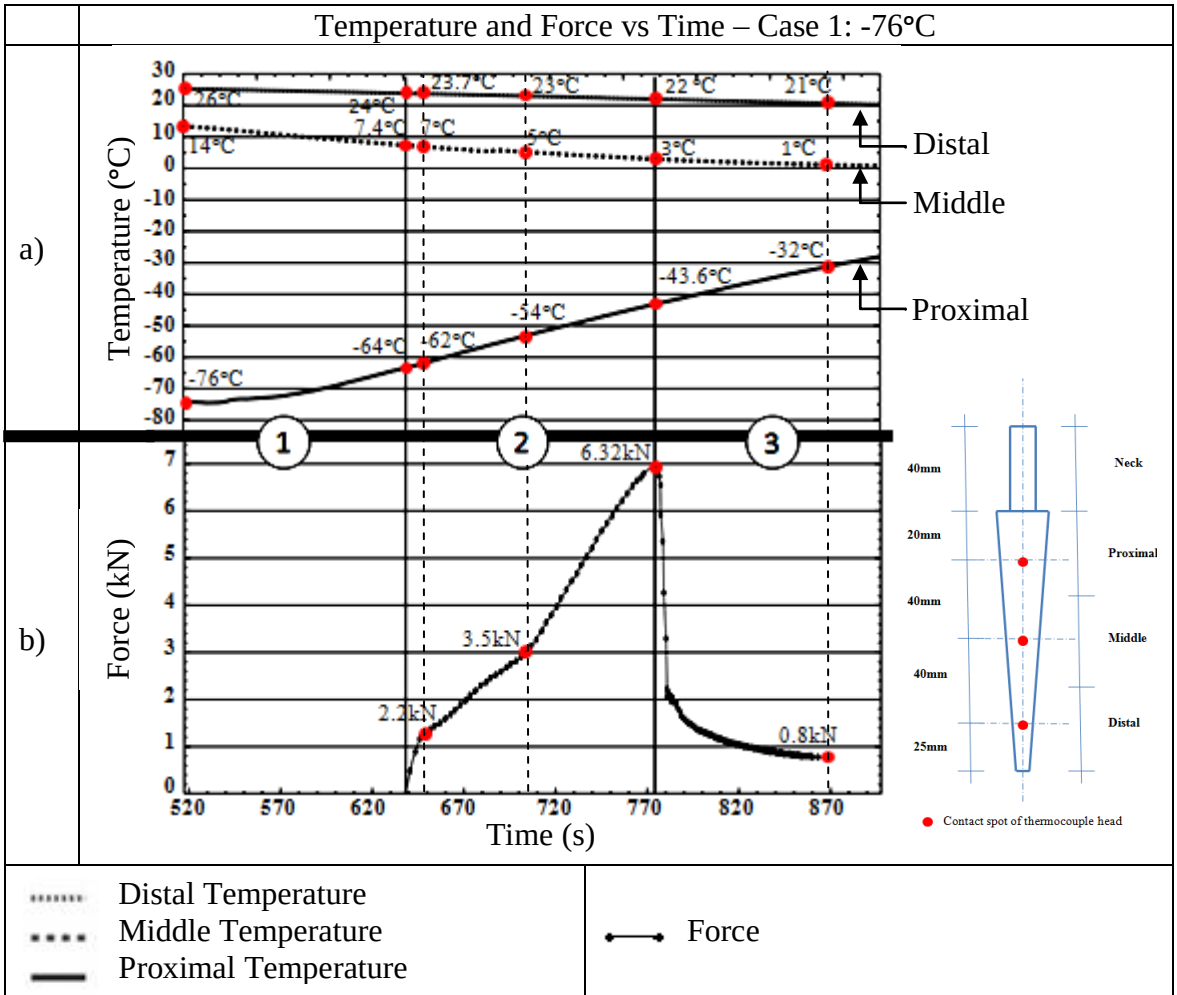

Figure 4.14 Experimental results for case study 1 on temperature of -76°C plotted after removing the specimen from the LN_2 bath. a) Temperature readings in the three zones of interest of the stem: distal, middle, and proximal. b) Pull-out test: force vs time; different stages in the experimental tests are marked as follows: 1) End of cooling, clamping interval, mechanical pull-out starts, 2) Elastic region, sudden drop in force and complete release of the stem, 3) End of mechanical loading stage.

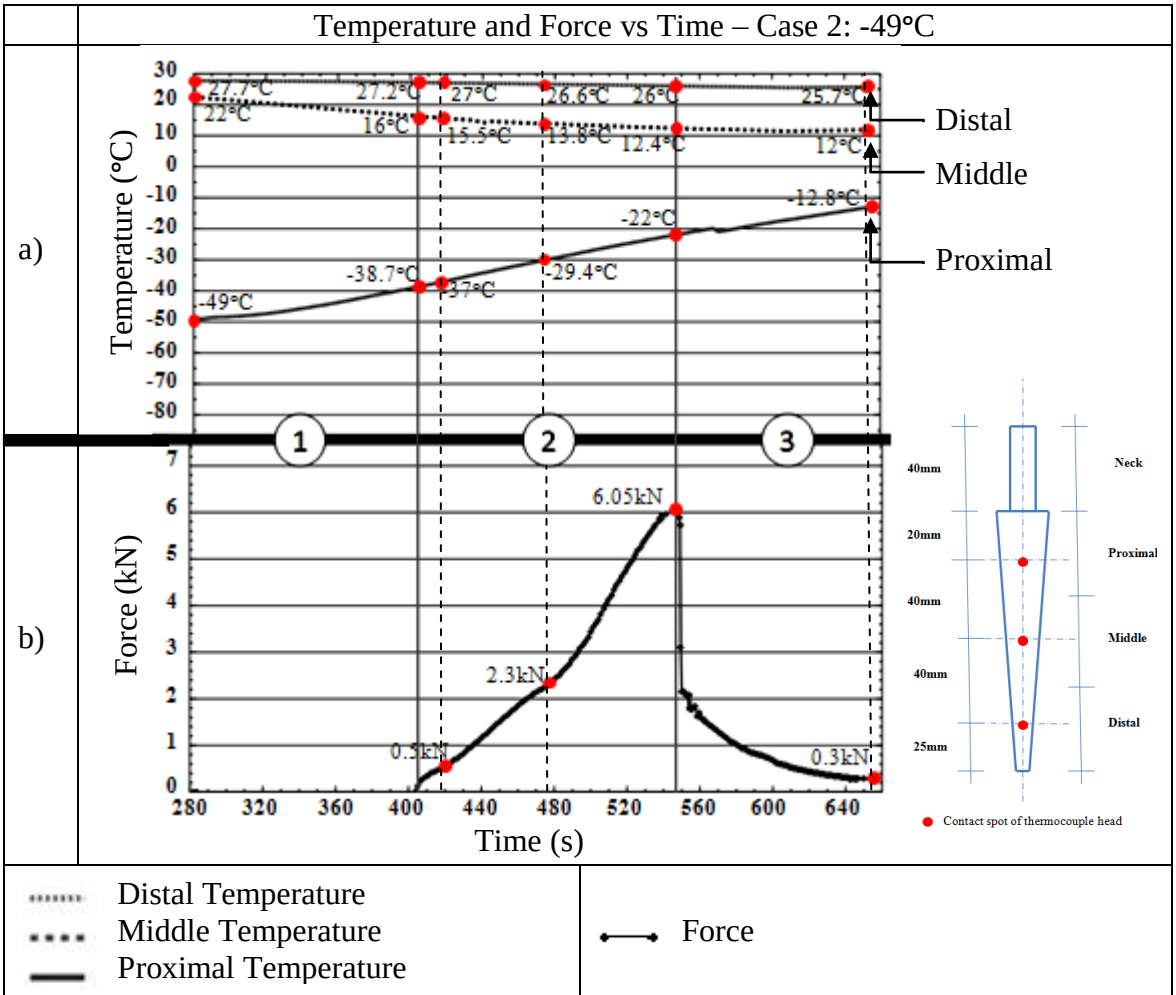

Figure 4.15 Experimental results for case study 2 on temperature of -49°C plotted after removing the specimen from the LN_2 bath. a) Temperature readings in the three zones of interest of the stem: distal, middle, and proximal. b) Pull-out test: force vs time; different stages in the experimental tests are marked as follows: 1) End of cooling, clamping interval, mechanical pull-out starts, 2) Elastic region, sudden drop in force and complete release of the stem, 3) End of mechanical loading stage.

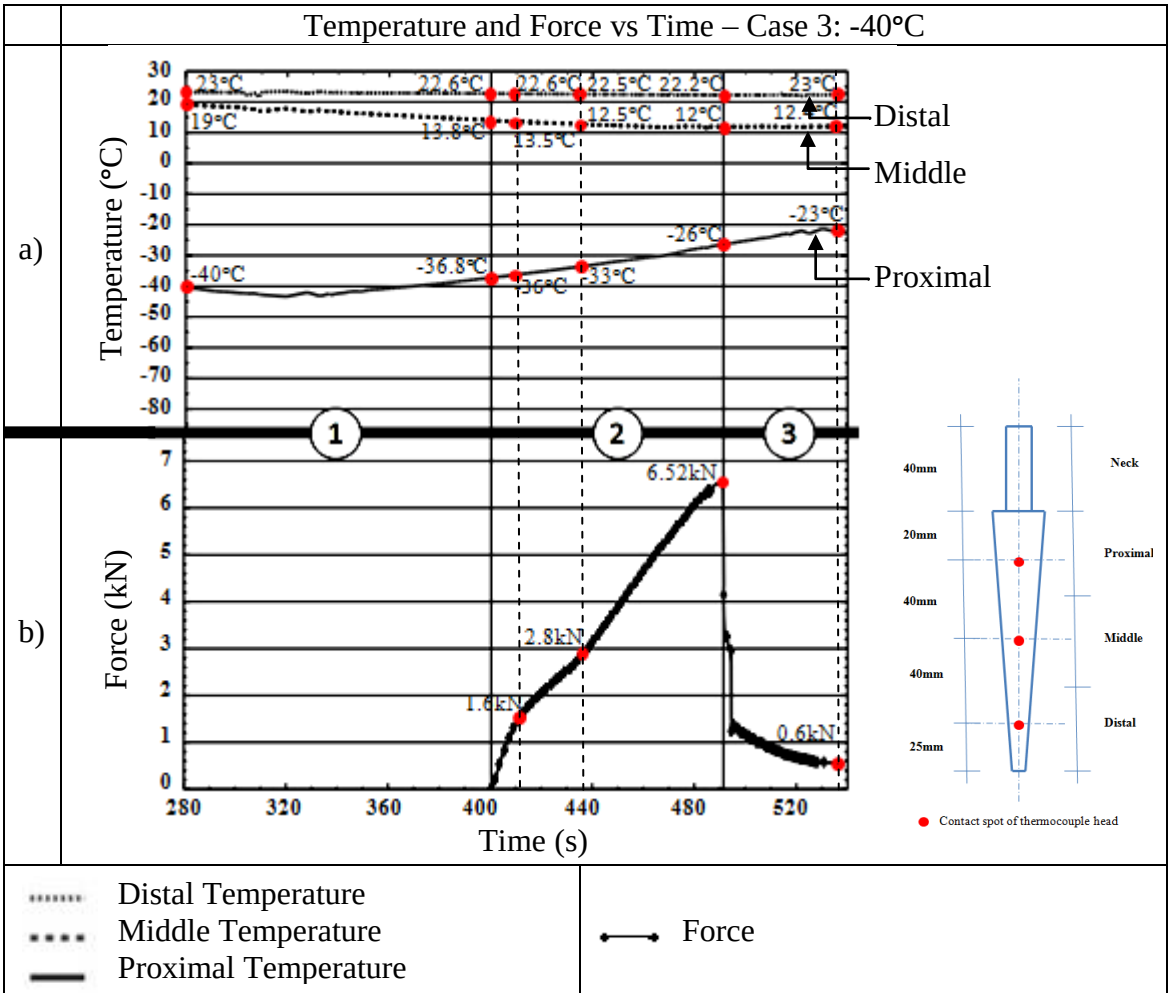

Figure 4.16 Experimental results for case study 3 on temperature of -40°C plotted after removing the specimen from the LN_2 bath. a) Temperature readings in the three zones of interest of the stem: distal, middle, and proximal. b) Pull-out test: force vs time; different stages in the experimental tests are marked as follows: 1) End of cooling, clamping interval, mechanical pull-out starts, 2) Elastic region, sudden drop in force and complete release of the stem, 3) End of mechanical loading stage.

Maximum shear stress was calculated by using equation 3.4 from Section 3.3.3.1. For Case 1 maximum shear stress showed a value of τ_{c1}= 1.07Mpa, a reduction of 50.42% compared to the control test. In contrast with the control test (τ_{cc}= 2.15 Mpa), the rest of cooling cases (Case 2 at -49°C, and Case 3 at -40°C) represented reductions of 56.7%, and 53.4% of the maximum shear respectively. Comparing these values with respect to the results obtained in the experiments with the steel mould the shear stress was lower in the composite cylinder by 3.92%, 42.1%, and 35.1% for the

tests at 22°C, -49°C, and -40°C respectively. however, in the case study at -76°C the shear stress was 9.66% higher than for the corresponding steel mould test.

Total strain energy was calculated by using equation 3.5 from Section 3.3.3.1. The total strain energy measures the amount of mechanical energy required to break the interface and remove the titanium stem, showed that the case studies at the temperatures of -40°C and -49°C required 74% and 70% of the energy needed to pull out the titanium stem at ambient temperature, which had a value of W_{cc} = 10.66 J. Case 1 at -76°C required less energy to release the stem from the cement mantle, 61.6%. In relation to the results of the experiments undertaken using the steel mould, the strain energy was reduced by 19.5%, 17.46%, 56.8%, and 61.5% for the tests at 22°C, -76°C, -49°C, and -40°C respectively.

4.4 Impact of Temperature on the Release Force of a Titanium Stem Cemented in Composite Femur

The experiments performed in Section 3.4 from Chapter 3 and the experiments with composite cylinders from Section 4.2 from Chapter 4 showed consistent results confirming that the thermal treatment effectively reduces the force required to extract a well cemented femoral stem.

As part of the second case scenario, this Section describes the experiments performed with composite femur from Sawbones®, which had the purpose of prove the cooling methodology in a closer approach to a real case by replacing the cylindrical composites, thus improving the specimen to be tested with an anatomic geometry.

The experiments consisted of testing the specimens mechanically pulling-out the femoral stem, in two case studies, one case by achieving an extreme temperature at -76°C, and the second case at the critical temperature of -40°C (as referenced in Section 2.5 and 2.6) at the proximal zone of the stem.

4.4.1 Materials Used for Composite Femur Specimens

4.4.1.1 Titanium Femoral Stem

As previously described in Section 4.2.1.1, customized Ti-6Al-4V stems were used for the experimental work presented in this section of Chapter 4.

4.4.1.2 Composite Femur

In order to implant the femoral stems with bone-cement, fourth generation Sawbones® composite femurs were used to reproduce a real case scenario of an implanted femoral prosthesis.

According to Sawbones and as described in Section 3.4.4 of Chapter 3, the composite femurs mimic the characteristics of both cortical and cancellous bone. The cortical bone is made of short fibre filled epoxy, and the cancellous bone is made of high-density polyurethane foam of 320 kg/m^3. A sample of a large composite femur is shown in Figure 4.17.

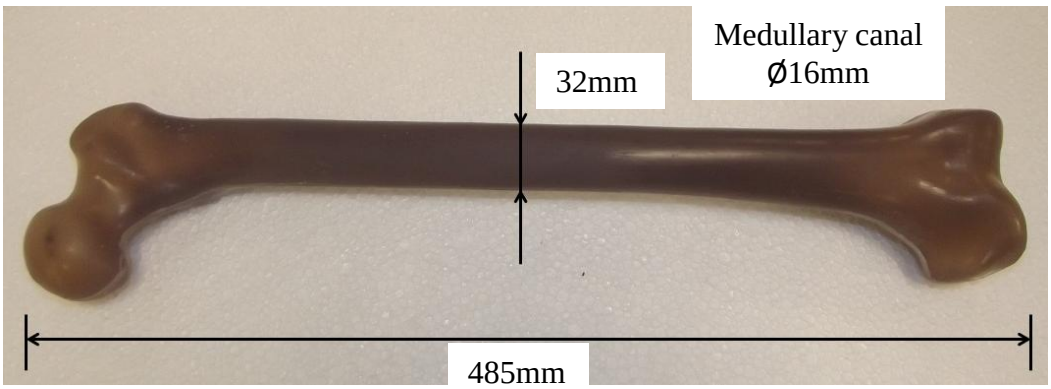

Figure 4.17 Dimensions of Sawbones' left composite femur, size large.

The preparation of the composite femurs started with a distal resection of the diaphysis 145 mm below the lesser trochanter; Figure 4.18 shows how it was marked.

The femoral head was resected as in surgery, approximately 20 mm above the lesser trochanter.

As mentioned by Breusch et al. [2], the exact osteotomy level is not critical if a collarless, tapered stem design is used as prosthesis. It is favourable to have a moderately high neck cut, between 30° and 35° to the femoral shaft axis, for partial preservation of the distal neck.

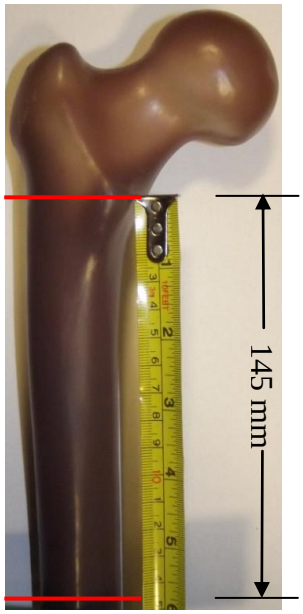

Figure 4.18 Sawbones large composite femur. Distance between the lesser trochanter and distal resection line, 145 mm.

Because a customized femoral stem was used in this research, the greater trochanter was resected in a horizontal line approximately 20-30 mm above the lesser trochanter, see Figure 4.19.

The composite bone was also prepared to facilitate the insertion of 12 T-Type thermocouples through its composite walls at strategic positions on the surface of the titanium stems. Figure 4.20 shows a total of 12 marked spots where 2 mm diameter holes were drilled. The distances between the holes were 20 mm, 60 mm, and 100 mm from the reference line, which represents the upper surface after the resection of the femoral head and greater trochanter previously explained.

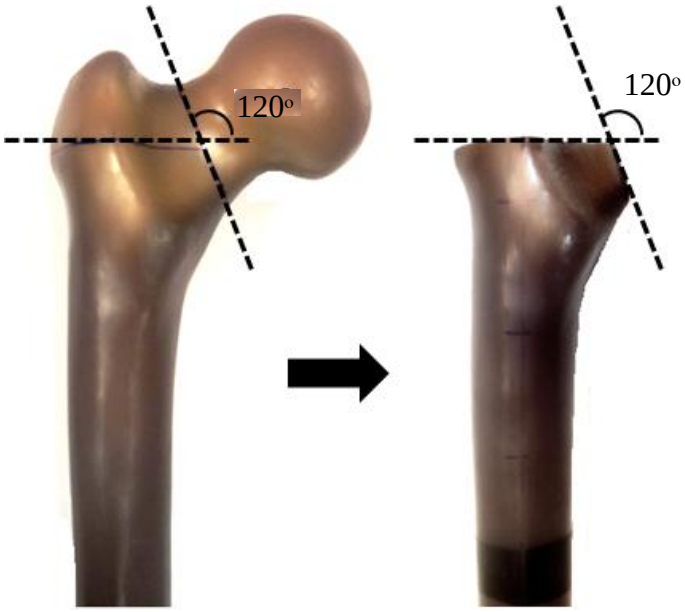

Figure 4.19 Composite femur. a) Guiding lines used to cut the femoral head and greater trochanter, and b) final resected geometry.

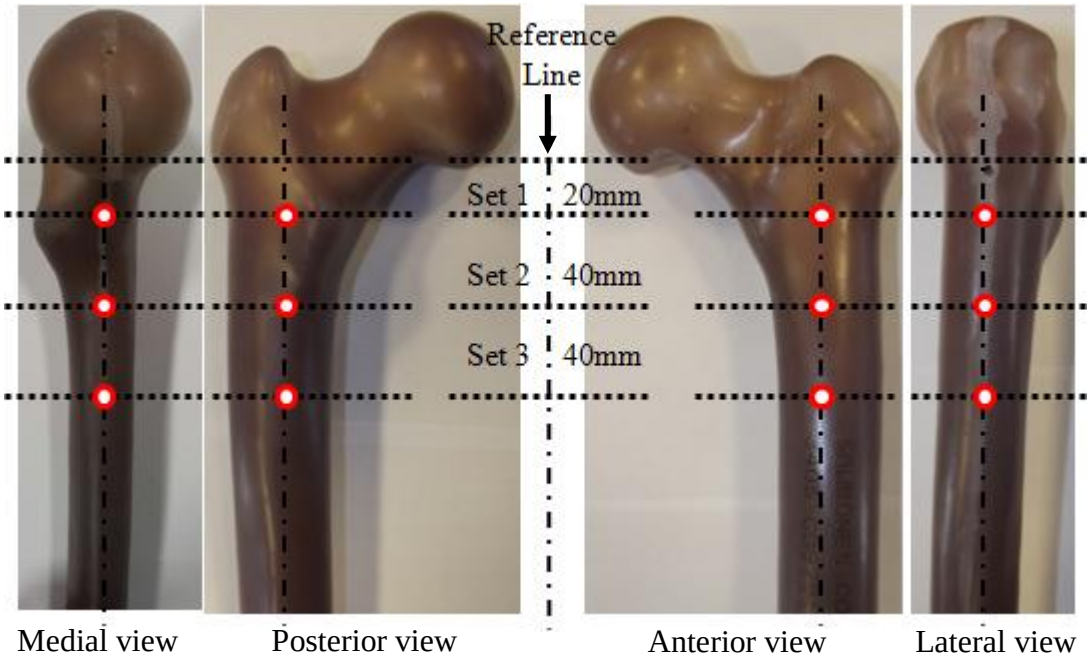

Figure 4.20 Guiding marks on the left femur of the set of drilling holes for thermocouples. Reference line is 20 mm above lesser trochanter.

In order to gain access to the medullary canal, a circle of Ø12 mm was drawn as a guide, as shown in Figure 4.21a. The circle was vertically aligned to the centre line of the femoral canal. Figure 4.21b shows the hole made with the aid of a circular broach. The medullary canal can be seen bellow the mantle of cancellous bone at approximately 30 mm. After this step, the trapezoidal shape of the stem was drawn as a guide to limit the expansion of the canal in the following step, see Figure 4.21b.

The expansion of the "medullary canal" in the cancellous bone followed the same process described in the previous Section 4.2.1.2 regarding the composite cylinders. The double tapered shape of the medullary canal was created using the custom made broaches.

As explained in the previous section, the positions correspond to the middle of the three zones of interest on the stem (proximal, middle, distal zones). Figure 4.22 shows the distances between a set of three holes drilled on the cylinder.

a)

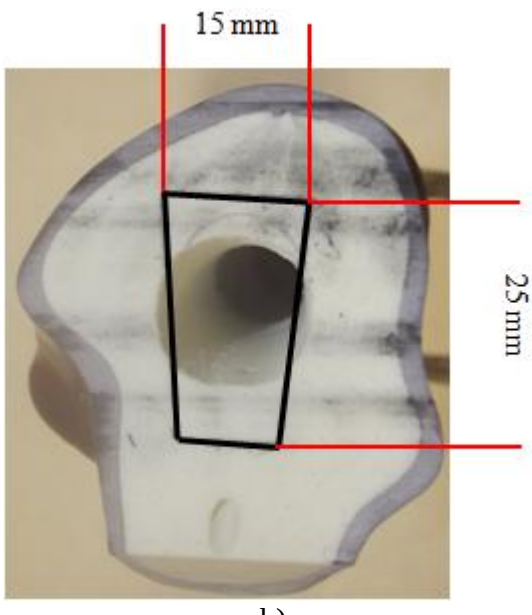

b)

Figure 4.21 Resected composite femur: a) circle guide to gain access to the medullary canal, b) access to the medullary canal and trapezoidal guide to expand the canal.

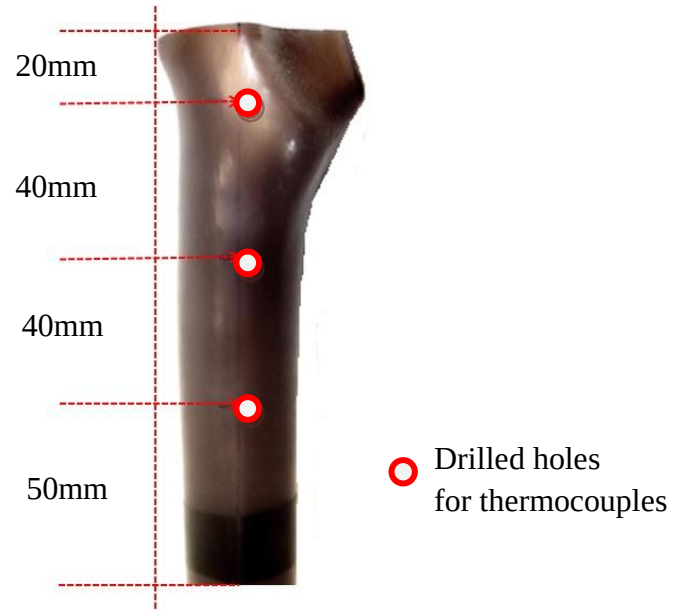

Figure 4.22 Sample set of drilled holes for thermocouples and distance between them on one side of the surface of a resected composite femur.

4.4.1.1 Bone Cement – Polymethyl-Methacrylate (PMMA), T-Type Thermocouples, and Liquid Nitrogen (NL_2)

For the experiments shown in this section, the same type bone cement was used (SmartSet CEMVAC), and was prepared by following the indications described in Section 4.2.2.1. Moreover, the T-Type thermocouples were used and liquid nitrogen as cooling agent, as described in Sections 3.3.1.4 to 3.3.1.5 from Chapter 3.

4.4.2 Experimental Methodology for Composite Femur Specimens

4.4.2.1 Cementing Procedure and Instrumentation of Composite Femurs

Following the same procedure explained in Section 4.2.2 of this chapter, the stems were cemented in the composite femurs with the clamp designed to firmly hold the specimen. Figure 4.23 shows the clamped composite femur and the cemented titanium stem with the 1.5 mm rods inserted through the drilled holes in the specimen. After 15 min setting time, the specimen was removed from the clamping system and the

steel rods were removed, before the T-Type thermocouples proceeded to be embedded. All specimens were allowed to set for 24 hours before being tested experimentally.

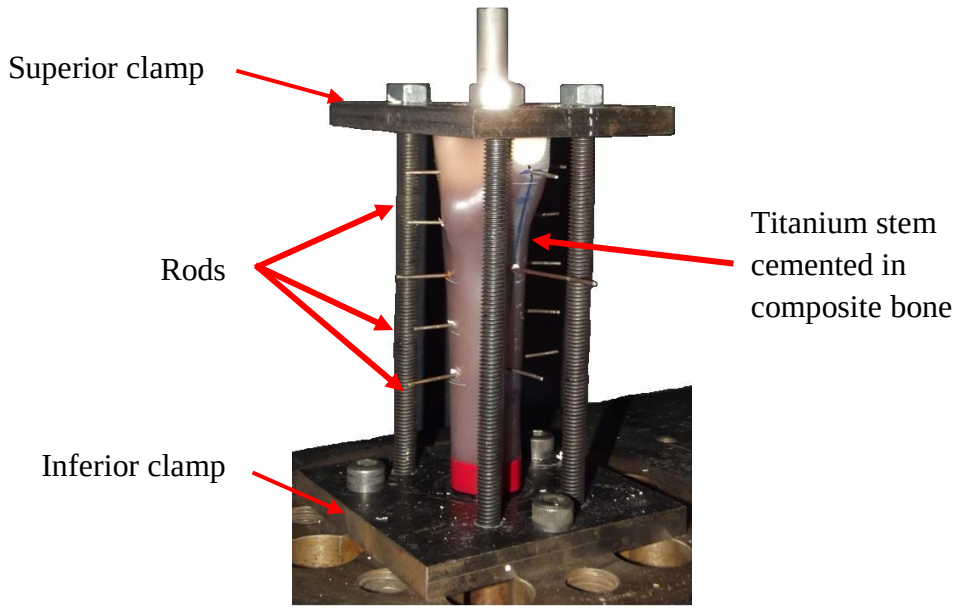

Figure 4.23 Femoral specimen after cementing procedure.

4.4.2.1 Cooling Stage Preparation: Composite Femurs

The cooling procedure was carefully followed as described in section 4.2.3. Figure 4.24 shows the specimen (2) clamped (1) with the neck of the stem facing down at a fixed height above a polystyrene container (4) filled with Liquid Nitrogen (LN_2). Thermocouples were connected to an Orion 3530 logging system (3). The neck of the stem was then lowered through the opening in the lid of the container until it was immersed in the LN_2. Two thermocouples (5) were attached through the lid to monitor the level of LN_2 in the container. When the level sensors showed a change in temperature, LN_2 was poured into the container through the attached funnel (6) to keep a constant level of LN_2 in the container.

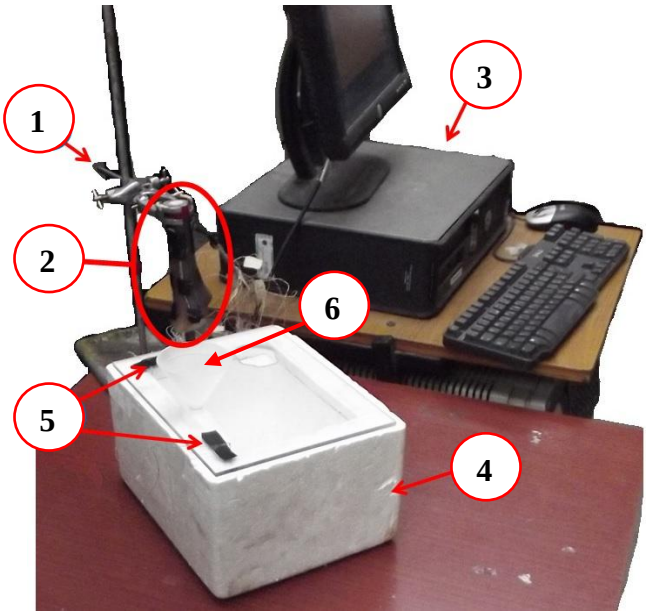

Figure 4.24 Setup for cooling procedure.1)Clamp, 2)Cemented specimen, 3) Orion 3530 data logger, 4)Container for LN_2, 5)Thermocouples as level sensors of LN_2, (6) Funnel.

Table 4.2 shows the temperatures of interest for the case studies. For this set of experiments, it was decided to test at temperatures of -76°C and at -40°C with the objective of analysing the force required to remove the femoral stem at an extreme temperature and at the critical temperature.

Table 4.2 Temperatures of Interest for Scenario Study with Composite Femurs

	Temperature (°C)
Case1	-76
Case 2	-40

4.4.2.2 Mechanical Loading Stage (Pull-out): Composite Femurs

For these tests, the same procedure explained in Section 4.2.4 was followed to perform the mechanical pull-out tests on the specimens. Figure 4.25 shows the specimens clamped in the Instron machine immediately after the cooling procedure.

The time between removing the specimen from the cooling bath, location in Instron machine and the start of the pull-out test was 120 seconds, which was the same standardized time taken in Section 4.2.4. As in all experimental tests, the stem was pulled from the composite femur at a constant crosshead speed of 0.5 mm/min until failure of the interface, when it became completely detached from the bone cement.

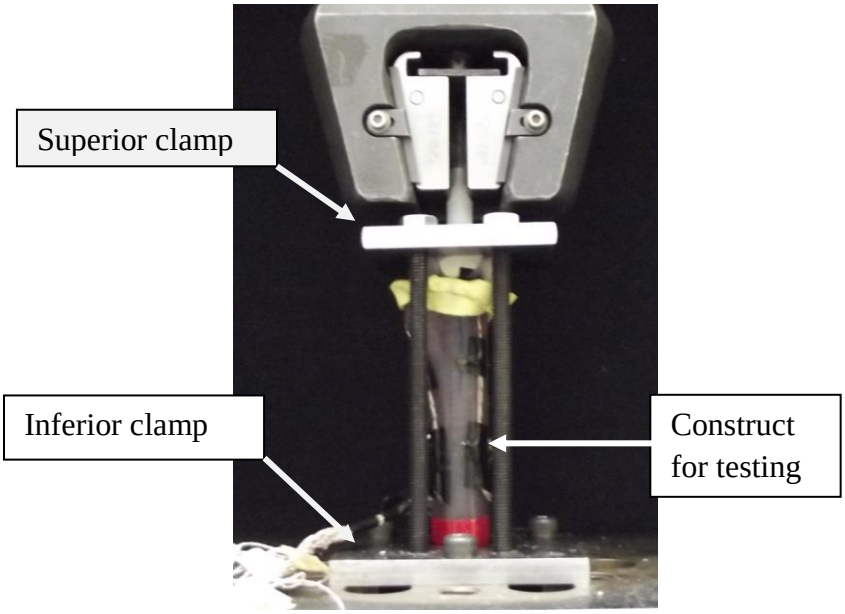

Figure 4.25 Mechanical pull-out test setup of a titanium stem cemented in composite bone.

4.5 Experimental Results of Cooled Composite Femurs

The readings of temperature and the results from the pull-out tests were averaged over a normalized time period as described in Chapter 3. In the absence of a control test for this particular case study with composite femurs, the control test performed with composite cylinders was used for comparison purposes for the cooled specimens, 1 test per case study at temperatures of -76°C and at -40°C.

Figure 4.26 shows the general experimental methodology that was explained and followed in Section 4.3.2.

a)

b)

c)

d)

e)

f)

g)

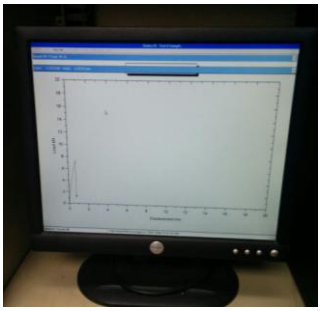

h)

i)

Figure 4.26 The various steps and stages while performing experimental tests with composite femurs. a) setup preparation, b) filling the container with LN_2, c) start of cooling stage, d) pouring LN_2 into the container to maintain the level constant, e) cooling state ended, proceed to fasten the specimen to Instron;s crosshead, f) clamping the neck of the stem to the superior clamp of Instron machine, g) start of mechanical pull-out test, h) and load-displacement data acquisition, i) specimen after titanium stem was removed.

At the end of the mechanical pull-out test, the specimen was visually inspected, it was observed that the cement mantle remained completely in the composite femur, and no residue of cement was found on the surfaces of the titanium stem. Figures 4.27a

and 4.27b show one of the titanium stems removed from a composite femur, and the cement mantle that remained in the femoral canal respectively.

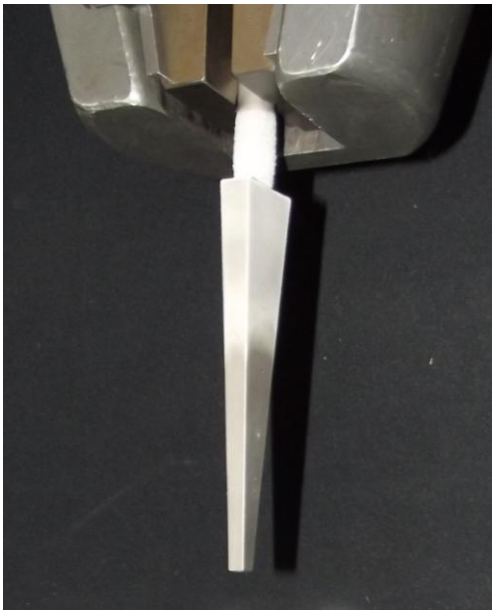

a)

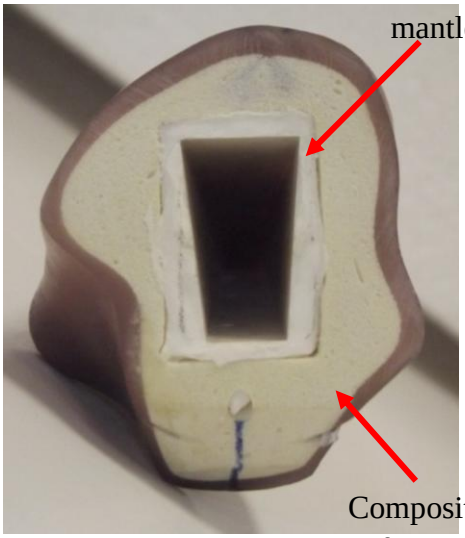

b)

Figure 4.27 a) Removed titanium stem, b) cement mantle in composite femur .

Similarly to previous Sections 4.2.3.2 and 3.3.3.2, the averaged results of temperature and force are shown in Figure 4.28 and Figure 4.29 for the case studies with temperature of interest at the proximal zone of the femoral stem of -76°C and -40°C respectively. The plots of temperature and force are described in the following two subsections respectively.

4.5.1 Temperature Results

The averaged temperature readings from the 12 thermocouples at the strategic points of interest on the surface of the titanium stem (proximal, middle, and distal) are shown in Figures 4.28a and 4.29a. Temperature units (-80°C to 30°C) are presented in Y axis while X axis present time in seconds. Similarly to previous Sections 4.2.3.2 and

3.3.3.2, the time interval of the plot starts at the end of the cooling stage and ends when the mechanical pull-out finalises, which was at the failure of the bonding interface. The numbered marks in the plots between the solid vertical lines indicate relevant stages in the experimental tests, and they are described similarly as in Section 4.3.1 as follows:

Zone#1: Temperature of the specimen recorded while being clamped in the Instron machine.

Zone#2: Temperature readings of the specimen during the mechanical pull-out stage, linear behaviour of the force. Failure of the interface and release of the stem.

Zone#3: Temperature readings of the specimen at the end of the mechanical pull-out stage.

Figures 4.28a and 4.29a show the results of the temperature readings for each case study undertaken for titanium stems cemented in composite femurs at the temperatures of interest, -76°C and -40°C in the proximal thermocouples. The temperature readings displayed a similar trend as in previous tests performed with the steel mould and composite cylinders. The cooling temperatures of interest, -76°C and -40°C, were achieved and registered by the proximal thermocouples at different times: 414 and 212 seconds respectively. Similar to previous tests, the specimens exhibited an increase in temperature after being removed from the bath of liquid nitrogen and as a consequence of the interaction of the specimen with the surrounding environment (average temperature 25°C) while preparing the specimens for the mechanical pull-out stage, Zone#1 of Figures 4.28a and 4.29a.

In Zone#2, and from the same Figures 4.28a and 4.29a, it was observed that the proximal temperature continued to warm-up at an approximate rate of 7.8 and 5.8°C/min for Case 1 and Case 2 respectively. The middle and distal temperatures remained practically constant with a rather small temperature change rate of approximately -1.6, and -0.4°C/min respectively for both case studies.

On the other hand, the temperature readings from the proximal thermocouples in Zone#3 of Figures 4.28a and 4.29a displayed a greater rate in temperature change for Case 1, 11.4°C/min, and a rather constant rate of 5.6°C/min for Case 2. The

temperature at middle of the stem continued to decrease at an approximate rate of 2.9 and -1.1°C/min for Case 1 and Case 2 respectively.

In general, the warming of the titanium stem was much more visible in the temperature readings of the thermocouples at the proximal zone. The proximal zone was observed to be warming up at an approximate average rate of 8 and 3.7°C/min for each case study (-76°C and -40°C respectively) and this was affected by the direct contact of the neck of the titanium stem with the superior clamp of the Instron machine, allowing thermal interaction between the two objects. For both case studies, the temperature in the middle zone continued to decrease at an average rate of -0.5 and -1.7°C/min approximately, while temperature at the distal zone remained almost constant, with an average decrease rate of 0.2 °C/min.

4.5.2 Force Results

Figure 4.28b and Figure 4.29b show the averaged results of force vs time for case studies, -76°C and -40°C respectively. On Y axis, the units of force are tabulated from 0 kN to 10 kN, and time is presented in seconds on X axis for each figure. Similarly to previous Sections 4.2.3.2 and 3.3.3.2, the time interval of the plot starts at the end of the cooling stage and ends when the mechanical pull-out finalises, which was at the failure of the bonding interface. The circled numbers (1 to 3) from the plots in Figures 4.28b and 4.29b, indicate relevant time interval zones from the mechanical pull-out test which are delimited by solid vertical lines, and they are described as in Section 4.3.2 as follows:

Zone#1: End of cooling, clamping of cylindrical specimen in the Instron machine, mechanical pull-out stage starts.

Zone#2: Linear behaviour of the force, failure of the interface and release of the stem.

Zone#3: End of the mechanical pull-out stage.

The force-time curves shown in Figures 4.28b and 4.29b exhibit the same behaviour as shown in previous results for the specimens with composite cylinders. Zone#1 represents the time taken to prepare the specimens to be mechanically tested by pulling-out the cemented femoral stem from the composite femur. The mechanical pull-out test started at an overall experimental time of 534, and 330 seconds for Case 1, and Case 2 respectively, the force at which the stem was released reached a maximum value of 4.9 kN and 9.44 kN for temperatures of -40°C and -76°C respectively. During the pull-out test, Zone#2, the force plots in showed one change in slope 40 and 19 seconds after the mechanical loading stage started for Case 1 and Case 2 respectively. At that specific moment, the proximal temperature increased 6°C for Case 1 and only 1°C for Case 2, after that change, the force plot had a constant linear behaviour until failure of the interface stem-cement causing the force to suddenly drop, a crack sound could be heard at failure and the stem was completely loosened from the cement mantle. The maximum force was achieved at 686 and 436 seconds after initiating the pull-out test, at that moment, the proximal temperature increased 20°C in Case 1, and 10°C in Case 2. Similar to the tests performed with composite cylinders, the tests with composite femurs did not display a non-linear deformation in the plots. Zone#3 is very short in time for these case studies since the force detected by the Instron machine immediately dropped to zero.

Comparing the results of the cooling cases with the force obtained in the control test for the composite cylinder (13.98 kN), there was a considerable reduction in the release force by 65% and 32.5% for the case study at -40°C and -76°C respectively. The different cooling temperatures demonstrated to have an effect on the force needed to release the femoral stem. The reduction of the release force was approximately 65% for a temperature of -40°C, which is 25% lower than the reduction achieved in former tests undertaken with the composite cylinder.

Displacement at failure, shear stress, and strain energy were calculated as in previous Sections 3.5.5 and 4.2.5. The displacement at failure for the case studies performed using the composite femurs at -76°C and -40°C, were of δ_{f1} = 1.28 mm, and δ_{f2} = 0.86 mm respectively. These represent reductions in extension of 25% and 50% compared to the cylinder control test, which had a total displacement at failure of δ_{cf} = 2.92 mm.

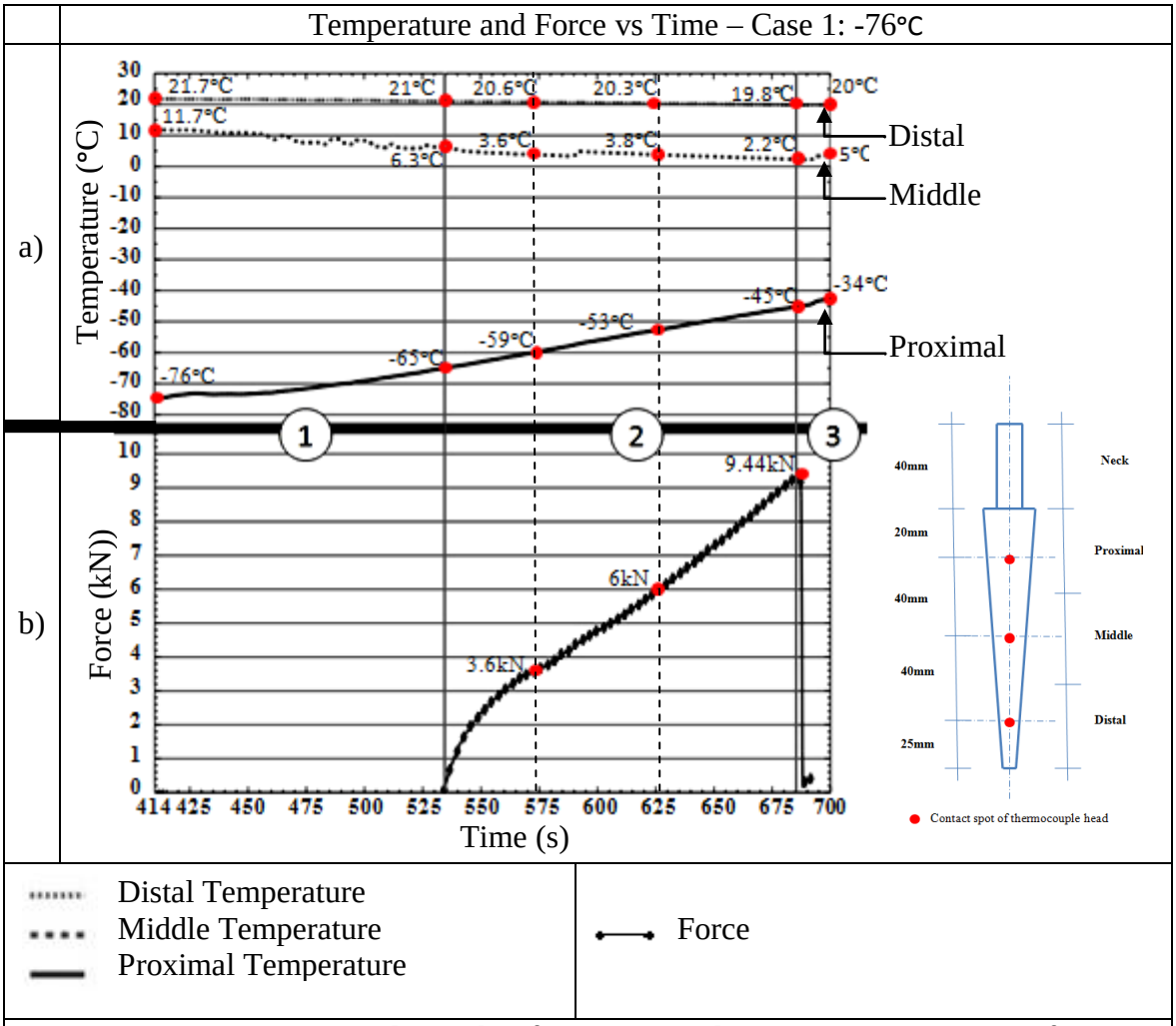

Figure 4.28 Experimental results for case study 1 on temperature of -76°C plotted after removing the specimen from the LN_2 bath. a) Temperature readings in the three zones of interest of the stem: distal, middle, and proximal. b) Pull-out test: force vs time; different stages in the experimental tests are marked as follows: 1) End of cooling, clamping interval, mechanical pull-out starts, 2) Elastic region, sudden drop in force and complete release of the stem, 3) End of mechanical loading stage.

On the other hand, by comparing the displacement between the corresponding femur and cylinder cooling cases (-76°C, and -40°C), there was an increase in extension by 12% and 12.8% respectively. In contrast with the studies using a steel mould, displacement decreased by 10.8% and 41% for the cooling tests at -76°C and -40°C respectively.

The maximum shear stress for Case 1 showed a value of τ_{f1}= 1.45 Mpa, and for Case 2 a value of τ_{f2}= 0.75 Mpa. This indicates a reduction of 32.4% and 65% compared to the control test (τ_{cc}= 2.15 Mpa). By comparing these values against the

results obtained with the steel mould and the composite cylinder, the shear stress was lower for the cooling case at -40°C by 51% and 24.8% respectively. In the other hand, the cooling case at -76°C showed an increment in shear stress by 49.5% and 36.3% respectively.

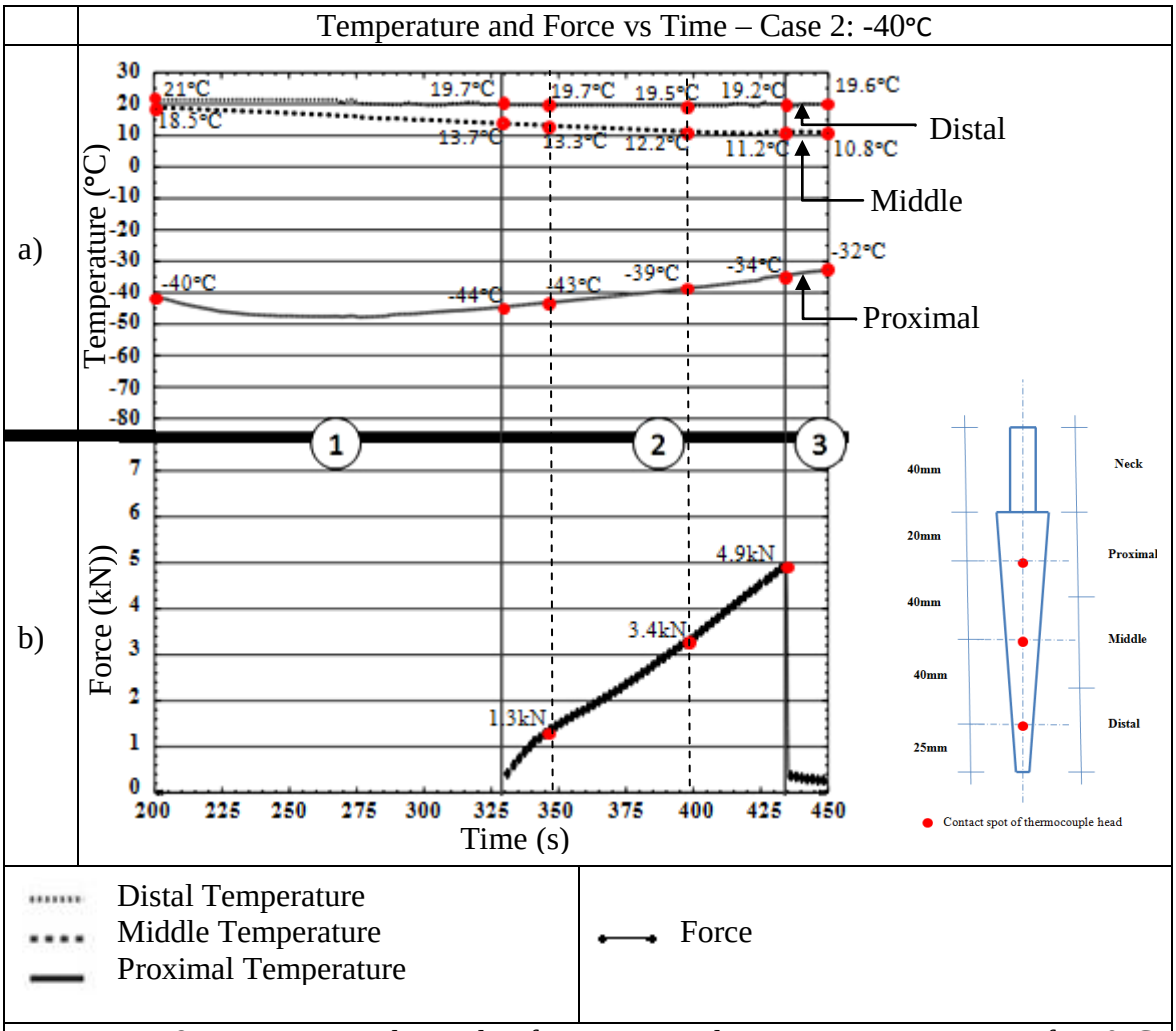

Figure 4.29 Experimental results for case study 2 on temperature of -40°C plotted after removing the specimen from the LN_2 bath. a) Temperature readings in the three zones of interest of the stem: distal, middle, and proximal. b) Pull-out test: force vs time; different stages in the experimental tests are marked as follows: 1) End of cooling, clamping interval, mechanical pull-out starts, 2) Elastic region, sudden drop in force and complete release of the stem, 3) End of mechanical loading stage.

The strain energy was lower for both case studies (-76°C and -40°C) by 36.2% and 78% compared to the control test of the composite cylinder, W_{cc} = 10.66 J. This

means that Case 2 required less energy to release the stem from the cement mantle. With respect to the results obtained with the steel mould and the composite cylinder, the strain energy was lower for the cooling case at -40°C by 67.4% and 15.3% respectively. Case 1 at -76°C required 37.3% more energy compared to the steel mould, and 66.3% more compared with the composite cylinder.

Table 4.3 shows the averaged results from the tests performed in titanium stems cemented in different materials, steel mould and composite bones (cylinders and femurs), at different cooling temperatures: -76°C, -58°C, -49°C, and -40°C depending on the case study for each scenario.

Regarding the maximum force obtained from the experimental investigation, the results indicate that there is an effect of the cooling temperature on the required force to release the femoral stem from the cement mantle holding the prosthesis to the container (steel mould or composite bones depending in the case scenario). Despite that the maximum force obtained with the cooled specimens for all case scenarios was reduced compared to the control tests, the specimens corresponding to steel mould displayed a different temperature trend compared to the tests performed with composite cylinders and composite femurs. Moreover, case studies performed at a temperature of interest of -76°C at the proximal zone of the stem, showed that for that particular range of temperature, the force required to release the prosthesis increased, compared to the values obtained for case studies at temperatures of interest of -40°C and -49°C in the tests performed with composite geometries (cylinder and femur), whereas for the steel mould specimens, the maximum force required to remove the cemented stem was lowest at -76°C. Nevertheless, the experiments performed with composite bones demonstrated that the maximum force required to remove the prosthesis from the cement mantle could be lowered from 53% to 65% compared to the force required at room temperature, and that reduction can be achieved by aiming to cool proximal zone of the stem down to temperature of -40C.

Strain energy was calculated by using equation 3.4 from Section 3.3.3.1, to visualize how much mechanical energy was required to break the interface between the femoral stem and the cement mantle and remove the femoral stem from where it was implanted (steel mould, composite cylinder, composite femur). Table 4.3 shows that the

cooled specimens of steel mould required much more energy, almost four times the value, than those cylinders and femurs equally cooled at the corresponding temperatures of interest, -40°C and -49°C for the cylinders and -40°C for the femur. The results of strain energy confirmed that by cooling the proximal zone of the femoral stem at -40°C, less mechanical energy is required to loosen and extract the prosthesis from the material were it was implanted.

Table 4.3 Experimental average results of the case studies using composite femurs.

Material Used	Case Study	Temperature (°C)	Maximum Pulling Force (kN)	Reduction Pulling Force compared to control kN-(%)	Maximum Shear Stress (MPa)	Total Strain Energy (J)
Steel Mould	Control	23	14.55	-	2.24	13.24
	1	-76	6.32	8.23 kN (56.5%)	0.97	9.9
	2	-58	8.85	5.7 kN (39%)	1.36	8.7
	3	-49	10.45	4.1 kN (28%)	1.61	11.8
	4	-40	10.04	4.5 kN (31%)	1.54	12.1
Sawbones Cylinders	Control	25	13.98	-	2.15	10.66
	1	-76	6.93	7 kN (50%)	1.07	4.01
	2	-49	6.05	7.9 kN (57%)	0.93	3.18
	3	-40	6.52	7.4 kN (53%)	1.01	3.16
Sawbones Femurs	Control Cylinder	25	13.98	-	2.15	10.66
	1	-76	9.44	4.5kN (32.5%)	1.45	6.8
	2	-40	4.9	9 kN (65%)	0.75	2.34

To know the interface strength between the titanium stem and the bone cement when structurally failing in shear, the maximum shear stress was calculated by using the maximum force required to release the cemented stem and the area of contact between the prosthesis and the cement in equation 3.5 from Section 3.3.3.1. As shown in Table 4.3, the maximum shear stress obtained for control specimens had a very similar value in al case scenarios. By comparing the thermally treated specimens, it was shown that the maximum shear stress was higher for the specimens of steel mould tested at temperatures of -40°C, -49°C, and -58°C, while for the cylindrical specimens the values were lower in the cases tested at -40°C, and -49°C, as well as for the composite femur tested at -40°C. Nevertheless, the case scenarios with composite bones showed that the maximum shear stress is practically the minimum, when the proximal zone of the femoral stem is cooled at -40°C, which also showed that the force required to remove the cemented femoral stem was lower and conveniently in the critical temperature of safety. Nevertheless, all thermally treated specimens showed a reduction of maximum shear stress compared to the control specimens.

The results shown in chapter 3 and chapter 4 have demonstrated that thermal treatment can be employed to effect a reduction on the force required to remove a well-cemented titanium stem, and these effects of the temperature can also be seen in the reduction of maximum shear stress and the total strain energy for each cooling case. The following chapter presents a concept design of a medical device which works based on this idea which forms the foundation for a new technique.

Chapter 5
Concept Design of the Medical Device

5.1 Introduction

The results of the experimental tests performed with composite bones in Chapter 4 confirmed that by applying the new methodology, the force required to remove a femoral stem at a temperature of -40ºC was considerably lowered by 53% and 65% when the stem was cemented in composite cylinders and composite femur respectively.

Based on the information gathered from the work presented in previous chapters of this thesis, a concept design of a medical device can be worked. The design of a medical device is a complex process that needs to be well planned with the objective of obtaining the final product that will be launched to the market.

This chapter describes the developing process of the concept design of the medical device. The process starts by defining the user which are the surgeon and medical personnel, and the patient. Once the needs have been identified, the specification requirements are addressed followed by the starting point of the concept design involving decision-making, leading to a final detailed concept design. It is crucial that the detailed concept design fulfils the needs of the users: medical professionals and patients while functioning under the characteristics of the new methodology.

5.2 General Description of the Design Process

In order to carry out a concept design, a framework that facilitates the selection process of product characteristics and decision-making was put into practice. A simplified framework, as shown in Figure 5.1, identifies the main activities that are systematically implicated in the design process [253-257].

Alonso-Rasgado et al. [257] reviewed diverse knowledge types that are required for service development process. Nevertheless, since service development and hardware design process have close similarities, the present research followed and fulfilled two of the three stages of concept development described in their research. The stages applied to the development of a concept design of a medical device are summarised as follows:

I. Concept development
    a. Identification of user's needs
    b. Specification of requirements
    c. Concept design of medical device

II. System design
    a. Detailed design

III. Testing and implementation. This stage was not covered in the present thesis, as it was visualised as future work.

The design process started by identifying the needs of the customer, in the present case, the surgeon and the medical personnel as well as the patient, were identified as the users/customer. Once the user's needs have been indicated, these were interpreted into requirements in order to fulfil specifications that established potential solutions. These possible solutions were compared and evaluated in the development of the concept design by following Pugh's matrix for decision-making [256]. A number of possible solutions for the medical device were generated and weighted against each other in the design criteria generated in the Pugh's matrix. The concept design that met the criteria was selected and the re-evaluated by following the same norm from the Pugh matrix. As a result, a more competitive concept design was attained, detailed design, and general description of the operation of the medical device were made.

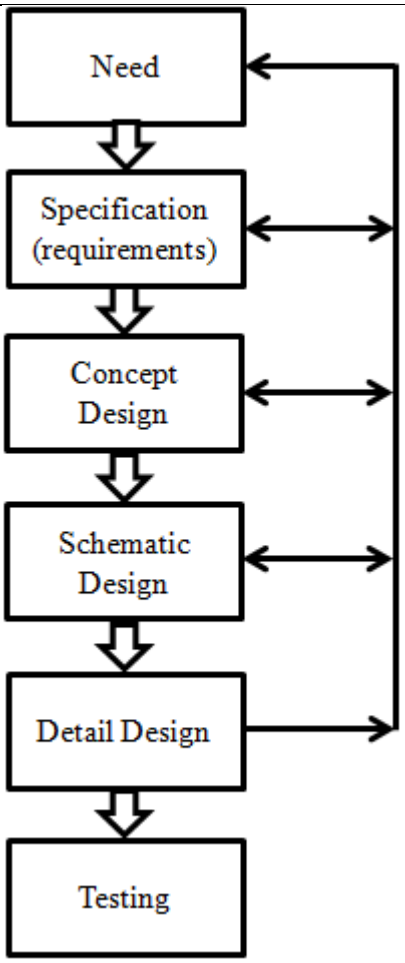

Figure 5.1 General design process [256, 257].

5.3 Concept Development of the Medical Device

This thesis was focused on a specific need which was to provide a new methodology to remove a femoral stem during revision total hip arthroplasty. This new methodology proved that by applying low temperatures on the femoral stem, the force required to remove a cemented prosthesis from bone-like material was considerably reduced. From these findings, the main purpose of the medical device is to safely remove a well-fixed femoral stem during revision total hip arthroplasty by using the new methodology.

In order to start the design process of the concept medical device, concept development began by identifying the needs of the user. After identifying the user's needs, specific requirements of the medical device were assessed in order to create the

suitable characteristics of the concept medical device. These phases of concept development are described in the following sections.

5.3.1 Identification of Device User Needs

Firstly, it was important to identify and understand the user's needs. The role of the user had to be comprehended in order to add design attributes to the concept.

5.3.1.1 Device User Needs

The user needs were classified into two groups, surgeon and medical personnel, patient as follows:

Surgeon and medical personnel:

1. The device should be easy and fast to mount and operate over the leg of the patient.
2. Detailed and clear user-guide protocol for the device.

Patient:

1. The patient's health shall not be put at risk when the device has been mounted and while the device is in operation.
2. The integrity of the living tissue near the medical device shall be safeguarded when the device is being mounted and while the device is in operation.

5.3.1.2 Operating Theatre Needs

In addition to surveying the surgeon and medical personnel, an extra need was found, the operating theatre. For the surgeon to freely manipulate the medical device, it must meet the characteristics of the operating theatre and its restrictions. Figure 5.2 shows the operating theatre, the red square limits the operating area (2.7 x 2.7 m).

Operating theatre:

1. The working space is limited (2.7 x 2.7 m), and the available space surrounding the operating area is narrow (1.5 m). Therefore, the various parts that constitute the medical device should occupy as little space as possible.

2. The operating theatre does not account of a cryogen agent station. Therefore, the device must have a source for the cooling agent.

3. The device should meet the regulations for use in the operating theatre as described in the following Section 5.3.2.

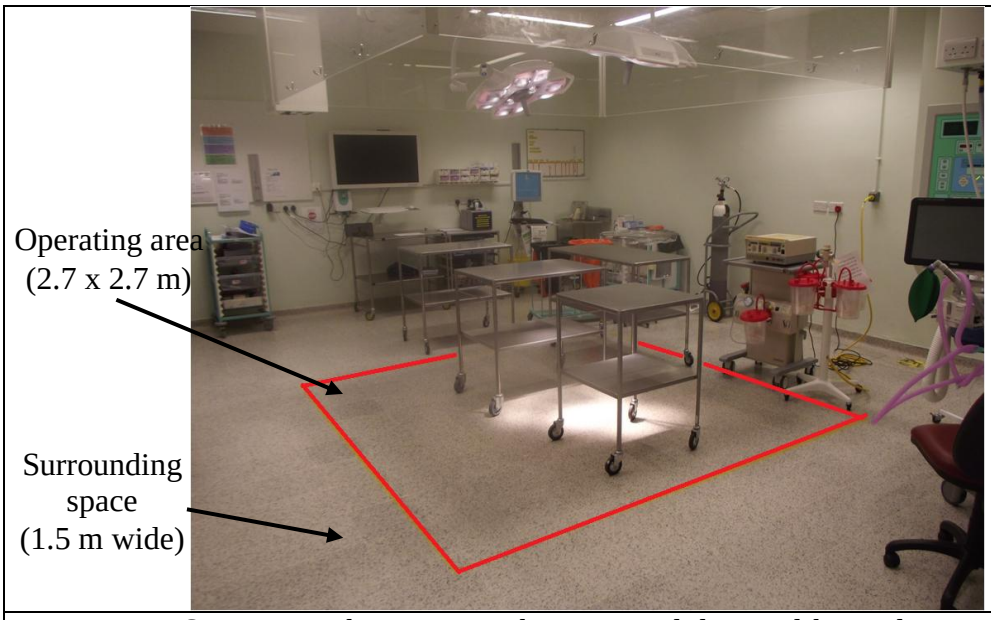

Figure 5.2 Operating theatre. Working area delimited by red square.

Figure 5.3 shows various characteristics of the operating theatre such as gas outlets (oxygen, nitrous oxide) and vacuum pressure, master control panel, lighting, diverse medical equipment stored around the operating area.

b)

c)

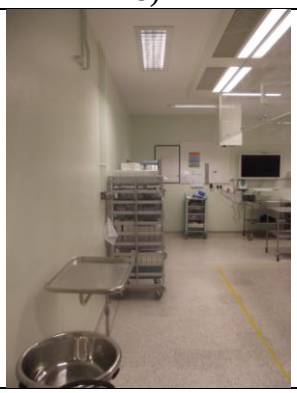

d)

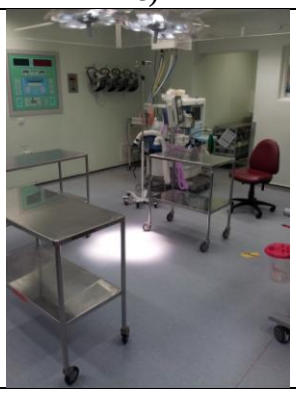

e)

f)

g)

Figure 5.3 The various characteristics of the operating theatre: a) gas outlets and vacuum pressure, b) master control panel, c) Space surrounding operating area and diverse medical equipment, d) distribution of equipment around operating area, f) lightning, g) operating area.

5.3.2 Specification of the Requirements for the Device

Since the health of patients can be compromised by a failure of the medical device, manufacturing and marketing of medical devices in the world must be regulated, checked, tested and analysed in an effort to ensure the effectiveness and safety of the device. Complying with these requirements constitutes a major key point in the development process to gain approval for medical devices research. In Europe, the device should be designed by following the guidance for researchers, manufacturers, and research ethics committees developed by the following European bodies:

I. Medicines and Healthcare Products Regulatory Agency – Devices Division (MHRA).

II. National Institute for Health and Care Excellence (NICE).

III. National Research Ethics Service (NRES).

IV. British Standards Institution (BSI).

V. CE Marking of Medical Devices in line with the European Devices Directive (MDD) in order to gain access to the market in Europe.

VI. Fulfil the following standards for British and European market:

   a. ISO 14971 “Medical Device Risk Management”.

   b. ISO 13485 “Quality Management System for Medical Devices”.

   c. ISO 14155-1 “Clinical Investigation of Medical Devices for Human Subjects – part1: General Requirements”.

   d. ISO 14155-2 “Clinical Investigation of Medical Devices for Human Subjects – part2: Clinical Investigation Plans”.

   e. EN 60601 “Medical Electrical Equipment and Systems”.

VII. Use of cryogenic fluids in operating theatre:

a. Code of Practice CP30 - "The Safe Use of Liquid Nitrogen Dewars up To 50 Litres", rev 1, 2008, published by the British Compressed Gases Association (BCGA).

b. SI 1992 No 2793 “The Manual Handling Operations Regulations”, 1992.

c. SI 1999 No 3242 “The Management of Health and Safety at Work Regulations” 1999.

d. SI 1992 No 2966 “The Personal Protective Equipment at Work Regulations” 1992.

It is possible that the list of regulations and guides should be revisited as the project advances in the design process and depending on the market it is intended for.

5.3.3 Concept Design of Medical Device

The concept design began after the user’s needs and requirements were classified. As the next step in the design process, diverse concept designs were generated through rough sketches, attributes and functions that fulfilled the needs and requirements. Posteriorly, they were evaluated through Pugh’s matrix for the decision-making. The Pugh’s matrix presented various criteria of the device in measurable terms in order to develop a final concept design.

Information gathered from the experimental work of the present study was essential for the design of the product:

a. Desired working cooling temperature: -40°C.

b. Cooling agent: liquid nitrogen (LN_2).

c. Maximum force required to remove cemented femoral stem: < 14 kN.

d. Minimum force required to remove cemented femoral stem: > 4 kN.

e. Approximate time to reach the cooling temperature of interest: 5 min.

f. The various parts of the device and its working station should not occupy an area bigger than 50x50 cm.

g. The medical device should be able to enclose the femoral neck should allow a minimum volume of 25 ml of cooling agent.

h. The medical device should have a pulling mechanism and it may rest over the dissected proximal zone of the femur.

i. The base of the medical device resting over the dissected proximal zone of the femur should not exceed the boundaries of that dissected area. This may vary according to the characteristics of the femur and age of the patient.

j. The base of medical device resting over the dissected proximal zone of the femur should not cause any potential damage to the bone structure.

5.3.3.1 Concept Development of the Medical Device

By a continuous search of ideas to fulfil the needs, the concept development phase was not restricted to only one design; a total of three concept designs were generated in order to search for the best idea that could meet all requirements for the medical device.

Once the needs and specifications for the design had been set, the search for the solutions started, with the objective of meeting the needs and requirements of the device.

As a first approach, Figure 5.4a shows the concept design #1. The concept consists of a cap encapsulating the neck of the stem. The cap has one coolant inlet and two outlets, one for the remaining liquid and one for the coolant that may evaporate due to the heat transfer process.

Figure 5.4b shows in more detail the possible construction of the concept design #1, called “cryo-cap”. The wall of the cryo-cap is made of three materials, the inner and outer walls are of stainless steel and the intermediate wall is made of an insulating

material. The insulating material used could vary from ceramic, fibreglass, or glass epoxy G-10. At the base of the cap, a cryogenic insulating seal is required as a way to protect from any leakage of coolant that may put at risk the soft tissue and health of the patient. The inlet of liquid coolant should allow a continuous flow into the cap and exit through the outlet at the bottom of the cap. A second outlet works as pressure relief and exit for the evaporated coolant.

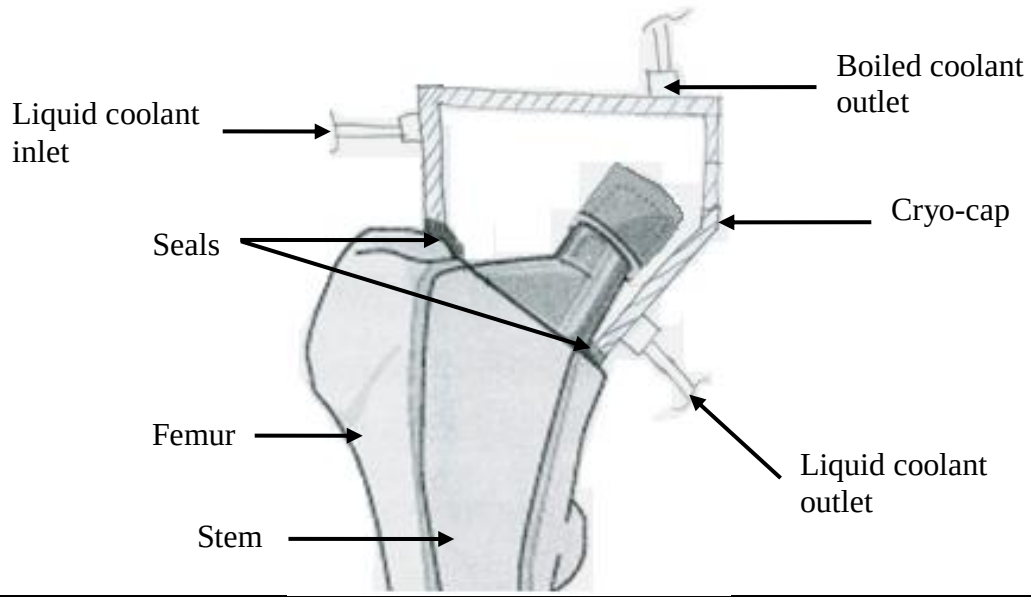

a)

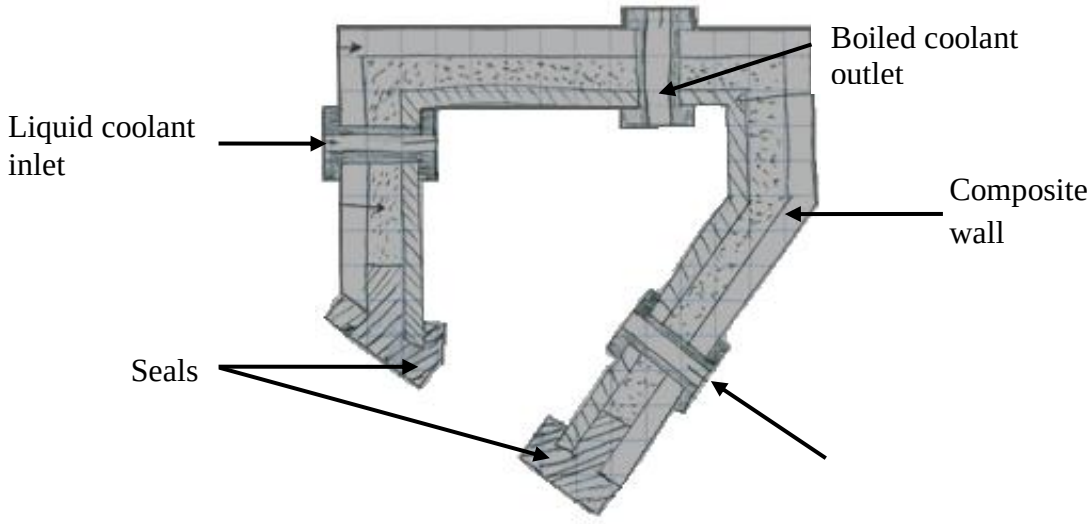

b)

Figure 5.4 Concept design #1 of "cryo-cap": a) general drawing, b) cryo-cap and its construction.

Figure 5.5 shows the concept design #2. This design is a variation from the concept #1, this "cryo-cap" includes an opening that allows the surgeon to introduce a threaded rod through the cap, as shown in Figure 5.5a.

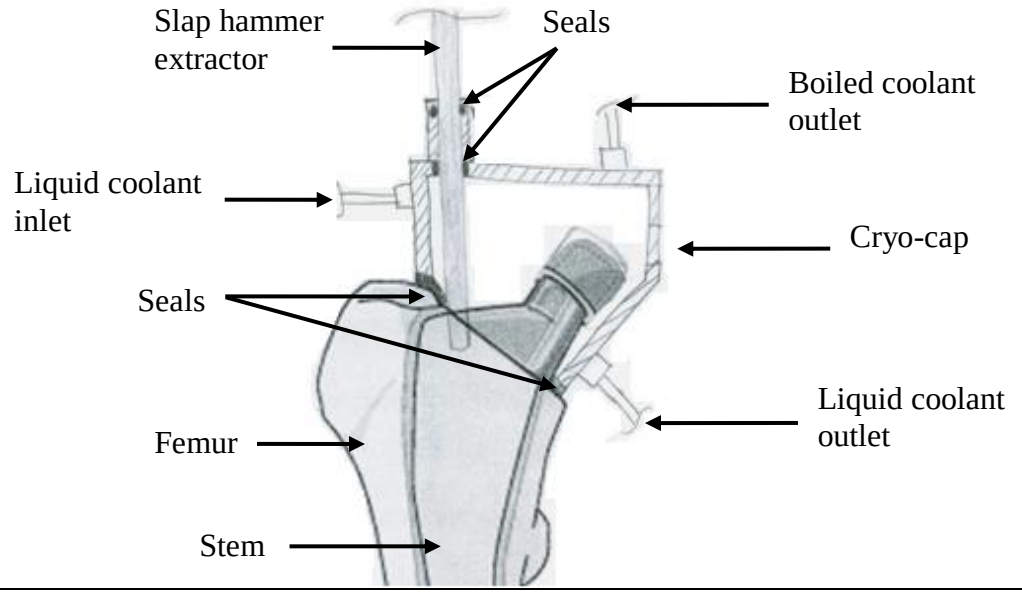

a)

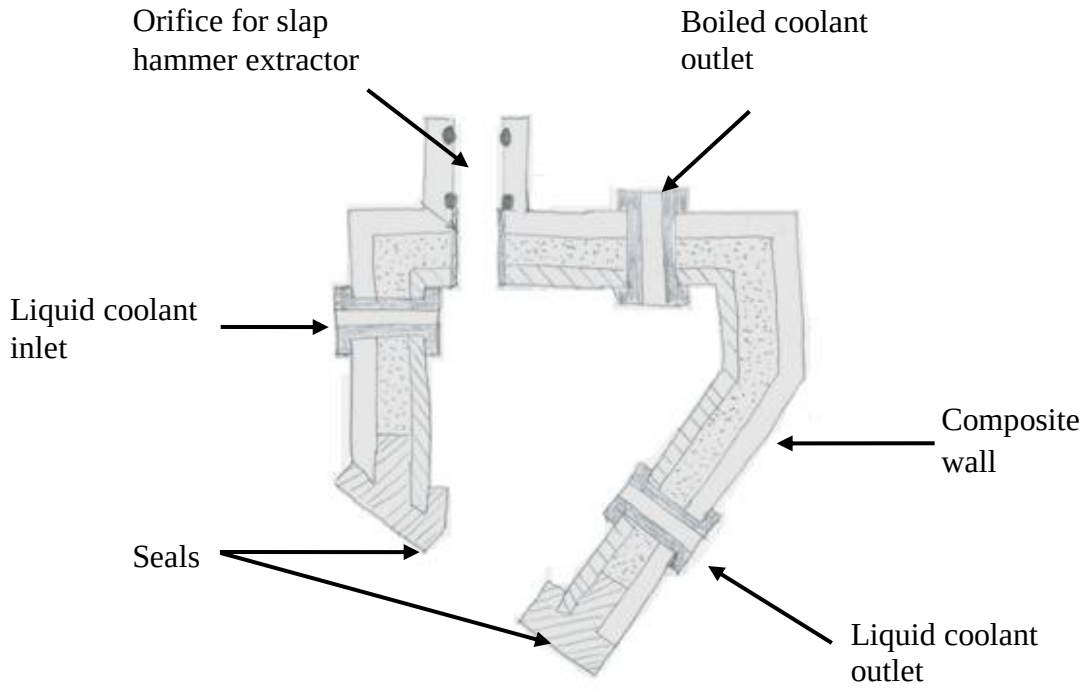

b)

Figure 5.5 Concept design #2 of "cryo-cap": a) general drawing, b) cryo-cap and its construction.

The opening, or orifice, allows the femoral stem to be fastened with a threaded rod. The rod should be part of a slap hammer, which will serve as the extractor. Inlets and outlets of the cooling agent remain the same as in the previous concept design.

Figure 5.5b shows a possible construction of the modified cryo-cap. Similarly, the cryo-cap is made of three materials: the interior and exterior walls are made of stainless steel and there is an insulating material in between.

A possible third concept was proposed. Figure 5.6 shows concept design #3, which is a variation of the cup where only the neck of the stem is surrounded and encapsulated. This new shape of the cup is now called "cryo-bell". In the same way as in the previous designs, the cryo-bell has one inlet for the cooling fluid and two outlets, one for evaporated coolant and pressure relief.

The cryogenic seal at the base of the cryo-bell should provide a hermetic seal and thus protects the living tissue from being damaged by the coolant. The composite wall of the bell is structured in tandem: insulating material between two walls of stainless steel. This design allows the surgeon to use a traditional tool, the slap hammer, to extract the femoral stem without worrying about how the cooling agent might affect the threaded stem of the slap hammer.

After designing three possible concepts of the medical device, a PUGH analysis was carried out. The PUGH analysis is a criteria-based matrix to quantitatively determine the best solutions for a problem or best characteristics of a design [253-255, 258, 259]. The baseline for the concepts is the current method of extraction of the femoral stem, which is manually done. Each of the alternative concept designs was evaluated using the criteria in the range from -1 to 1, with -1 being a poor solution or characteristic from the criteria and +1 being the best match to a criterion. The relevance of each criterion was weighted in the range from 1 to 3, 3 being the most important.

Table 5.1 shows the concept designs mentioned earlier and their comparison to one another with the criteria alternatives and their subdivisions:

1. Operation process:

    a) Modes of use: Automatic, manual, on/off switch

b) Infrastructure: Energy use (electricity, hydraulic)

2. Operational performance:

a) Physical characteristics: Geometry, materials

b) Performance parameters

c) User interface

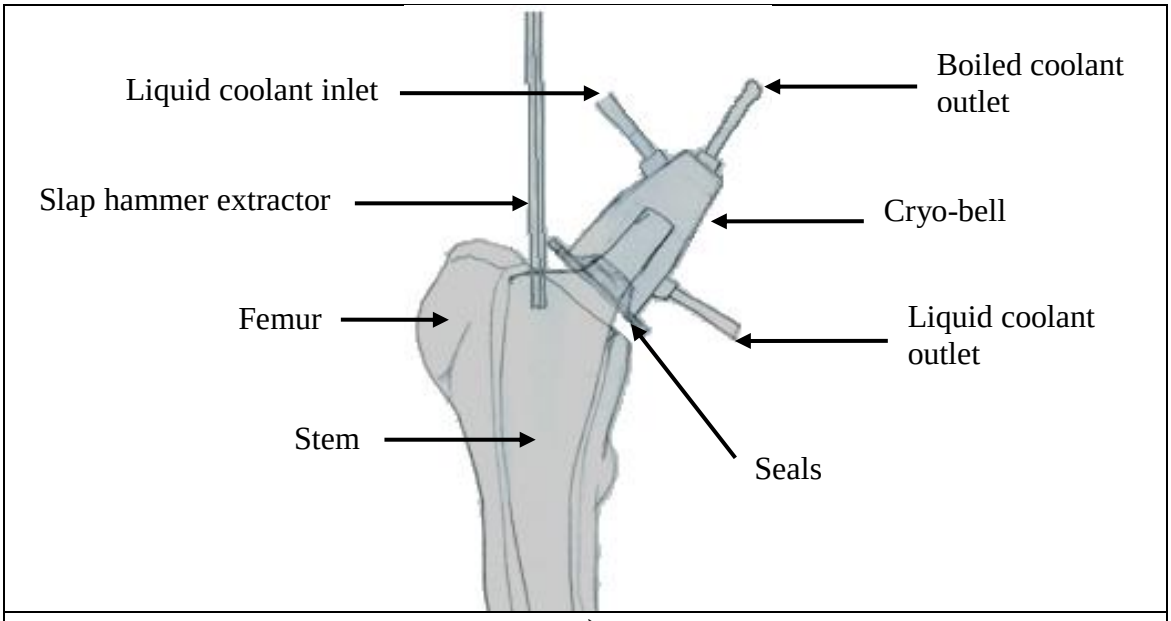

a)

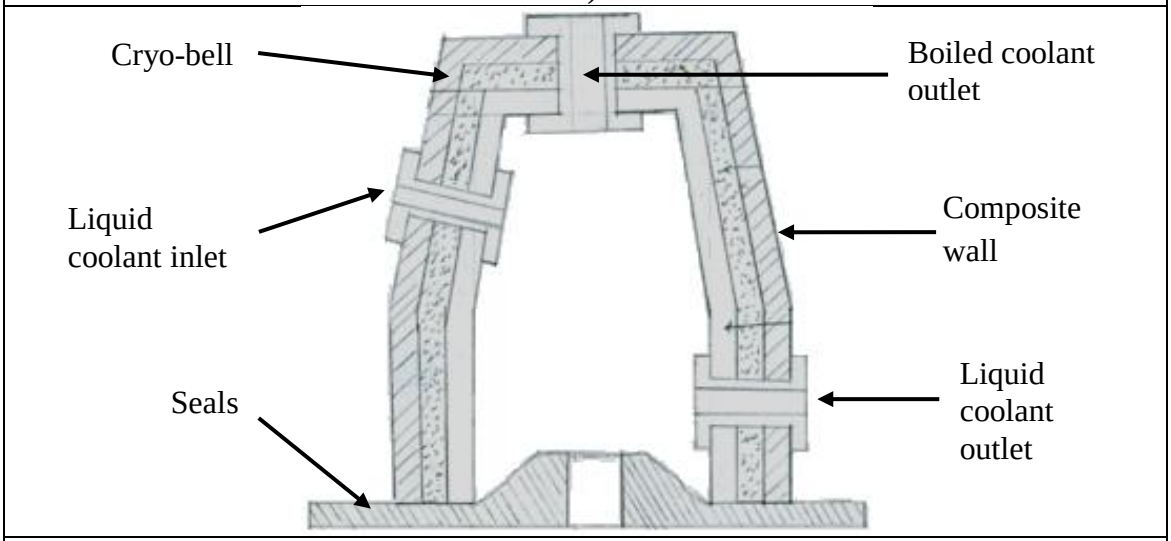

b)

Figure 5.6 Concept design #3 - "cryo-bell": a) general drawing, b) cryo-bell and its construction.

After analysing the three concept designs with the PUGH method [256], it was found that the third concept design obtained a higher score. As the next step, a second analysis was undertaken from Concept #3, in order to improve some of its characteristics to create a much more effective design.

Table 5.1 PUGH analysis of developed concept designs [253-255, 258, 259].

Alternatives	**Weight**	**Concept 1**	**Concept 2**	**Concept 3**
Criteria (-1, 0, 1)	1,2,3			
Operation Process				
Modes of Use				
automatic	3	-1	-1	-1
manual	1	0	0	0
on/off	3	0	0	0
Identify Infrastructure Reqs.				
energy (electricity, hydraulic power)	3	-1	-1	-1
Operational Performance				
Physical Characteristics				
Geometry:				
shape	2	-1	0	1
size (height length, volume, diameter)	3	1	1	1
space requirement	3	0	0	0
maximum dimensions	3	1	1	1
weight	3	0	0	0
operating temperature range	3	1	1	1
operating pressure range	3	-1	-1	-1
forces (maximum magnitude)	3	0	0	0
Materials:				
corrosion resistance	3	1	1	1
sterilizability	3	1	1	1
insulation	3	1	1	1
manufacturability	2	1	1	1
Performance Parameters				
speed of operation	2	0	0	1
capacity	2	1	1	1
accuracy	3	0	0	0
repeatability	2	0	0	0
response time	3	0	0	0
User Interface				
man-machine relationship	2	0	0	0
operator skill/training requirements	2	1	1	1
Clarity of interface:				
operator input	2	0	0	0

Continues on next page

Continuation of Table 5.1

operator output	3	1	1	1
feedback to user	3	0	0	0
Ergonomics:				
posture of operator	1	0	0	0
operator fatigue	1	-1	-1	-1
ease of assembly	3	1	1	1
Score		**18**	**20**	**24**

The additional alternatives taken into consideration were: controlled and automatic operation of the pulling mechanism with the use of hydraulic power; better accuracy; and better mechanical and thermal performance. To do this, the characteristics of concept design #3 were taken as the base line to improve the design [253-255, 258, 259].

Table 5.2 presents the analysis of both concept designs where concept design #4 shows a higher score meaning an improvement in the design. The following sections of Chapter 7 present the details and specifications of the selected concept design.

Table 5.2 PUGH analysis concept design #3 vs improved concept design [253-255, 258, 259].

Alternatives	**Weight**	**Base Line Design - Concept 3**	**Improved Design - Concept 4**
Criteria (-1, 0, 1)	1,2,3		
Operation Process			
Modes of Use			
automatic	3	-1	1
manual	1	0	0
on/off	3	0	1
Identify Infrastructure Requirements			
energy (electricity, hydraulic power)	3	-1	1
Operational Performance			
Physical Characteristics			
Geometry:			
shape	2	1	1
size (height length, volume, diameter)	3	1	1
space requirement	3	0	-1
maximum dimensions	3	1	-1

Continues on next page

Continuation of Table 5.2

weight	3	0	-1
operating temperature range	3	1	1
operating pressure range	3	-1	1
forces (maximum magnitude)	3	0	1
Materials:			
corrosion resistance	3	1	1
sterilizability	3	1	1
insulation	3	1	1
manufacturability	2	1	0
Performance Parameters			
speed of operation	2	1	1
capacity	2	1	1
accuracy	3	0	1
repeatability	2	0	0
response time	3	0	1
User Interface			
man-machine relationship	2	0	1
operator skill/training requirements	2	1	1
Clarity of interface:			
operator input	2	0	1
operator output	3	1	0
feedback to user	3	0	1
Ergonomics:			
posture of operator	1	0	1
operator fatigue	1	-1	1
ease of assembly	3	1	0
Score		**24**	**44**

5.3.4 System Design: Detailed Design of the Selected Concept 4

The system design phase has the task of transcribing concepts into specific elements that comprise the design as a whole. After identifying the various elements that will constitute the concept design of the medical device, a detailed description of the design criteria for each element of the design is carried out. Once the best characteristics and the most suitable solution ideas had been selected from the preliminary concepts, the development of the concept design continued.

A medical device composed of two parts is presented next: a component whose function is to apply the cooling procedure, and a component which mechanically removes the femoral prosthesis by means of a pulling mechanism. The cooling

procedure from the new methodology takes part in the cryo-bell that will encapsulate the neck of the femoral stem. In order to remove the femoral stem, instead of applying the traditional removal method of hammering the prosthesis with the retrograde technique, a hydraulic extraction mechanism is included in the device. Details and specifications of these two components are presented in the following section.

5.3.4.1 Detailed Design: "Cryo-bell"

Figure 5.7 shows the concept design of the cap that will encapsulate the femoral neck so that the cooling agent can flow inside and cool the neck. Figure 5.8 shows the dimensions of the cryo-bell, and the specifications of the design are listed below:

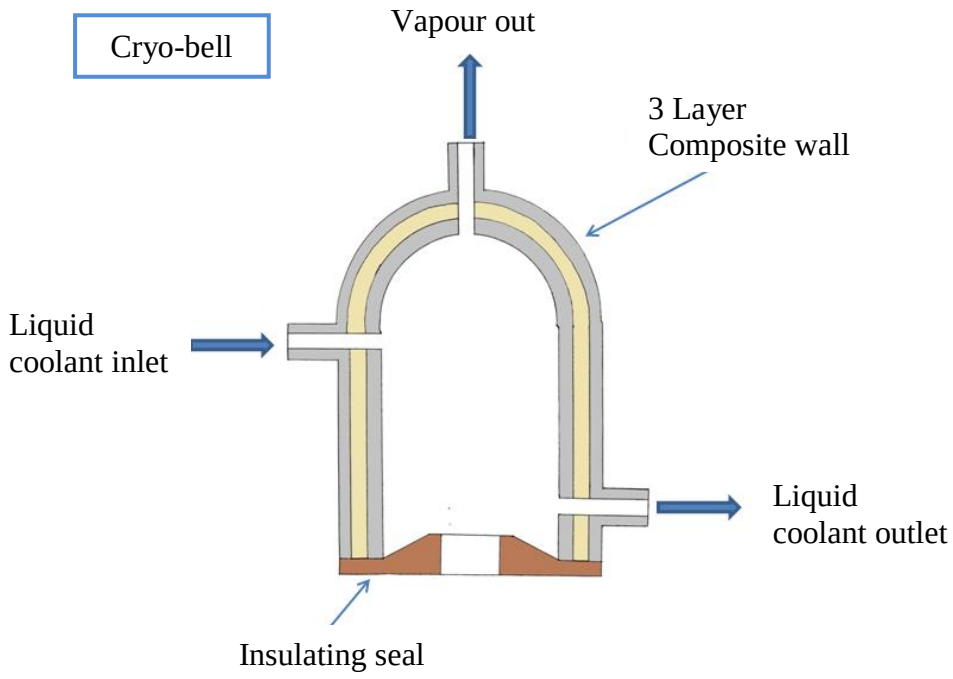

Figure 5.7 "Cryo-bell", descriptive schematic of the concept design.

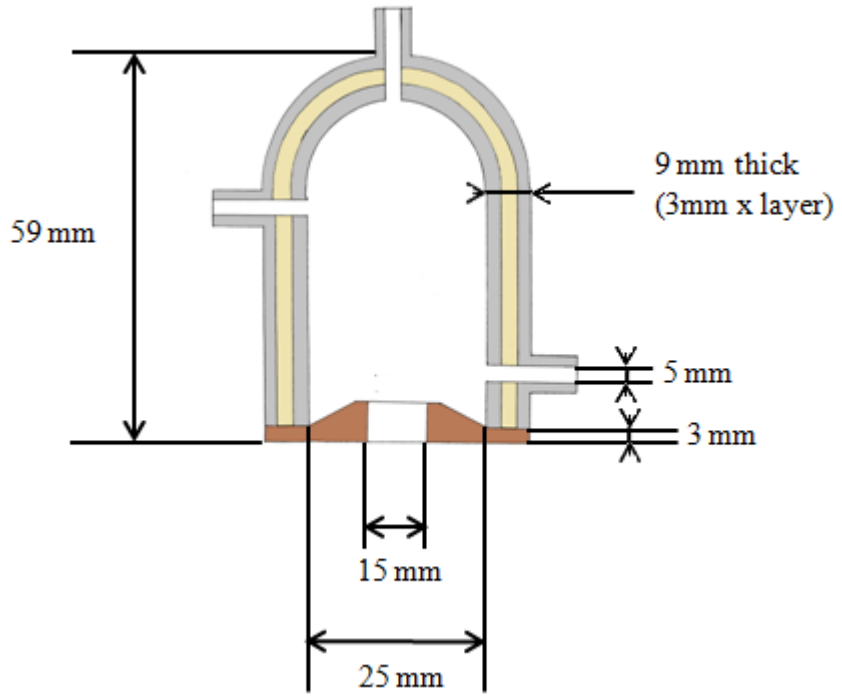

Figure 5.8 “Cryo-bell”, dimensions.

a. The cooling cap “cryo-bell” should be manufactured with materials that can withstand cryogenic temperatures.

b. The “cryo-bell” should have approximate internal dimensions of 25 mm diameter and 50 mm height thus having a capacity of 25 ml of cooling fluid.

c. The “cryo-bell” has one inlet for the cooling agent and two outlets, one as exit and purge of the remaining liquid cooling agent, and one as exit and purge of the evaporated cooling agent.

d. The “cryo-bell” must completely cover the neck of the femoral stem.

    a. At the bottom of the “cryo-bell”, a fitted indium cryogenic seal prevents any leakage of the cooling agent and further damage to living tissue.

e. The structure of the “cryo-bell” should be a composite wall in tandem. Each wall should have a thickness of no less than 3mm but the outer diameter should not exceed 45 mm.

5.3.4.2 Material Selection of the Cryo-Bell

a. Exterior wall: 303 stainless steel was chosen as the primary material since it is widely used for cryogenic devices due to its mechanical and thermal properties, and it is also used for medical purposes because it can be sterilised.

b. Middle wall: made of fibre glass epoxy G-10. Chosen as insulation wall due to its low conductivity coefficient.

c. Interior wall: 303 stainless steel.

5.3.4.3 Detailed Design: Pulling mechanism - hydraulic piston

Figure 5.9 shows the concept design of the pulling mechanism, which is a double-acting, hollow plunger cylinder mounted on a saddle. Dimensions of the pulling mechanism are shown in Figure 5.10 and the detailed characteristics are as follows:

a. The saddle is shaped as an inverted U shape where the hollow plunger is fixed.

b. The saddle rests over the resected area of the femur, allowing the mechanism to have a support area while pulling the femoral stem.

c. The inverted U-shape of the saddle allows the femoral stem to move freely upwards while being pulled by the plunger.

d. The hollow plunger should have a minimum stroke of 5 mm and a maximum of 10 mm.

e. The maximum capacity of the plunger should be 14 kN.

f. The hydraulic fluid of the plunger should be non-toxic and meet safety and sanitary requirements.

g. The hollow plunger should have a minimum centre hole diameter of 9 mm and a maximum of 10 mm.

h. The double-acting cylinder must be powered by a pump with a 4-way valve.

i. The hollow plunger allows the insertion of a threaded stem into the femoral prosthesis.

j. The threaded stem is screwed into the threaded hole of the femoral stem.

k. The threaded rod should be 65 mm longer than the total height of the pulling mechanism. This will allow the threaded stem to be nut-fixed to the plunger.

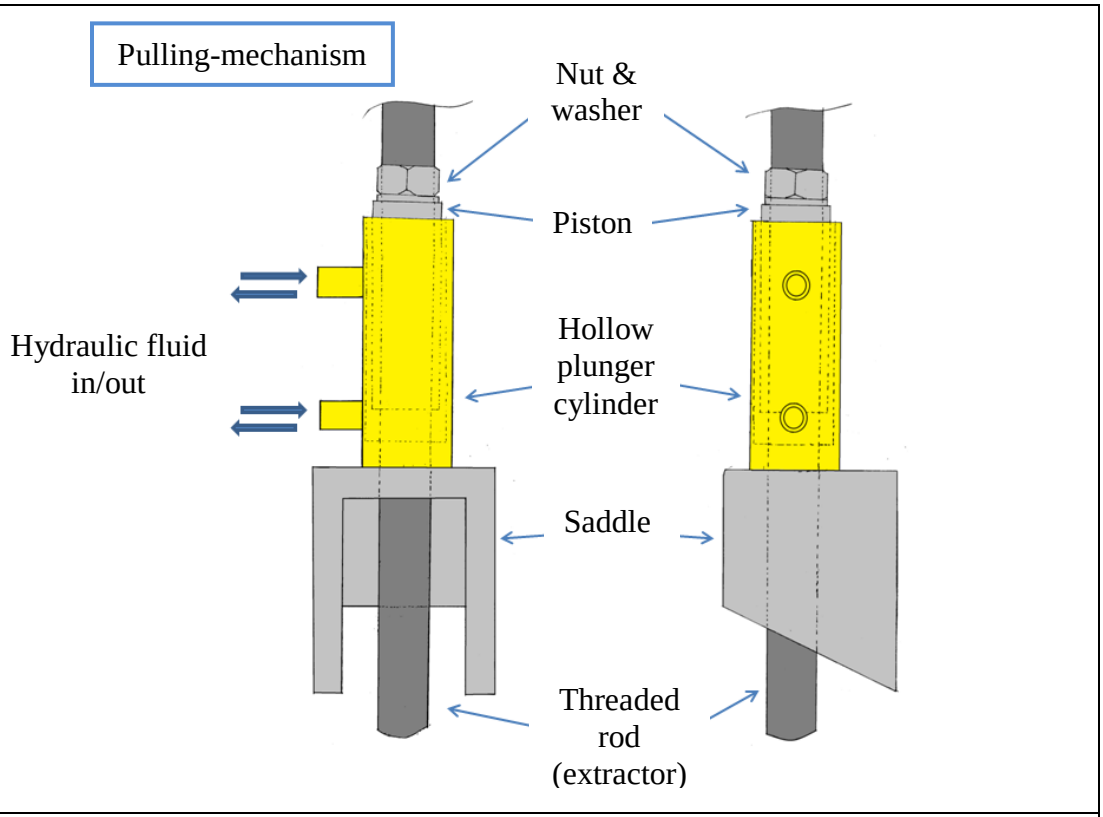

Figure 5.9 “Pulling-mechanism”, schematic of the concept design.

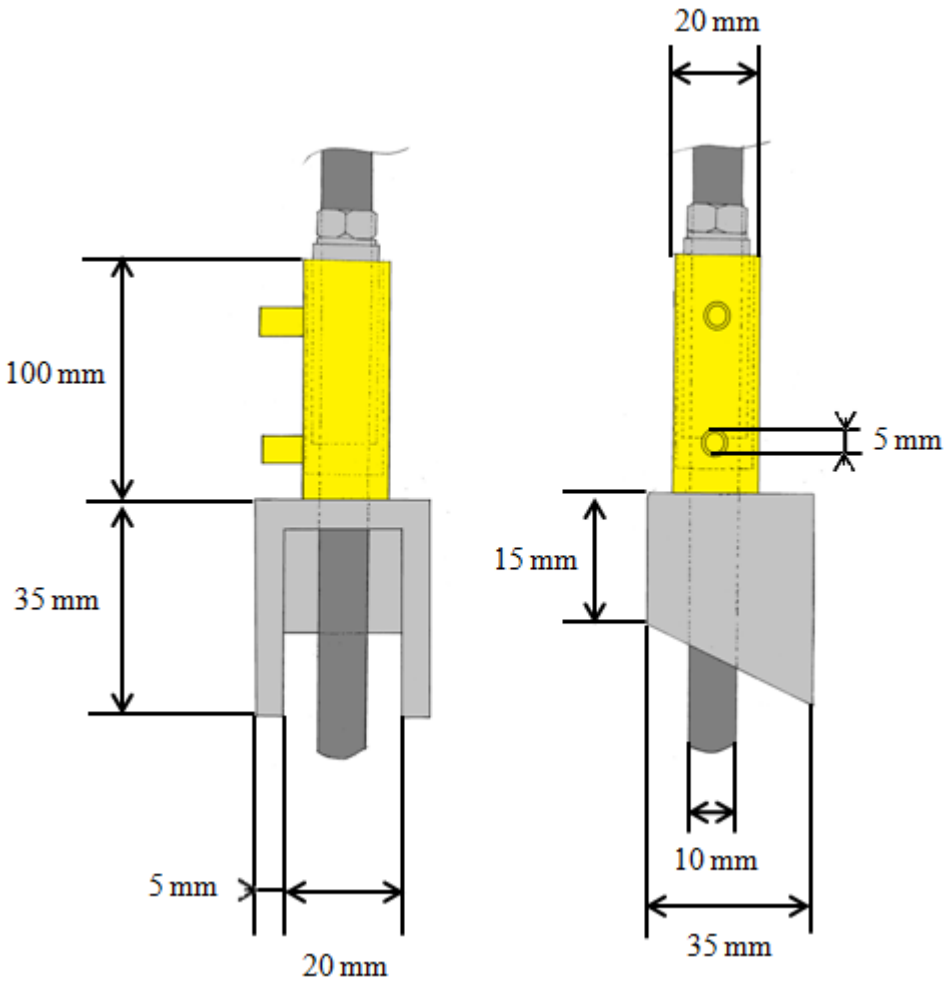

Figure 5.10 “Pulling-mechanism”, dimensions.

5.3.5 General Description of the Operation of the Selected Medical Device

A design concept of an orthopaedic medical device utilising low temperatures in the surgical treatment of revision hip arthroplasty is presented. Figure 5.11 shows the device mounted on the femur and femoral stem.

Once the surgeon has exposed the hip and the femoral prosthesis, the general operation of the medical device is as follows:

1. The neck of the femoral stem is plugged into a “cryo-bell” which completely encapsulates the neck.

2. The pulling mechanism is mounted on the femoral stem. This pulling mechanism consists of a double-acting, hollow plunger mounted on a saddle, which rests on the surface of the resected femur.

3. The hollow plunger allows the surgeon to insert a threaded steel stem into the femoral prosthesis. Once the threaded stem has been inserted, it is secured by the other end to the hollow plunger with a washer and nut.

4. The "cryo-bell" is filled with the cooling agent, LN_2, pumped at regulated volumetric flow of Q = 0.25 L/min from a cryogenic storage Dewar by using a Norhof® - micro LN_2 pump. Filling time: $t = \frac{V}{Q} = \frac{0.025\ L}{0.25\ L/min}$ = 0.1 min = 6 seconds.

5. While heat transfer occurs inside the "cryo-bell", the cooling agent partially evaporates and the vapour is allowed to escape through an exit/outlet port to prevent overpressure inside the "cryo-bell".

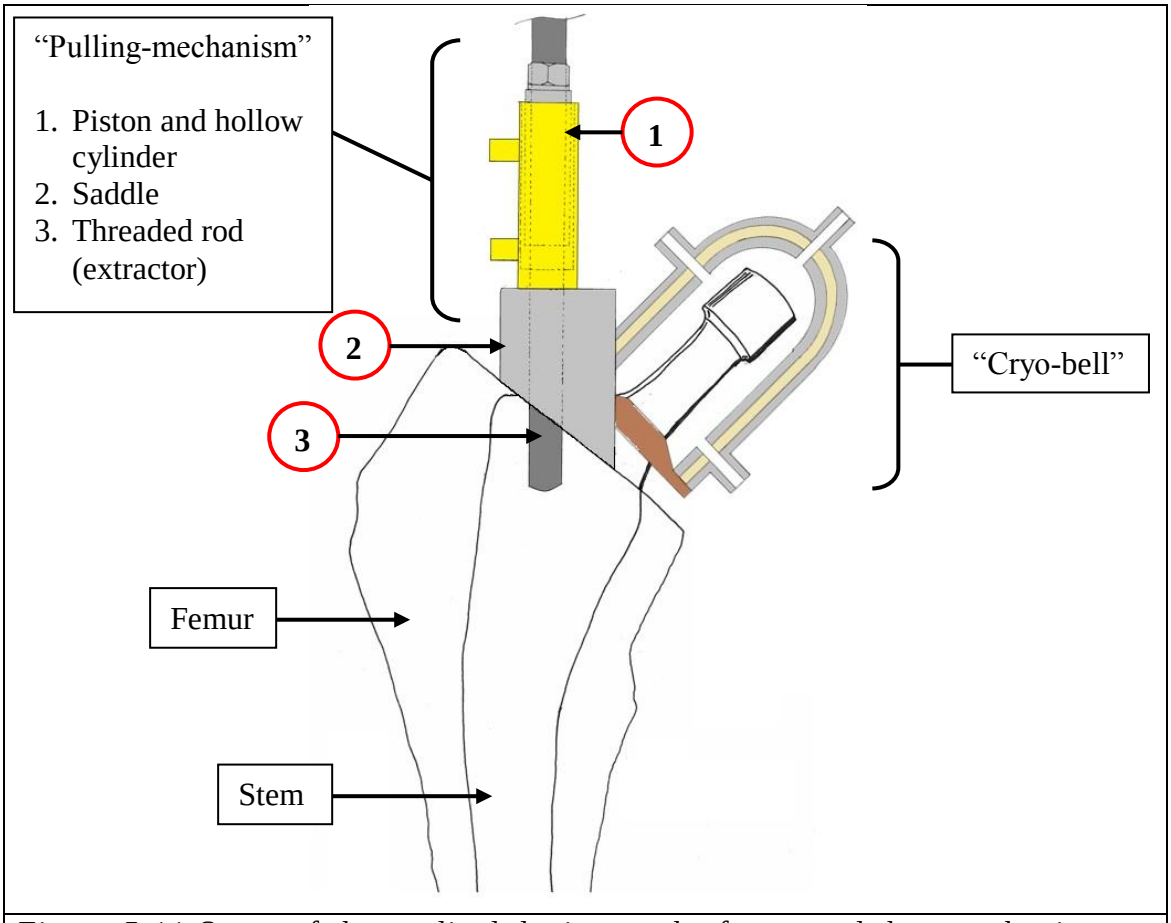

Figure 5.11 Setup of the medical device on the femur and the prosthesis.

6. A second exit/outlet port allows the coolant to flow constantly and be collected in a reservoir.

7. The pump is allowed to function until the cooling temperature is reached, which is -40°C.

8. Once the temperature of interest has been reached the pump is turned off, the security valves from the feeding line are closed to stop the flow of coolant into the "cryo-bell", while the second exit/outlet port is used to drain/purge the coolant that may remain in the "cryo-bell".

9. Once the "cryo-bell" has been emptied, the pulling process starts.

10. The plunger starts pulling the femoral stem at a rate of 0.5 mm/min. The allowed time interval to start pulling the femoral stem should be between 120 seconds and should not exceed 300 seconds. This is recommended because the prosthesis would be warming up quickly due to the body heat generation, and its interaction with air in the room.

11. Once the femoral stem has been released from the femur, the pulling mechanism is stopped and the device is un-mounted.

In case there is no thread hole in the femoral stem to secure the slap hammer or threaded rod of the pulling mechanism, a hole would have to be drilled in the implanted stem. This would be possible only on stainless steel femoral stems since cobalt-chromium and titanium alloy stems would be very difficult to drill while in surgery. On the other hand, the medical device would have to pass through other PUGH analysis.

The following chapter presents a computational model of an artificial specimen that mimics a femoral stem implanted with bone cement. The numerical analysis of the cooling process helps in understanding the heat transfer process by visualising the temperature fields in the specimen and thus predicting an ideal cooling regime to determine the margins of safety.

Chapter 6
Finite Element Thermal Analysis

6.1 Introduction

An understanding of mechanical and thermal properties of human tissues and the physics governing the biological processes has been gained by studying engineering principles of structural mechanics, materials science, and the application of heat and mass transfer concepts in medicine.

The application of numerical methods in the bioengineering field includes studies of stresses in bones in healthy conditions or with a pathological indication. Heat and mass transfer within the body such as blood flow, breathing, design of surgical tools, devices of cryopreservation and infant incubators are some examples found in bioengineering/medical engineering [78, 181, 183, 237, 238, 260-263].

In previous chapters the new methodology to remove a femoral stem during an RTHA was introduced, demonstrated, and tested in a closer approach to a real case. The results proved that by applying low temperature on the neck of the femoral stem, the force required to remove a cemented femoral stem is reduced by nearly 65% compared to the control tests. Furthermore, the development of a concept design of a medical device functioning under the new methodology was presented.

This Chapter describes the development of a three-dimensional (3D) finite element thermal analysis of the geometry representing the specimen that was experimentally tested presented as first case scenario in Chapter 3 (femoral stem, bone cement and steel mould). The thermal analysis was modelled as a phenomena of conduction heat transfer in the titanium stem cemented in a steel mould, all the specimen considered as a solid body. The creation of the finite element model is explained in detail, as well as the thermal properties of the materials used (stem, bone cement, and steel), the thermal loads to simulate the various temperatures of interest: -76^{o}C, -58^{o}C, -49^{o}C, and -40^{o}C. The distribution of temperature was estimated in the femoral stem after the neck had been exposed to the mentioned temperatures of interest.

Since the new methodology utilizes low temperature as a treatment, and knowing that the critical temperature is -40°C as mentioned in Section 2.5 and 2.6, the findings from the computational model can be used as a tool to determine approximate margins of safety for bone and soft tissue to prevent necrosis, and also to establish the safe cooling temperature of the femoral stem during the cooling procedure by means of visualizing the predicted temperature distribution in the femoral stem and the surrounding materials in various cooling situations.

6.2 Finite Element Method (FEM)

The Finite Element Method (FEM) or finite element analysis is a numerical technique used to find approximate solutions to partial differential equations in boundary value problems. Finite element analysis has been developed to the extent that it is considered an essential tool for the analysis and design of a wide range number of applications in diverse areas of industry such as solid mechanics, fluid mechanics, electromagnetism, heat and mass transfer, and bioengineering.

The modern finite element method can be traced back to the work of Hrennikoff in 1941 when he developed a model of a membrane and plate bending of structures called the lattice analogy [264]. His work marked the starting point of the development of the finite element method, but it was two years later that Courant first introduced the finite element technique in his paper "Variational methods for the solution of problems of equilibrium and vibrations" [265, 266].

The first significant and practical use of the finite element method was in the 1950s in the aircraft industry by Boeing; in their studies, they used triangular stress elements to model the dynamic stiffness properties and displacements of aircraft wings [267]. In the 1960s Clough introduced the term "finite element" in the paper "The finite element method in plane stress analysis" and it has been used as such ever since. Clough used the Ritz numerical method with the modified methodology proposed by Courant [268]. The first study in the biomechanical field that used finite element analysis took place in the early 1970s when Brekelmans et al. investigated the stress affecting a human femur under the action of physiological forces [269].

The typical finite element procedure employed by commercial software can be seen in the diagram shown in Figure 6.1.

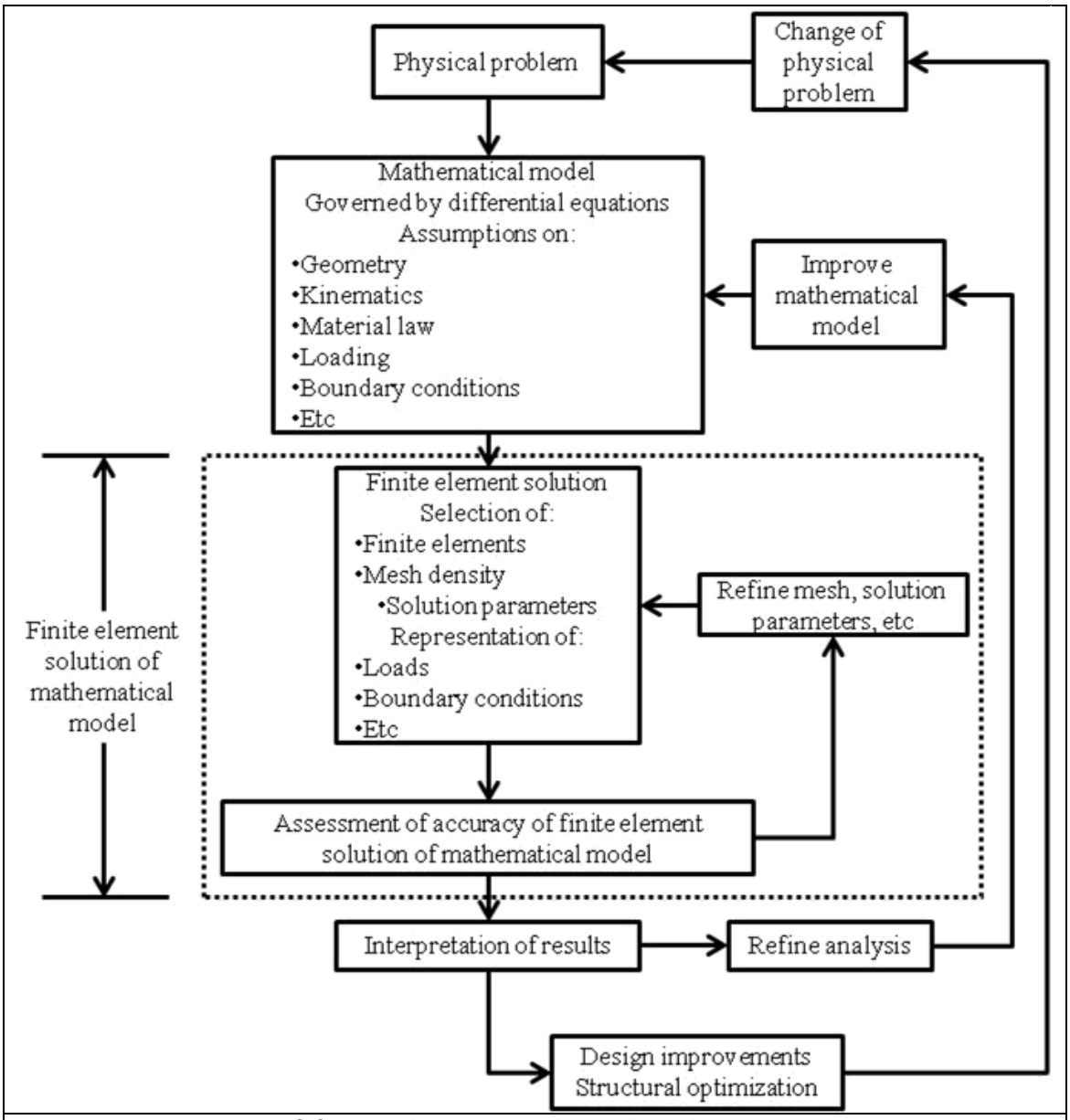

Figure 6.1 Process of finite element analysis [270].

A physical problem must be represented as a mathematical model governed by differential equations, with specific assumptions based on the laws of physics, thermodynamics, or kinematics, depending on the nature of the problem to be analysed. The finite element method solves the mathematical model. A correct formulation of the numerical model leads to a correct and approximate solution. If the accuracy criterion is

not met, the solution parameters must be refined and the calculation repeated until sufficient accuracy is reached.

ABAQUS CAE®, like other commercial computational software, solves the proposed coupled mechanical-thermal systems numerically, based on a finite element method. The solution scheme of the partial differential equations, such as the continuity, energy and mechanical stress equations, starts from the analysis of finite elements generated from nodes in the mesh of the system to be analysed. The governing equations of the phenomena are applied to each and every one of the created elements.

The process of discretization runs from the integration of those equations in the defined vector field in such a way that the equations are transformed into surface integrals [271].

Abaqus/Standard has the capability to model heat transfer by conduction in a solid body with general temperature-dependent conductivity, internal energy, convective and radiative boundary conditions [271].

From the equation of energy balance expressed in the integral form [272], where the internal energy of the system is a function only of the temperature of the material, $U = U(T)$:

$$\int_V \rho \dot{U} dV = \int_S q" dS + \int_V r dV \tag{4.1}$$

Where V is the volume and S is the surface area of the solid body, ρ is the density of the material, $\dot{U}$ is the change of the internal energy in time, q'' is the heat flux per unit area flowing into the solid body, r is the external energy per unit volume supplied into the body.

Heat conduction is governed by Fourier's Law:

$$q" = -k\left(\frac{\partial T}{\partial x} + \frac{\partial T}{\partial y} + \frac{\partial T}{\partial z}\right) = -k\nabla T \tag{4.2}$$

where k is the conductivity of the material and is a function of the temperature T; q'' is the heat flux; (x,y,z) are position coordinates. For simplicity, the conductivity of the material is considered as isotropic.

Therefore, transforming equation 4.1 to its differential form and substituting equation 4.2 in it, results in a well-posed problem in heat conduction without internal energy generation as follows:

$$\nabla \cdot (k\nabla T) = \rho c \frac{\partial T}{\partial t} \tag{4.3}$$

where c is the heat capacity of the material and ∇ is the gradient operator, and a time $0<t<J$ (where J can $\rightarrow \infty$) for (x, y, z) belonging to some region, R, of the solid body.

To find the temperature fields, $T(x, y, z, t)$, Abaqus needs:

1. An initial condition where $T = T_i(x, y, z)$ at a time t=0.
2. The temperature T must satisfy two boundary conditions for each direction in the coordinate system:
    I. T is specified on a boundary of the surface of the body for a time $t >$ 0, i.e. cold temperature at the neck of the stem.
    II. A convective condition on the surface of the body, i.e. the external surface of the steel mould where the stem is cemented, and considering the convective coefficient h:

$$-k\nabla T|_{boundary} = h(T - T_\infty)_{boundary} \tag{4.4}$$

Once the correct information has been entered in Abaqus, the software solves the equations by obtaining a variational statement of the energy balance using the Galerkin approach which assumes that the temperature T, the variational field, is interpolated by the same functions. Therefore, the solid is geometrically approximated with finite elements and the temperature is interpolated as:

$$T = N^N(x)T^N \tag{4.5}$$

where T^N is the temperature at the N node, N = 1,2,...,

For time integration of the equation, transient analysis, Abaqus/Standard uses the backward difference algorithm:

$$\dot{U}_{t+\Delta t} = (U_{t+\Delta t} - U_t)(1/\Delta t\,) \tag{4.6}$$

Substituting equation 4.6 in the energy balance after applying the Galerkin approach, the nonlinear system in equation 4.7 is obtained.

$$\frac{1}{\Delta t}\int_V N^N \rho(U_{t+\Delta t} - U_t)dV + k\int_V \nabla N^N \cdot \nabla T\, dV - \int_S N^N q"dS = 0 \tag{4.7}$$

With these computational tools, the process for a solution of an engineering system can be considerably reduced, decreasing the time to calculate the solutions and the costs of this process.

6.3 Geometry of the Model

The purpose of conducting a numerical analysis is to investigate and understand the heat transfer phenomena in the various parts that form the specimen with the cemented femoral stem. This kind of analysis can be performed with the computational software ABAQUS CAE® 6.10.

The development of the three-dimensional (3D) geometry used to predict the temperature fields was constructed in the framework of a bone-cement-prosthesis system, based on the materials employed in the experimental work. The geometries were drawn in the solid modelling CAD software SOLIDWORKS® 2010, Education Edition Software, (Dassault Systemes Corporation). Figure 6.2 shows the dimensions (mm) of the femoral stem and the solid model.

The walls of the mould were of 3 mm thickness, and the mould was designed tso that the cement mantle could have 3 mm thickness. The dimensions of the mould and final solid geometry are shown in Figure 6.3.

These geometries were imported from SOLIDWORKS® as solids (.sat files) into Abaqus CAE. Once imported, the cavity of the mould was used to create a volume representing a block of cement; the volume of the femoral stem was subtracted from the block of cement, thus creating a cement mantle as shown in Figure 6.4.

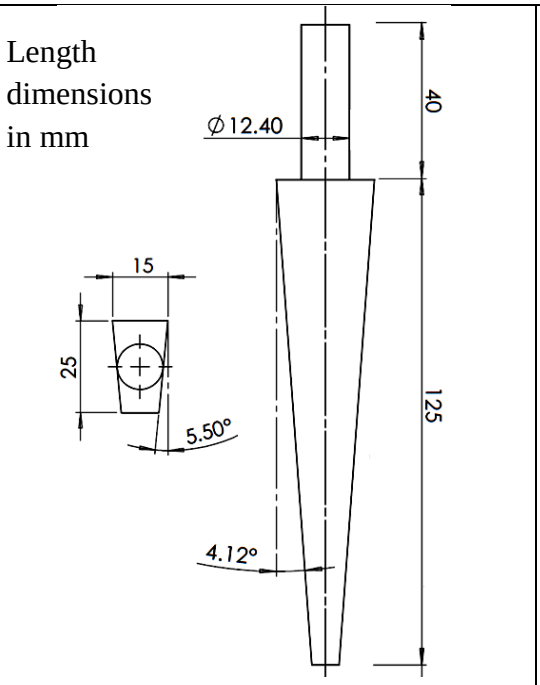

a)

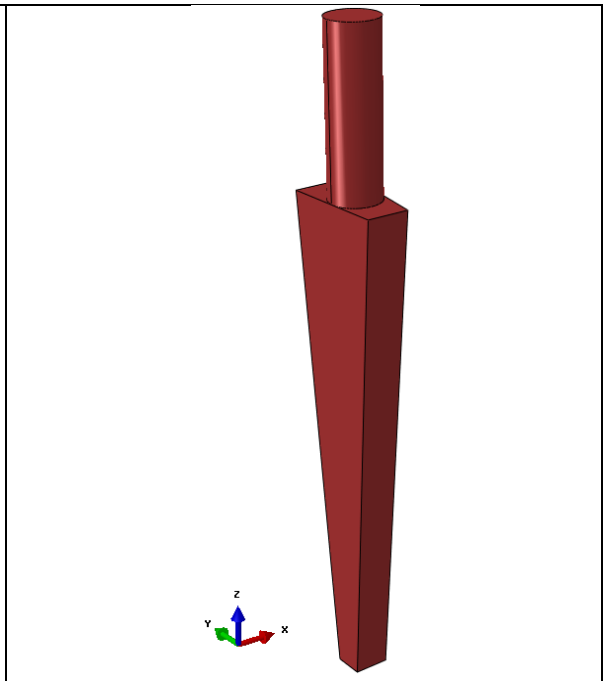

b)

Figure 6.2 a) Drawing of customised femoral stem with dimensions in mm, and b) final solid model in ABAQUS CAE® 6.10.

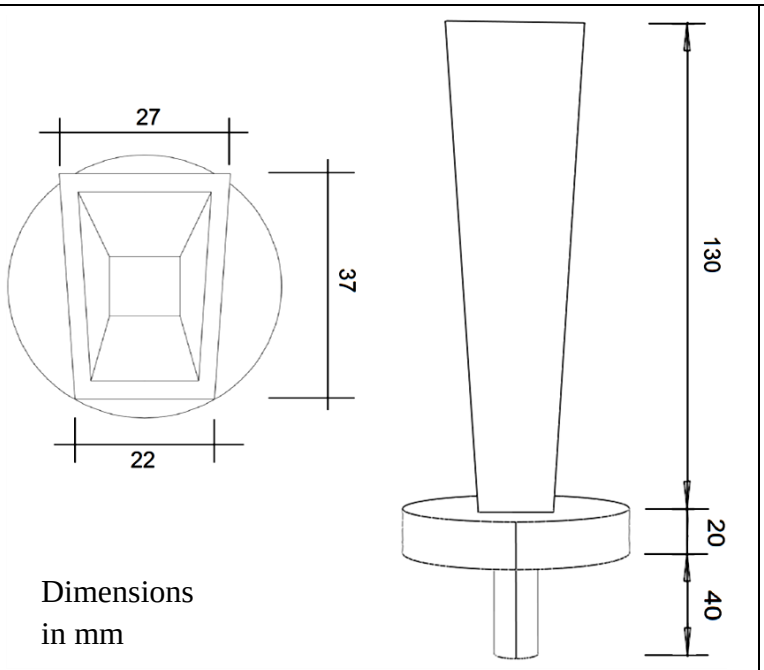

a)

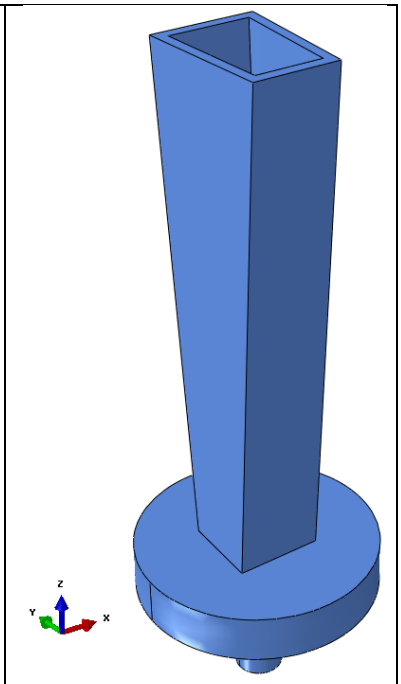

b)

Figure 6.3 a) Drawing of the steel mould with dimensions in mm, and final solid model in ABAQUS CAE® 6.10.

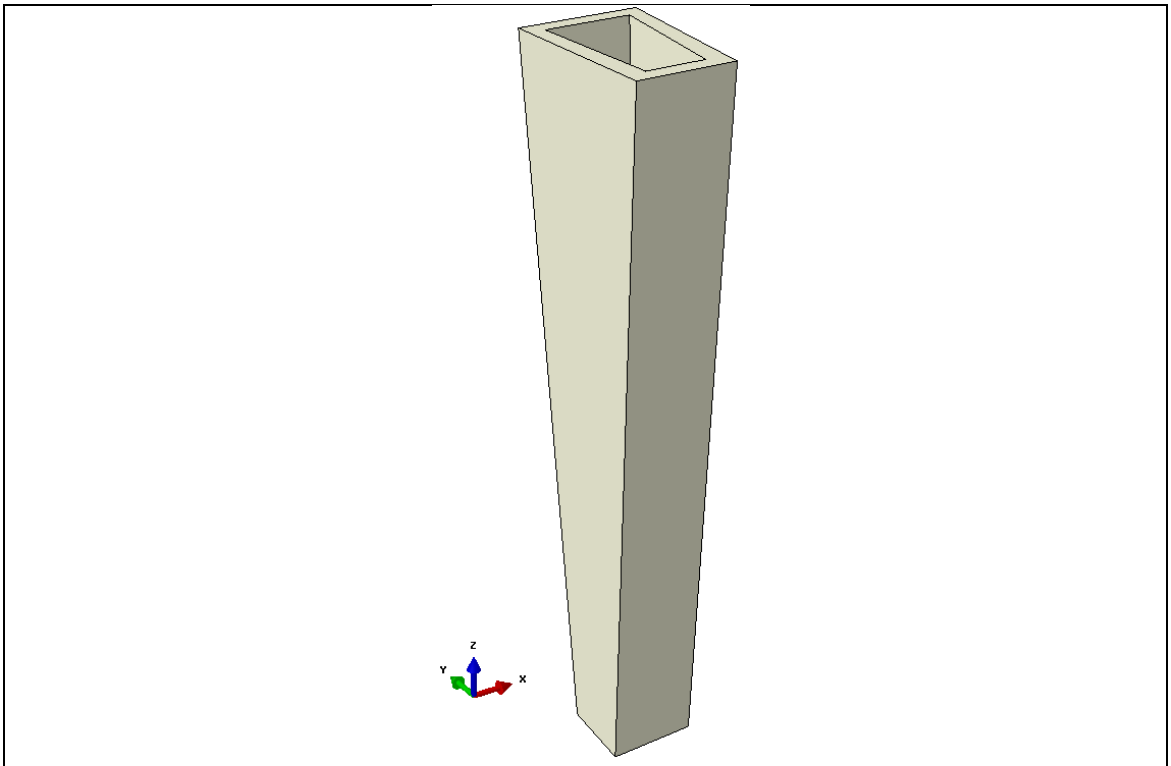

Figure 6.4 Solid model of cement mantle in ABAQUS CAE® 6.10.

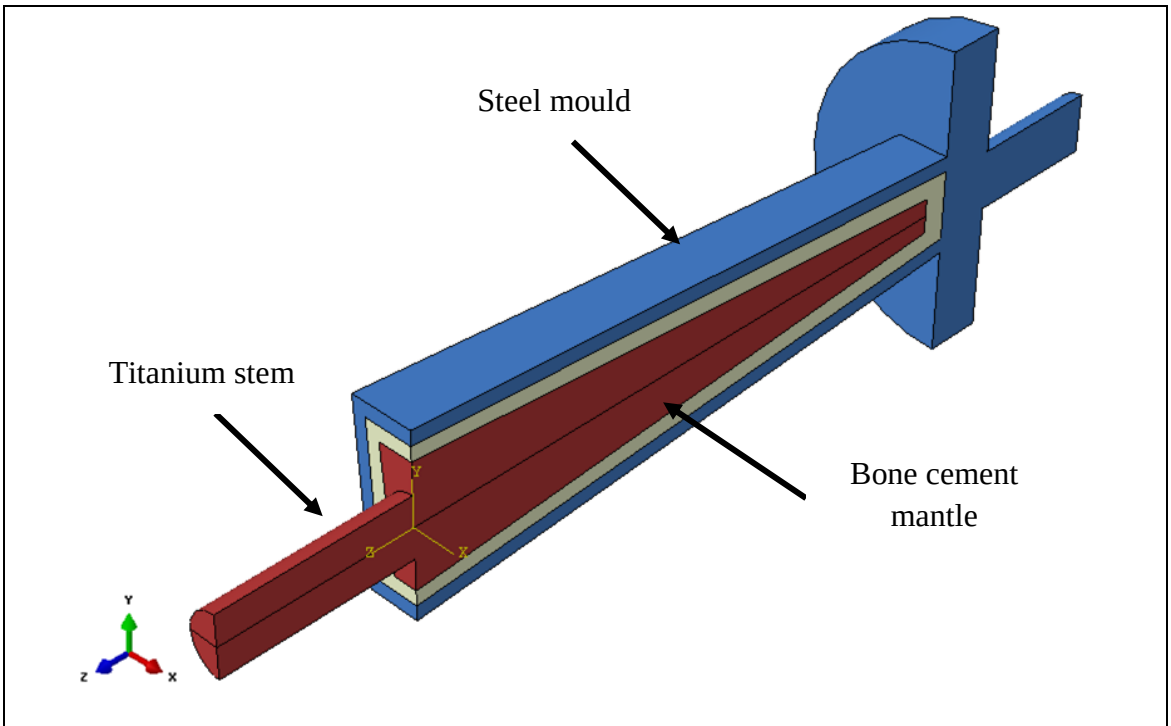

Figure 6.5 Final computational domain, femoral stem, cement and mould. View in the symmetrical YZ plane. Geometry from ABAQUS CAE® 6.10.

The three geometries: mould, cement mantle, and titanium stem were assembled into a unit to form the specimen of interest. To simplify the model and to reduce computing time, the specimen was reduced to a symmetric geometry in the YZ plane as shown in Figure 6.5.

6.4 Materials and Thermal Properties

The material properties of each part/element of the geometry are conditions required to accurately recreate or generate the model of the specimen to be studied. For this research, the materials were assumed to be homogeneous, isotropic, and elasto-plastic. The thermal properties of the materials to be used in the material database of ABAQUS are shown in Table 6.1, and are the average values from those found in the literature corresponding to a material at an ambient temperature of 22^{o}C [50, 53, 180, 199, 210, 223].

Table 6.1 Material thermal properties of materials at 22^{o}C [50, 53, 180, 199, 210, 212, 223, 273].

	Density (t/mm^3)	Coefficient of Thermal Conductivity (mW/mm^{o}C)	Heat Capacity (mJ/t^{o}C)
Titanium alloy Ti-6Al-4V	4.85x10^{-9}	7.44	5.443x10^{8}
Stainless Steel	8x10^{-9}	16.2	5x10^{8}
Bone cement (PMMA)	1.19x10^{-9}	0.18	1.45x10^{9}

For the titanium stem: density, heat capacity and thermal conductivity were considered to be temperature dependent, as shown in Chapter 3 [210, 212]. The density, heat capacity, and thermal conductivity of the steel and bone cement were considered as

constant properties. Properties at sub-zero temperatures were not assumed since the thermal properties for bone cement, as functions of sub-zero temperatures, are not available in the literature, moreover, the author decided not to assume the behaviour of acrylic bone cement if unknown. Nevertheless, reference values at room temperature were considered from studies performed on various types of acrylic bone cements found [50, 53, 180, 223, 273].

6.5 Contacts and Boundary Conditions

The proposed numerical model reproduces the experimental work of an idealised cemented stem. With the objective of determining the correct temperature distribution in the medium, it is important to keep in mind that the appropriate solution of the heat equation, Equation 6.3, depends on the physical conditions of the surrounding environment, such as room temperature, radiation, or humidity. These parameters affect heat transfer processes, hence defining the boundary conditions.

The modelling of the interface between surfaces of various materials, i.e. prosthesis-bone cement and bone cement-steel mould, was represented using a surface-surface tie constraint resulting in a perfect bonding to optimise the heat transfer between materials, thus thermal contact resistance was neglected. This thermal resistance may be caused by the effects of surface roughness and contact spots mainly filled by air in the bonding of the composite walls, formed by the three different materials [199]. The symmetry condition in the YZ plane is shown in Figure 6.6a.

To model the immersion of the neck of the stem (zone 1) into the liquid nitrogen (LN_2), a boundary condition of constant temperature was applied to the neck of the stem with a value of -196°C, which is the boiling temperature of liquid nitrogen [46, 274].

The boundary condition of convective heat transfer over the outer surface of the steel mould was based on different numerical and experimental studies of heat transfer. These works studied the cooling dynamics and interactions of boiling liquid nitrogen and refrigerant R-134a used in cryogenic medical devices [183, 199, 274-278].

Jin et al. [275] measured the boiling heat transfer coefficient on a stainless steel block immersed in liquid nitrogen (LN_2) using inverse heat conduction analysis. The steel block was instrumented with three T-Type thermocouples (Cu-Constantan) to measure the changes in temperature inside the steel block. After recording the temperature readings, the surface heat flux was deduced using the inverse heat conduction method in an explicit finite difference model. The heat transfer coefficient, h ($W/m^{2o}C$), was defined by the ratio of the heat flux and the temperature gap between the surface temperature of the steel block and the liquid nitrogen. The correlations obtained are shown in the following expressions:

$$h=125+0.069x\Delta T \quad , \quad 52 \leq \Delta T \leq 214 \qquad (6.8a)$$

$$h=13087.8 - 723.04\Delta T + 13.47\Delta T^2 - 0.084\Delta T^3 \quad , \quad 19.6 \leq \Delta T < 52 \qquad (6.8b)$$

$$h=82.74 - 131.22\Delta T + 37.64\Delta T^2 - 1.13\Delta T^3 \quad , \quad 4 \leq \Delta T < 19.6 \qquad (6.8c)$$

$$h=21.945x\Delta T \quad , \quad 0 \leq \Delta T < 4 \qquad (6.8d)$$

Sansinena et al. [274] compared the cooling rates between slush nitrogen and liquid nitrogen. Heat transfer coefficients in the range of film boiling, 125 – 1000 ($W/m^{2o}C$), were used to predict the cooling rates in the numerical simulation of the heat conduction equation with a convective boundary condition.

Crowley et al. [278] performed an experimental study of the parametric effects of vapour quality and flow rate on the convective heat transfer coefficient. The experiments were undertaken to reduce heat generation from high-performance electronics. Values of the convective heat transfer coefficient were in the range of 20,000 - 60,000 ($W/m^{2}{}^{o}C$).

Figure 6.6b and Table 6.2 show the boundary conditions employed for the present study. Based on the above mentioned works, and from the studies performed by Franco et al. [183, 262, 276] and Aguilar et al. [277, 279], the temperature variation along the length of the mould was obtained experimentally at six locations.

Table 6.2 shows the experimental readings at 30, 50, 80, 110, and 120 mm from the proximal edge of the mould. These values were used in the numerical model as sink temperatures, since a layer of LN_2 vapour at very low temperature was present over the surface.

The surface of the modelled steel mould was then divided into 13 zones equally spaced (10 mm) with the objective of setting a local convective heat transfer coefficient by regions (or zone); three other zones correspond to the base of the mould, and two small areas (steel mould, bone cement and the titanium stem) facing the liquid nitrogen, see Figure 6.6 for details.

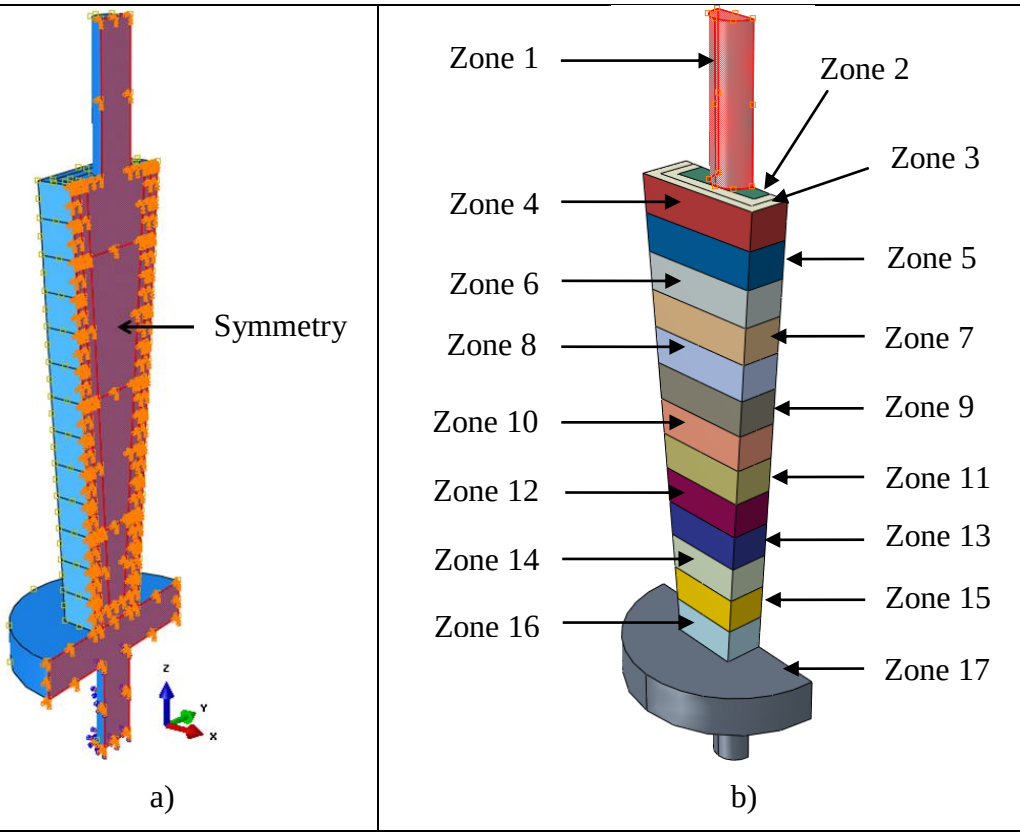

Figure 6.6 Boundary conditions in the model: a) symmetry condition, b) thermal boundary zones. Geometries from ABAQUS CAE® 6.10.

In total, there are 16 zones and each has a local convective heat transfer coefficient as a boundary condition and a local sink temperature T_s(°C). The convective coefficient varies by decreasing its value along the length of the mould, from Zone 2 to Zone 17. Incropera et al. and Welty et al. [199, 201], state that the higher values of *h*

correspond to the areas (or zones) most affected by the evaporation of liquid nitrogen and layer of nitrogen vapour, and this can be seen in the values shown in Table 6.2.

Table 6.2 Thermal boundary conditions applied in the numerical model.

Zone	Thermal Condition	
1	Constant temperature $T_c = -196^oC$	-
Exposed surfaces (mould and cement)	$T_{film}\ (^oC)$	$h\ \left(\frac{mW}{mm^{2o}C}\right)$
2	-80	10
3	-80	10
4	-60	0.5
5	-60	0.5
6	-60	0.1
7	-50	0.1
8	-50	0.1
9	-40	0.1
10	-40	0.1
11	-35	0.05
12	-35	0.05
13	-25	0.01
14	-25	0.01
15	-10	0.01
16	-10	0.01
17	-5	0.005

In addition, the variation of temperature on the surface of the titanium stem was monitored by three nodes generated at one of the surfaces of the stem, see Figure 6.7. Node 1 was positioned at 20 mm, Node 2 at 60 mm, and Node 3 at 100 mm from the proximal edge of the stem [280]. The data obtained from these temperature readings were used to validate the numerical model.

The model solved the heat transfer equation as time dependent with running time t= 20 minutes, ambient temperature was set as the initial condition of the model.

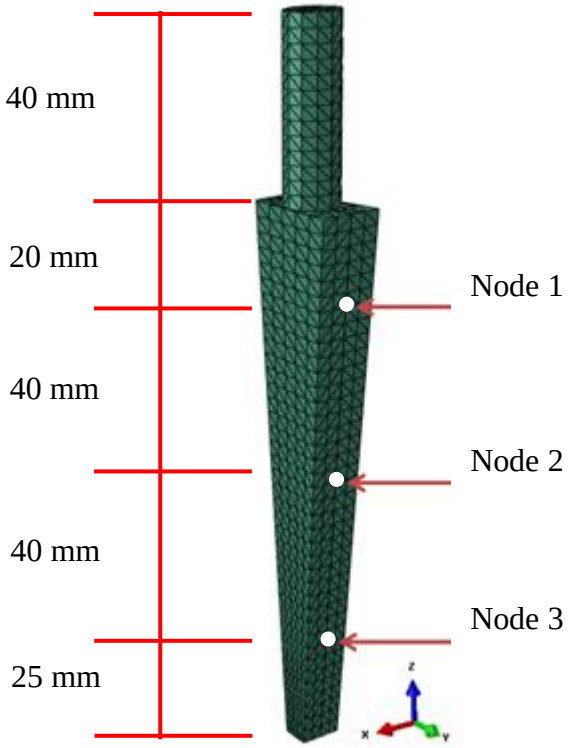

Figure 6.7 Location of the temperature monitoring nodes in the modelled titanium stem. Geometry from ABAQUS CAE® 6.10.

6.6 Mesh Sensitivity Analysis

The creation of the mesh is one of the most important steps of the pre-processing stage in all computational modelling. The distribution of the nodes and the selection of element type for the mesh depend on the geometry of the model and the nature of the problem to be solved, in this case, a non-linear heat transfer process is studied. The model representing the specimen is geometrically complex because it is double tapered and, therefore, has various changes in area; consequently, 4-node linear tetrahedral elements were chosen to mesh the domain, and specific elements for diffusion heat transfer in a 3D continuum were used, DC3D4. Figure 6.8a and Figure 6.8b show the hypothetical tetrahedron element of 4-nodes and a section of the meshed geometry.

To ensure precision in the results, a mesh analysis was performed by assigning different global element sizes in the mesh of a single model. To illustrate this step, Figure 6.9 shows the meshed model with different global element sizes.

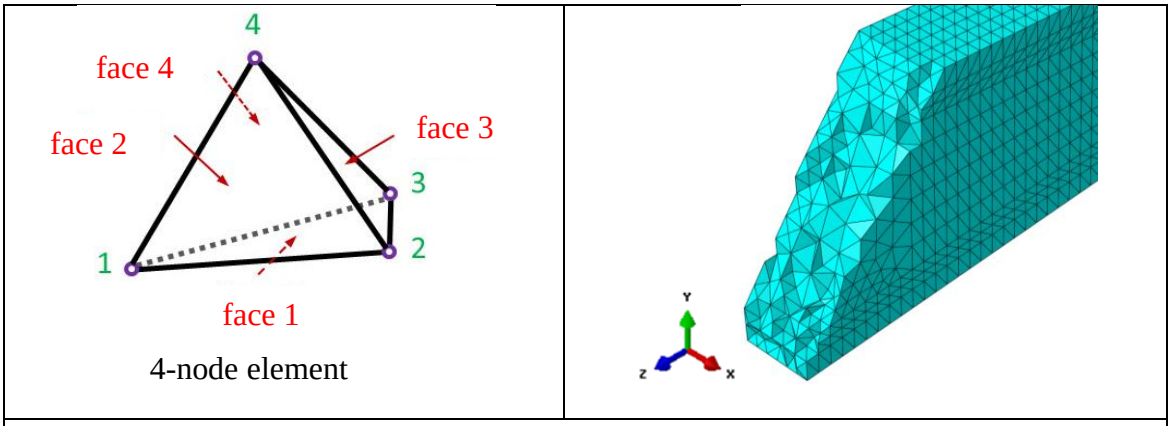

Figure 6.8 Tetrahedral element. a) Hypothetical 3D representation of the element, b) Meshed geometry using tetrahedral elements in ABAQUS CAE® 6.10.

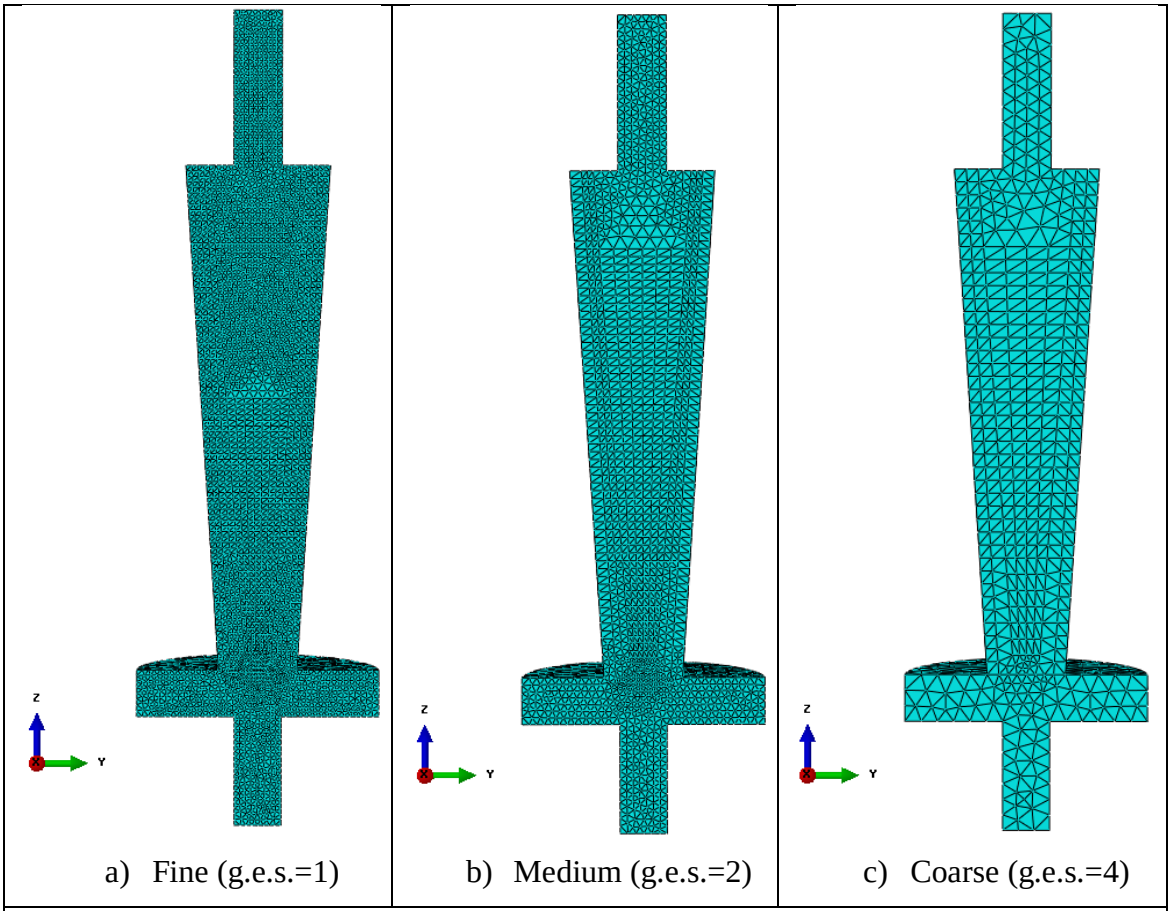

Figure 6.9 Types of mesh depending on the global element size (g.e.s.) used in the model. Geometries from ABAQUS CAE® 6.10.

The global element sizes were chosen between 1 and 4 and the mesh density varied between a coarse mesh of 10193 elements and a very fine mesh of 403539 elements. Each case of mesh density was processed with the same conditions and the variations in the results were analysed.

Table 6.3 shows the analysis of the mesh by comparing the difference between the temperature measured experimentally in the proximal monitor and the numerical nodal monitor; the global element size of 2 was chosen because the percentage error between the calculated temperature and the temperature of interest was less than 1%, 0.31°C, and the computing time was acceptable.

Table 6.3 Mesh sensitivity analysis.

Mesh Case	Global element size	Number of elements	Temp difference vs experimental values (°C)	Temperature (°C)	Computing time
A	1	403539	1.6885	-74.3115	4507.9sec
B	1.5	141692	0.6885	-75.3155	1486.7sec
C	2	59215	0.3141	-76.3141	1215.7 sec
D	2.5	31873	1.2622	-77.2622	330.90 sec
E	3	19520	2.0889	-78.0889	199.30 sec
F	4	10193	1.9466	-77.9466	109.40 sec

Figure 6.10 shows the final distribution of the elements in the geometry with the selected global element size, g.e.s.=2.

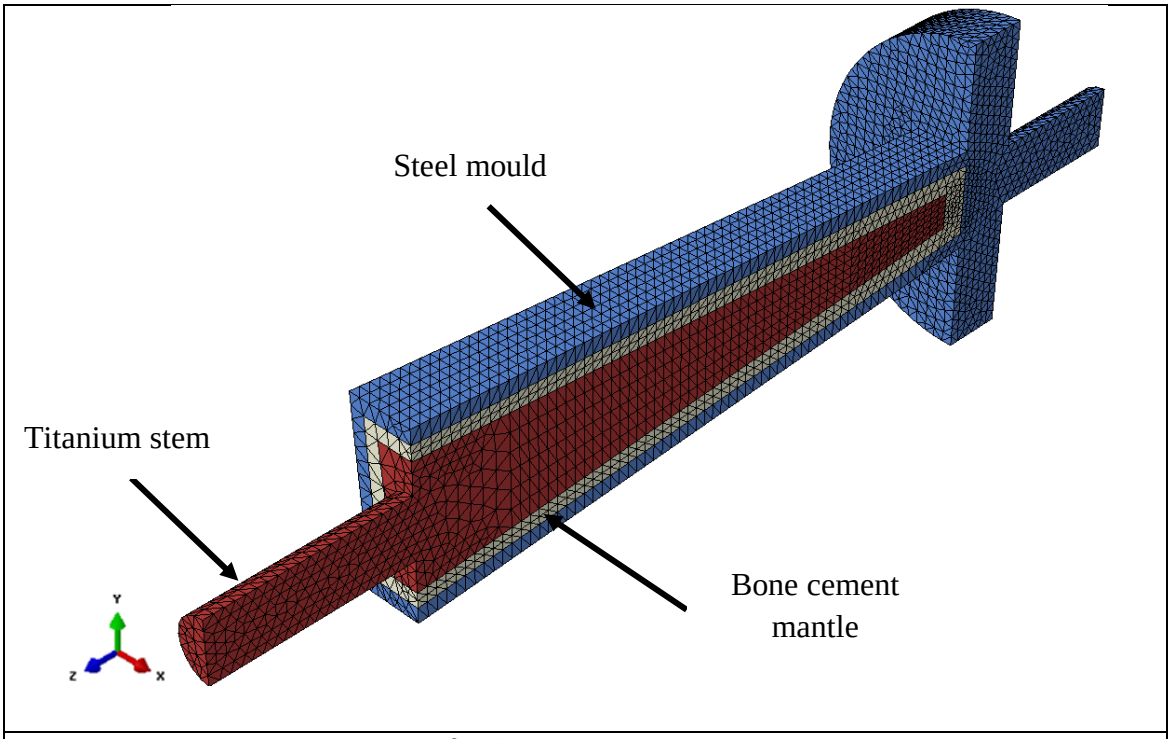

Figure 6.10 Distribution of elements in the geometry. View in the symmetrical YZ plane, ABAQUS CAE® 6.10.

6.7 Finite Element Thermal Results

Five (3D) thermal numerical models from the geometry representing the titanium stem cemented in a steel mould were developed as part of future computational work. The numerical model provided relevant information regarding the distribution of temperatures in the femoral stem, and the appropriate thermal conditions of safety for the surrounding materials after being exposed to low temperatures. The following case studies were simulated:

1. Simulation of the cooling procedure over the specimen for 20 minutes.
2. Simulation of the cooling procedure to four different cooling temperatures of interest as shown in Table 6.4.

Table 6.4 Temperatures of Interest for the Thermal Numerical Analysis with Steel Mould

	Temperature (^{o}C)
Case 1	-76
Case 2	-58
Case 3	-49
Case 4	-40

6.7.1 Temperature Change Rate and Temperature Distribution

A preliminary analysis was carried out to visualise the temperature distribution and the variation of temperature in time at specific points in the specimen during the simulated cooling process, see Figure 6.11. Nodal temperatures corresponding to the three points of interest in the physical stem were monitored: proximal, middle, and distal. From the plot, it can be seen that during the first 100 seconds of cooling, temperature readings from the proximal node show a temperature change rate of -0.5^{o}C/s, while the middle and proximal temperatures decreased at a rate of -0.1^{o}C/s and -0.02^{o}C/s respectively.

After 100 seconds, middle and distal temperatures decreased rapidly while the proximal rate of temperature change decreased from -0.5^{o}C/s to -0.34^{o}C/s. In the cooling time interval of 200 – 600 seconds, the variation of temperature starts to stabilise as the slope is less steep. From 600 seconds onwards, temperature change is approximately linear with an average rate of -0.02^{o}C/s. The minimum nodal temperatures registered at the end of the running time were -96^{o}C, -63^{o}C, and -34^{o}C in the proximal, middle, and distal monitoring nodes respectively.

Figure 6.12 shows the temperature distribution of the specimen after 20 minutes of cooling; the edges of the titanium stem have been highlighted for better visualisation. Analysing the image along the Z axis, the minimum temperature reached in the proximal zone had an average value of -100^{o}C for the titanium stem. The major temperature change effect can be seen at the junction of the neck and the body of the stem in the middle region, the temperature contours vary from -75C^{o} to -45^{o}C, whereas

for the distal region the average temperature is -25°C. In the proximal zone of the cement mantle and the steel mould, the minimum temperatures reached are -90°C and -86°C respectively. The middle and distal regions have almost uniform and similar temperatures in the perpendicular direction of the Z axis.

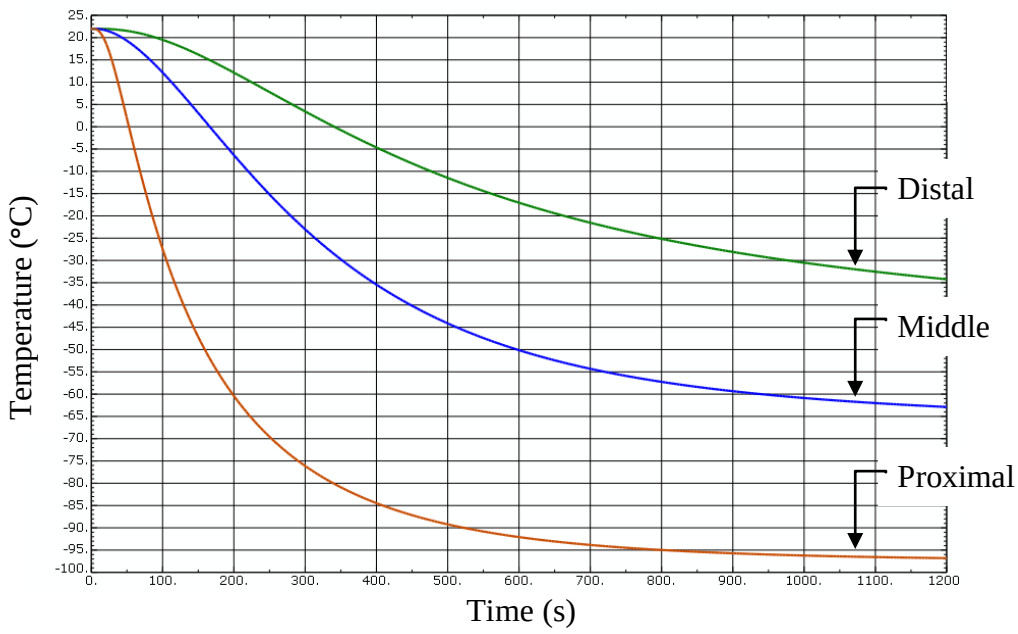

Figure 6.11 Numerical prediction of temperatures at three positions of interest over the titanium stem: distal, middle, proximal.

Moreover, after predicting the temperature distribution of the specimen, numerical simulations were performed for the four case studies of the present research. Different cooling temperatures were analysed for further study and these are shown in Table 6.4. A maximum value of -76°C was chosen as an extreme cooling case, and a value of -40°C was chosen as a critical temperature limit of thermal safety as mentioned in Section 2.5.1. Two other temperatures were studied: -49°C and -58°C at intervals of 9°C and 18°C from the critical temperature of -40°C.

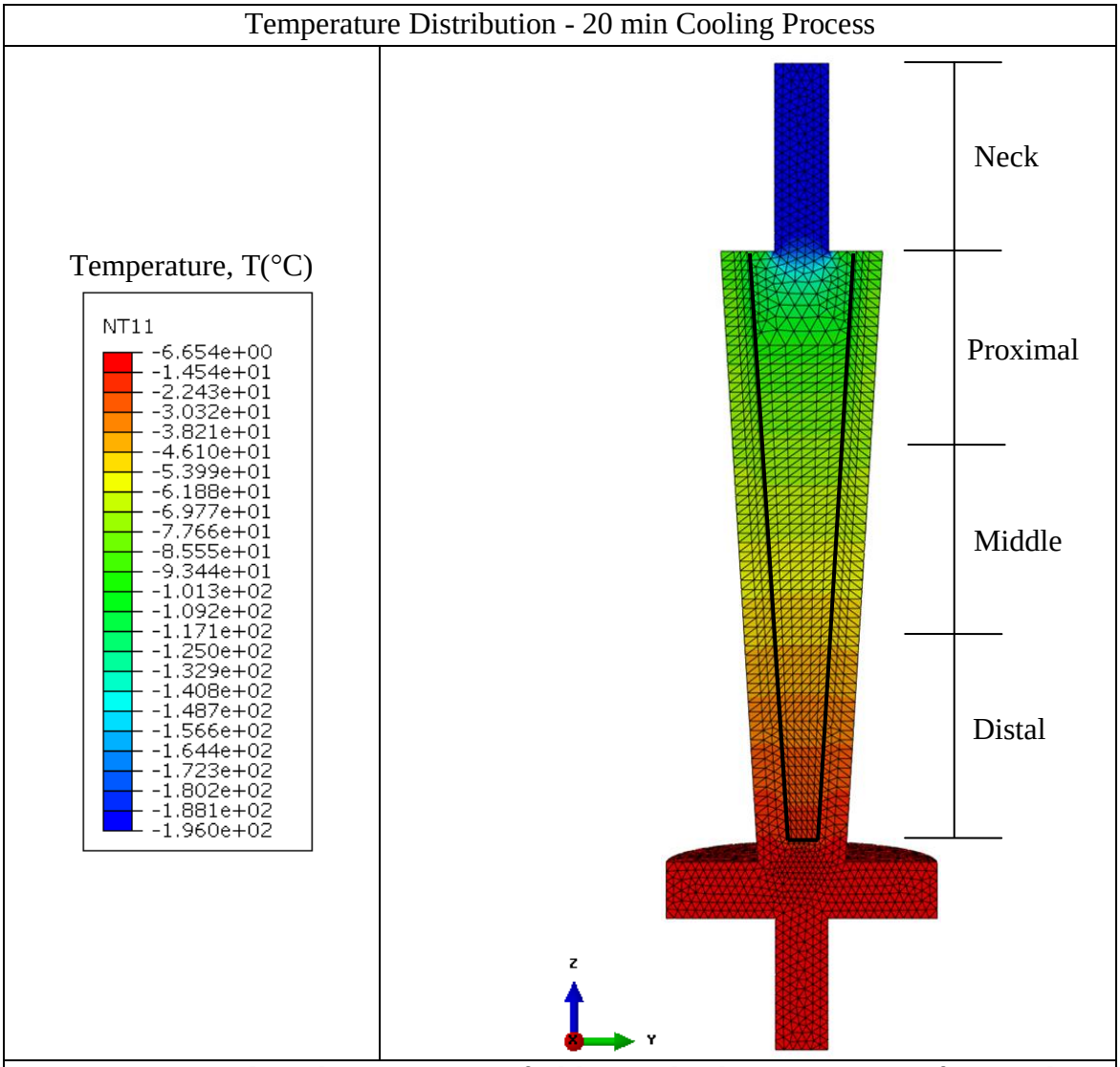

Figure 6.12 Predicted temperature fields inside the specimen, after cooling time t=20min. View at symmetry plane YZ , ABAQUS CAE® 6.10.

Table 6.5 Temperatures of Interest for the Finite Element Thermal Analysis

	Temperature (°C)
Case1	-76
Case 2	-58
Case 3	-49
Case 4	-40

Figure 6.13 to Figure 6.16 show the numerical prediction of temperature (solid lines) and temperature readings of the thermocouples (dotted lines) for each case study. In all cases the cooling temperature at the distal and middle nodal monitors from the model are very close to the experimental values, with a maximum difference of 2°C between the 30 and 120 seconds of the cooling procedure. Proximal nodal and experimental temperature readings differ by up to 10°C caused by the large amount of heat transfer in that zone of the material in the experimental test, this is mainly seen in the time interval of transition, from 0 to a maximum of 100 seconds. This effect of sudden heat transfer is much more marked in the experimental readings from Case 1 (-76°C) and Case 2 (-58°C), i.e. the thermal shock of the bath in the LN_2.

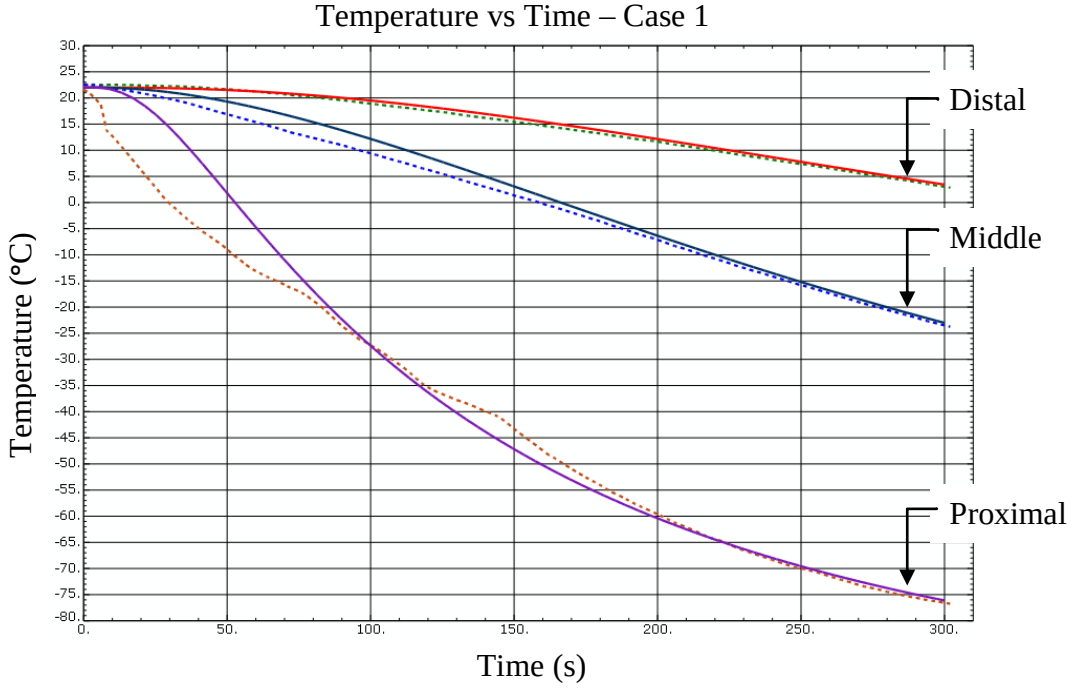

NUMERICAL	EXPERIMENTAL
Distal Temperature – Case 1	Distal Temperature – Case 1
Middle Temperature – Case 1	Middle Temperature – Case 1
Proximal Temperature – Case 1	Proximal Temperature – Case 1

Figure 6.13 Numerical prediction of temperatures vs experimental temperature readings at three positions of interest over the titanium stem: distal, middle, proximal. Cooling simulation compared to the experimental temperature readings of case study 1 with temperature of -76°C.

The energy transfer begins to stabilise after 80 seconds of cooling. At that moment, evaporation of LN_2 at the surface of the titanium stem ceases. Regarding Case 3 (-49°C) and Case 4 (-40°C), the abrupt heat transfer effect caused by the layer of nitrogen gas surrounding the steel mould can be seen in the readings of the proximal thermocouples over the entire cooling process. For Case 3 and Case 4, the temperatures of interest are reached in less time than required for Case 1 and Case 2.

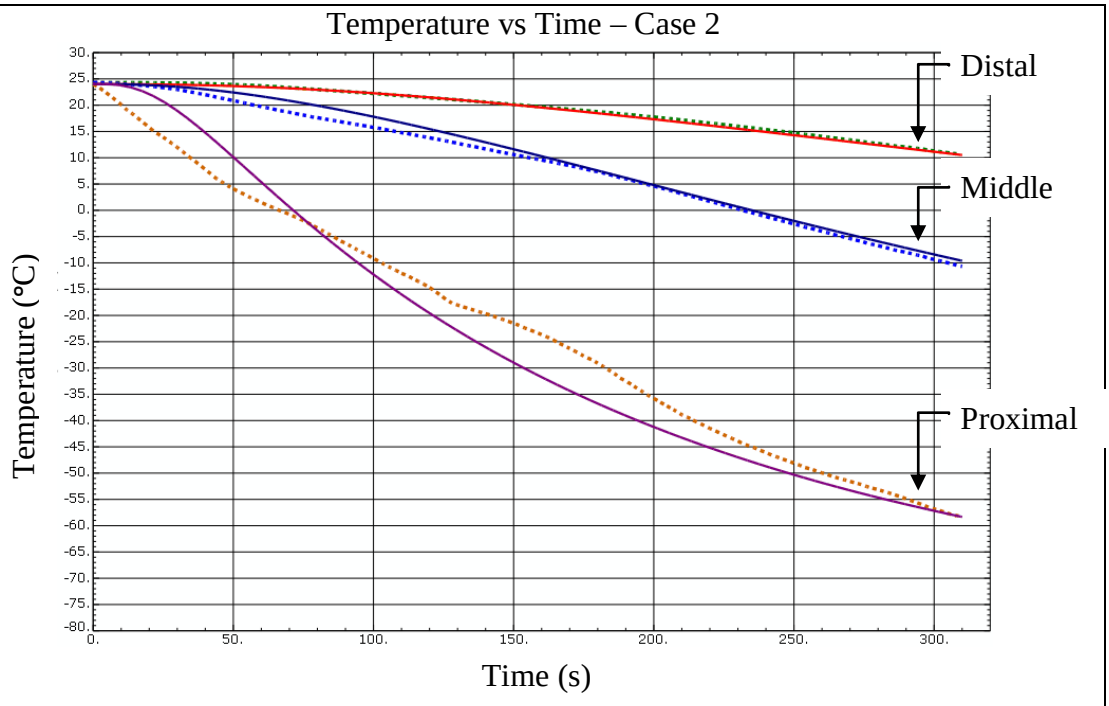

NUMERICAL	EXPERIMENTAL
Distal Temperature– Case 2	Distal Temperature – Case 2
Middle Temperature – Case 2	Middle Temperature – Case 2
Proximal Temperature – Case 2	Proximal Temperature – Case 2

Figure 6.14 Numerical prediction of temperatures vs experimental temperature readings at three positions of interest over the titanium stem: distal, middle, proximal. Cooling simulation compared to the experimental temperature readings of case study 2 with temperature of -58°C.

The maximum error was calculated for at the transition, 0 to 100 seconds, and at the achievement of the cooling temperature of interest for each case study. The error in the transition for Case 1 was of 14% but it was gradually reduced to 1.4% as the heat transfer stabilized and reached the temperature of interest of -76°C. Similarly the error

at the transition was of 6.3%, 8.3% and 8% for Case studies at -58°C, -49°C, and -40°C respectively. The error was reduced to 3.4%, 3.1%, and 1.9% when the temperature of interest was achieved, -58°C, -49°C, and -40°C respectively.

The trend of computed cooling rate for nodal temperatures from three points of interest, Figures 6.13 to 6.16, is similar to the experimental values in each monitored position for all four cases.

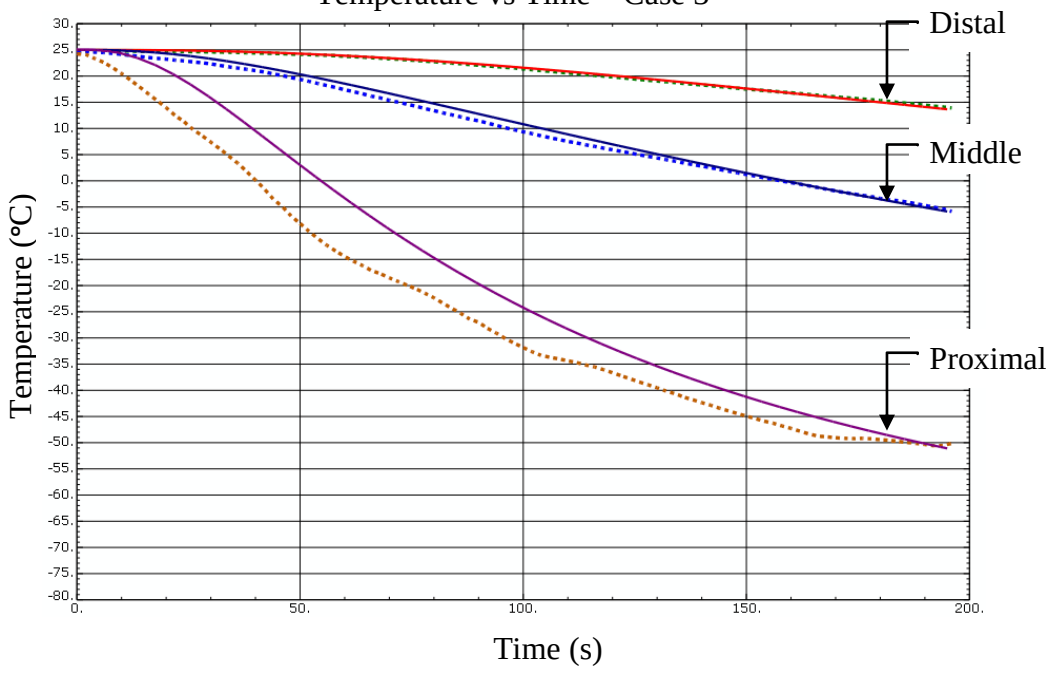

NUMERICAL	EXPERIMENTAL
Distal Temperature – Case 3	Distal Temperature – Case 3
Middle Temperature – Case 3	Middle Temperature – Case
Proximal Temperature– Case 3	Proximal Temperature – Case 3

Figure 6.15 Numerical prediction of temperatures vs experimental temperature readings at three positions of interest over the titanium stem: distal, middle, proximal. Cooling simulation compared to the experimental temperature readings of case study 3 with temperature of -49°C.

Distal and middle cooling rates ranged from -0.04 to -0.065 °C/s and -0.11 to -0.157 °C/s respectively, and the trend showed good consistency with experimental values. With respect to cooling rates for the proximal zone, the values ranged from -0.3 to -0.35 °C/s, and the trend of temperature change rate differed from the experimental

data in the first 80 seconds of the cooling process caused by the accelerated energy transfer in that zone for Case 1 and Case 2, but remained consistent afterwards.

The average time required to end the cooling process ranged from 300 to 192 seconds, depending on the case study.

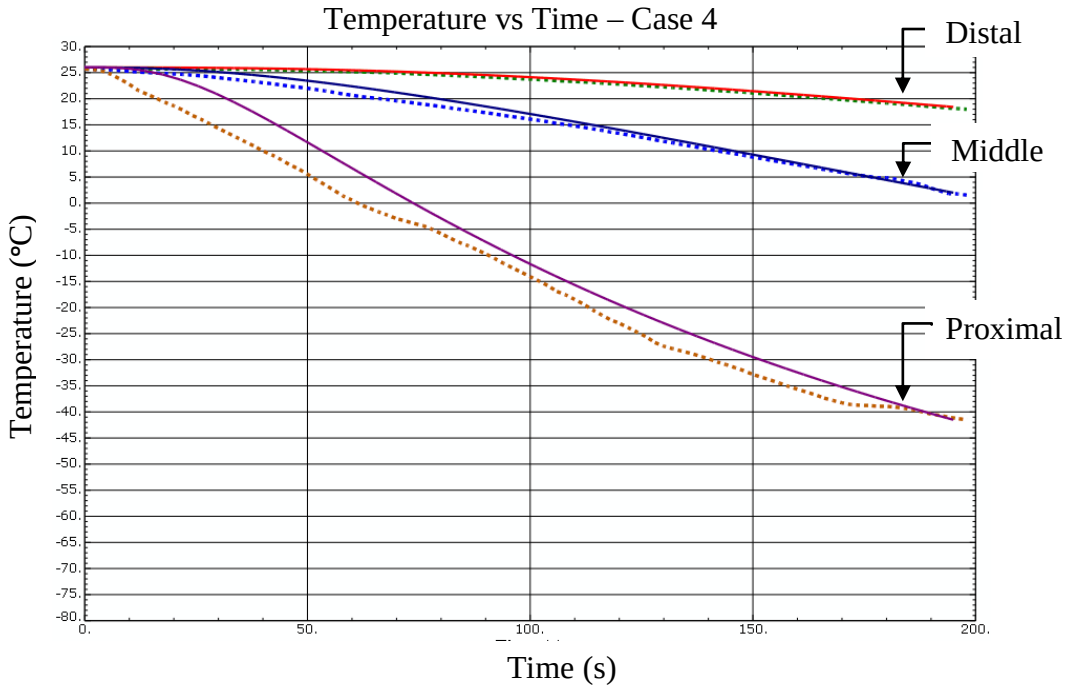

NUMERICAL	EXPERIMENTAL
Distal Temperature – Case 4	Distal Temperature – Case 4
Middle Temperature – Case 4	Middle Temperature – Case 4
Proximal Temperature – Case 4	Proximal Temperature – Case 4

Figure 6.16 Numerical prediction of temperatures vs experimental temperature readings at three positions of interest over the titanium stem: distal, middle, proximal. Cooling compared to the experimental temperature readings of case study 4 with temperature of -40°C.

Figures 6.17 to 6.20 show the temperature distribution of the specimen after reaching the specified temperature of interest for each case study, -76°C, -58°C, -49°C, and -40°C respectively. By analysing the images along the Z axis, all figures show the neck of the stem with constant temperature of -196°C, which is the temperature of liquid nitrogen.

The average temperature at the junction between the neck and the body of the stem was -150°C for all cases. The warmest temperature is observed on the base of the mould with values of 15°C, 20°C, 21°C, and 24°C, for case 1 to case 4 respectively. Compared to the other materials and due to the high conductivity of the steel mould, the walls have higher temperature in the middle and proximal zones of the specimen.

By analysing the variation of temperature in the Y direction, it can be seen that the cement mantle acts as insulation between the titanium stem and the steel mould since the temperature differs by nearly 10°C between materials.

Temperature Distribution - Case 1

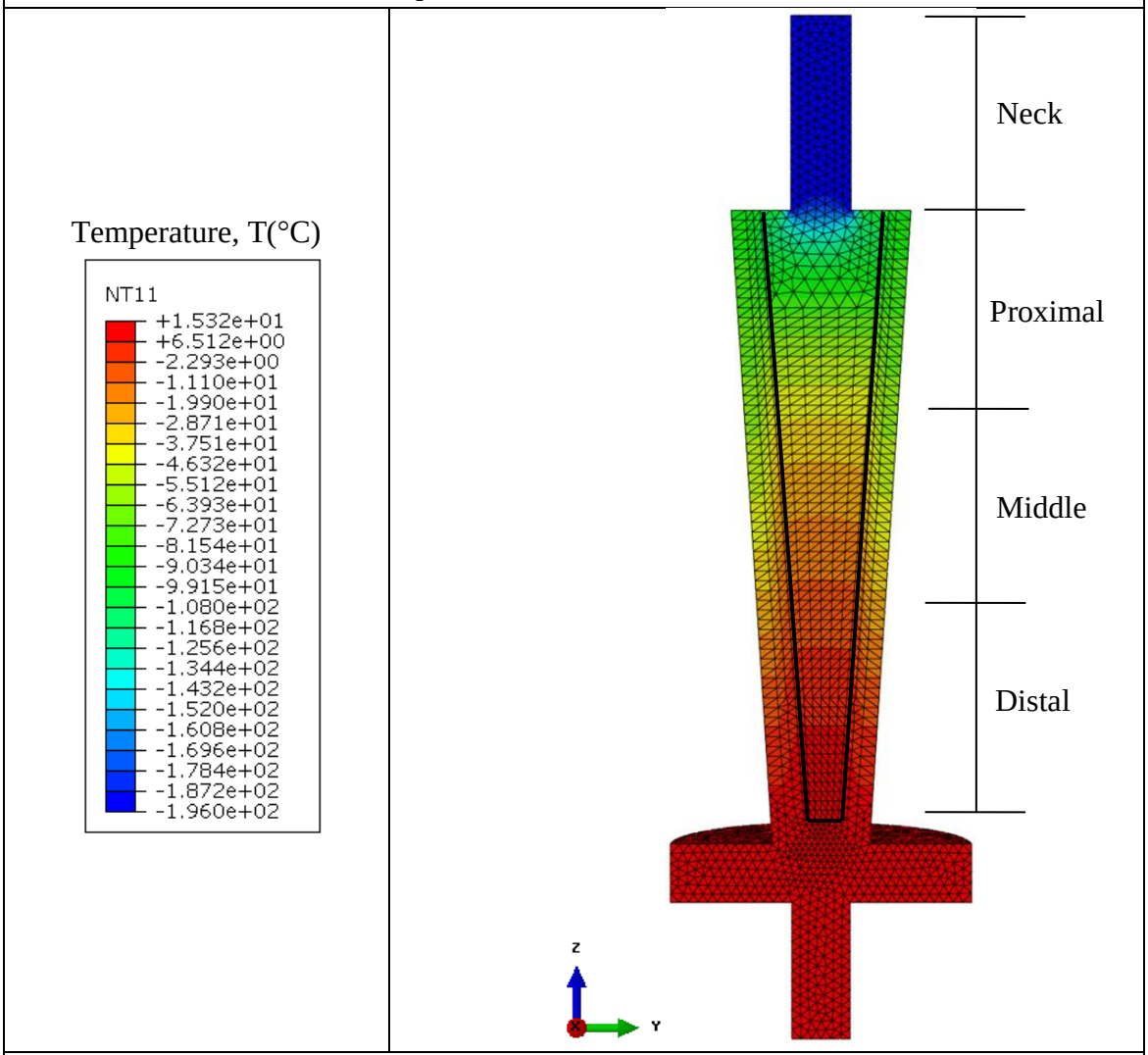

Figure 6.17 Temperature fields inside the specimen for Case 1, temperature of -76°C. Viewed at symmetry plane YZ, ABAQUS CAE® 6.10.

Referring to the temperature field in the titanium stem, for Case 1 shown in Figure 6.17, at the proximal zone of the specimen, which extends to a length of 55 mm of the stem's body, a high temperature gradient can be found with isotherms ranging from -156 to -38°C. The minimum temperature reached at the proximal zone had an average value of -85°C for the titanium stem.

Temperature Distribution - Case 2

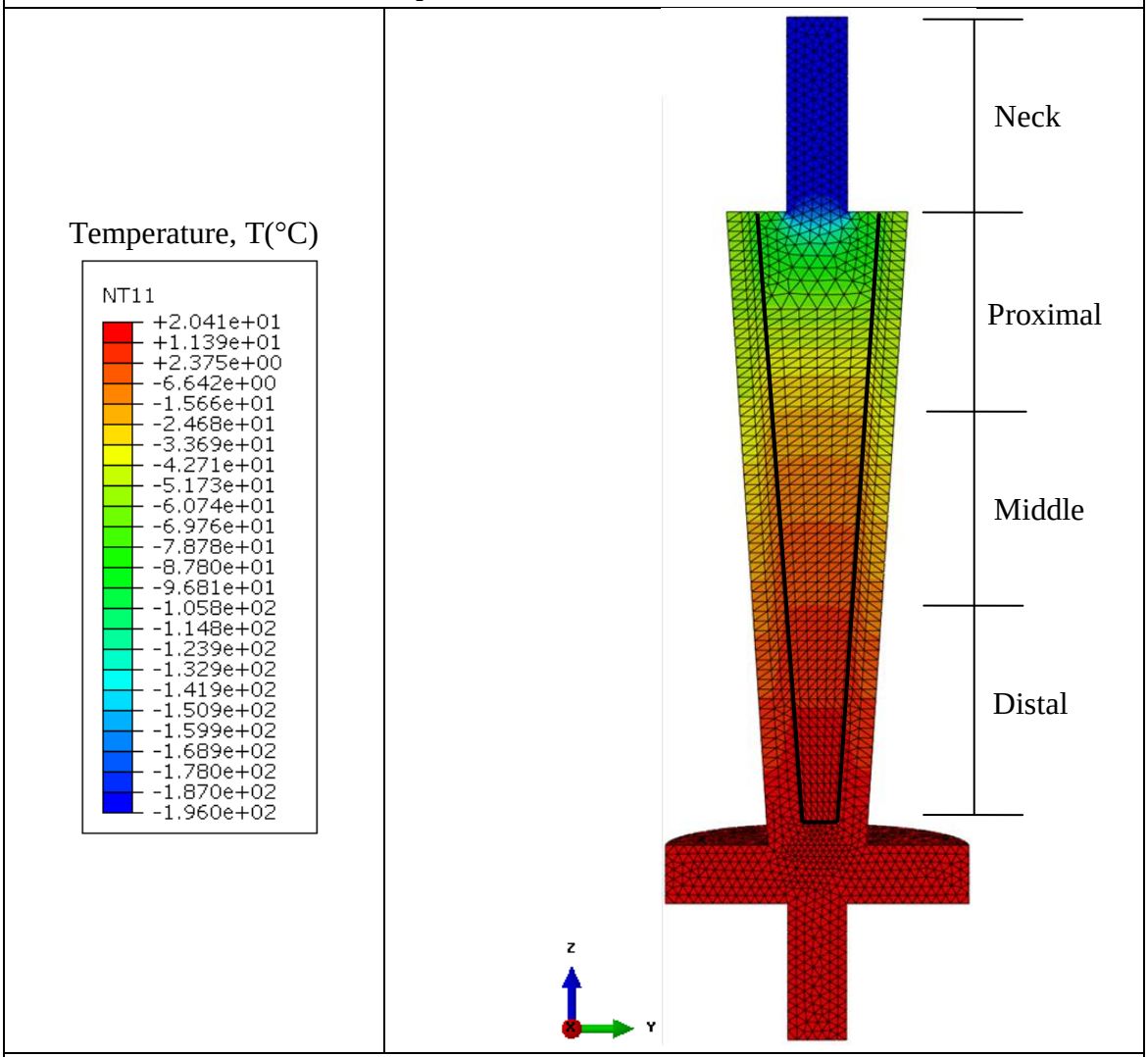

Figure 6.18 Temperature fields inside the specimen for Case 2, temperature of -58°C. Viewed at symmetry plane YZ, ABAQUS CAE® 6.10.

For Case 2, seen in Figure 6.18, temperature varied from -150 to -24°C with an average temperature of -68°C for the proximal zone. Case 3, shown in Figure 6.19, had an average temperature of -55°C at the same zone, the minimum and maximum

temperatures were -145 and -16°C. Finally, Figure 6.20 shows the temperatures in Case study 4, which varied from -140 to -4°C, with an average temperature of -47°C in the proximal zone.

By inspecting the figures, it can be seen how the cold area of the proximal zone gradually reduces as the temperature varies from -76°C to -40°C. This can be seen at the middle zone of the stem as the warmer isotherms approach the proximal zone. The average temperatures in the middle zone from Case 1 to Case 4 were -25, -7, -3, and 2°C respectively.

Temperature Distribution - Case 3

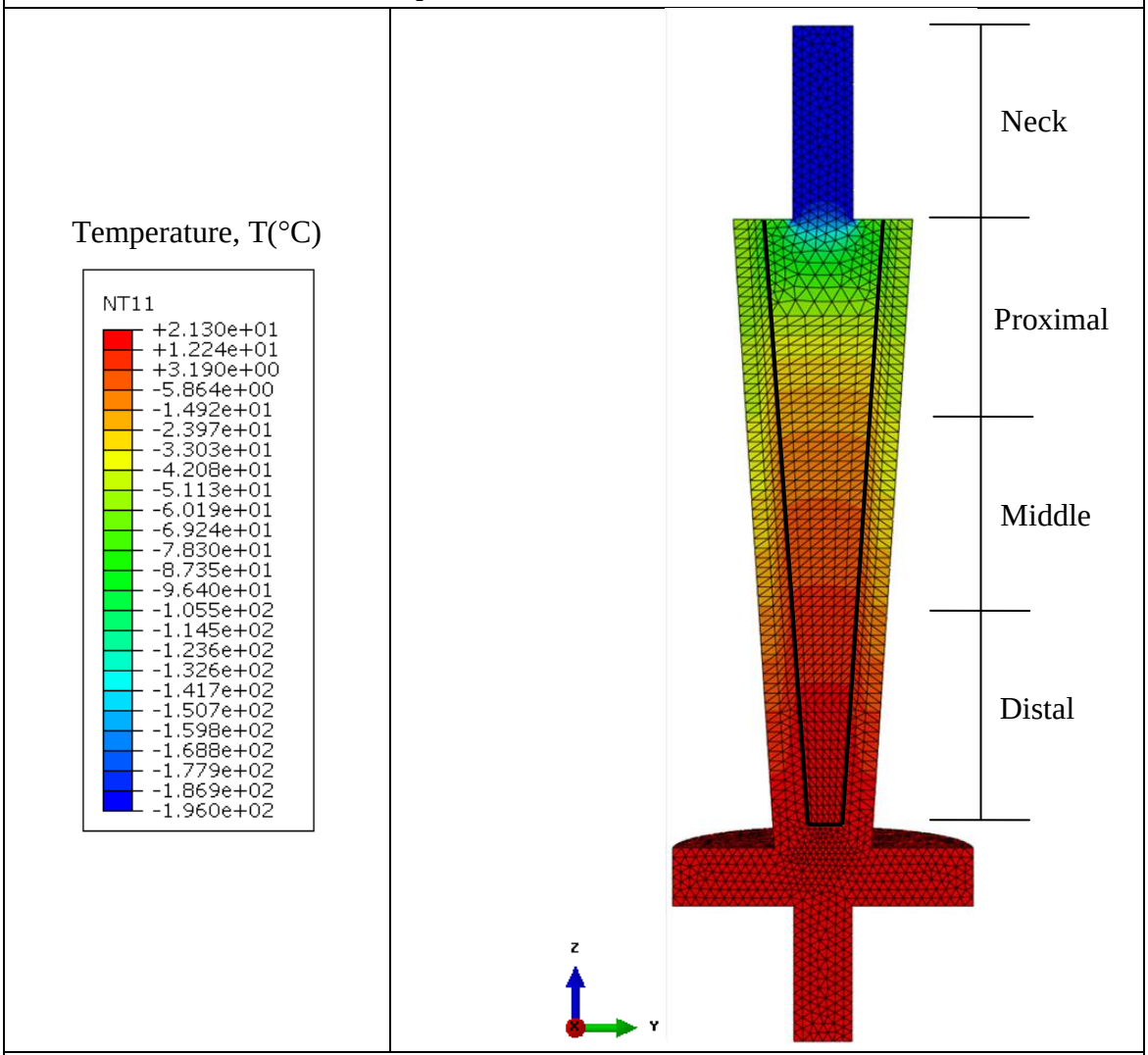

Figure 6.19 Temperature fields inside the specimen for Case 3, temperature of -49°C. Viewed at symmetry plane YZ, ABAQUS CAE® 6.10.

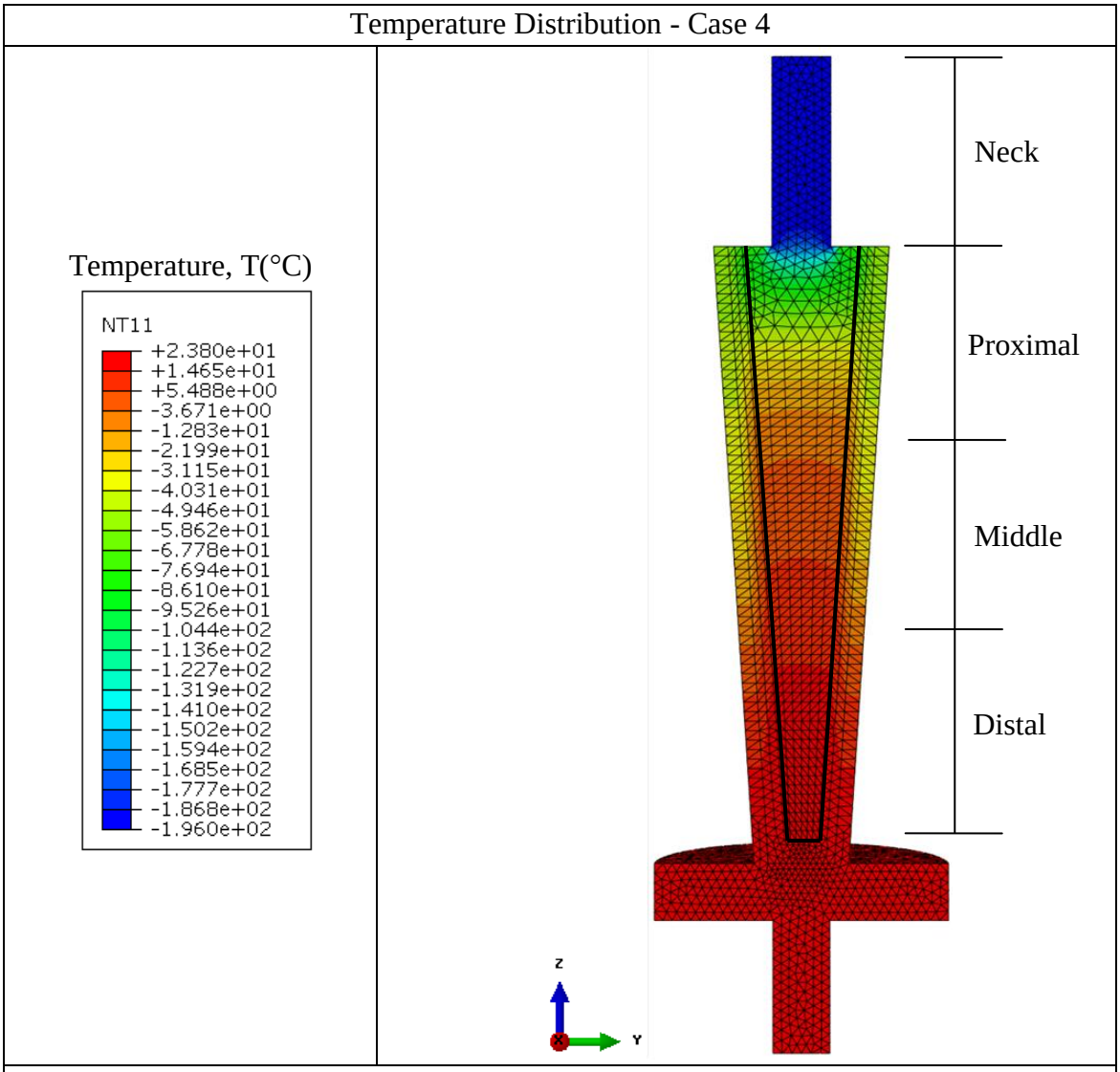

Figure 6.20 Temperature fields inside the specimen for Case 4, temperature of -40°C. Viewed at symmetry plane YZ, ABAQUS CAE® 6.10.

Regarding the distal zone of the stem, the average temperatures were 3.5, 10, 12, and 18°C for Case 1 to Case 4 respectively. In all cases, the distal part of the stem and the specimen in general was the warmer zone.

In this Chapter, a thermal computational model was presented. The temperature distribution in the specimen was estimated and analysed. The analyses confirmed the margins of safety for bone and soft tissue when performing the cooling of the stem at -40°C. Nevertheless, a coupled thermo-mechanical computational analysis needs to be performed by modelling the femur, soft tissue, body heat generation, and interface properties in order to have a better understanding of the effects and interaction of the

methodology to the components of the real artificial hip during a surgery of revision THA.

To finalise this thesis, the next chapter discusses and provides conclusions from investigative work described in this research as well as the future challenges that the proposed methodology and the medical device must face before its application in the operating theatre.

Chapter 7
Discussion and Conclusions

7.1 Impact of Temperature on the Release Force of a Cemented Titanium Stem in a Steel Mould

The experimental tests performed in Chapter 3 reproduced the removal of a cemented femoral stem from a steel mould as a first scenario study with the objective of investigating the impact of applying cooling to the femoral stem on the force required to release a cemented femoral implant. A total of 10 tests were performed, 8 following the cooling process to achieve the specific temperature of interest at the proximal zone of the titanium stem for each case study (-76°C, -58°C, -49°C, and -40°C) and 2 control specimens performed at room temperature (23°C).

In the results shown in Chapter 3 regarding the specimens implanted in the steel mould, the plot of the control test in Figure 3.22, showed a linear increment of the force. The results suggest that a brittle fracture of the interface is occurring since there is a dramatic failure without appreciable plastic deformation.

For all the thermally treated case studies presented in this chapter, at the moment the force shows the first sign of failure (Zone#2 from Figure 3.24 to 3.27) it seems likely that some area of the stem-cement interface had failed completely, but part of the stem-cement interface was still bonded to some extent, which could explain the existence of the second rise in the force shown at Zone#3 from Figure 3.24 to 3.27. It is important to mention that for these case studies, the femoral stem was considered loose from the cement mantle at the first force drop, even though it was not released from the specimen until the second rise in force. The second rise in force will be discussed in the following sections of this chapter; however, the author discards the roughness of the femoral stem as the causative factor to the second tier release of the force.

In the cases were the specimens were thermally treated, the force required to remove the implanted stem showed a non-linear trend but still a visible association between force value and temperature, this means that the force required to remove the

stem was reduced as the temperature at the proximal zone of the stem was lowered. The value of maximum force was reduced from 14 kN at room temperature to 10.04 kN, 10.45 kN, 8.85kN, and 6.32 kN for the temperatures of interest at the proximal zone, that is -40°C, -49°C, -58°C, and -76°C respectively.

Maximum shear stress was reported for all cases, which can be interpreted as the interface shear strength between the titanium stem and bone cement [31, 34, 42]. The present set of experiments showed that the control test had an interface shear strength of 2.24 MPa, which is by 80% similar to the value reported by Perez et al. [281] for a femoral stem with a polished surface finishing. On the other hand, it was found that the apparent decrease in shear strength measured in the present research is related to the cooling temperature applied in each case study (-40°C to -76°C), 0.97 MPa being the lowest value found corresponding to a temperature of -76°C. The values obtained are in good agreement with those found by Zelle et al. [33] in their study regarding mixed mode failure strength of implant-cement interfaces. They reported an interface shear strength in the range 0.45 – 3.11 Mpa for a loading angle from 60° to 90°, and a roughness of 0.89 μm. From the values obtained, the maximum shear stress showed a non-linear trend where the maximum value of 2.24 MPa at a room temperature of 23°C, was reduced as the temperature of interest at the proximal zone of the stem decreased: 1.54 MPa, 1.61Mpa, 1.36 MPa, and 0.97 MPa for the studied temperatures of -40°C, -49°C, -58°C, and -76°C respectively. Although the value obtained at a temperature of -58°C was 0.07 MPa higher than the value obtained at -49°C, there was a strong relationship between maximum shear stress and temperature.

The analysis of the strain energy indicated a significant decrease of 44% and 62.6% between the control test at 23°C and the case studies at their elastic zone, the lowest values being at temperatures of -58°C and -76°C, 5.2 J and 4.9 J respectively. For these particular case studies performed with a steel mould, this means that at lower cooling temperatures, less mechanical energy is needed in order to break the stem-cement interface. Similarly to the plots of force and maximum shear stress, the strain energy showed a relation with temperature as its values were reduced with respect to the temperature of interest. The values obtained were 12.1, 11.8, 8.7, and 9.9 J for case studies at -40°C, -49°C, -58°C, and -76°C respectively, all lower than the strain energy obtained for the control test at room temperature: 13.24 J.

In the absence of the mechanical characteristics of a bond interface from experimental data in conjunction with an appropriate numerical model to clarify the failure mechanism, it is only possible to obtain an approximation of the failure mechanism.

Although there have been many investigations regarding the mechanical behaviour of joints and bimetallic strips, whether they were bonded mechanically or with the use of an adhesive, the complexity of the mechanical behaviour of the interface between the materials involved is still not entirely understood [195, 252]. It is agreed that the failure mechanism and the strength of the bond depend on the particular mechanical characteristics found at the interface. To obtain the mechanical characteristics of the interface, it is important to implement a systematic series of experiments based on standardised tests for tensile, in-plane shear, tear, and mixed mode failure. Fracture energy, bonding strength, separation strength, and yield strength, as well as the components of the stiffness matrix can be obtained from such tests and, therefore, a possible failure mechanism can be proposed [194, 195, 252, 282-284]. In the present research, it was only possible to obtain an apparent bonding strength and strain energy from the mechanical tests.

As a way to understand the force-time curves obtained from the experiments, the studies by Di Franco et al. [197] were reviewed. Di Franco et al. described the failure mechanisms in tension found in one experimental study of metal-composite joints, bonded with adhesive or as a hybrid adhesive-rivet. They observed that the failure mechanism of an ordinary composite joint began at the edges of the bonded joint, extending to the centre of the bonded area. On the other hand, a hybrid joint starts to fail with delamination of the adhesive at one edge of the joint before the opposite edge starts to delaminate. Delamination of the adhesive at the edges continues centripetally to the rivet which mechanically fastens the composite plies. The load is then transferred to the rivet in its entirety, causing deformation and subsequent failure of the rivet.

In the present study, when the titanium stem is extracted from the bone cement at room temperature (no cooling treatment) it seems likely that the failure of the interface follows the mechanism described by Di Franco et al. Failure could start at both the interior and exterior edges, extending to the centre of each face in contact with the

bone cement. It is also likely that the smallest areas of the stem-cement interface are the first to fail.

In the case of the cooled titanium stems, the failure mechanism could be expected to be similar to that without thermal treatment, starting at the edges and extending to the centre of the surfaces. Since the neck of the stem was being cooled, there was a temperature gradient along the length of the stem-cement interface, with the coldest part in the proximal zone and the distal zone being relatively warmer than the proximal zone but still colder than ambient temperature. This difference in temperature along the length of the stem clearly affected the interface bonding strength in all cooling cases studied, from -76°C to -40°C, demonstrated by the reduction in the required force to remove the titanium stem from the bone cement, the strain energy, and the maximum shear stress from each case.

The following conclusions can be drawn from the experiments performed in four case studies:

I. Cooling the titanium stem does have an impact on the required force to remove it from the cement mantle. By comparing the maximum force for the Control tests, which was 14.55 kN, to the cooling case studies, a maximum reduction of 56.5% of the force for a temperature of -76°C, and a reduction of 31% for a temperature of -40°C were obtained. From the above, it can be stated that the lower the cooling temperature of the stem the lower the required force to remove the femoral stem from the cement mantle.

II. The energy needed to release the titanium stem (strain energy) obtained for each case study also demonstrates that the cooling process is effective. Release energy was reduced by 45% and 62.5% compared to a test performed at ambient temperature (22°C). This means that by cooling the femoral stem, the surgeon would need to exert less energy to remove the femoral stem.

III. The maximum shear stress is reduced by 28% to 56.5% compared to the control tests at 23°C. This means that the apparent interface strength between

the titanium stem and the bone cement is affected by exposing the titanium stem to low temperatures.

IV. Force-time curves from all case studies are characterised by two reductions in force; first a sudden failure as a brittle material, and then the force increases until the interface completely fails. As for the failure mechanism, it is thought that debonding is triggered at the edges and rapidly progresses to the centre of the surfaces of the stem. When the stems are subjected to the cooling process, debonding would be expected to occur at the edges of the interface with lower temperature (these in the proximal zone). Since the titanium stem has a temperature distribution, colder in the proximal zone and warmer in the distal zone, the smaller interfaces fail first and the larger interfaces at the end.

The proposed cooling methodology has been shown to offer a potential improvement by reducing the release force of a cemented titanium stem in comparison to ambient conditions, which would serve to facilitate the surgery in revision total hip arthroplasty.

7.2 Impact of Temperature on the Release Force of a Cemented Titanium Stem in a Composite Cylinder

Chapter 4 presented experiments performed with composite cylinders as part of the second scenario study. The cylinders had similar mechanical and thermal properties of human cortical and trabecular bone. The objective of these experiments was to test the cooling methodology, in a closer approach, on specimens made of materials that mimic human bone mechanical and thermal properties.

The results from these experiments demonstrated that the cooling process does have an effect on the force required to remove titanium stems cemented in composite cylinders. The plots of force showed a linear trend and the relation between the force required and the low temperature remained visible. The force required to release the stem was lowered in relation to the temperature of study at the proximal zone of the

prosthesis. The values were of 6.52 kN, 6.05 kN, and 6.93 kN for the case studies at -40°C, -49°C, and -76°C compared to the control specimen which was of 13.98 kN. It was observed that for the scenario study with composite cylinders, and while aiming to a proximal temperature of 76°C, the force required to remove the stem had a small increment in value of 0.41 kN and 0.88 kN compared to case studies at -40°C and -49°C respectively.

Differences were found between the experiments shown in Section 4.2 of Chapter 4 and those shown in Section 3.4 from Chapter 3. As a first observation, the titanium stems extracted at room temperature (25°C), had a very similar value of maximum force (13.98 kN) compared to the control specimens for steel moulds (14.55 kN). For the tests performed with composite cylinders, the force-time curve smoothly increased to the maximum value that the interface could withstand.

The cooling case studies demonstrated a maximum reduction of nearly 50% of the control force (13.98 kN) for a temperature of -76°C, and a reduction of almost 53% for a temperature of -40°C. The curves showed elastic deformation with a single maximum force; plastic deformation was not present in these cases.

By comparing the results from the cooled specimens in Section 3.3 and the thermally treated specimens from Section 4.2, it can be observed from the temperature plots that the steel mould specimens are colder at the middle and distal zones of the stem than the specimens with composite cylinders at the same spots, middle and distal. The lower temperature at those points was caused by the vapour of nitrogen surrounding the exterior surfaces of the steel mould while in the cooling stage, situation that was avoided when performing the experiments with composite bones. The lower temperature could have affected much more the bonding interface between the titanium stem and the bone cement in the steel mould specimens causing a lower force required to remove the stem at -76°C.

For these case studies, the maximum shear stress (which represented the interface shear strength) was reduced by 50.42% to 56.7% compared to the control test. Particular attention was paid to the interface shear strength obtained in Case 1 at -76°C since it resulted in a higher shear strength compared to the case studies at -40°C and -49°C. This difference is thought to be related to the contraction of the materials at the

proximal zone caused by the effects of temperature over the thermo-mechanical properties, particularly from the composite cylinder. It is known that the composite bone has a similar thermal expansion coefficient to that of bone cement ($63e^{-6}$ 1/°C and $72.2e^{-6}$ 1/°C respectively), but considerably greater compared to the titanium stem and the steel mould ($9.5e^{-6}$ 1/°C and $17e^{-6}$ 1/°C respectively). Maximum shear stress maintained a non-linear trend and the relation between the cooling temperature and the resulting maximum shear stress remained strong. From the calculated maximum shear stress, it was observed that, as the temperature at the proximal zone of the prosthesis is lowered, the value of maximum shear stress decreases. Compared to the specimens at room temperature, which had a value of 2.15 MPa, the values obtained were of 1.01 MPa, 0.93 MPa, and 1.07 MPa for the cooling temperatures of interest of -40°C, -49°C, and -76°C at the proximal zone respectively.

The cooling cases showed that the mechanical energy required to remove the femoral stem (strain energy) was considerably lower than the energy needed to remove the stem at ambient temperature, lower by 74% and 70% for a temperature of -40°C and -49°C respectively. However, it was observed that for a cooling temperature of -76°C, the energy was 22% and 32% higher than the values obtained for -40°C and -49°C respectively. This increment in strain energy is also thought to be related to the effects of thermal contraction of the materials, particularly at the proximal zone of the specimen, causing a tighter hold of the femoral stem in that area. Strain energy was observed to have linear trend for the case studies at low temperature, keeping a visible relation between mechanical energy required and temperature of interest at the proximal zone of the femoral stem. Though the results showed a reduction compared to the control test, 10.66 J, the thermally treated specimens showed a linear increase in the value of strain energy. The calculated values of strain energy were of 3.16 J, 3.18 J, and 4.01 J, for the cooling temperatures -40°C, -49°C, and -76°C at the proximal zone respectively.

The following points can be inferred from the results obtained in this section of Chapter 4:

I. It was observed that in the test undertaken at different cooling temperatures with composite cylinders, a lower release force was required compared to the

tests done with a steel mould. As a result, the strain energy, and the interface shear strength were also lowered.

II. The non-linear behaviour obtained in the tests from Chapter 3 could have been caused by two means: first, the clamping system (steel mould) used and the interaction between the bone-cement and the internal surfaces of the steel mould; and second, the thermal contraction of the steel followed by a thermal expansion once clamped in the Instron machine. This would confirm the mechanical failure similar to the hybrid bonded joints mentioned in the studies of Di Franco et al. [197], and would also discard the roughness of the femoral stem as factor to create a second tier release of the force.

III. All cooled studies exhibit brittle behaviour as shown in their force-time plots in which the force suddenly drops, with force values as low as 57% of that obtained at room temperature.

IV. The interface fails as described in the literature for ordinary composite-metal bonded joints [197]: when the stems are subjected to low temperatures, the debonding of the proximal zone is triggered by the edges with lower temperature in that zone, it continues rapidly and progressively to the centre of the surfaces of the stem since the titanium stem. The interfaces with smaller area are the first to fail and the larger areas are the last to yield.

Finally, it can be confirmed that by cooling the titanium stem, the force required to remove the cemented titanium stem from bone-like composite cylinders is reduced. This is also demonstrated by the reduction of work needed to remove the femoral stem. The methodology proposed offered a reduction in the release force of a cemented titanium stem in comparison to ambient conditions to facilitate the extraction of the stem in Revision THA.

7.3 Impact of Temperature on the Release Force of a Cemented Titanium Stem in a Composite Femur

To validate further the impact of the cooling procedure, a second experimental work presented in Chapter 4 was performed by "implanting" the titanium stem in composite femurs which were resected and prepared as in a real case scenario. This set of experiments had two temperatures of interest: one at -40°C labelled as critical temperature, and one at -76°C as an extreme cooling case scenario.

Regarding the cooling cases, the release force obtained from the test performed at a temperature of -40°C showed a reduction of nearly 65% of the value of the control force from the composite cylinder, which had a value of 13.98 kN. The release force required (5 kN) is in agreement with the results from previous experiments which showed a reduction of 31% and 53% of the overall force for a temperature of -40°C. On the other hand, the cooling case at -76°C showed a reduction of the force by 32.5%. Similar to the previous case with a composite cylinder, the force required to remove the stem was higher at the cooling temperature of -76°C than the required force at -40°C. This is thought to have been caused by the contraction of the composite bone in the proximal zone. Nevertheless, the effect of the cooling temperature was observed as the value of the force required to remove the femoral stem was reduced from 13.98 kN at room temperature to 4.9 kN and 9.44 kN for the temperatures of interest of -40°C and -76°C respectively.

The results from this case study showed that the interface shear strength of the stem-cement interface is reduced with temperature. Nevertheless, it was observed that the interface shear strength corresponding to a temperature of -40°C, was lower by 48% than the strength at -76°C. This was also observed for the studies performed with composite cylinders. It is thought that the increase of interface shear strength with temperatures lower than -40°C is the result of the effects of temperature on the thermal properties of the composites, principally the thermal expansion/contraction which is greater for the composites than the titanium stem, $63e^{-6}$ 1/°C and $9.5e^{-6}$ 1/°C respectively. For this scenario study performed with composite femurs, the maximum shear stress had a similar trend as the one found with the composite cylinders. The

maximum shear stress that could withstand the interface at room temperature was reduced from 2.15 MPa to 0.75 MPa and 1.45 MPa for case studies at -40°C and -76°C respectively. In the case study were the cooling temperature was aimed to be -76°C at the proximal zone, the value of shear stress increased compared to the value obtained at a cooling temperature of -40°C, a behaviour also observed found in the tests performed with composite cylinders.

The mechanical energy needed to release the titanium stem (strain energy) was also found to be lower for a temperature of -40°C by 65.5% compared to the case study at -76°C. Although, both strain energies at -40°C and -76°C were lower compared to the control test of the composite cylinder by 78% and 36.2% respectively. The strain energy calculated for this case scenario with composite femurs showed a close value at a temperature of -40°C, 2.34 J, compared to the composite cylinder, 3.16 J. The case study when the proximal zone of the stem was at -76°C showed that the strain energy was higher by 41% for the composite femur compared to the cylinder specimens at the same cooling temperature, the values were of 6.8 J and 4.01 J respectively. By comparing the calculated strain energy between the case scenario with steel mould and case scenario with composite bones, the thermally treated composites showed a significant reduction of the mechanical energy required to release the stem by 74% and 80% compared to the thermally treated steel mould specimens, this at a temperature of interest of -40°C.

It was mentioned in the experimental work performed with composite bones that the mechanical pull-out stage started after 120 seconds of removing the femoral stem from the bath of liquid nitrogen. In clinical practice the pull-out should start as soon as possible while taking advantage of the mentioned thermal inertia of the cooling stage, however, it is known that some unpredictable situations may occur while in surgery, nevertheless, 120 seconds and up to 300 seconds should be an acceptable time period to start the mechanical pull-out. It is important to remark that the bonding interface between prosthesis-bone or prosthesis-cement has been broken already at this point as demonstrated in the present study.

Some factors need to be considered in order to comprehend why the force required to remove the femoral stem increased from 6.93 KN for the composite cylinder to 9.44 KN for the composite femur. Some of the factors to be considered are:

1. Different geometry and structure of the composite bone used to implant the femoral stems, cylinder and femur like geometries.

2. The amount of cortical and trabecular bone-like material. The composite cylinder contains a greater amount of simulated trabecular bone than the composite femur. regarding the simulated cortical bone, the cylinder has an uniform shell of 3mm thick whereas the composite femur properly simulates the thickness of cortical bone of a human femur.

3. The process of preparing the medullary canal to implant the titanium stems in the composite femurs required a process were the amount of trabecular bone was none in the proximal region of the composite femur, thus the bone cement at that zone would not count with the porosity of the trabecular bone to have a better mechanical bonding.

4. A possible manufacture defect of the composite femur that could not be assessed prior to the experiment.

The following points can be concluded from the results obtained in this section of Chapter 4:

I. It was observed that in the tests undertaken at different cooling temperatures with composite femurs, a lower release force was required compared to the tests undertaken using a steel mould. As a result, the strain energy, and the interface shear strength are also significantly reduced.

II. All cooled studies exhibit brittle behaviour as the force drops abruptly with no sign of non-linear behaviour. The release force for a temperature of -40°C had a value as low as 4.8 kN, reducing by 65% compared to the required force at room temperature.

III. The failure mechanism of the interface is thought to happen as described in for composite-metal bonded joints [197]: first, the proximal zone is affected

by low temperatures, and it triggers by continually breaking the interface to the centre of the surfaces of the stem since the titanium stem.

IV. Finally, from the observed results regarding maximum force, interface shear strength, and strain energy, it is concluded that by cooling the proximal zone of the titanium stem down to -40^{o}C, considered as the optimal temperature, the removal of a cemented titanium stem can be achieved with the lowest amount of work exerted by the surgeon.

7.4 Concept Design

Based on the results of the work presented in this thesis, the feasibility of the new methodology for removing a cemented femoral stem during a revision total hip arthroplasty surgery has been demonstrated. Furthermore, the framework of the design process of a medical device was presented. The functioning of the medical device is based on the proposed new methodology of cooling the femoral prosthesis of an artificial hip. The development of the concept design is currently in the verification phase. Once verification is completed, the author is planning to patent the medical device.

The proposed medical device takes into account a design based on the femoral prosthesis from DePuy Corail size 11, however, it is known that the design, size, and shape of the femoral stems in the market is wide. The proposed components of the medical device, i.e. cryo-bell and pulling-mechanism, should be manufactured in various sizes in order to fit the femoral stem to be removed.

7.5 Finite Element Thermal Analysis

In Chapter 6 of this thesis, a computational model was developed to predict and analyse the temperature distribution of a titanium stem cemented in a steel mould. The first model predicted the distribution of temperature after simulating the cooling of the

titanium stem by the neck for 20 minutes. Furthermore, four case studies were undertaken to predict the change of temperature that occurs while applying the cooling technique at each cooling temperature: -76°C, -58°C, -49°C, and -40°C.

The thermal analysis showed the behaviour of energy exchange due to temperature differences along the length of the specimen, i.e. the temperature distribution. In all analyses, the zone most affected by temperature is the proximal region of the stem, which is clearly seen in the temperature contour plots, Figures 6.17 to 6.20.

With regard to the cement mantle, it was observed from the temperature fields that it is affected by the heat transfer from both sides, from the titanium stem and the steel mould. The lowest temperature reached at the proximal zone was approximately -50°C for the cooling case at -40°C, and -100°C for the cooling case at -76°C. Even though the temperature of the cement mantle is 10°C below the critical safety temperature, it is correct to state that cooling the femoral stem to -40°C is the optimal cooling temperature. This is supported by the fact that, in a better approach such as case scenarios with composites, the cement mantle would surrounded by much more insulating material, that is composite bone, thus the temperature of the cement is less likely to reach temperatures below the critical temperature.

The model accurately predicted the temperature distribution in the titanium stem for the four case studies of interest, and it was demonstrated that the thermal gradient is unidirectional in the main axis of the femoral stem, where the most affected zone by temperature is the proximal region.

7.6 Limitations to the Research

Limitations and difficulties of measuring the mechanical and thermal properties as a function of cryogenic temperatures limit complete understanding of the behaviour of the materials involved in the present study. However, data concerning the specific heat, thermal conductivity, and the thermal coefficient of expansion were obtained from the literature. These three thermal properties are the three most important parameters

used for heat transfer analysis and applications. The material characteristics mentioned work as control of the thermal input, the cool-down time, and the mechanical stability of the device [285].

7.7 Recommendations and Future Challenges

Some challenges must be faced in the subsequent development of the final medical device:

- The process of manufacturing and assembling the "cryo-bell" based on the recommended selection of materials given for the design concept.
- Experiments need to be conducted with the femoral stem used in real surgery, DePuy's Corail; either in vitro or in vivo. These experiments should be carefully planned, following the relevant ethical practices.
- Experiments in vivo with animals need to be conducted in order to obtain an osseointegrated prosthesis, either into the cement mantle or directly to the coated femoral stem.

Another suggested major research project would be the investigation of the fracture mechanics of the interface between the titanium stem and the bone cement, the fracture mechanics of the interface of a hybrid hip arthroplasty which comprises stem-cement-bone.

Experimentation in-vivo/in-vitro could be conducted to determine the mechanical properties in torsion, tension, and shear of the interface between surgical implant and bone tissue. In addition, mechanical and thermal properties of the most commonly used bone cement could be obtained since this data is stored by manufacturers. This useful information could be used to numerically model with high precision the extraction of the femoral stem by applying the methodology proposed in the present work.

For in vivo experimentation and future clinical practice, liquid nitrogen would have to be used with extreme care. Extreme security measures must be done to safeguard the living tissue that is exposed to low temperature as liquid nitrogen would be flowing through the proposed cryo-bell to cool the neck of the femoral stem. To avoid thermal damage of muscle and bone, insulating materials such as cryogels and cryogel membranes could be applied over the living tissue.

It is recommended to work on a refined thermo-mechanical numerical model with the objective of visualising and understanding much more the mechanics of failure at the interface after applying the cooling process on the femoral stem.

References

1. Pivec R, Johnson AJ, Mears SC, Mont MA. Hip arthroplasty. The Lancet. 2012;380(9855):1768-77.
2. Breusch S, Malchau H. The Well-Cemented Total Hip Arthroplasty: Theory and Practice: Springer; 2005.
3. Migaud H, Girard J, May O, Soenen M, Pinoit Y, Laffargue P, et al. Contemporary total hip arthroplasty: Materials and surgical approaches. Revue du Rhumatisme (Edition Francaise). 2009;76(4):367-73.
4. Mulliken BD, Rorabeck CH, Bourne RB, Nayak N. The surgical approach to total hip arthroplasty: complications and utility of a modified direct lateral approach. The Iowa Orthopaedic Journal. 1995;15:48-61.
5. Mantovani G, Lamontagne M, Varin D, Cerulli GG, Beaulé PE. Comparison of total hip arthroplasty surgical approaches by Principal Component Analysis. Journal of Biomechanics. 2012;45(12):2109-15.
6. Maheshwari AV, Ranawat AS, Ranawat CS. The use of hydroxyapatite on press-fit tapered femoral stems. Orthopedics. 2008;31(9):882-4.
7. Lesur E, Laude F. Arthroplastie totale de hanche par voie antérieure et son évolution mini-invasive. EMC - Rhumatologie-Orthopédie. 2004;1(5):445-53.
8. Healthbase-Online-Inc. Total hip replacement surgery implants. Available from: http://www.healthbase.com/resources/orthopedics/total-hip-replacement-surgery-implants/frequently-asked-questions-faqs-total-hip-replacement-surgery-implants-india-mexico-price-cost.html.
9. Lee YK, Yoo JJ, Koo KH, Yoon KS, Kim HJ. Metal neck and liner impingement in ceramic bearing total hip arthroplasty. Journal of Orthopaedic Research. 2011;29(2):218-22.
10. Haddad FS, Thakrar RR, Hart AJ, Skinner JA, Nargol AVF, Nolan JF, et al. Metal-on-metal bearings: The evidence so far. Journal of Bone and Joint Surgery - Series B. 2011;93 B(5):572-9.
11. Bonnaig NS, Freiberg RA, Freiberg AA. Total hip arthroplasty with ceramic-on-ceramic bearing failure from third-body wear. Orthopedics. 2011;34(2).
12. Poss R, Walker P, Spector M, Reilly DT, Robertson DD, Sledge CB. Strategies for improving fixation of femoral components in total hip arthroplasty. Clinical Orthopaedics and Related Research. 1988(235):181-94.
13. Sumner DR, Kienapfel H, Jacobs JJ, Urban RM, Turner TM, Galante JO. Bone ingrowth and wear debris in well-fixed cementless porous-coated tibial components removed from patients. The Journal of Arthroplasty. [doi: DOI: 10.1016/S0883-5403(05)80122-6]. 1995;10(2):157-67.
14. Bertani A, Helix M, Louis ML, Rochwerger A, Curvale G. Total hip arthroplasty in severe segmental femoral bone loss situations: Use of a reconstruction modular stem design (JVC IX™). Orthopaedics and Traumatology: Surgery and Research. 2009;95(7):491-7.
15. Baudriller H, Chabrand P, Dubois F. Failure of total hip arthroplasties. Numerical modeling of debris formation through plastic strains. Computer Methods in Biomechanics and Biomedical Engineering. 2004;7(4):227-44.
16. von Knoch M, A. Engh SC, Sychterz CJ, Engh JCA, Willert H-G. Migration of polyethylene wear debris in one type of uncemented femoral component with circumferential porous coating: An autopsy study of 5 femurs. The Journal of Arthroplasty. [doi: DOI: 10.1016/S0883-5403(00)91259-2]. 2000;15(1):72-8.

17. Engh CA, Bobyn JD. The influence of stem size and extent of porous coating on femoral bone resorption after primary cementless hip arthroplasty. Clinical Orthopaedics and Related Research. 1988(231):7-28.
18. Arif M, Sivananthan S, Choon DS. Revision of total hip arthroplasty using an anterior cortical window, extensive strut allografts, and an impaction graft: follow-up study. Journal of orthopaedic surgery (Hong Kong). 2004;12(1):25-30.
19. Glassman AH, Engh CA, Bobyn JD. Proximal femoral osteotomy as an adjunct in cementless revision total hip arthroplasty. Journal of Arthroplasty. 1987;2(1):47-63.
20. Garino JP, Ferrante CR. Femoral component exposure and removal technique. Techniques in Orthopaedics. 2001;16(3):245-57.
21. Chen WM, McAuley JP, Engh C.A, Jr., Hopper R.H, Jr., Engh CA. Extended slide trochanteric osteotomy for revision total hip arthroplasty. Journal of Bone and Joint Surgery - Series A. 2000;82(9):1215-9.
22. Glassman AH. Exposure for Revision: Total Hip Replacement. Clinical Orthopaedics and Related Research. 2004(420):39-47.
23. Sabboubeh A, Al Khatib M. A technique for removing a well-fixed cemented acetabular component in revision total hip arthroplasty. Journal of Arthroplasty. 2005;20(6):800-1.
24. Li C, Granger C, Schutte Jr HD, Biggers Jr SB, Kennedy JM, Latour Jr RA. Progressive failure analysis of laminated composite femoral prostheses for total hip arthroplasty. Biomaterials. 2002;23(21):4249-62.
25. Jack CM, Molloy DO, Esposito C, Walter WL, Zicat B, Walter WK. Limited slot femorotomy for removal of proximally coated cementless stems. A 10-year follow-up of an unreported surgical technique. Journal of Arthroplasty. 2013;28(6):1000-4.
26. National-Joint-Registry. 10th Annual Report 2013: Pad Creative Ltd; 2013. Available from: www.njrcentre.org.uk.
27. National-Joint-Registry. 11th Annual Report 2014: Pad Creative Ltd; 2014. Available from: www.njrcentre.org.uk.
28. National-Joint-Registry. 12th Annual Report 2015: Pad Creative Ltd; 2015. Available from: www.njrcentre.org.uk.
29. Bobyn JD, Wilson GJ, MacGregor DC, Pilliar RM, Weatherly GC. Effect of pore size on the peel strength of attachment of fibrous tissue to porous-surfaced implants. Journal of Biomedical Materials Research. 1982;16(5):571-84.
30. Bobyn JD, Pilliar RM, Cameron HU. The effect of porous surface configuration on the tensile strength of fixation of implants by bone ingrowth. Clinical Orthopaedics and Related Research. 1980;NO 149:291-8.
31. Hayashi K, Inadome T, Tsumura H, Nakashima Y, Sugioka Y. Effect of surface roughness of hydroxyapatite--coated titanium on the bone-implant interface shear strength. Biomaterials. [doi: DOI: 10.1016/0142-9612(94)90241-0]. 1994;15(14):1187-91.
32. Müller RT, Schürmann N. Shear strength of the cement metal interface - An experimental study. Archives of Orthopaedic and Trauma Surgery. 1999;119(3-4):133-8.
33. Zelle J, Janssen D, Peeters S, Brouwer C, Verdonschot N. Mixed-mode failure strength of implant-cement interface specimens with varying surface roughness. Journal of Biomechanics. 2011;44(4):780-3.
34. Stone MH, Wilkinson R, Stother I. Some factors affecting the strength of the cement-metal interface. Journal of Bone and Joint Surgery - Series B. 1989;71(2):217.
35. Wang BC, Lee TM, Chang E, Yang CY. The shear strength and the failure mode of plasma-sprayed hydroxyapatite coating to bone: The effect of coating thickness. Journal of Biomedical Materials Research. 1993;27(10):1315-27.

36. Wang X, Subramanian A, Dhanda R, Agrawal CM. Testing of bone-biomaterial interfacial bonding strength: A comparison of different techniques. Journal of Biomedical Materials Research. 1996;33(3):133-8.
37. Cook SD, Barrack RL, Dalton JE, Thomas KA, Brown TD. Effects of indomethacin on biologic fixation of porous-coated titanium implants. The Journal of Arthroplasty. [doi: DOI: 10.1016/S0883-5403(05)80184-6]. 1995;10(3):351-5, 7-8.
38. Cook SD, Thomas KA, Dalton JE, Volkman TK, Whitecloud TS, Kay JF. Hydroxylapatite coating of porous implants improves bone ingrowth and interface attachment strength. Journal of Biomedical Materials Research. 1992;26(8):989-1001.
39. Oonishi H, Yamamoto M, Ishimaru H, Tsuji E, Kushitani S, Aono M, et al. The effect of hydroxyapatite coating on bone growth into porous titanium alloy implants. Journal of Bone and Joint Surgery - Series B. 1989;71(2):213-6.
40. Oonishi H, Noda T, Ito S, Kohda A, Ishimaru H, Yamamoto M, et al. Effect of hydroxyapatite coating on bone growth into porous titanium alloy implants under loaded conditions. Journal of applied biomaterials. 1994;5(1):23-37.
41. Raab S, Ahmed AM, Provan JW. The quasistatic and fatigue performance of the implant/bone-cement interface. Journal of Biomedical Materials Research. 1981;15(2):159-82.
42. Ahmed AM, Raab S, Miller JE. Metal/cement interface strength in cemented stem fixation. Journal of Orthopaedic Research. 1984;2(2):105-18.
43. Tóth K, Sisák K, Wellinger K, Manó S, Horváth G, Szendröi M, et al. Biomechanical comparison of three cemented stem removal techniques in revision hip surgery. Archives of Orthopaedic and Trauma Surgery. 2011;131(7):1007-12.
44. Costa FWG, Brito GAC, Pessoa RMA, Studart-Soares EC. Histomorphometric assessment of bone necrosis produced by two cryosurgery protocols using liquid nitrogen: An experimental study on rat femurs. Journal of Applied Oral Science. 2011;19(6):604-9.
45. Gage AA, Baust JM, Baust JG. Experimental cryosurgery investigations in vivo. Cryobiology. 2009;59(3):229-43.
46. Salmassy DA, Pogrel MA. Liquid nitrogen cryosurgery and immediate bone grafting in the management of aggressive primary jaw lesions. Journal of Oral and Maxillofacial Surgery. 1995;53(7):784-90.
47. Diefenbeck M, Thomas M, Sergiy Z, Jörg B, Klaus DJ, Christian S, et al. Freezing of Rat Tibiae at -20°C Does Not Affect the Mechanical Properties of Intramedullary Bone/Implant-Interface: Brief Report. The Open Orthopaedics Journal. 2011;5.
48. Huss BT, Anderson MA, Wagner-Mann CC, Payne JT. Effects of temperature and storage time on pin pull-out testing in harvested canine femurs. American Journal of Veterinary Research. 1995;56(6):715-9.
49. Biyikli S, Modest MF, Tarr R. Measurements of thermal properties for human femora. Journal of Biomedical Materials Research. 1986;20(9):1335-45.
50. Hansen E. Modelling heat transfer in a bone–cement–prosthesis system. Journal of Biomechanics. 2003;36(6):787-95.
51. Carter DR, Spengler DM. Mechanical properties and composition of cortical bone. Clinical Orthopaedics and Related Research. 1978;NO. 135:192-217.
52. Swenson Jr LW, Schurman DJ, Piziali RL. Finite element temperature analysis of a total hip replacement and measurement of PMMA curing temperatures. Journal of Biomedical Materials Research. 1981;15(1):83-96.
53. Stańczyk M. Study on modelling of PMMA bone cement polymerisation. Journal of Biomechanics. 2005;38(7):1397-403.
54. Kim SY, Kim DH, Oh CW, Kim PT, Ihn JC. Total hip arthroplasty with the use of nonmodular cementless acetabular component. Journal of Arthroplasty. 2005;20(5):632-8.

55. Moore KL, Dalley AF. Clinically Oriented Anatomy. 5th Edition ed: Lippincott Williams & Wilkins; 2006.
56. Tortora GJ. Principles of anatomy and physiology. 12 ed: John Wiley and Sons, Inc.; 2009.
57. Muller H. The Hip. Haderer & Muller Biomedical Art, LLC; 2013; Available from: http://www.haderermuller.com/.
58. Klemm D. Hip anatomy. New York Dynamic Neuromuscular Rehabilitation & Physical Therapy; 2009; Available from: http://nydnrehab.com/what-we-treat/hip-pain/hip-groin-pain/.
59. Malchau H, Herberts P, Ahnfelt L. Prognosis of total hip replacement in Sweden: Follow-up of 92,675 operations performed 1978–1990. Acta Orthopaedica. 1993;64(5):497-506.
60. Beckenbaugh RD, Ilstrup DM. Total hip arthroplasty. A review of three hundred and thirty-three cases with long follow-up. Journal of Bone and Joint Surgery - Series A. 1978;60 A(3):306-13.
61. Erdemli B, Yilmaz C, Atalar H, Güzel B, Cetin I. Total hip arthroplasty in developmental high dislocation of the hip. Journal of Arthroplasty. 2005;20(8):1021-8.
62. Morsi E. Total Hip Arthroplasty for Fused Hips; Planning and Techniques. Journal of Arthroplasty. 2007;22(6):871-5.
63. Swanson MA, Knight JR, Huo MH. Total Hip Arthroplasty Following Previous Acetabular Fracture. Operative Techniques in Orthopaedics. 2009;19(3):150-4.
64. van Dijk CM, Bimmel R, Haddad FS. (iv) Surgical approaches in primary total hip arthroplasty - pros and cons. Orthopaedics and Trauma. 2009;23(1):27-34.
65. Queen RM, Butler RJ, Watters TS, Kelley SS, Attarian DE, Bolognesi MP. The effect of total hip arthroplasty surgical approach on postoperative gait mechanics. Journal of Arthroplasty. 2011;26(SUPPL. 6):66-71.
66. Anderson RH, Baker EJ, Redington AN, Rigby ML, Penny DJ, Wernovsky G. Surgical Treatment of Hip Arthritis: Reconstruction, Replacement, and Revision: Elsevier Health Sciences; 2009.
67. Pfeil J, Siebert WE. Minimally invasive surgery in total hip arthroplasty2010.
68. Total Hip Replacement Surgery. Available from: http://www.medicinenet.com.
69. Total Hip Replacement. Available from: http://orthoinfo.aaos.org.
70. Hip Replacement. Available from: http://www.niams.nih.gov.
71. Rack HJ, Qazi JI. Titanium alloys for biomedical applications. Materials Science and Engineering: C. [doi: DOI: 10.1016/j.msec.2005.08.032]. 2006;26(8):1269-77.
72. Albrektsson T, Branemark PI, Hansson HA, Lindstrom J. Osseointegrated titanium implants. Requirements for ensuring a long-lasting, direct bone-to-implant anchorage in man. Acta Orthopaedica Scandinavica. 1981;52(2):155-70.
73. TIG. Titanium for medical applications. Titanium Information Group; 2012; Available from: http://www.titaniuminfogroup.co.uk/data-sheets.
74. Niinomi M. Mechanical properties of biomedical titanium alloys. Materials Science and Engineering A. [doi: DOI: 10.1016/S0921-5093(97)00806-X]. 1998;243(1-2):231-6.
75. Artificial hip components. Available from: http://www.hipsforyou.com/.
76. Teoh SH. Engineering Materials for Biomedical Applications: World Scientific Pub.; 2004.
77. Nag S, Banerjee R. Fundamentals of medical implant materials: ASM Handbook; 2012.
78. Wnek GE, Bowlin GL. Encyclopedia of Biomaterials and Biomedical Engineering (Print): Taylor & Francis; 2004.
79. Berry DJ, Steinmann S. Adult Reconstruction: Wolters Kluwer Health/Lippincott Williams & Wilkins; 2007.

80. Elkins JM, O'Brien MK, Stroud NJ, Pedersen DR, Callaghan JJ, Brown TD. Hard-on-hard total hip impingement causes extreme contact stress concentrations. Clinical Orthopaedics and Related Research. 2011;469(2):454-63.
81. Walsh AJ, Nikolaou VS, Antoniou J. Inflammatory pseudotumor complicating metal-on-highly cross-linked polyethylene total hip arthroplasty. Journal of Arthroplasty. 2012;27(2):324.e5-.e8.
82. Schlegel UJ, Bishop N, Sobottke R, Perka C, Eysel P, Morlock MM. Squeaking as a cause for revision of a composite ceramic cup. Orthopade. 2011;40(9):812-6.
83. Mesko JW, D'Antonio JA, Capello WN, Bierbaum BE, Naughton M. Ceramic-on-Ceramic Hip Outcome at a 5- to 10-Year Interval. Has it Lived Up to Its Expectations? Journal of Arthroplasty. 2011;26(2):172-7.
84. Ki SC, Kim BH, Ryu JH, Yoon DH, Chung YY. Squeaking sound in total hip arthroplasty using ceramic-on-ceramic bearing surfaces. Journal of Orthopaedic Science. 2011;16(1):21-5.
85. Carli A, Reuven A, Zukor DJ, Antoniou J. Adverse soft-tissue reactions around non-metal-on-metal total hip arthroplasty: A systematic review of the literature. Bulletin of the NYU Hospital for Joint Diseases. 2011;69(SUPPL. 1):S47-S51.
86. Callaghan JJ, Liu SS, Firestone DE, Yehyawi TM, Goetz DD, Sullivan J, et al. Total hip arthroplasty with cement and use of a collared matte-finish femoral component nineteen to twenty-year follow-up. Journal of Bone and Joint Surgery - Series A. 2008;90(2):299-306.
87. Hongyu Z. The Influence of Stem Design and Fixation Methods on the Lifetime of Total Hip Replacement [Medical Engineering]. Huddersfield: University of Huddersfield; 2009.
88. Bidar R, Kouyoumdjian P, Munini E, Asencio G. Long-term results of the ABG-1 hydroxyapatite coated total hip arthroplasty: Analysis of 111 cases with a minimum follow-up of 10 years. Orthopaedics and Traumatology: Surgery and Research. 2009;95(8):579-87.
89. Bobyn JD, Pilliar RM, Cameron HU, Weatherly GC. The optimum pore size for the fixation of porous surfaced metal implants by the ingrowth of bone. Clinical Orthopaedics and Related Research. 1980;NO. 150:263-70.
90. Bobyn JD, Stackpool GJ, Hacking SA, Tanzer M, Krygier JJ. Characteristics of bone ingrowth and interface mechanics of a new porous tantalum biomaterial. Journal of Bone and Joint Surgery - Series B. 1999 September 1, 1999;81-B(5):907-14.
91. Chambers B, St. Clair SF, Froimson MI. Hydroxyapatite-Coated Tapered Cementless Femoral Components in Total Hip Arthroplasty. Journal of Arthroplasty. 2007;22(4 SUPPL.):71-4.
92. Hacking SA, Bobyn JD, Toh KK, Tanzer M, Krygier JJ. Fibrous tissue ingrowth and attachment to porous tantalum. Journal of Biomedical Materials Research. 2000;52(4):631-8.
93. Keaveny TM, Bartel DL. Effects of porous coating, with and without collar support, on early relative motion for a cementless hip prosthesis. Journal of Biomechanics. [doi: DOI: 10.1016/0021-9290(93)90087-U]. 1993;26(12):1355-68.
94. Li J, de Wijn J, van Blitterswijk C, de. Groot K. Porous Ti6Al4V scaffolds directly fabricated by 3D fibre deposition technique: Effect of nozzle diameter. Journal of Materials Science: Materials in Medicine. 2005;16(12):1159-63.
95. Li X, Wang CT, Zhang WG, Li YC. Properties of a porous Ti-6Al-4V implant with a low stiffness for biomedical application. Proceedings of the Institution of Mechanical Engineers, Part H: Journal of Engineering in Medicine. 2009;223(2):173-8.
96. Soballe K. Hydroxyapatite ceramic coating for bone implant fixation: Mechanical anf histological studies in dogs. Acta Orthopaedica Scandinavica, Supplement. 1993;64(255):1-58.
97. Race A, Miller M, Ayers D, Cleary R, Mann K. The influence of surface roughness on stem-cement gaps. Journal of Bone and Joint Surgery - Series B. 2002;84(8):1199.

98. Verdonscbot N, Huiskes R. Surface roughness of debonded straight-tapered stems in cemented THA reduces subsidence but not cement damage. Biomaterials. 1998;19(19):1773-80.
99. Wirz D, Daniels AU, Göpfert B, Morscher EW. Clinical development and current status: Europe. Orthopedic Clinics of North America. [doi: DOI: 10.1016/j.ocl.2004.07.002]. 2005;36(1):63-73.
100. Morscher EW, Wirz D. Current state of cement fixation in THR. Acta Orthopaedica Belgica. 2002;68(1):1-12.
101. Pal B, Puthumanapully PK, Amis AA. (ii) Biomechanics of implant fixation. Orthopaedics and Trauma. 2013;27(2):76-84.
102. Gomez PF, Morcuende JA. Early Attempts at Hip Arthroplasty: 1700s to 1950s. The Iowa Orthopaedic Journal. 2005;25:25-9.
103. Nottrott M. Acrylic bone cements. Acta Orthopaedica. 2010;81(S341):1-27.
104. Nottrott M, Mølster AO, Moldestad IO, Walsh WR, Gjerdet NR. Performance of bone cements: Are current preclinical specifications adequate? Acta Orthopaedica. 2008;79(6):826-31.
105. Kenny SM, Buggy M. Bone cements and fillers: A review. Journal of Materials Science: Materials in Medicine. 2003;14(11):923-38.
106. Harper EJ. Bioactive bone cements. Proceedings of the Institution of Mechanical Engineers, Part H: Journal of Engineering in Medicine. 1998;212(2):113-20.
107. Lautenschlager EP, Jacobs JJ, Marshall GW, Meyer PR. Mechanical properties of bone cements containing large doses of antibiotic powders. Journal of Biomedical Materials Research. 1976;10(6):929-38.
108. Thielen T, Maas S, Zuerbes A, Waldmann D, Keim J. Mechanical material properties of polymethylmethacrylate (PMMA) for medical applications. Materialpruefung/Materials Testing. 2009;51(4):203-9.
109. Bello DG, Hernández ML, Guerra NB. Determinacion de propiedades mecanicas y temperatura maxima de polimerizacion de cementos oseos acrilicos modificados con micro y nanoparticulas de hidroxyapatita. Revista Latinoamericana de Metalurgia y Materiales. 2011(31):91-8.
110. Chou PM, Mariatti M. The properties of polymethyl methacrylate (PMMA) bone cement filled with titania and hydroxyapatite fillers. Polymer - Plastics Technology and Engineering. 2010;49(12):1163-71.
111. Daglilar S, Erkan ME. A study on bioceramic reinforced bone cements. Materials Letters. [doi: DOI: 10.1016/j.matlet.2006.07.068]. 2007;61(7):1456-9.
112. Harper EJ, Behiri JC, Bonfield W. Flexural and fatigue properties of a bone cement based upon polyethylmethacrylate and hydroxyapatite. Journal of Materials Science: Materials in Medicine. 1995;6(12):799-803.
113. Lewis G. Fatigue testing and performance of acrylic bone-cement materials: State-of-the-art review. Journal of Biomedical Materials Research Part B: Applied Biomaterials. 2003;66B(1):457-86.
114. Emerson RH, Sanders SB, Head WC, Higgins L. Effect of Circumferential Plasma-Spray Porous Coating on the Rate of Femoral Osteolysis After Total Hip Arthroplasty. Journal of Bone and Joint Surgery - Series A. 1999 September 1, 1999;81(9):1291-8.
115. Pilliar RM. Cementless implant fixation-toward improved reliability. Orthopedic Clinics of North America. 2005;36(1):113-9.
116. Kienapfel H, Sprey C, Wilke A, Griss P. Implant fixation by bone ingrowth. The Journal of Arthroplasty. [doi: DOI: 10.1016/S0883-5403(99)90063-3]. 1999;14(3):355-68.

117. Soballe K, Hansen ES, Rasmussen BH, Jorgensen PH, Bunger C. Tissue ingrowth into titanium and hydroxyapatite-coated implants during stable and unstable mechanical conditions. Journal of Orthopaedic Research. 1992;10(2):285-99.
118. Tsui Y, Doyle C, Clyne T. Plasma sprayed hydroxyapatite coatings on titanium substrates. Part 2: optimisation of coating properties. Biomaterials. 1998;19(22):2031-44.
119. Judet R, Siguier M, Brumpt B, Judet T. A noncemented total hip prosthesis. Clinical Orthopaedics and Related Research. 1978;NO. 137:76-84.
120. Lord GA, Hardy JR, Kummer FJ. An uncemented total hip replacement. Experimental study and review of 300 madreporique arthroplasties. Clinical Orthopaedics and Related Research. 1979;NO 141:2-16.
121. Pilliar RM, Cameron HU, Macnab I. Porous surface layered prosthetic devices. Bio-Medical Engineering. 1975;10(4):126-31.
122. Galante J, Rostoker W, Lueck R, Ray RD. Sintered fiber metal composites as a basis for attachment of implants to bone. Journal of Bone and Joint Surgery - Series A. 1971;53(1):101-14.
123. Cameron HU, Pilliar RM, Macnab I. The rate of bone ingrowth into porous metal. Journal of Biomedical Materials Research. 1976;10(2):295-302.
124. Lueck RA, Galante J, Rostoker W, Ray RD. Development of an open pore metallic implant to permit attachment to bone. Surgical Forum. 1969;20:456-7.
125. Sangiorgio SN, Longjohn DB, Dorr LD, Ebramzadeh E. The influence of proximal stem geometry and surface finish on the fixation of a double-tapered cemented femoral stem. Journal of Biomechanics. 2011;44(1):22-7.
126. Urban RM, Jacobs JJ, Sumner DR, Peters CL, Voss FR, Galante JO. The Bone-Implant Interface of Femoral Stems with Non-Circumferential Porous Coating. A Study of Specimens Retrieved at Autopsy. Journal of Bone and Joint Surgery - Series A. 1996 July 1, 1996;78(7):1068-81.
127. Thomas KA, Kay JF, Cook SD, Jarcho M. The effect of surface macrotexture and hydroxylapatite coating on the mechanical strengths and histologic profiles of titanium implant materials. Journal of Biomedical Materials Research. 1987;21(12):1395-414.
128. Tonino AJ, Thèrin M, Doyle C. Hydroxyapatite-coated femoral stems. Journal of Bone and Joint Surgery - Series B. 1999;81(1):148-54.
129. Soballe K, Hansen E, Brockstedt-Rasmussen H, Bunger C. Hydroxyapatite coating converts fibrous tissue to bone around loaded implants. Journal of Bone and Joint Surgery - Series B. 1993 March 1, 1993;75-B(2):270-8.
130. Engh CA, Bobyn JD, Glassman AH. Porous-coated hip replacement. The factors governing bone ingrowth, stress shielding, and clinical results. Journal of Bone and Joint Surgery - Series B. 1987;69(1):45-55.
131. Folgado J, Fernandes PR, Jacobs CR, Pellegrini VD. Influence of femoral stem geometry, material and extent of porous coating on bone ingrowth and atrophy in cementless total hip arthroplasty: an iterative finite element model. Computer Methods in Biomechanics and Biomedical Engineering. 2009;12(2):135-45.
132. Malchau H, Herberts P. Prognosis of total hip replacement. International Journal of Risk and Safety in Medicine. 1996;8(1):27-45.
133. Khanuja HS, Vakil JJ, Goddard MS, Mont MA. Cementless Femoral Fixation in Total Hip Arthroplasty. The Journal of Bone & Joint Surgery. [10.2106/JBJS.J.00774]. 2011;93(5):500.
134. Spotorno L, Romagnoli S, Ivaldo N, Grappiolo G, Bibbiani E, Blaha DJ, et al. The CLS system. Theoretical concept and results. Acta Orthopaedica Belgica. 1993;59 Suppl 1:144-8.
135. Renkawitz T, Santori FS, Grifka J, Valverde C, Morlock MM, Learmonth ID. A new short uncemented, proximally fixed anatomic femoral implant with a prominent lateral flare: Design

rationals and study design of an international clinical trial. BMC Musculoskeletal Disorders. 2008;9.
136. Ghera S, Pavan L. The DePuy Proxima hip: a short stem for total hip arthroplasty. Early experience and technical considerations. Hip international : the journal of clinical and experimental research on hip pathology and therapy. 2009;19(3):215-20.
137. Eskelinen A, Remes V, Helenius I, Pulkkinen P, Nevalainen J, Paavolainen P. Uncemented total hip arthroplasty for primary osteoarthritis in young patients: A mid- to long-term follow-up study from the Finnish Arthroplasty Register. Acta Orthopaedica. 2006;77(1):57-70.
138. Lazarinis S, Krärholm J, Hailer NP. Increased risk of revision of acetabular cups coated with hydroxyapatite: A Swedish Hip Arthroplasty Register study involving 8,043 total hip replacements. Acta Orthopaedica. 2010;81(1):53-9.
139. Adolphson P. Femoral cortical remodeling after uncemented total hip arthroplasty: A prospective radiologic study of 26 hips followed for 2 to 4 years. Journal of Arthroplasty. 1997;12(1):99-105.
140. Stryker. Orthopaedics Femoral Stems. Stryker Corporation; 2013; Available from: http://www.aboutstryker.com/hip/why-stryker/fit-fixation.php.
141. Landa J, Benke M, Dayan A, Pereira G, Di Cesare PE. Fracture of Fully Coated Echelon Femoral Stems in Revision Total Hip Arthroplasty. Journal of Arthroplasty. 2009;24(2).
142. Götze C, Tschugunow A, Götze HG, Böttner F, Pötzl W, Gosheger G. Long-term results of the metal-cancellous cementless Lübeck total hip arthroplasty: A critical review at 12.8 years. Archives of Orthopaedic and Trauma Surgery. 2006;126(1):28-35.
143. Phillips TW, Nguyen LT, Munro SD. Loosening of cementless femoral stems: A biomechanical analysis of immediate fixation with loading vertical, femur horizontal. Journal of Biomechanics. 1991;24(1):37-48.
144. Tóth K, Sisák K, Nagy J, Manó S, Csernátony Z. Retrograde stem removal in revision hip surgery: Removing a loose or broken femoral component with a retrograde nail. Archives of Orthopaedic and Trauma Surgery. 2010;130(7):813-8.
145. Nabors ED, Liebelt R, Mattingly DA, Bierbaum BE. Removal and reinsertion of cemented femoral components during acetabular revision. Journal of Arthroplasty. 1996;11(2):146-52.
146. Pabinger C, Geissler A. Utilization rates of hip arthroplasty in OECD countries. Osteoarthritis and Cartilage. 2014;22(6):734-41.
147. NICE. Guidance on the selection of prostheses for primary total hip replacement. London: NICE - National Institute for Health and Clinical Excellence; 2000.
148. Grünig R, Morscher E, Ochsner PE. Three- to 7-year results with the uncemented SL femoral revision prosthesis. Archives of Orthopaedic and Trauma Surgery. 1997;116(4):187-97.
149. Dunn AW. Total hip arthroplasty: revision in long-term results of 185 cases. Shouthern Medical Journal. 1982 August 1982;75(8):937-40.
150. Lakstein D, Backstein D, Safir O, Kosashvili Y, Gross AE. Revision total hip arthroplasty with a porous-coated modular stem : 5 to 10 years followup. Clinical Orthopaedics and Related Research. 2010;468(5):1310-5.
151. Manktelow ARJ. (ii) Implant removal in revision hip surgery. Orthopaedics and Trauma. 2009;23(5):307-21.
152. Holt G, Hook S, Hubble M. Revision total hip arthroplasty: The femoral side using cemented implants. International Orthopaedics. 2011;35(2):267-73.
153. Brooks AT, Nelson CL, Stewart CL, Skinner RA, Siems ML. Effect of an ultrasonic device on temperatures generated in bone and on bone-cement structure. Journal of Arthroplasty. 1993;8(4):413-8.

154. Park YS, Moon YW, Lim SJ. Revision Total Hip Arthroplasty Using a Fluted and Tapered Modular Distal Fixation Stem With and Without Extended Trochanteric Osteotomy. Journal of Arthroplasty. 2007;22(7):993-9.
155. Mardones R, Gonzalez C, Cabanela ME, Trousdale RT, Berry DJ. Extended femoral osteotomy for revision of hip arthroplasty: Results and complications. Journal of Arthroplasty. 2005;20(1):79-83.
156. Younger TI, Bradford MS, Magnus RE, Paprosky WG. Extended proximal femoral osteotomy: A new technique for femoral revision arthroplasty. Journal of Arthroplasty. 1995;10(3):329-38.
157. Callaghan JJ, Rosenberg AG, Rubash HE. The Adult Hip: Lippincott Williams & Wilkins; 2007.
158. Morrey BF, Kavanagh BF. Complications with revision of the femoral component of total hip arthroplasty: Comparison between cemented and uncemented techniques. Journal of Arthroplasty. 1992;7(1):71-9.
159. Smith SE, Estok Ii DM, Harris WH. 20-year experience with cemented primary and conversion total hip arthroplasty using so-called second-generation cementing techniques in patients aged 50 years or younger. The Journal of Arthroplasty. [doi: DOI: 10.1016/S0883-5403(00)90463-7]. 2000;15(3):263-73.
160. Gramkow J, Jensen TH, Varmarken JE, Retpen JB. Long-term results after cemented revision of the femoral component in total hip arthroplasty. Journal of Arthroplasty. 2001;16(6):777-83.
161. Malkani AL, Lewallen DG, Cabanela ME, Wallrichs SL. Femoral component revision using an uncemented, proximally coated, long-stem prosthesis. Journal of Arthroplasty. 1996;11(4):411-8.
162. Sporer SM, Paprosky WG. (iii) Cementless femoral revision: The role of monoblock versus modular stems. Current Orthopaedics. 2006;20(3):171-8.
163. Dennis DA. Removal of well-fixed cementless metal-backed patellar components. Journal of Arthroplasty. 1992;7(2):217-20.
164. Blumenfeld TJ. Removing a well-fixed nonmodular large-bearing cementless acetabular component. A simple modification of an existing removal device. Journal of Arthroplasty. 2010;25(3).
165. Kim YM, Lim ST, Yoo JJ, Kim HJ. Removal of a well-fixed cementless femoral stem using a microsagittal saw. Journal of Arthroplasty. 2003;18(4):511-2.
166. Olyslaegers C, Wainwright T, Middleton RG. A Novel Technique for the Removal of Well-Fixed Cementless, Large-Diameter Metal-on-Metal Acetabular Components. Journal of Arthroplasty. 2008;23(7):1071-3.
167. Freiman A, Bouganim N. History of cryotherapy. Dermatology Online Journal. 2005;11(2).
168. Shepherd J, Dawber RPR. The historical and scientific basis of cryosurgery. Clinical and Experimental Dermatology. 1982;7(3):321-8.
169. Gage AA. History of cryosurgery. Seminars in Surgical Oncology. 1998;14(2):99-109.
170. Keijser LCM, Schreuder HWB, Buma P, Weinans H, Veth RPH. Cryosurgery in long bones; An experimental study of necrosis and revitalization in rabbits. Archives of Orthopaedic and Trauma Surgery. 1999;119(7-8):440-4.
171. Woods EJ, Benson JD, Agca Y, Critser JK. Fundamental cryobiology of reproductive cells and tissues. Cryobiology. 2004;48(2):146-56.
172. Korpan NN. Cryosurgery: Ultrastructural changes in pancreas tissue after low temperature exposure. Technology in Cancer Research and Treatment. 2007;6(2):59-67.
173. Korpan NN, Hochwarter G, Sellner F. Cryoscience and cryomedicine: new mechanisms of biological tissue injury following low temperature exposure. Experimental study. Klinichna

khirurhiia / Ministerstvo okhorony zdorov'ia Ukraïny, Naukove tovarystvo khirurhiv Ukraïny. 2009(7-8):80-5.
174. Kuylenstierna R, Lundquist P-G. Bone destruction by direct cryoapplication: A temperature study in rabbits. Cryobiology. 1982;19(3):231-6.
175. Keijser LCM, Schreuder HWB, Boons HW, Keulers BJ, Buma P, Huiskes R, et al. Bone grafting of cryosurgically treated bone defects: Experiments in goats. Clinical Orthopaedics and Related Research. 2002(396):215-22.
176. Severs NJ, Shotton DM. Rapid Freezing of Biological Specimens for Freeze Fracture and Deep Etching. Cell Biology, Four-Volume Set2006. p. 249-55.
177. Whittaker DK. Mechanisms of tissue destruction following cryosurgery. Annals of the Royal College of Surgeons of England. 1984;66(5):313-8.
178. Kang Q, An YH, Friedman RJ. Effects of multiple freezing-thawing cycles on ultimate indentation load and stiffness of bovine cancellous bone. American Journal of Veterinary Research. 1997;58(10):1171-3.
179. Madrala A, Nuño N. Effect of stem preheating and precooling on residual stress formation at stem/cement interface for cemented hip implants. Journal of Biomedical Materials Research - Part B Applied Biomaterials. 2010;93(1):258-65.
180. Pérez MA, Nuño N, Madrala A, García-Aznar JM, Doblaré M. Computational modelling of bone cement polymerization: Temperature and residual stresses. Computers in Biology and Medicine. [doi: DOI: 10.1016/j.compbiomed.2009.06.002]. 2009;39(9):751-9.
181. Gage AA, Baust J. Mechanisms of Tissue Injury in Cryosurgery. Cryobiology. 1998;37(3):171-86.
182. Brown NJ, Pollock KJ, Bayjoo P, Reed MWR. The effect of cryotherapy on the cremaster muscle microcirculation in vivo. British Journal of Cancer. 1994;69(4):706-10.
183. Franco W, Vu H, Jia W, Nelson JS, Aguilar G, editors. Spray and cooling dynamics of cryogen sprays impinging on a human skin model. 2007 Proceedings of the ASME/JSME Thermal Engineering Summer Heat Transfer Conference; 2007.
184. CSA. Cryosurgery. 2008; Available from: http://www.cryogenicsociety.org/.
185. Popken F, Meschede P, Erberich H, Koy T, Bosse M, Fischer JH, et al. Complications after cryosurgery with new miniature cryoprobes in long hollow bones: An animal trial. BMC Surgery. [Article]. 2005;5.
186. Steu S, Baucamp M, Von Dach G, Bawohl M, Dettwiler S, Storz M, et al. A procedure for tissue freezing and processing applicable to both intra-operative frozen section diagnosis and tissue banking in surgical pathology. Virchows Archiv. 2008;452(3):305-12.
187. Karlsson JOM, Toner M. Long-term storage of tissues by cryopreservation: Critical issues. Biomaterials. 1996;17(3):243-56.
188. Sapanathan T, Ibrahim R, Khoddam S, Zahiri SH. Shear blanking test of a mechanically bonded aluminum/copper composite using experimental and numerical methods. Materials Science and Engineering: A. 2015 1/19/;623:153-64.
189. Sapanathan T, Khoddam S, Zahiri SH, Zarei-Hanzaki A. Strength changes and bonded interface investigations in a spiral extruded aluminum/copper composite. Materials & Design. 2014 5//;57:306-14.
190. Pishbin H, Parsa MH, Dastvareh A. An analytical modified model of clad sheet bonding by cold rolling using upper bond theorem. Journal of Materials Engineering and Performance. 2010;19(7):936-41.
191. Pan D, Gao K, Yu J. Cold roll bonding of bimetallic sheets and strips. Materials Science and Technology. 1989;5(9):934-9.
192. Maleki H, Bagherzadeh S, Mollaei-Dariani B, Abrinia K. Analysis of bonding behavior and critical reduction of two-layer strips in clad cold rolling process. Journal of Materials Engineering and Performance. 2013;22(4):917-25.

193. Meng L, Zhou SP, Yang FT, Shen QJ, Liu MS. Diffusion annealing of copper–silver bimetallic strips at different temperatures. Materials Characterization. 2001 9//;47(3–4):269-74.
194. Matsuzaki R, Shibata M, Todoroki A. Improving performance of GFRP/aluminum single lap joints using bolted/co-cured hybrid method. Composites Part A: Applied Science and Manufacturing. 2008;39(2):154-63.
195. Álvarez D, Blackman BRK, Guild FJ, Kinloch AJ. Mode I fracture in adhesively-bonded joints: A mesh-size independent modelling approach using cohesive elements. Engineering Fracture Mechanics. 2014;115(0):73-95.
196. Camanho PP, Tavares CML, de Oliveira R, Marques AT, Ferreira AJM. Increasing the efficiency of composite single-shear lap joints using bonded inserts. Composites Part B: Engineering. 2005;36(5):372-83.
197. Di Franco G, Fratini L, Pasta A. Analysis of the mechanical performance of hybrid (SPR/bonded) single-lap joints between CFRP panels and aluminum blanks. International Journal of Adhesion and Adhesives. 2013;41(0):24-32.
198. Gage AA, Caruana Jr JA, Montes M. Critical temperature for skin necrosis in experimental cryosurgery. Cryobiology. [Article]. 1982;19(3):273-82.
199. Incropera DW, Bergman, Lavine. Fundamentals of heat and mass transfer. sixth ed: John Wiley & Sons Inc.; 2007.
200. Arpaci VS. Conduction heat transfer: Addison-Wesley Pub. Co.; 1966.
201. Welty J, Rorrer GL, Foster DG. Fundamentals of Momentum, Heat and Mass Transfer, 6th Edition: Wiley; 2014.
202. Ozisik N. Heat Conduction: Wiley; 1993.
203. Bejan A. Convection Heat Transfer: Wiley; 2013.
204. Novitskaya E, Chen PY, Lee S, Castro-Ceseña A, Hirata G, Lubarda VA, et al. Anisotropy in the compressive mechanical properties of bovine cortical bone and the mineral and protein constituents. Acta Biomaterialia. 2011;7(8):3170-7.
205. Dick C, Georgii J, Burgkart R, Westermann R. Stress tensor field visualization for implant planning in orthopedics. IEEE Transactions on Visualization and Computer Graphics. 2009;15(6):1399-406.
206. Reilly DT, Burstein AH. The mechanical properties of cortical bone. Journal of Bone and Joint Surgery - Series A. 1974;56(5):1001-22.
207. Galante J, Rostoker W, Ray RD. Physical properties of trabecular bone. Calcified Tissue International. 1970;5(1):236-46.
208. Cowin SC. Bone Mechanics: CRC Press; 1989.
209. Head WC, Bauk DJM, Emerson RH. Titanium As the Material of Choice for Cementless Femoral Components in Total Hip Arthroplasty. Clinical Orthopaedics & Related Research. 1995;311:85-90.
210. Leyens C, Peters M. Titanium and Titanium Alloys, Fundamentals and Applications: Wiley-VCH; 2003.
211. Down GM. Use of Titanium as an Implant Material. Engineering in Medicine. 1973;2(3):58-9, 63.
212. Donachie MJ. Materials Properties Handbook - Titanium Alloys: ASM International; 1988.
213. Ivasishin OM, Markovsky PE, Pakharenko GA, Shevchenko AV. Mechanical properties of (α + β)-titanium alloy at cryogenic temperatures. Materials Science and Engineering: A. [doi: 10.1016/0921-5093(94)09707-0]. 1995;196(1-2):65-70.
214. Cohen BI, Deutsch AS, Musikant BL. The effect of cold treatment on the physical properties of stainless steel and titanium alloy endodontic posts. The Journal of Prosthetic Dentistry. [doi: 10.1016/0022-3913(92)90377-M]. 1992;68(4):625-8.

215. Conrad H. Plastic flow and fracture of titanium at low temperatures. Cryogenics. 1984;24(6):293-304.
216. Touloukran YS. Thermophysical Properties of Matter. New York: Plenum Press; 1970.
217. Ziegler W, Mullins J, Hwa S. Specific Heat and Thermal Conductivity of Four Commercial Titanium Alloys: Plenum Press; 1963.
218. McGann M. Determination of Design Data for Heat Treated Titanium Alloy Sheet: Aerospace Structural Metals Handbook; 1962.
219. Queheillalt DT, Wadley HNG. Titanium alloy lattice truss structures. Materials & Design. [doi: DOI: 10.1016/j.matdes.2008.09.015]. 2009;30(6):1966-75.
220. Serbetci K, Korkusuz F, Hasirci N. Thermal and mechanical properties of hydroxyapatite impregnated acrylic bone cements. Polymer Testing. 2004;23(2):145-55.
221. Eyerer P, Jin R. Influence of mixing technique on some properties of PMMA bone cement. Journal of Biomedical Materials Research. 1986;20(8):1057-94.
222. Shrivastava S, editor. Medical Device Materials I. Proceedings from the 2003 Materials & Processes for Medical Devices Conference; 2003; Anaheim, California: ASM International.
223. Fukushima H, Hashimoto Y, Yoshiya S, Kurosaka M. Conduction analysis of cement interface temperature in total knee arthroplasty. Journal of Medical Sciences. 2002;48(1-2):63-72.
224. Mousa WF, Kobayashi M, Shinzato S, Kamimura M, Neo M, Yoshihara S, et al. Biological and mechanical properties of PMMA-based bioactive bone cements. Biomaterials. [doi: DOI: 10.1016/S0142-9612(00)00097-1]. 2000;21(21):2137-46.
225. Lewis G. Properties of acrylic bone cement: State of the art review. Journal of Biomedical Materials Research. 1997;38(2):155-82.
226. Saha S, Pal S. Mechanical properties of bone cement: A review. Journal of Biomedical Materials Research. 1984;18(4):435-62.
227. Nottrott M, Mølster AO, Gjerdet NR. Time dependent mechanical properties of bone cement. An in vitro study over one year. Journal of biomedical materials research Part B, Applied biomaterials. 2007;83(2):416-21.
228. Grant JA, Bishop NE, Götzen N, Sprecher C, Honl M, Morlock MM. Artificial composite bone as a model of human trabecular bone: The implant-bone interface. Journal of Biomechanics. 2007;40(5):1158-64.
229. Elfar J, Menorca RM, Reed JD, Stanbury S. Composite bone models in orthopaedic surgery research and education. The Journal of the American Academy of Orthopaedic Surgeons. 2014;22(2):111-20.
230. Crookshank M, Coquim J, Olsen M, Schemitsch EH, Bougherara H, Zdero R. Biomechanical measurements of axial crush injury to the distal condyles of human and synthetic femurs. Proceedings of the Institution of Mechanical Engineers, Part H: Journal of Engineering in Medicine. 2012;226(4):320-9.
231. Nicayenzi B, Shah S, Schemitsch EH, Bougherara H, Zdero R. The biomechanical effect of changes in cancellous bone density on synthetic femur behaviour. Proceedings of the Institution of Mechanical Engineers, Part H: Journal of Engineering in Medicine. 2011;225(11):1050-60.
232. Zdero R, Olsen M, Bougherara H, Schemitsch EH. Cancellous bone screw purchase: A comparison of synthetic femurs, human femurs, and finite element analysis. Proceedings of the Institution of Mechanical Engineers, Part H: Journal of Engineering in Medicine. 2008;222(8):1175-83.
233. Heiner AD, Brown TD. Structural properties of a new design of composite replicate femurs and tibias. Journal of Biomechanics. 2001;34(6):773-81.
234. Heiner AD. Structural properties of fourth-generation composite femurs and tibias. Journal of Biomechanics. 2008;41(15):3282-4.

235. Gardner MP, Chong ACM, Pollock AG, Wooley PH. Mechanical evaluation of large-size fourth-generation composite femur and tibia models. Annals of Biomedical Engineering. 2010;38(3):613-20.
236. Dunlap J, Chong A, Lucas G, Cooke F. Structural Properties of a Novel Design of Composite Analogue Humeri Models. Annals of Biomedical Engineering. 2008;36(11):1922-6.
237. Zdero R, Shah S, Mosli M, Schemitsch EH. The effect of load application rate on the biomechanics of synthetic femurs. Proceedings of the Institution of Mechanical Engineers, Part H: Journal of Engineering in Medicine. 2010;224(4):599-605.
238. Zdero R, Bougherara H, Dubov A, Shah S, Zalzal P, Mahfud A, et al. The effect of cortex thickness on intact femur biomechanics: A comparison of finite element analysis with synthetic femurs. Proceedings of the Institution of Mechanical Engineers, Part H: Journal of Engineering in Medicine. 2010;224(7):831-40.
239. Chong A, Friis E, Ballard G, Czuwala P, Cooke F. Fatigue Performance of Composite Analogue Femur Constructs under High Activity Loading. Annals of Biomedical Engineering. 2007;35(7):1196-205.
240. Chong ACM, Miller F, Buxton M, Friis EA. Fracture toughness and fatigue crack propagation rate of short fiber reinforced epoxy composites for analogue cortical bone. Journal of Biomechanical Engineering. 2007;129(4):487-93.
241. Tu YK, Chen LW, Ciou JS, Hsiao CK, Chen UC. Finite element simulations of bone temperature rise during bone drilling based on a bone analog. Journal of Medical and Biological Engineering. 2013;33(3):269-74.
242. Huang CC, Liu YC, Chen LW, Chen YC. Temperature rise of alveolar bone during dental implant drilling using the finite element simulation. Life Science Journal. 2010;7(1):68-72.
243. Da Matta Sellani G, Valois C, de Albuquerque Pereira W, Machado C. Thermographic Analysis of Block and Cylindrical Bone Phantoms and In Vitro Human Bone Samples after Therapeutic Ultrasound Stimulation. In: Lacković I, Vasic D, editors. 6th European Conference of the International Federation for Medical and Biological Engineering: Springer International Publishing; 2015. p. 192-5.
244. Sawbones. Biomechanical Test Materials. Pacific Research Laboratories, Inc.; 2015; Available from: http://www.sawbones.com/UserFiles/Docs/biomechanical_catalog.pdf.
245. Petheram TG, Bone M, Joyce TJ, Serrano-Pedraza I, Reed MR, Partington PF. Surface finish of the Exeter Trauma Stem. A cause for concern? 2013;95-B(2):173-6.
246. Riede U, Lüem M, Ilchmann T, Eucker M, Ochsner PE. The M.E Müller straight stem prosthesis: 15 year follow-up. Survivorship and clinical results. Archives of Orthopaedic and Trauma Surgery. [journal article]. 2007;127(7):587-92.
247. Campbell P, Takamura K, Lundergan W, Esposito C, Amstutz HC. Cement technique changes improved hip resurfacing longevity: Implant retrieval findings. Bulletin of the NYU Hospital for Joint Diseases. 2009;67(2):146-53.
248. Fisher DA, Tsang AC, Paydar N, Milionis S, Turner CH. Cement-mantle thickness affects cement strains in total hip replacement. Journal of Biomechanics. 1997;30(11-12):1173-7.
249. Flynn T. Cryogenic Engineering, Second Edition, Revised and Expanded: Taylor & Francis; 2004.
250. DePuy-International-Ltd. Acrylic Bone Cement Instruction Leaflet. In: Johnson Ja, editor. Blackpool, UK: DePuy International Ltd.
251. Khandaker M, Tarantini S, editors. Nanoscale fracture resistance measurement of a composite bone cement. Conference Proceedings of the Society for Experimental Mechanics Series; 2011.
252. Xu W, Wei Y. Strength and interface failure mechanism of adhesive joints. International Journal of Adhesion and Adhesives. 2012;34(0):80-92.

253. Alexander KL, Clarkson J, Bishop D, Fox S. Good Design Practice for Medical Devices and Equipment: A Framework, vol 1: University of Cambridge Engineering Design Centre/University of Cambridge Institute of Manufacturing; 2001.
254. Ward J, Clarkson J. Good Design Practice for Medical Devices and Equipment: Design Verification: University of Cambridge Engineering Design Centre/University of Cambridge Institute of Manufacturing; 2002.
255. Shefelbine S, Clarkson J, Farmer R. Good Design Practice for Medical Devices and Equipment: Requirements Capture: University of Cambridge Engineering Design Centre/University of Cambridge Institute of Manufacturing; 2002.
256. Pugh S. Total Design: Integrated Methods for Successful Product Engineering: Addison-Wesley Publishing Company; 1991.
257. Alonso-Rasgado T, Thompson G. A rapid design process for total care product creation. Journal of Engineering Design. [Article]. 2006;17(6):509-31.
258. iSixSigma. Pugh Matrix. Cyger, Michael; Available from: http://www.isixsigma.com/featured/resource-page-pugh-matrix/.
259. Optimal-Design-Laboratory. Pugh Chart Worksheet. University of Michigan-Optimal Design Laboratory; Available from: http://ode.engin.umich.edu/APD12/readings/5%20EMBODIMENT%20&%20EVALUATION.
260. Ginalski MK, Nowak AJ, Wrobel LC. A combined study of heat and mass transfer in an infant incubator with an overhead screen. Medical Engineering and Physics. 2007;29(5):531-41.
261. Fic AM, Ingham DB, Ginalski MK, Nowak AJ, Wrobel LC. Modelling and optimisation of the operation of a radiant warmer. Medical Engineering and Physics. 2014;36(1):81-7.
262. Franco W, Vu H, Jia W, Nelson JS, Aguilar G. Fluid and thermal dynamics of cryogen sprays impinging on a human tissue phantom. Journal of Biomechanical Engineering. 2008;130(5).
263. Andrade MGS, Sá CN, Marchionni AMT, Bório dos Santos Calmonde Bittencourt TC, Sadigursky M. Effects of freezing on bone histological morphology. Cell and Tissue Banking. 2008;9(4):279-87.
264. Hrennikoff A. Solution of Problems of Elasticity by the Frame-Work Method. ASME Journal of Applied Mechanics. 1941;8:A619 - A715.
265. Courant R. Variational methods for the solution of problems of equilibrium and vibrations. 1943 1943/01(1):1-23.
266. Pelosi G. The finite-element method, Part I: R. L. Courant [Historical Corner]. Antennas and Propagation Magazine, IEEE. 2007;49(2):180-2.
267. Turner MJ. Stiffness and Deflection Analysis of Complex Structures. Journal of the Aeronautical Sciences (Institute of the Aeronautical Sciences). [doi: 10.2514/8.3664]. 1956 1956/09/01;23(9):805-23.
268. Clough RW. The finite element method in plane stress analysis. 1960.
269. Brekelmans WAM, Poort HW, Slooff TJJH. A new method to analyse the mechanical behaviour of skeletal parts. Acta Orthopaedica. 1972;43(5):301-17.
270. Bathe KJ. Finite Element Procedures: Prentice Hall; 2006.
271. SIMULIA DS. ABAQUS/CAE 6.10 User's Manual: Dessault Systèmes; 2010.
272. Green AE, Naghdi PM. A general theory of an elastic-plastic continuum. Arch Rational Mech Anal. 1965 1965/01/01;18(4):251-81.
273. Li C, Kotha S, Huang CH, Mason J, Yakimicki D, Hawkins M. Finite element thermal analysis of bone cement for joint replacements. Journal of Biomechanical Engineering. 2003;125(3):315-22.

274. Sansinena M, Santos MV, Zaritzky N, Chirife J. Comparison of heat transfer in liquid and slush nitrogen by numerical simulation of cooling rates for French straws used for sperm cryopreservation. Theriogenology. 2012;77(8):1717-21.
275. Jin T, Hong JP, Zheng H, Tang K, Gan ZH. Measurement of boiling heat transfer coefficient in liquid nitrogen bath by inverse heat conduction method. Journal of Zhejiang University: Science A. 2009;10(5):691-6.
276. Franco W, Liu J, Aguilar G, editors. Interaction of cryogen spray with human skin under vacuum pressures. WIT Transactions on the Built Environment; 2005.
277. Aguilar G, Díaz SH, Lavernia EJ, Nelson JS. Cryogen spray cooling efficiency: Improvement of port wine stain laser therapy through multiple-intermittent cryogen spurts and laser pulses. Lasers in Surgery and Medicine. 2002;31(1):27-35.
278. Crowley TJ, Tuzla R, Wenzel LA, Chen JC. Convective boiling of nitrogen on a short vertical surface. Thermal Phenomena in the Fabrication and Operation of Electronic Components: IEEE; 1988. p. 127-31.
279. Aguilar G, Verkruysse W, Majaron B, Svaasand LO, Lavernia EJ, Nelson JS. Measurement of heat flux and heat transfer coefficient during continuous cryogen spray cooling for laser dermatologic surgery. IEEE Journal of Selected Topics in Quantum Electronics. 2001;7(6):1013-21.
280. Ashtiani MN, Imani R. Transient heat transfer in a dental prosthesis implanted in mandibular bone. 26th Southern Biomedical Engineering Conference: International Federation for Medical and Biological Engineering; 2010. p. 376-9.
281. Pérez MA, García JM, Doblaré M. Analysis of the debonding of the stem-cement interface in intramedullary fixation using a non-linear fracture mechanics approach. Engineering Fracture Mechanics. 2005;72(8):1123-4.
282. He X. Effect of mechanical properties of adhesives on stress distributions in structural bonded joints. World Congress on Engineering. 2010;2:1168-72.
283. Kweon J-H, Jung J-W, Kim T-H, Choi J-H, Kim D-H. Failure of carbon composite-to-aluminum joints with combined mechanical fastening and adhesive bonding. Composite Structures. 2006;75(1–4):192-8.
284. Park S-J, Seo M-K. Chapter 4 - Solid-Solid Interfaces. In: Soo-Jin P, Min-Kang S, editors. Interface Science and Technology: Elsevier; 2011. p. 253-331.
285. Risegari L, Barucci M, Lolli L, Ventura G. Low temperature thermal conductivity of Ti6Al4V alloy. Journal of Low Temperature Physics. 2008;151(3-4 PART 2):645-9.

APPENDIX

Appendix A1: DePuy®'s Corail® femoral stem - size 11 (length dimensions in mm)

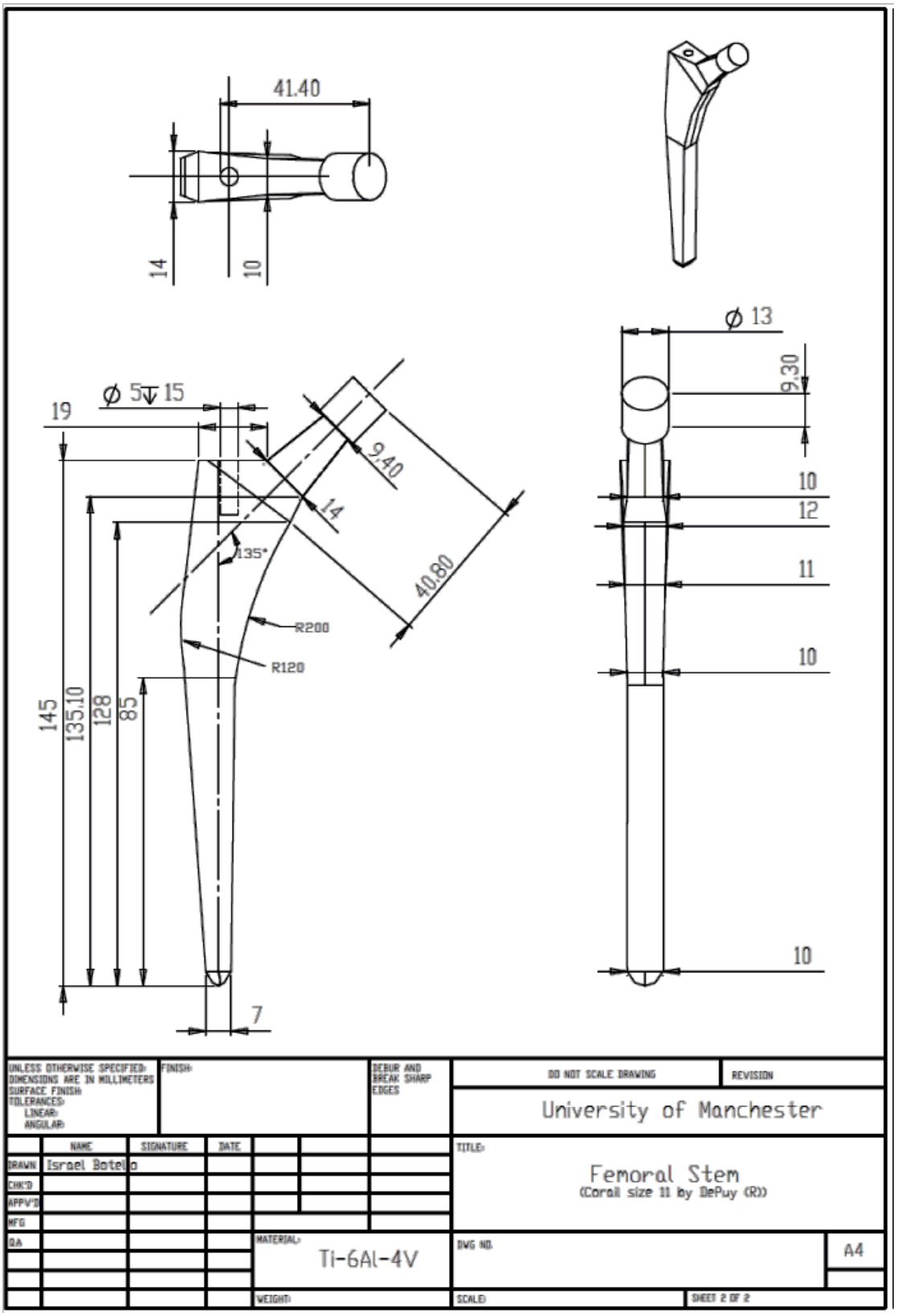

Appendix A2: Customized titanium stem (length dimensions in mm)

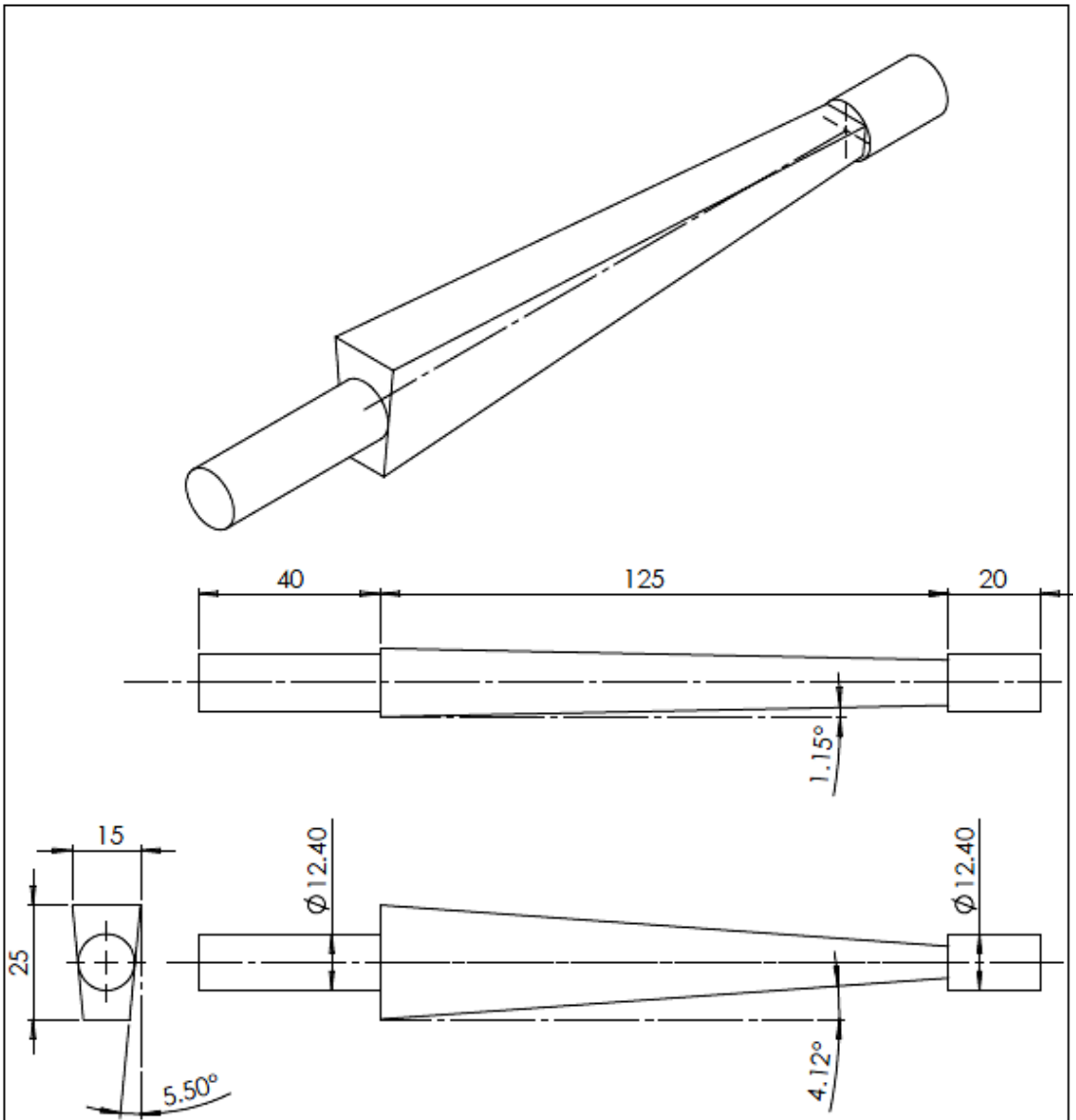

UNLESS OTHERWISE SPECIFIED: DIMENSIONS ARE IN MILLIMETERS SURFACE FINISH: TOLERANCES: LINEAR: ANGULAR:		FINISH:		DEBUR AND BREAK SHARP EDGES			DO NOT SCALE DRAWING	REVISION
							University of Manchester	
	NAME	SIGNATURE	DATE				TITLE:	
DRAWN	Israel Botello						Stem Probe	
CHK'D								
APPV'D								
MFG								
Q.A				MATERIAL:			DWG NO.	A4
				Ti-6Al-4V				
				WEIGHT:			SCALE:1:2	SHEET 1 OF 1

Appendix A3: Clamping system – Bottom plate (length dimensions in mm)

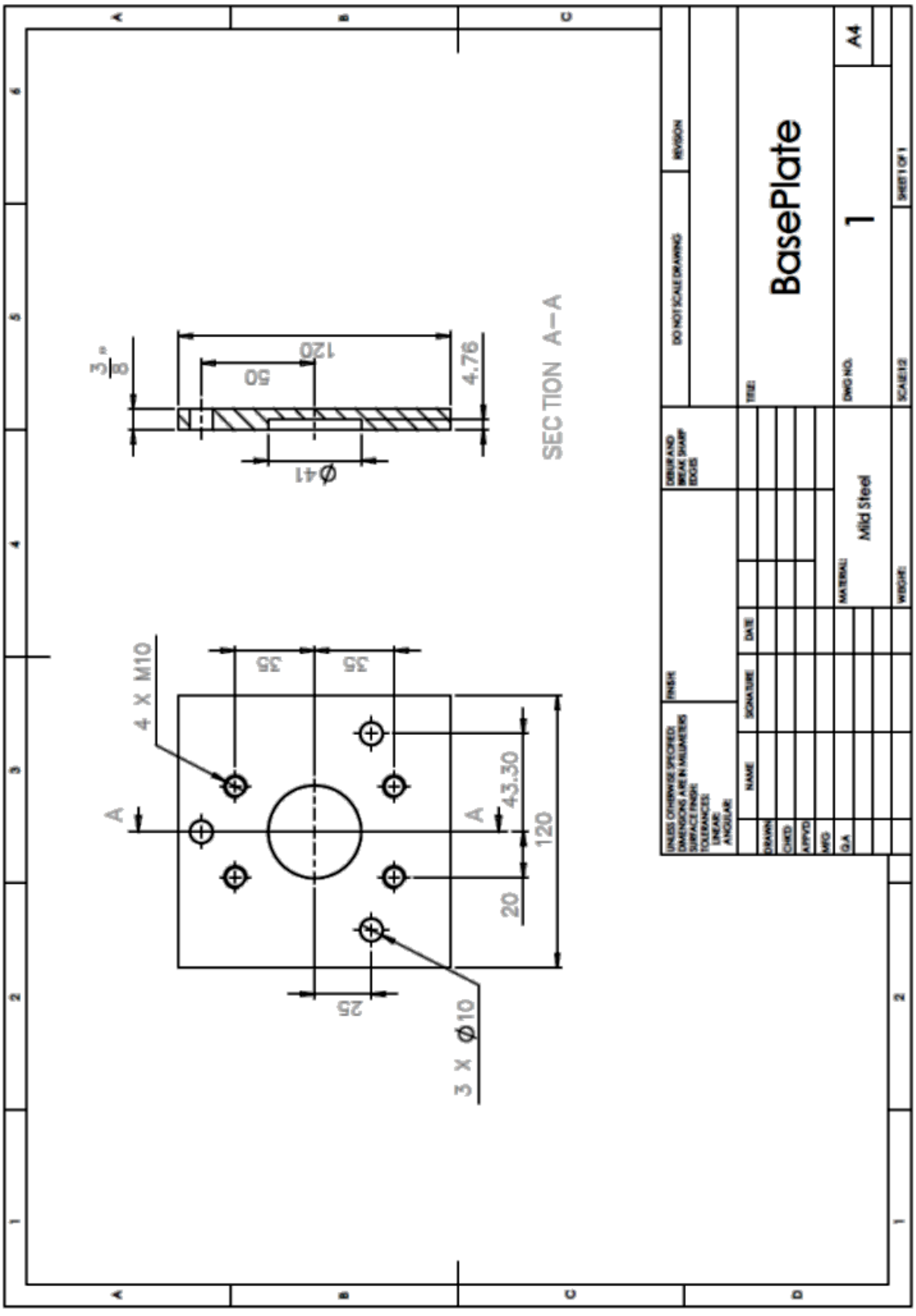

Appendix A4: Clamping system – Top plate (length dimensions in mm)